

EXPERIMENTAL AND ANALYTICAL INVESTIGATIONS ON A CLASS OF DYNAMIC PROBLEMS IN BEAM-FOUNDATION INTERACTION

A Thesis Submitted
**In Partial Fulfilment of the Requirements
for the Degree of
DOCTOR OF PHILOSOPHY**

by
ASHOK KUMAR JAIN

to the

**DEPARTMENT OF CIVIL ENGINEERING
INDIAN INSTITUTE OF TECHNOLOGY KANPUR
SEPTEMBER 1977**

I.I.T. KANPUR
CENTRAL LIBRARY
Acc. No. A 54248

M1 JUN 1978

CE-1977-D-JAI-EXP

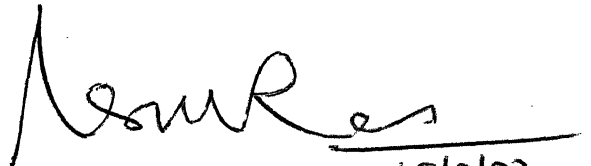
TH
624.17723
J 199 e

132

CERTIFICATE

Certified that the work contained in this thesis entitled "Experimental and analytical Investigations on a class of dynamic problems in Beam-foundation Interaction" has been carried out by Shri Ashok Kumar Jain under my supervision and the same has not been submitted elsewhere for a degree. In the initial phases, Dr. M. Anandakrishnan, Professor in Department of Civil Engineering, (Presently the Science Counsellor, Indian Embassy, Washington) has been associated with the investigation.

September 1977

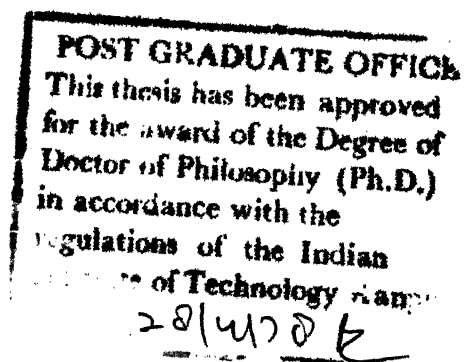


(N. S. V. Kameswara Rao)

15/9/77

Professor

Department of Civil Engineering
Indian Institute of Technology, Kanpur



To
my
parents

Acknowledgements

The author is deeply indebted to Dr. N.S.V. Kameswara Rao for the inspiring guidance, constructive suggestions and encouragement at each stage of the work. Dr. Kameswara Rao always inspired the author in difficult moments. The author gratefully acknowledges the guidance of him.

The author expresses his gratitude to Dr. M. Anandakrishnan who had initiated him into this problem and provided him with constant guidance in the initial phases of the investigations.

The help rendered by his friend, Mr. K.V. Lakshmidhar, Foreman, Soil Mechanics Lab. in setting up the experiments and in conducting the tests, is gratefully acknowledged.

The author is indebted to his friends, Mrs. and Mr. Afsar Hussain who always cheered and brought relief to him. He sincerely thanks Mr. Somnath Bandyopadhyay and many other friends who helped him in difficult moments.

His appreciations are to M/S R.P. Trivedi, Gulab Chand, R.K.Verma, G.S. Trivedi, Parasuram for thier help in the investigations. Thanks are due to M/S S.K. Tewari and G.L. Misra for their efficient typing and Mr. B.B. Srivastava for his neat tracings. The facilities provided by Computer Centre is thankfully acknowledged.

Words are inadequate to express the author's sentiments to his wife, Savita. She shared all the responsibilities of the author and this has allowed him to devote completely on the research work. Author pays high regards to his in-laws who were a constant source of inspiration.

Ashok Kumar Jain

Table of Contents

| | Page |
|--|------|
| Title page | |
| Certificate | i |
| Acknowledgements | ii |
| Table of Contents | iii |
| List of figures | iv |
| List of Tables | x |
| Synopsis | xi |
| Chapter 1 Introduction | 1 |
| 1.1 General | 1 |
| 1.2 Brief review of literature | 3 |
| 1.3 Scope of the present investigation | 11 |
| 1.4 Notations | 14 |
| Chapter 2 Experimental investigations | 20 |
| 2.1 General | 20 |
| 2.2 Soil properties | 20 |
| 2.3 Dynamic soil structure interaction studies | 25 |
| 2.4 Experimentation for Winkler model verification | 39 |
| Chapter 3 Dynamic Response of Beams on Elastic Foundation Carrying a Concentrated Mass | 81 |
| 3.1 General | 81 |
| 3.2 General theory | 82 |
| 3.3 Finite beam on Winkler foundation | 90 |
| 3.4 Infinite beam on Pasternak foundation | 93 |
| 3.5 Infinite beam on Winkler foundation | 94 |
| 3.6 Results | 95 |
| 3.7 Verification of solutions and Results | 104 |
| Chapter 4 Dynamic Response of Beams on Elastic Foundation Subjected to Impulse Loads | 144 |
| 4.1 General | 144 |
| 4.2 General formulation | 146 |
| 4.3 Inversion of Laplace transform | 152 |
| 4.4 Results | 158 |
| Chapter 5 Conclusions and Recommendations | 173 |
| 5.1 Conclusions | 173 |
| 5.2 Recommendations | 175 |
| References | 176 |

LIST OF FIGURES

| Figure | | Page |
|--------|--|------|
| 2.1 | Results of plate load test of a 1640 cm ² plate on stabilized soil | 54 |
| 2.2 | Results of a cyclic plate load test of a 1640 cm ² plate on Stabilized Soil | 55 |
| 2.3 | Relationship between pressure versus elastic settlement of a 1640 cm ² plate on stabilized soil | 56 |
| 2.4 | A schematic diagram of the test frame for soil contained in a bin | 57 |
| 2.5 | A schematic diagram of the test frame for field tests | 58 |
| 2.6(a) | A block diagram showing the arrangements of instruments for constant amplitude excitation on the footings | 59 |
| 2.6(b) | Idealized Winkler model | 59 |
| 2.7 | Displacement frequency curve for soil contained in the bin (for circular plate) | 60 |
| 2.8 | Displacement frequency response curve for soil contained in the bin (for Square Plate) | 61 |
| 2.9 | Displacement frequency response curve for soil contained in the bin (for Rectangular Plate) | 62 |
| 2.10 | Displacement frequency response curve for soil contained in the bin (for long stip) | 63 |
| 2.11 | Displacement frequency response curve for stabilized soil (for circular plate) | 64 |
| 2.12 | Displacement frequency response for stabilized soil (for square plate) | 65 |
| 2.13 | Displacement frequency response for stabilized soil (for rectangular plate) | 66 |

| Figure | | Page |
|--------|--|------|
| 2.14 | Displacement frequency response for stabilized soil (for long strip) | 67 |
| 2.15 | Displacement frequency response for natural soil (for circular plate) | 68 |
| 2.16 | Displacement frequency response for natural soil (for square plate) | 69 |
| 2.17 | Displacement frequency response for natural soil (for rectangular plate) | 70 |
| 2.18 | Displacement frequency response for natural soil (for long strip) | 71 |
| 2.19 | Variation of frequency with L/B ratio | 72 |
| 2.20 | Variation of maximum deflection with L/B ratio | 73 |
| 2.21 | Variation of maximum displacement with force | 74 |
| 2.22 | Variation of spring constant ratio with L/B ratio | 75 |
| 2.23 | Variation in damping factor with L/B ratio | 76 |
| 2.24 | Displacement frequency response curve for a beam resting on ideal springs | 77 |
| 2.25 | Maximum displacement variation along the length of beam at different frequencies for force 5.15 kg. | 78 |
| 2.26 | Maximum displacement variation along the length of the beam at different frequencies for force 9.40 kg. | 79 |
| 2.27 | Maximum displacement variation along the length of beam at different frequencies for force 12.0 kg. | 80 |
| 3.1(a) | A beam element on Pasternak foundation | 112 |
| 3.1(b) | A uniform beam on Pasternak foundation | 112 |
| 3.2 | Displacement frequency response curves for beam on Winkler foundation | 113 |
| 3.3 | Displacement response curve for beam with concentrated mass at the centre of beam resting on Winkler foundation. | 114 |

| Figure | Page |
|---|------|
| 3.4 Displacement frequency response for beam with concentrated mass and resting on Winkler foundation ($R=1.0$) | 115 |
| 3.5 Displacement frequency responses at various points along the length of the beam ($R=0.6$) | 116 |
| 3.6 Displacement frequency response at various points along the length of beam ($R=0.8$) | 117 |
| 3.7 Displacement frequency response at various points along the length of beam ($R=1.0$) | 118 |
| 3.8 Variation of maximum displacement with damping factor for various concentrated mass ratio | 119 |
| 3.9 Displacement variation along the length of beam for undamped case | 119 |
| 3.10 Displacement variation along the length of beam for damped case ($R=0.5$) | 120 |
| 3.11 Displacement variation along the length of beam for damped case ($R=0.6$) | 120 |
| 3.12 Displacement variation along the length of beam for damped case ($R=0.8$) | 121 |
| 3.13 Displacement variation along the length of beam for damped case ($R=1.0$) | 121 |
| 3.14 Variation of displacement with concentrated mass ratio for undamped case | 122 |
| 3.15 Variation of displacement with concentrated mass ratio for damped case ($R=0.5$) | |
| 3.16 Variation of displacement with concentrated mass ratio for damped case ($R=0.6$) | 123 |
| 3.17 Variation of displacement with concentrated mass ratio for damped case ($R=0.8$) | 124 |
| 3.18 Variation of displacement with concentrated mass ratio for damped case ($R=1.0$) | 125 |
| 3.19 Displacement variation with non-dimensional length R | 125 |
| 3.20 Displacement frequency response of an infinite beam along the length of the beam | 126 |

| Figure | Page |
|--|------|
| 3.21 Variation of maximum displacement with concentrated mass ratio | 127 |
| 3.22 Variation of maximum displacement along the length of the beam | 127 |
| 3.23 Displacement frequency response curve for an infinite beam on Pasternak foundation (variation along the length of the beam) $A=1.0$ | 128 |
| 3.24 Displacement frequency response for an infinite beam on Pasternak foundation ($A=0.5$) (variation along the length of the beam) | 129 |
| 3.25 Displacement frequency response for an infinite beam with no concentrated mass (variation with shear coefficient A) | 130 |
| 3.26 Displacement frequency response of infinite beam with concentrated mass (variation with shear coefficient A) | 131 |
| 3.27 Displacement frequency response of an infinite beam with concentrated mass ($\alpha=0.4$) (variation with the shear coefficient A) | 132 |
| 3.28 Displacement frequency response for an infinite beam on Pasternak foundation with damping | 133 |
| 3.29 Maximum displacement variation with concentrated mass ratio | 134 |
| 3.30 Displacement variation along the length of the beam | 135 |
| 3.31 Maximum displacement variation with shear coefficient A | 136 |
| 3.32 Displacement frequency response of a finite beam on Pasternak foundation (variation of concentrated mass) | 137 |
| 3.33 Displacement frequency response of a finite beam on Pasternak foundation ($A=1.4141$) variation of concentrated mass | 138 |
| 3.34 Variation of maximum displacement with shear coefficient | 139 |
| 3.35 Variation of maximum displacement along the length of the beam | 139 |

| Figure | | Page |
|---------|--|------|
| 3.36(a) | A line diagram of test arrangement | 140 |
| 3.36(b) | A block diagram for the test of a beam carrying a concentrated mass at its centre | 140 |
| 3.37 | Displacement frequency response of channel section for frequency dependent force | 141 |
| 3.38 | Maximum displacement variation along the length of channel for frequency dependent force | 142 |
| 3.39 | Comparision of test results with theoretical results for beam with concentrated mass on it and resting on elastic foundation | 143 |
| 4.1 | Variation of displacement with time of an infinite beam on Winkler foundation subjected to impulse load (Set No. 1) | 165 |
| 4.2 | Variation of displacement with time of an infinite beam on Winkler foundation subjected to impulse load (Set 2) | 165 |
| 4.3 | Comparison of time period of the response by numerical inversion with that of exact solution | 166 |
| 4.4 | Variation of maximum displacement at the centre of the beam with time (Set 1) | 166 |
| 4.5 | Variation of maximum displacement at the centre of the beam with time (Set 2) | 167 |
| 4.6 | Variation of maximum displacement with damping factor (Berger's technique) | 167 |
| 4.7 | Variation of maximum displacement along the length of beam (Set 1) | 168 |
| 4.8 | Variation of maximum displacement along the length of beam (Set 2) | 169 |
| 4.9 | Variation of maximum displacement along the length of beam (Post & Widder's technique) | 170 |

| Figure | Page |
|--|------|
| 4.10 Variation of maximum displacement at the centre of beam with damping factor (Post & Widder's technique) | 171 |
| 4.11 Variation of maximum displacement at the centre of the finite beam ($R=0.6$) (Berger's technique) | 172 |
| 4.12 Variation of maximum displacement of finite beam ($R = 0.6$) along the length of the beam (Berger's technique). | 172 |

List of Tables

| <u>Tables</u> | Description | Page |
|---------------|--|-------|
| 1.1 | Criteria for Flexibility of beams | 19 |
| 1.2 | Values of C_s for flexible and rigid beams for various L/B ratios | 19 |
| 2.1 | Properties of stabilized soil medium | 42 |
| 2.2 | Properties of natural soil deposit | 43 |
| 2.3 | Summary of properties of soil media on which the experiments were conducted | 44 |
| 2.4 | Data regarding footings used in the Experiments | 45 |
| 2.5 | Data for soil contained in bin, and formulae used for evaluation | 46-47 |
| 2.6 | Data for stabilized soil | 48-49 |
| 2.7 | Data for natural soil deposit | 50-51 |
| 2.8 | Increase in spring constant ratio for L/B=16 | 52 |
| 2.9 | Details of beam and spring used for Winkler model idealisation | 52 |
| 2.10 | Displacement values with frequency at force level 9.4 kg. | 53 |
| 4.1 | Soil and beam parameters used for numerical results by inversion technique | 164 |

SYNOPSIS

ASHOK KUMAR JAIN

Ph.D. Thesis

Department of Civil Engineering

I.I.T. Kanpur September - 1977

Thesis Title :- "Experimental and Analytical Investigations on a Class of Dynamic Problems in Beam-Foundation Interaction".

Thesis Supervisor Dr. N.S.V. Kameswara Rao

In the present work, experimental and analytical investigations have been carried out on some dynamic problems in beam-foundation interaction. Effect of size, shape of the footing, degree of flexibility of the footing and magnitude of force levels to which the footing is subjected, have been experimentally investigated. Various types of soil media, such as a loosely compacted, uniform, medium to fine dry sand; fine sand stabilized by adding some percentage of cement; and a natural silty soil have been selected for the studies. From the test results, it has been found that the maximum displacement varies proportionately with the force applied. The effect of the flexibility on the spring constant was found to be negligible as predicted from theoretical results. On the effect of the size, and shape of the footing, the spring constant ratio and damping factor showed variation with length/width ratio. The spring constant ratio have been found to be increasing with L/B ratio while the damping factor is decreasing.

with L/B ratio. An attempt has been made to analyse this observed behaviour.

Solutions for the response of beams carrying concentrated mass, resting on soil medium have been presented idealizing the soil medium as Winkler model and as Pasternak model. Damping has also been included in these models. The beam with concentrated mass attached to it and resting on elastic foundation has been analysed for steady state dynamic force. The displacement magnitudes have been calculated for infinite and finite beams with different values of concentrated mass attached to it. It has been found, from the analysis, that with concentrated mass increasing, the maximum displacement at the centre and at points along the length of the beam, decreases. The rate of decrease in maximum displacement have been found to be nonlinear with concentrated mass. The displacement magnitudes have also been evaluated at various points along the length of the beam, for beams of different length. From the theoretical results, it has been observed that along the length of beam, the maximum displacement decreases, with the rate being non-uniform along the length of beam. However, with the beam length, the maximum displacements have been found to be increasing, though marginally.

Beams resting on elastic foundations subjected to impulse loads have also been analysed. A general solution for displacement response at any point along the length of the beam has been derived through numerical inversion of Laplace transforms. Post and Widder's formula

has been used for numerical inversion of Laplace transform for infinite beam on elastic foundation. Berger's technique of Laplace inversion for infinite and finite beams has been used to get the numerical values of the response functions. From the results, it has been observed that with damping, the maximum displacement decreases. Also, along the length of the beam, the maximum displacement has been found to be decreasing.

CHAPTER 1

INTRODUCTION

1.1 GENERAL.

The dynamic analysis of foundations finds many applications in modern technology such as strip footings, railway tracks, aircraft runways, buried pipes, rocket testing tracks etc. Such problems of foundation-soil interaction are generally solved by incorporating the reaction from the foundation into the response mechanism of the structure by idealizing the foundation by a suitable mathematical model. In majority of the cases, the response of the structure at the contact surface is of prime interest. Thus it would be of immense help in the analysis, if the foundation can be represented by a simple mathematical model with the parameters of the model characterizing the true behaviour of the system as closely as possible. To accomplish this objective, many foundation models, from the Winkler foundation to the elastic continuum idealisation have been evolved. A comprehensive review of some of these foundation models is given in reference (29).

For any method of analysis, the critical step would be the correct evaluation of soil parameters which characterize the behaviour of soil media. These soil parameters will be different for different media. Furthermore these parameters will depend on loading conditions, strain distributions developed in the soil mass,

size and shape of the structure etc. Through various testing procedures, either by testing the soil samples in the laboratory or by performing the tests in-situ, these parameters are evaluated. In both types of testing, the values of these parameters depend on testing procedure, environmental conditions and the extent of medium. Then the question arises: Can these values be used as such for the analysis of various foundation soil interaction problems in all situations?

The dynamic loading effects on stationary structure have been the subject of great interest. A lot of work has been done on the behaviour of beams subjected to steady state forces and transient loads. But for beams, resting on soil media, the available literature is quite meagre. In technical applications it is not infrequent that a beam resting on soil media which is under vibration carries a lumped or concentrated mass somewhere along the length of the beam. A machine resting on a deep beam is an example. No solutions have been reported so far on such problems also.

The vibrations, due to aircraft landing on airstrips, due to rocket movement on rocket-sled-track, due to transient loads on buried pipes, due to dynamic loads on column-foundation system etc. are few examples which require the analysis of beam-foundation system, simulating the field conditions. The dynamic soil parameters, also, require to be critically examined whether they require any modifications in their values for changed situations of the vibrating systems. Some theoretical and experimental investigations are presented and analysed for some aspects of these problems.

1.2 BRIEF REVIEW OF LITERATURE

The earliest formulation of elastic foundations was due to Winkler who assumed that the foundation model consisted of closely spaced independent linear springs (29). The Winkler model approximates the reaction of the continuum by a simple expression which results in a single ordinary differential equation governing the responses of the beam. The solution is straight-forward for any loading configuration. A more difficult analysis by idealising the foundation as an elastic continuum or models derived from the continuum hypothesis is only possible in most cases through essentially approximate and numerical methods. Several other authors have evolved various partly continuous models conceptually developed from the Winkler model, such as Pasternak, Filonenko-Borodich, Wieghardt, Hetenyi, Kerr etc. (29). The objectives in employing a model are mathematical simplicity and relatively accurate representation of the real system. Often, the Visco-elastic model (Spring-Dashpot system) is used in dynamic analysis owing to mathematical simplicity, though the above mentioned models which are used for static loads, can also be used for dynamic analysis with appropriate inclusion of damping. In visco-elastic model, the soil medium is idealised in terms of physical constants—such as spring constant, damping coefficient and the equivalent mass of soil participating in the vibration. Attempts have been made to evaluate these parameters appropriate to represent the media as closely as possible. Fletcher and Hermann (17) developed foundation

parameters based on elastic constants, considering the foundation model in which the soil reaction is given by,

$$q(x) = k_1 w - k_2 \frac{\partial^2 w}{\partial x^2} - k_3 \frac{\partial^4 w}{\partial x^4} \quad (1.2.1)$$

where $q(x)$ is foundation reaction, w the deflection, and k the foundation modulus. In another discrete model (54), the foundation reaction has been expressed in terms of spring constant and damping constant as follows

$$q(x) = K_{st} (k_d + i a_o c_d) \quad (1.2.2)$$

where $q(x)$ = foundation reaction

K_{st} = static stiffness of the footing

k_d = dynamic spring factor

c_d = dynamic damping factor

a_o = nondimensional frequency, $\frac{\omega}{v_s} \cdot \frac{r_{eq}}{2}$

ω = circular frequency

r_{eq} = radius of the equivalent circular footing

v_s = shear wave velocity in the medium.

These spring and damping parameters k_d and c_d are the functions of coefficients that have been calculated and presented for various foundation shapes by Veletsos and Verbic (55) for footings resting on elastic halfspace, on the basis of Parmelee's (38) work. Luco and Westmann (31), Rainer (41) Sarrazin, Rosset and Whitman (47) presented the variation of the dynamic spring factor parameter with the frequency

of vibrations. Structure-foundation interaction studies were extended by Jennings and Bielak (24), Novak (35), Szuladzinski (52) etc. for various other aspects of loading conditions on the basis of this soil reaction. Analysis of the change in the dynamic spring factors and the damping factors were carried by Rosset, Whitman and Dobry (45) and Rainer (42). The damping is attributed to radiation of energy due to the propagation of the waves in the medium, and the energy dissipation through intergranular friction. Through experimental evidence, Kausel and Rosset (27) indicated that the energy dissipation takes place largely due to internal friction. It was also indicated that this energy dissipation is independent of frequency. About the spring constant, most of the methods presume that the spring constant is independent of amplitude of motion. This assumption is not strictly valid (59). However, so long as the motions are within certain limits, the behaviour of foundations may be taken as linear.

From the experimental and theoretical work, it is clear that the stress distribution for the static load at the interface of structure and soil may be quite different from the presumed distribution in the Winkler model. Yet from a bending moment diagram of an infinite beam acted upon by a concentrated load, derived by Biot (8), it is evident that for certain values of spring constant based on Winkler model, these bending moment diagrams are in reasonable agreement (56). After conducting some experiments, it was shown by Vesic (57) that Winkler hypothesis is practically satisfied, not only for long beams but also, for beams for moderate lengths. If the beams of infinite length on

an ideally elastic continuum are analysed by Winkler foundation, the bending moments are overestimated, contact pressure and deflections of the beam are underestimated (56).

Using Biot's theory of bending of beams, Vesic (56) derived the expressions for the coefficient of subgrade reaction \underline{K}_∞ , \underline{K} , for an infinite and finite beam respectively and developed a relationship between them in terms of elastic constants as given by

$$\underline{K} = 1.23 \left[\frac{E_s \cdot B^4}{C_p (1-\mu_s^2) E_b I} \right]^{0.11} \frac{E_s}{1-\mu_s^2} \quad (1.2.3a)$$

$$\underline{K}_\infty = 0.65 \sqrt[12]{\frac{E_s B^4}{E_b \cdot I}} \frac{E_s}{1-\mu_s^2} \quad (1.2.3b)$$

and

$$\underline{K}_\infty = 0.52 \sqrt[12]{\frac{\underline{K} B^4}{E_b I}} \underline{K} \quad (1.2.4)$$

where B = width of beam

E_b = modulus of elasticity of Beam

I = moment of inertia of Beam

E_s = modulus of elasticity of soil

μ_s = Poission's ratio of soil medium

C_p = coefficient of pressure distribution

Vesic and Johnson (58) substantiated later the reliability of the expressions by model studies of beams on silt. A variation of subgrade reaction with L/B ratios is given in Bowles (11).

From the theory of beams on an elastic foundation a foundation can be evaluated as rigid or flexible. Hetenyi (20) proposed the flexibility criteria depending on the value of λL (which considers the width, length and elastic properties of the medium), where

$$\lambda L = \sqrt{\frac{K_s L^4}{4E_b I}} \quad (1.2.5)$$

in which K_s is modulus of subgrade reaction.

Vesic (56) also proposed the criteria that was quite similar to the one proposed by Hetenyi. Depending on the flexibility of the beam, Vesic recommended the procedure for approximate analysis (Table 1.1).

If the foundation is absolutely flexible, ^{uniformly} loaded by a vertical pressure, then the stresses in the soil under the foundation will be distributed uniformly, but settlement under the foundation will vary. The average settlement is directly proportional to the pressure applied, with the coefficient of proportionality 1C_u , called the coefficient of elastic uniform compression, given by

$$C_u = \frac{p_s}{S_{av}} \quad (1.2.6)$$

Using Schleicher's solution (3) for an average settlement, a coefficient C_s which depends on L/B ratio, can be derived. Then 1C_u can be written as

$$C_u = \frac{C_s C_r}{\sqrt{A_b}} \quad (1.2.7)$$

where C_u is coefficient of elastic uniform compression,

p_s is uniform pressure under the foundation,

S_{av} is average settlement under the foundation,

A_b is base area of foundation

C_r is $\frac{E}{1-\nu^2}$ ν, E elastic constants

The expression for C_s is given by

$$C_s = \frac{\pi \sqrt{\alpha}}{\log_e \frac{\sqrt{1+\alpha^2} + \alpha}{\sqrt{1+\alpha^2} - \alpha} + \alpha \log_e \frac{\sqrt{1+\alpha^2} + 1}{\sqrt{1+\alpha^2} - 1} - \frac{2}{3} \left[\frac{(1+\alpha^2)^{3/2} - (1+\alpha^3)}{\alpha} \right]} \quad (1.2.8)$$

where $\alpha = L/B$

Thus the spring constant K for absolutely flexible foundation is given by

$$K = \frac{2G}{(1-\nu)} C_s \sqrt{BL} \quad (1.2.9)$$

where L is the length of the foundation.

For an absolutely rigid rectangular foundation Gorbunov-Posadov (3) computed the values of the spring constants and it was found that there is hardly a difference of 3% in the values. A comparative values of C_s for different L/B ratios for rigid and flexible foundation are presented in the table 1.2. A general review on the dynamic soil-structure interaction is provided by Kameswra Rao (26).

Theoretical investigations on beam vibrations find its origin in curvature-bending relationship derived by Bernoulli. Perhaps Euler and Bernoulli were the first to find the fundamental frequency of a cantilever bar and apparently, Ludwig was the first to deal with steady state dynamic solution of an infinite beam on an elastic foundation (32). In 1954 Kenny (28) included linear viscous damping in the basic equilibrium equation and solved for the corresponding steady state response. The steady state solution with a forcing function $F_0 \cos \omega t$ instead of F was obtained by Mathews (33). Nowacki (36) solved the basic equilibrium equation,

$$EI \frac{\partial^4 w}{\partial x^4} + Kw + m \frac{\partial^2 w}{\partial t^2} = F \delta(x) \cdot \delta(t) \quad (1.2.10)$$

For the transient loads, Stadler and Shreeves (50), Rades (40) presented the analytical solutions for infinite and finite beams respectively for the dynamic response of the Euler-Bernoulli beam including the effects of damping, axial load or shear layer etc. as given by the equation

$$EI \frac{\partial^4 w}{\partial x^4} + T \frac{\partial^2 w}{\partial x^2} + Kw + C \frac{\partial w}{\partial t} + m \frac{\partial^2 w}{\partial t^2} = q(x,t) \quad (1.2.11)$$

where T is axial load or shear coefficient

Based on Galerkin's method, Eringen (16) derived deflection equations for transverse, time dependent, force. Boley and Chao (9,10) analysed approximately the Timoshenko beam (Rotary inertia and shearing force of the beam is included in the basic equation), based

on a 'Travelling Wave' approach and the principle of virtual work. Miklowitz (34) in his analysis of Timoshenko beam, divided the total deflection into its bending and shear components and solved these equivalent set of coupled equations. Anderson (1) presented the general series solution for the flexural vibration of Timoshenko beam. For short beams, some discrepancy in the deflection from theoretical shear coefficient of a Timoshenko beam was reported by Krishnamurthy (30) after conducting some experimental investigations. Thus he presented a new formulation in which governing equations are two simultaneous partial-integro-differential equations.

For beams on elastic foundation, some analytical results are available where the foundation moduli are nonlinear (19, 18). Saito and Tomizo (46) studied the effect of mass of the soil in deriving frequency equations for an infinite beam resting on elastic foundation using the wave propagation theory. Berger (5) considered the effect of shear force, rotary inertia and viscoelastic damping on the response functions of the beam.

The problem of lateral vibration of a simply supported beam with concentrated mass attached at the centre was studied by Hoppman II (22), taking the Euler-Bernoulli beam. Chen (12) presented a new formulation in which the Dirac-delta function is used in differential equation. Frequency equations for the normal modes of vibration were obtained by Baker (2). Srinath and Das (49) presented the analysis for simply supported beam having rotary inertia.

Later Das and Deshmukh (15) derived a general expression for Timoshenko beam with concentrated mass at the centre. So far, no solution is reported for beams on elastic foundations with concentrated mass attached to it.

On the effect of impact on the beam resting on the elastic foundation, there is very little information available. Besides Nowacki (36), Hoppman (21) derived expressions for simply supported beams with or without damping, using energy method. Schwieger (48) collected some experimental data to check the central deflection of the beam. Prasad (39) also conducted some experiments and model analysis for theoretical prediction of response for impact load.

1.3 SCOPE OF THE PRESENT INVESTIGATION

In this thesis experimental investigations have been carried out to study the effect of size, shape of the foundation, degree of flexibility and magnitude of force levels to which it is subjected. Attempts have been made to analyse these observed results in the light of available theories on dynamic soil behaviour.

The present work also includes the study of beams resting on soil media subjected to steady state vibrations and impulse loads. The soil media is idealized as Winkler model as well as Pasternak model with damping included in both the models. A beam with concentrated mass attached to it, is analysed for steady state vibrations. A general solution for displacement at any point along the length of

the beam subjected to impulse load is derived through numerical inversion of Laplace transform for finite and infinite beams on elastic foundations.

The procedure and results of experiments to evaluate the soil parameters through cyclic plate load test, cross-hole-seismic test, block test are presented in Chapter 2. Experiments have been conducted to study the effect of size, shape of the structure, degree of flexibility of the structures and magnitude of force levels on these soil parameters. Chapter 2 also presents the experimental details and results of these studies. On the basis of existing theories on the behaviour of soil media an attempt is made to analyse these results. To verify the Winkler model hypothesis, a flexible beam resting on ideal springs is tested and the results are compared with the analytical solution for sinusoidal force.

In chapter 3, the beam carrying a concentrated mass and resting on soil medium is analysed for steady state vibration. Two mathematical models, namely the Winkler model and the Pasternak model with and without damping are taken for the analysis of Euler-Bernoulli beams. Expressions and results are presented for the general solution of finite and infinite beams with concentrated mass at the centre of the beam. These solutions which can be used for any boundary conditions are checked with the existing solutions for the beams carrying a concentrated mass with end supports (without foundation). Variation of magnitude of displacements along the length of the beam for various

values of concentrated mass, shear values of Pasternak foundation model, and with the change in the length of the beam is presented in this chapter. Comparisons have been made with some existing solutions. Experimental results for the response of a beam resting on soil medium with concentrated mass attached to it have also been discussed.

For finite and infinite beams, resting on elastic foundation, general solution for displacement at any point along the length of the beam for an impulse load have been derived through numerical inversion of the Laplace transform of the basic equations of motion. In Chapter 4, various inversion techniques of Laplace transform are enumerated and Post & Widders, and Berger's techniques are used in deriving the solution. Solutions have been compared with existing results.

The general conclusions and the scope for further work have been presented in Chapter 5.

1.4 NOTATIONS

Each symbol is defined when first introduced and some of the common symbols used in this thesis are listed below

| | | |
|--------------------------------|---|--|
| A | = | shear coefficient of Pasternak foundation |
| A_b | = | Base area of foundation |
| A_c | = | cross sectional area of the beam |
| A_{max} | = | maximum amplitude |
| a_o | = | non-dimensional frequency $\frac{\omega \cdot r}{v_s}$ |
| $A_1, A_2, A_3, A_4, A_5, A_6$ | = | arbitrary constants |
| B | = | width of the beam |
| b | = | $\sqrt{\frac{\rho A_c}{EI}} L^2 \omega^2$ |
| C_a | = | shear parameter |
| \bar{C}_a | = | Laplace transform of shear parameter |
| C_r | = | $\frac{E}{1-\nu^2}$ |
| C_s | = | a coefficient |
| C_u | = | coefficient of elastic uniform compression |
| C_1, C_2 | = | initial constants |
| c | = | damping constant |
| c_c | = | critical damping constant |
| c_d | = | dynamic damping factor |
| c_e | = | external damping |
| c_f | = | internal damping |
| c_p | = | coefficient of pressure distribution |

| | |
|------------------------|--|
| D | = damping factor |
| D_a | = shear parameter |
| \bar{D}_a | = Laplace transform of shear parameter |
| E | = modulus of Elasticity |
| E_b | = elastic modulus of beam |
| E_s | = modulus of elasticity of soil |
| e_o | = coefficient of restitution |
| F | = a concentrated sinusoidal forcing function |
| F_o | = force of constant magnitude |
| G, G_o | = shear modulus of soil |
| g | = arbitrary constant |
| I | = moment of inertia of beam |
| $J_{-1/4}, J_{1/4}$ | = Bessel's function |
| K | = spring constant of the soil medium |
| \underline{K} | = coefficient of subgrade reaction for finite beam |
| \underline{K}_∞ | = coefficient of subgrade reaction for infinite beam |
| K_s | = modulus of subgrade reaction |
| K_{st} | = static stiffness of footing |
| k_d | = Dynamic spring factor |
| k_1, k_2, k_3 | = foundation model parameter |
| L | = length of the foundation |
| $L(F)$ | = Laplace transform of the function F |
| M | = concentrated mass attached to the beam |
| $M(z)$ | = bending moment of beam at z |

m = unit mass of the beam

m_s = mass of falling body

$N_1, N_2, N_3, N_4, N_5, N_6$ = arbitrary constants

n = integer number

$P_n^{(p_1, p_2)}$ = Jacobi Polynomial

$F(z)$ = soil reaction on beam at z

(p) = transform variable

p_s = uniform pressure under the footing

p_1, p_2 = arbitrary constants

$q(x)$ = foundation reaction in vertical direction

$q(x, t)$ = foundation reaction in vertical direction at a distance x at time t

R = nondimensional beam length = L/λ

r = $\frac{\omega}{\omega_n}$

r_{eq} = radius of the equivalent circular footing

S_{av} = Average settlement under the footing

$S(z)$ = slope of the deflection curve at z

T = axial load

T_L = time of contact

$T(z)$ = shear force of beam at z

t = time parameter

v_s = shear wave velocity in the medium

v_o = velocity of freely falling mass just before collision

W = weight of falling body

w = deflection in vertical direction

w_f = foundation deflection beyond the length of the beam
 x = distance parameter
 y = non-dimensional vertical displacement
 $y_f = \frac{w_f}{\lambda}$ = non-dimensional displacement of foundation beyond beam
 $\bar{y}(p)$ = laplace transform for $y(z)$
 $y(z)$ = non-dimensional vertical displacement at $z = w/\lambda$
 $y(z, \theta)$ = non-dimensional vertical displacement at a distance z and at time θ .
 z = non-dimensional distance x/λ
 α = concentrated mass ratio = $\frac{M}{2\rho A_c L}$, and L/B in equation (1.2.8)
 $\beta = \sqrt{2} \mu$
 $\bar{\beta} = \frac{1}{\sqrt{b}}$
 $\beta_1 = 4(1+2Dp + p^2)$
 $\gamma = \left(\frac{KL^2}{G}\right)^{1/2}$
 σ = arbitrary constant
 ρA_c = mass density of soil media
 $\mu = 4\sqrt{(1-r^2)^2 + (2Dr)^2}$
 $\bar{\mu} = (-2m^2 + 2(m^4 + n^4)^{1/2})^{1/2}$
 ν, μ_s = Poission's ratio of soil medium
 ω = circular frequency
 ω_n = natural circular frequency
 θ = non-dimensional time variable
 ϕ = phase angle

$\phi_1, \phi_2, \phi_3, \phi_4$ = Cauchy's function

λ = Characteristic length = $4\sqrt{\frac{4EI}{K}}$

$\bar{\lambda}$ = $(2m^2 + 2(m^4 + n^4)^{1/2})^{1/2}$

$\delta(x)$ = Kronecker delta of x

$\delta(t)$ = Kronecker delta of t

η = characteristic shear value of soil medium

ψ = a function

ξ = Notation .

Displacement Ratio = $\frac{\text{Dynamic Displacement}}{\text{Static Displacement.}}$

Table 1.1
Criteria for Flexibility of Beams

| S.No. | Size of Beam | Criteria for Distinction | Procedure Recommended |
|-------|---------------------|-------------------------------|---|
| 1 | long beam | $\bar{\lambda}L > 5.0$ | Winkler analysis assuming infinite beam |
| 2 | Moderately long | $2.25 < \bar{\lambda}L < 5.0$ | Winkler analysis |
| 3 | Short moderate beam | $0.8 < \bar{\lambda}L < 2.25$ | De Beer Method |
| 4 | Short beam | $\bar{\lambda}L < 0.8$ | Treat as perfectly rigid |

(Based on Vesic 56)

Table 1.2
Values of C_s for flexible and rigid beams for various L/B ratios

| L/B | 1 | 1.5 | 2 | 3 | 5 | 10 | 16 |
|-------------------------|------|------|------|------|------|------|-------|
| C_s for flexible beam | 1.06 | 1.07 | 1.09 | 1.13 | 1.22 | 1.41 | 1.507 |
| C_s for rigid beam | 1.08 | - | 1.10 | 1.15 | 1.24 | 1.41 | - |

Barkan (3)

CHAPTER 2

EXPERIMENTAL INVESTIGATIONS

2.1 GENERAL

For the experimental investigations on dynamic soil-structure interaction, a variety of soil media; a loosely compacted, well graded, medium to fine sand; a fine sand-stabilized by adding some percentage of cement; and a natural soil deposit are taken. These investigations are carried out to study the effect of shape, size of footing on the foundation parameters of soil, represented by a Visco-elastic model (spring and dashpot in series, that is Winkler's model with viscous damper). Studies also include, the effect of magnitude of force level to which the footing-soil system is subjected and the effect of flexibility of footing. Experimental results of a beam resting on ideal springs are compared with analytical solution of a beam resting on a Winkler foundation. In this chapter, the procedures and results are presented for these investigations besides the soil properties and its evaluation procedures.

2.2.1. Soil Properties-Evaluation Procedures.

The procedure for basic physical soil properties are quite standard and are available in most of the text books on soil mechanics. For dynamic studies, soil parameters in terms of shear modulus, Poisson's ratio, elastic modulus or alternatively, spring constant and damping factor of the soil medium need to be evaluated.

IS 5249-1969 (23) provides a standard procedure for obtaining these parameters. By conducting cyclic plate load test, the soil parameters for dynamic studies can also be ascertained in terms of coefficient of subgrade reaction and coefficient of elastic uniform compression (3) while from the block test (23), the soil parameters are evaluated in terms of elastic constants. Another procedure, Cross-hole test, was presented by Stokoe II and Woods (51) which facilitates the evaluation of the dynamic soil parameters in terms of elastic constants. This procedure seems to be better, compared to block test, as the time taken in setting up the experiment and conducting the test is far less, and the ability of this method to probe deeper depths. In evaluating the parameters, however, all the three methods were adopted. While the block test procedure is quite established (23), the cross-hole test and cyclic plate load test are described very briefly.

2.2.1.1. Cross-hole Method. (Stokoe II & Wood)

The procedure followed is to advance two vertical boreholes some distance apart into the ground to the same depth. A transducer is placed at the bottom of one of the boreholes. The transducer is a vertical velocity pickup attached to a pipe that allows the transducer to be placed at the bottom of the borehole and can be removed. An impulse rod is placed down the other borehole. A small top plate with a vertical velocity transducer attached at the bottom of the first borehole is connected to the input of an

oscilloscope while transducer attached to the impulse rod is connected to the trigger of the oscilloscope.

The test is conducted by striking the plate on the top of impulse rod with a hammer which triggers the oscilloscope and also sends a compression wave down the rod. The compression wave from the rod starts the wave propagation into the soil at the bottom of the rod. Body waves are generated in the soil and their arrivals at the velocity transducer in the opposite borehole are displayed on the oscilloscope. This procedure of striking the impulse rod and recording of the wave arrival is done several times with the equipment in the initial position to determine an average time. The impulse rod and velocity transducer are removed and placed down the opposite borehole and the test repeated. Then the seismic equipment removed from the borehole and boreholes are advanced to the next depth and the procedure is repeated. The primary wave velocity and shear wave velocity are determined by dividing the distance between the boreholes by total travel time taken by primary wave and shear wave respectively. Using the density values, the shear modulus, elastic modulus and Poisson's ratio are evaluated. Expressions (44) for these moduli can be written as

$$\begin{aligned} \text{shear modulus } G &= \frac{v_s^2}{\rho} \\ \text{Elastic modulus } E &= \frac{v_c^2}{\rho} \\ \text{Poisson's ratio} &= \frac{E_s}{2G} - 1 \end{aligned}$$

where v_c is primary wave velocity in the medium

v_s = shear wave velocity in the medium

ρ = mass density of the medium.

2.2.1.2 Cyclic Plate Load Test (Barkan 1962).

In this method, a square or circular rigid plate is loaded and unloaded in increments, with the record of settlement and recovery in settlement, in the soil beneath the plate. The plate is reloaded to a higher increment and then unloaded. Each higher loading increment makes the plate settle more and unloading allows the plate to reduce this increased settlement. The part of the settlement which does not recover after unloading is called permanent settlement and the remaining part of the settlement which is recoverable on unloading, is called elastic settlement. This elastic settlement increases with increase in vertical stress. The ratio of the vertical stress to this settlement is called the coefficient of elastic uniform compression. In the present work, a circular plate of area 1640 cm^2 was used for the test. Fig. 2.1 shows the load and total settlement (elastic + plastic) relation. This relation is quite linear. Results of cyclic plate load test are shown in Fig. 2.2. Out of the elastic and plastic settlement, the elastic settlement is separated out and plotted with vertical stress in Fig. 2.3. It can be observed from the graph, that the elastic settlement is proportional to pressure applied.

2.2.2 Soil Properties-Results.

For the investigations, a variety of soil media were taken. In the laboratory, a well graded dry sand, with a uniformity coefficient of 2.1, was filled in a large container. This sand with density of 1.62 gm/cm^3 and void ratio of 0.65 was poured and compacted in layers of 10 cm throughout the area by a rammer imparting the equal energy everywhere. In the field, two types of soil media were selected. While one soil medium was a natural soil deposit of silty sand (Density 1.62 gm/cm^3), having liquid limit and plasticity index equal to 27.5 and 10 respectively, the other was micaceous fine sand filled in a trench of size $20\text{m} \times 5\text{m} \times 2\text{m}$. This sand was stabilized by adding 5% cement and compacting it at the optimum moisture content. The density of the soil was 1.55 gm/cm^3 .

While the soil in the container and in the trench was more homogeneous, isotropic and uniform, the natural soil deposit has a range of particle sizes. These three different soil media were selected to represent various soil conditions. The loose dry sand may absorb the wave energy more thus increasing the damping coefficient, the stabilized soil may increase the stiffness of the soil thus increasing the spring constant. While both these soils are extending to a limited length, the natural soil deposit extends upto infinite extent.

Evaluated soil properties are presented in Tables 2.1, 2.2, 2.3. Where Tables 2.1 and 2.2 show the primary, shear wave velocity,

elastic constants, soil density etc. for stabilized and natural soil deposits respectively, Table 2.3 presents the summary of these elastic constants and soil parameters for all the soil media.

2.3 DYNAMIC SOIL-STRUCTURE INTERACTION STUDIES

The effect of size, shape of the footing, magnitude of force applied and the flexibility of the footing on soil-structure interaction are dealt in this section. Experiments were conducted on (i) a circular plate of 22.9 cm diameter and thickness of 1.25 cm, (ii) a square plate of size 20.4 cm × 20.4 cm × 1.25 cm, (iii) a rectangular plate of size 40.8 cm × 10.16 cm × 1.25 cm, and (iv) a long strip of dimension 81.3 cm × 5.08 cm × 1.25 cm, resting on three different soil media. The base area of all the plates and beam have been chosen to be same and equal to 413.0 cm^2 , with the weight approximately 4.0 kg. The frequency independent sinusoidal force was applied on the centres of these footings by an electromagnetic exciter. The magnitude of the force level was varied on these footings. Following sub-sections describe, the experimental set up, instrumentation, sequence of operations, results and discussion of the results.

2.3.1 Experimental Set-up.

The various instruments used for excitation, measurement and control of dynamic characteristics of the experimental system are briefly presented. Care was taken at each step to check the calibration and rating of the primary equipments during their operation.

Each reading was repeated several times in the course of single measurement or over a period of time to ensure the consistency of the results.

2.3.1.1 Test Frame for Dynamic Tests for Soil in the Laboratory.

A schematic diagram of the frame is shown in Fig. 2.4. It consists of a large bin filled with loosely compacted, well graded sand. The plates and beam were tested one after another, after keeping them on the surface of sand so that uniform contact between soil and the footing is maintained. Before, during and after the testing, the footings were checked for uniform contact of these with soil, and horizontal level of these plates. The exciter's moving table was fixed at the centre of the footings. To keep the exciter in inverted position so that its moving table just rests on the footings without adding any weight of its own on the footing, a frame made up of steel angles was fabricated. The position of the exciter could be vertically adjusted by means of a central screw arrangement in the steel frame. The frame is big enough to accommodate the sand container. The exciter was fixed tightly to the frame so that at the time of resonance, there should not be any movement of the exciter. The moving table of the exciter was along the axis of the footing.

2.3.1.2 Test Frame for Dynamic Tests of Soils in the Field.

Fig. 2.5 presents a schematic diagram of the frame, for testing in the field. This frame made up of steel angles, was fabricated

with modifications suitable to field conditions. Instead of a central screw arrangement, the exciter in a steel cabinet was kept in inverted position by steel ropes. The weight of the exciter and the cabinet was balanced by three sets of equal weights, hanging on the same rope on the other end as shown in the schematic diagram (Fig. 2.5). The rope passes through a set of frictionless pulleys specially fabricated for the purpose. During preliminary investigations, when the exciter was kept by a central screw arrangement, it was found at certain frequency, this frame was vibrating at its resonant frequency. Thus, by adopting this method for keeping the exciter in inverted position and lowering it to the footing so that it just rests on the footing, the problem of frame resonance was avoided. Besides the fact that the exciter does not add its own weight to the footing, another advantage derived from this method, was that during the vibration, footing did not loose its contact with soil medium at any time.

2.3.2 Instrumentation

2.3.2.1 Oscillator

An oscillator (Model 200AB Audio Oscillator) capable of generating sinusoidal pulse of constant voltage in the frequency range of 20-10000 cps was used for excitation. Maximum output power of the signal was 1 watt with an overall accuracy of 2%. The desired frequency and output voltage were controlled by the frequency dial and amplitude knob respectively. The output signal was amplified

2.3.2.2 Amplifier.

A power amplifier (Model 2120 MB Power Amplifier) used to amplify the output signal from the oscillator. The frequency of sinusoidal pulse remained unaltered and only the output voltage was amplified. The signal distortion through the amplifier was less than 2% within the frequency range of 20-1000 cps. The maximum output power of the amplifier was 125 VA and input signal voltage was 1 V. rms.

2.3.2.3 Exciter.

The exciter used was an electromagnetic device (Model EA 1250 MB) which could produce the maximum force levels of 12 kg and maximum displacement of 1.25 cm at different pay loads and accelerations. The exciter had a frequency range of 5-10,000 cps with total weight of moving table 0.323 kg. Its signal distortion was less than 5%. The frequency of the exciter was controlled through the oscillator. The maximum power input to the exciter was limited to 15 volts, 7 amps, 76 watts and controlled through an amplifier.

2.3.2.4 Vibration Transducer. (GR-1566 P-52).

In the accelerometer type of pickup which was used in the experiments, the transducer is made of a piezo-electric crystal. A piezo-electric crystal develops an electrical charge directly proportional to the pressure applied to it. This pressure is due to the acceleration of the base on which the transducer is fixed. This pickup was used to measure amplitudes of displacement, velocity

and acceleration of the base. This was held in position with the magnetic clamp or fixed otherwise.

2.3.2.5 Vibration Meter (GR-1553 AK)

This instrument consisted of a sensitive vacuum tube voltmeter. The vacuum tube voltmeter included a high gain band amplifier, a calibrated attenuator, average reading, peak reading, and peak to peak reading voltmeters, integrating circuits to convert acceleration signals to velocity or displacement signals. Its operation range was to 2 - 20,000 cps. An outlet was provided to connect it with the oscilloscope.

2.3.2.6 Oscilloscope.

For the visual display of waveform, a cathode ray oscilloscope with storage facility was used for visual check of forcing function or alternatively to facilitate to photograph the waveform trace. It consisted of a cathode ray tube in which a beam of electrons illuminates a spot on the screen. This spot can be accurately positioned both horizontally and vertically by application of voltage across the pair of deflection plates between which the beam passes. One set is used to control the vertical position and the other, horizontal position of the beam. For most applications, a calibrated saw-tooth voltage is applied to the horizontal deflection plates so that beam moves from left to right at a known velocity and rapidly returns to the left side of the tube to repeat its sweep from left to right. This provides a time scale on the screen of cathode ray tube. The signal to be measured is amplified and applied to the vertical deflection plates.

2.3.3 Sequence of Operation.

Before starting the test, the soil, contained in the bin, and in the field, on which these plates or beam rests, was made even and level. It was ensured that footing is in contact with soil medium at every point and was level. The axis of the moving table and the axis of centre of gravity of footings were checked to coincide and remain vertical. The level of the footing and the axis of vibration were checked intermittently.

After resting the footing (circular, square, rectangular plate or beam having the same base area of 413 cm^2) on the soil media, the exciter was fixed on the footing. The exciter was connected to an oscillator through an amplifier. An electric sinusoidal force signal was fed from the oscillator to the power amplifier from where, after getting the signal amplified, it was fed into the exciter. The exciter, in turn, converted this electric signal into mechanical oscillation which was transmitted to the footing soil system. As mentioned earlier, the frequency and the amplitude of force level was controlled through the oscillator. The nature of sinusoidal force produced by exciter was visually verified through an accelerometer attached to exciter, which fed the signal to oscilloscope through a vibrationmeter.

The response of the footing soil system was measured through a system of vibration pickup and vibrationmeter. The displacements, velocities and accelerations were measured at various points on the

footing through an accelerometer type of pickup which was attached to the footing. This transducer picked up the vibration and fed into the vibrationmeter. The nature of oscillations of the footing soil system was monitored on oscilloscope by taking out the signal from vibrationmeter and feeding it into oscilloscope. Fig. 2.6(a) shows a block diagram of the test set up. Starting from very low frequency, the responses were noted in terms of frequency, displacement, velocity and acceleration of the footing soil system over a large frequency range. The force level was constant throughout the frequency range and was increased for the next set of readings. For each type of footing (circular, square, rectangular shapes or beam) three to five force levels were applied for the response curves. The frequency ranged from 300 to 600 cps.

2.3.4 Presentation of Results.

The experimental results, of the tests conducted on circular plate, square plate, rectangular plate and long strip (beam) resting on three different soil media, are presented in this section. The base areas, the thickness and the weights of these footings were the same. Table 2.4 provides relevant information of these footings.

2.3.4.1 Tests for Soil in the Laboratory.

In the first set of experiments, these four footings (circular plate of dia 22.9 cm, square plate of 20.4 cm × 20.4 cm, rectangular plate of 40.6 cm × 10.2 cm and a long strip of 81.2 cm × 5.08 cm) of base area of 413 cm², resting on the soil contained in bin were tested

in the laboratory. These were subjected to sinusoidal force at their centres. The magnitude of force level ranged from 3.0 kg to 9.0 kg. The response curves were obtained for deflection, velocity and acceleration at each frequency. The velocity, acceleration values were utilized for the verification of displacement values.

Fig. 2.7 shows the response curves of a circular plate for four different force levels. The plot is between frequency (cps) versus magnitude of displacement (in m.m.). It can be observed that resonance occurs at 385 cps in the frequency range of 300-600 cps. With increase in force level, the resonant frequency does not change. Only maximum deflection is increasing with increase in force level.

The frequency displacement curve for square plate is shown in Fig. 2.8. The response curves for four different force levels were obtained as for circular plate.

For this plate also, frequency ranges from 300 to 600 cps with the resonance at the frequency of 385 cps. With increase in force level, maximum displacement was increasing while resonance frequency was not much different.

For rectangular plate, the resonance shifted to a higher frequency 410 cps. Fig. 2.9 shows the response curve for four different force levels. Magnitude of displacement increase with the increase in force level. For the rectangular plate, the displacements were measured at more points than for circular plate or square plate and an average value was plotted with the frequency.

In Fig. 2.10, frequency-displacement response is plotted for the long strip. During testing, it was observed that the displacement along the length of the beam was varying at any particular frequency. This figure shows the deflection of the beam at its centre. It can be seen that like other footings, the resonant frequency was not varying much with the magnitude of force level and remain at 510 cps. Only maximum deflection is increasing with force level.

From these figures (Fig. 2.7, 2.8, 2.9, 2.10), it can be observed that resonant frequency is increasing from square plate to beam. As the base area, thickness, and the mass of the footings are same, the increase in frequency and maximum displacement, could be attributed to the shape of the footing. Maximum displacement and frequency are plotted against L/B (the length of the plate or beam/width of the plate or beam), in Figs. 2.19 and Fig. 2.20 for all the soil media. Another observation can be made from Figs. 2.7, 2.8, 2.9, 2.10, that there is some proportionality in the increase of maximum displacement with increase in force levels. Both the maximum displacement and resonant frequency are increasing with the L/B ratio as shown in (Figs. 2.19, 2.20).

From these curves, the spring constant and the damping factor are calculated assuming the plates and the beam as rigid. Table 2.5 presents these values for various force levels applied on them with the formulae used in the calculations to evaluate these values.

2.3.4.2 Test Results for Stabilized Soil Medium.

The response curves for circular plate, square plate, rectangular plate and long beam resting on stabilized soil are presented in Figures 2.11 to 2.14 respectively. For this soil medium also, four to five force levels, varying from 3.0 kg to 7.0 kg were selected for all the footings. The frequency ranges from 300 cps to 600 cps. Like in previous case, the displacements for rectangular plate were measured at more points and average was plotted (Fig. 2.13) while for long beam, the displacements at the centre of gravity were measured several times and plotted in Fig. 2.14.

There was hardly any variation in resonant frequency with magnitude of force level. With L/B ratio, the maximum displacement and resonant frequency were increasing (Fig. 2.19, 2.20), as was found for the soil in the container. Same way, there was some proportionality noticed in the increase of maximum displacement with the force level.

Treating the plates and beam as rigid, the spring constant and damping factor are calculated and tabulated in Table 2.6.

2.3.4.3 Test Results for Natural Soil Deposit.

In the last set of results, the circular plate, square plate, rectangular plate and the long beam, resting on the natural soil deposit, were subjected to steady state oscillation of constant force as was the case for the previous two types of soil media. Figs. 2.15 to 2.18 show the frequency displacement curves for three

to four force levels. As usual, the frequency ranges from 300 cps to 600 cps. Maximum displacement increases with force levels as can be seen from the Figures (2.15, 2.16, 2.17, 2.18). Maximum displacement also increases with L/B ratio. The resonant frequency does not vary much with force levels. It varies with L/B ratio only (Fig. 2.19, 2.20). Table 2.7 presents the spring constant and damping factor values for these footings. These values are calculated treating the plates and the beam as rigid.

Taking the averages of the values of spring constant and damping factor, calculated from the response curves for circular, square, rectangular plates and the long beam on the three different soil media, the variation of spring constant and damping factor with L/B ratio is plotted. Fig. 2.22 shows the spring constant ratio variation (spring constant for any L/B ratio/spring constant of circular plate of the same base area) with L/B ratio. The spring constant ratio is increasing with increase in L/B ratio. Fig. 2.23 presents the variation of damping factor with increase in L/B ratio. The damping factor decreases with the increase in L/B ratio. The rate of increment of spring constant ratio, and rate of decrement of damping factor is not the same for three different soil media, but there is a definite trend with increase in L/B ratio.

2.3.5 Discussion.

Based on these observations, the effect of magnitude of force levels, the effect of size and shape of the footing, and the flexibility of the footing on dynamic foundation parameters are discussed in this section.

2.3.5.1 Magnitude of Force.

From the response curves (Figs. 2.7 to 2.21 and Table 2.5 to 2.7 it can be seen that there is some proportionality in the increase of maximum displacement with the increase in force levels. Generally, the increase in displacement is linear with force levels, as in the theoretical analysis the maximum displacement is directly proportional to the force level. Thus, it may be taken that the maximum displacement is directly proportional to the force level.

2.3.5.2 Effect of Size and Shape.

2.3.5.2.1 Spring Constant.

In the theoretical visco-elastic model, the footing, resting on it, experiences same stiffness at all points below the footing when the footing-soil system undergoes vibration. In practice, however, it is not always true. Stresses below the plate vary from point to point depending on the nature of soil medium and flexibility or rigidity of the footing. A rigid or flexible plate on soil does not have uniform stress distribution. It may vary from outer edge to inner area. Also with the change in the base area, if the load distribution remains the same, the stress below the footing at a point does not remain constant (3). Thus the coefficient of elastic uniform compression depend on the area and the shape of the footing. In another words, the spring constant will depend on the shape of the footing, if the base area remains the same.

Below a circular or square plate, the stress distribution and thus the stiffness at the edges will be different from that in the inner portion. Thus the net sum of the stiffness will be less than the values if the stiffness had been uniform throughout the area below the plate. Having the same base area, if the length increases and width decreases, the stress distribution becomes more and more uniform. This uniformity in stiffness brings the net sum to a little higher value. Thus, as the length increases and width decreases, the value of spring constant appears to be increasing.

For rigid rectangular plate, Gorbunov-Posadov calculated the values of a coefficient which can be equated to spring constant ratio for various values of L/B ratio. Barkan (3) has presented those values in tabular form. According to them, if the base area of a footing remains constant, the coefficient of elastic uniform compression increases with an increase in L/B ratio. The variation of spring constant ratio based on this theory is shown by dotted line in figure 2.22.

2.3.5.2.2 Damping Factor.

From the figure 2.23, it can be observed that damping factor is decreasing with the increase in L/B ratio. This damping which the soil medium possesses, arises because the energy is dissipated through intergranular friction and due to wave propagation in the medium (42). The energy dissipation through intergranular friction is called material damping and reveals in a hysteretic load deformation curve

for the soil. The energy loss due to propagation of waves is called geometric damping or radiation damping. This damping is a function of frequency of the system (59) while the material damping or internal damping is frequency independent to a large extent (27).

The decrease in damping may be attributed to the increase in stiffness and probably the reduction in material damping. As the damping factor is a function of damping constant, spring constant and mass of the soil participating in vibration, the increase in spring constant may result in a decrease in the damping factor. As analysed, it is taken that with increasing L/B ratio, the stiffness of the soil will increase, thus, resulting in the higher spring constant value.

2.3.5.3 Effect of Flexibility.

Based on elastic theory, Barkan (3) has presented the relationship between spring constant ratio and L/B ratio (Equation 1.2.8) for flexible rectangular plate and compared these values with the values for rigid plates. The difference between these values is not larger than 3 percent. From the experiments the value of spring constant ratio is calculated for the long beam with reference to square plate, treating the beam and square plate as rigid in one case, and as absolutely flexible in the other case. Table 2.8 presents the comparison of the these two cases. For this L/B ratio, the theoretical values of spring constant ratio for flexible and rigid cases are also presented in this table. From the experimental results, the spring constant ratio does not seem to be different for flexible case in comparison to rigid case. Within experimental errors, these values may be taken as equal to the theoretical values.

2.4 EXPERIMENTATION FOR WINKLER MODEL VERIFICATION

To study the response of beam on elastic foundation, often the foundation is idealised as Winkler model. An experiment has been designed to verify the theoretical values based on Winkler model. A schematic diagram is shown in Figure 2.6.

2.4.1 Experimental Setup

Beam of mild steel and of uniform cross-section was put on ten almost identical linear springs at a spacing of 10.16 cm. The details of the characteristics of the beam and springs used for the experimental study are given in table 2.9. These springs were welded to a fairly heavy channel making the base rigid. The ends of the beam were kept free. Thus a uniform free-free Euler-Bernoulli beam resting on Winkler model of foundation was simulated in the experimental set up.

In studying experimentally, the response of the beam subjected to steady state sinusoidal force, various parameters such as displacement, acceleration, velocity of the beam were measured. Instrumentation arrangements were the same as for the studies on dynamic footing-soil interaction. Block diagram is shown in Fig. 2.6(a). Instrumentation details are given in the section 2.3.2.

All the ten springs which were used in the model were tested on a uni-axial compression testing machine. It was found that the load deflection relationship was fairly linear during loading, unloading

and reloading. Table 2.9 presents the value of spring constant, characteristic length etc.

2.4.2 Results and Discussion.

For three different set of force levels, the beam was subjected to steady state sinusoidal force which varies from 5.15 kg to 12.0 kg. Frequency ranges from 30 cps to 120 cps. The displacement, acceleration and velocity were measured at centre of the beam and along the length of the beam at the interval of 10.2 cm. A typical set of measured displacements along these points are presented in Table 2.10. With the increase in frequency, the maximum displacement was increasing, and it reached its first peak at the frequency of 55 cps, indicating that beam is under first mode of vibration. In this mode, maximum displacement occurs at the centre and the point of zero deflection, at $1/4$ th distance from the one end of the beam. Besides the centre of the beam, displacements were higher at the free ends.

Frequency displacement responses at the centre of the beam, for the force levels 5.15 kg, 9.4 kg and 12.0 kg are shown in figure 2.24. Peak of the displacement at first mode of vibration occurs at 55 cps. The variations of displacement along the length of the beam for few values of the frequencies of vibration are presented in Figures 2.25, 2.26, 2.27 for force levels of 5.15 kg, 9.4 kg, and 12 kg respectively. From these figures, it can be observed that the amplitude of deflection is decreasing at every point on the beam as the frequency goes on increasing. Also, the point of zero deflection shifts towards the free-free end.

Based on the theoretical solution of a beam resting on the Winkler foundation, the values of the amplitude of displacement are calculated. The expression is given by

$$y(z) = -\frac{F_0 \lambda^2}{2EI} \frac{1}{\mu^3} \left[\frac{(1+\cos \mu R \cosh \mu R) (\cos \mu z + \cosh \mu z)}{(\sin \mu R \cosh \mu R + \cos \mu R \sinh \mu R)} + \frac{(1+\sin \mu R \sinh \mu z) (\cos \mu z - \cosh \mu z)}{(\sin \mu R \cosh \mu R + \cos \mu R \sinh \mu R)} \right] \quad (2.4.1)$$

For the first mode of vibration of beam, the amplitudes of displacement along the length of the beam, for all the three force levels were calculated and are plotted by dotted lines in Figures 2.25, 2.26 and 2.27.

The experimental curve is in good agreement with the values, calculated from theoretical analysis of Beam on Winkler foundation. This probably reinforces the confidence in modelling the foundation medium as per Winkler's hypothesis.

Table 2.1
Properties of Stabilized Soil Medium

| Bore log | Depth in m. | Time taken by P wave in millisecc. | Time taken by S wave in millisecc. | P Wave velocity m/sec. | S Wave velocity m/sec. | Poisson's Ratio | Density gm/cc. | E kg/cm ² | Shear Modulus kg/cm ² |
|--|-------------|------------------------------------|------------------------------------|--|------------------------|--|----------------|----------------------|----------------------------------|
| | 0.0m | | | | | | | | |
| Stabilized soil sand | 0 | 39 | 64 | 256 | 156 | .30 | 1.60 | 1030 | 397 |
| | 1.83m | 0.60 39 | 63 | 256 | 159 | .30 | 1.55 | 1040 | 400 |
| Silt clay | | | | | | | | | |
| | 2.13m | | | | | | | | |
| Silt clay with Kankar | 1.22 | 38 | 63 | 263 | 159 | .35 | 1.55 | 1090 | 400 |
| | 1.83 | 38 | 62 | 263 | 161 | .33 | 1.55 | 1090 | 410 |
| Distance between Trigger hole and Receiver hole=10m. | | | | Average G=402 kg/cm ² Poisson's Ratio=0.32 | | Average E=1060 kg/cm ² Density=1.56 gm/c. c. | | | |

Table 2.2
Properties of Natural Soil Deposit

| Bore log | Depth in m | Time taken by P wave in milli sec | Time taken by S wave in milli sec | P wave velocity m/sec | S wave velocity m/sec | Poisson's Ratio | Density gm/cm ³ | E Elastic modulus kg/cm ² | G Shear modulus kg/cm ² |
|------------------------|------------|-----------------------------------|-----------------------------------|-----------------------|-----------------------|-----------------|----------------------------|--------------------------------------|------------------------------------|
| | 0.00' | | | | | | | | |
| Silt with clay | 0 | 33.0 | 51 | 280 | 180 | 0.250 | 1.60 | 1275 | 509 |
| | 0.62 | 31.5 | 50 | 291 | 183 | 0.266 | 1.65 | 1425 | 562 |
| | 2.13m | | | | | | | | |
| Silty clay with Kankar | 1.20 | 30.0 | 50 | 305 | 183 | 0.380 | 1.60 | 1520 | 548 |
| | 1.83 | 28.0 | 48 | 327 | 191 | . | 1.65 | 1790 | 615 |
| | 3.36m | | | | | | | | |
| Sandy silt with Bajari | 2.44 | 29.0 | 49 | 315 | 186 | 0.370 | 1.65 | 1620 | 585 |

Average $G=550 \text{ Kg/cm}^2$ Poisson's Ratio=0.31

Distance between trigger hole and Receiver hole=9.15m.

Average $E=1460 \text{ Kg/cm}^2$ Density = 1.62 gm/cm^3

Table 2.3

Summary of Properties of Soil Media on which the Experiments
were conducted

| Type of Soil Medium | Medium and Fine Uniform Sand in the bin | Stabilized Sand | Natural Soil Deposit |
|---|---|--|-------------------------|
| Soil identification | Badarpur Fine uniform sand | Micaceous sand stabilized with 5% cement | Silty clay |
| Void Ratio | 0.60 | 0.65 | 0.50 |
| Liquid Limit | - | - | 27.5 |
| Elasticity index | - | - | 10.0 |
| Total unit weight gm/cc. | 1.62 | 1.56 | 1.62 |
| Total mass density $\frac{\text{kg sec}^2}{\text{cm}^4}$ | 1.65×10^{-6} | 1.59×10^{-6} | 1.65×10^{-6} |
| Elastic modulus kg/cm^2 | - | 1060 | 1460 |
| Shear modulus kg/cm^2 | 395 | 402 | 550 |
| Poisson's Ratio | 0.30 | 0.32 | 0.31 |

Table 2.4

Data regarding footings used in the Experiments

| Serial No. | Properties | Circular Plate | Square Plate | Rectangular Plate | Long Strip |
|------------|----------------------------|---|--|---|--------------------------------------|
| 1 | Dimensions | 22.9 cm dia (9") | 20.4 x 20.4 cm ² (8" x 8") | 40.6 cm x 10.2 cm (16" x 4") | 81.2 cm x 5.08 cm (32" x 2") |
| 2 | Thickness | 1.27 cm. (0.5") | 1.27 cm. (0.5") | 1.27 cm. (0.5") | 1.27 cm. (0.5") |
| 3 | Weight | 4.048 kg | 4.055 kg | 4.032 kg | 3.93 kg |
| 4 | E Modulus of Elasticity | 2.1×10^6 kg/cm ² | 2.1×10^6 kg/cm ² | 2.1×10^6 kg/cm ² | 2.1×10^6 kg/cm ² |
| 5 | I Moment of Inertia | - | 3.48 cm ⁴ | 1.74 cm ⁴ | 0.87 cm ⁴ |

Table 2.5

Data for Soil Contained in bin, and formulae used for evaluation

a. Circular Plate

| Plate dimension 9" dia. 1/2" thickness | | | | Weight = 4.048 kg. | |
|--|-------------|----------------------------|---------------------------|---------------------------|----------------|
| Sr.No. | Force in kg | Resonant frequency in cps. | Maximum Amplitude in m.m. | Spring constant in kg/cm. | Damping factor |
| 1 | 3.0 | 380 | 0.0072 | 24000 | .090 |
| 2 | 5.1 | 385 | 0.0100 | 24600 | .104 |
| 3 | 7.0 | 385 | 0.0110 | 24900 | .129 |
| 4 | 7.5 | 385 | 0.0220 | 24500 | .072 |

b. Square Plate

| Plate dimension 8" x 8" x 1/2" | | | | Weight = 4.055 kg. | |
|--------------------------------|-------------|----------------------------|---------------------------|---------------------------|----------------|
| Sr.No. | Force in kg | Resonant frequency in cps. | maximum amplitude in m.m. | Spring constant in kg/cm. | Damping factor |
| 1 | 3.2 | 385 | 0.0075 | 24600 | .090 |
| 2 | 5.0 | 385 | 0.0090 | 24800 | .113 |
| 3 | 5.3 | 390 | 0.0095 | 25400 | .110 |
| 4 | 7.0 | 385 | 0.0180 | 24550 | .080 |

c. Rectangular Plate

| Plate dimension 16"x 4" x 1/2" | | | | Weight = 4.032 kg. | |
|--------------------------------|--------------|----------------------------|---------------------------|----------------------------|-----------------|
| Sr.No. | Force in kg. | Resonant frequency in cps. | maximum amplitude in m.m. | Spring constant* in kg/cm. | Damping factor* |
| 1 | 3.1 | 410 | 0.0055 | 27900 | .102 |
| 2 | 5.0 | 410 | 0.0099 | 27800 | .100 |
| 3 | 5.2 | 415 | 0.0180 | 28000 | .051 |
| 4 | 7.5 | 420 | 0.0225 | 28400 | .058 |

* Assuming the plate is rigid

Table 2.5 (contd.)

d. Long Beam

| Beam Dimension 32" x 2" x 1/2" | | | | Weight = 3.93 kg. | |
|--------------------------------|-----------------|----------------------------------|---------------------------------|------------------------------|-----------------|
| Sr.No. | Force in kg. | Resonant frequency in cps. | Maximum amplitude in m.m. | *Spring constant in kg/cm | Damping factor* |
| 1 | 3.4 | 500 | .0133 | 39620 | .032 |
| 2 | 5.0 | 510 | .0174 | 41230 | .035 |
| 3 | 7.4 | 510 | .0230 | 41260 | .039 |
| 4 | 9.5 | 520 | .0270 | 42910 | .041 |

*Assuming the plate as rigid

e. Formulae Used

| Parameters | Formulae |
|--------------------------------|---|
| Known parameters - F , f_m | A_{max} , m , F = Force, f_m = Resonant frequency = $f_n \sqrt{1-2D^2}$, A_{max} = Maximum Amplitude, m = mass of Plate |
| f_n = natural frequency | $= \frac{1}{2\pi} \sqrt{\frac{K}{m}}$ |
| D = Damping factor | $\frac{1-2D^2}{2D(1-D^2)^{1/2}} = \left(\frac{A_{max} \cdot m}{F} \right) (2\pi f_m)^2$ |
| K = Spring constant | $K = \frac{F}{A_{max} \cdot 2D \sqrt{1-D^2}}$ |

Table 2.6

Data for Stabilized Soil

a. Circular Plate

Plate dimension = 9" dia 1/2" thickness

weight of the plate
4.048 kg

| Sr.No. | Force in kg. | Resonant Frequency in cps. | Maximum Amplitude in m.m. | Spring constant in kg/cm. | Damping factor |
|--------|-----------------|----------------------------------|---------------------------------|------------------------------|----------------|
| 1 | 3.0 | 375 | 0.0062 | 23900 | .105 |
| 2 | 4.2 | 375 | 0.0073 | 24200 | .123 |
| 3 | 5.3 | 380 | 0.0086 | 24600 | .129 |
| 4 | 6.0 | 385 | 0.0100 | 24900 | .122 |

b. Square Plate

Plate dimension = 8" x 8" x 1/2"

weight of the plate
= 4.055 kg.

| | | | | | |
|---|-----|-----|-------|-------|------|
| 1 | 3.3 | 385 | .0075 | 24500 | .090 |
| 2 | 4.6 | 385 | .0078 | 25000 | .120 |
| 3 | 6.2 | 385 | .0096 | 25100 | .130 |
| 4 | 7.1 | 385 | .0100 | 25100 | .130 |

Table 2.6 (contd.)

c. Rectangular Plate

| Plate dimension = 16" x 4" x 1/2" | | | | Weight of the plate=4.032kg. | |
|-----------------------------------|-----------------|----------------------------------|---------------------------------|-------------------------------|-----------------|
| Sr.N. | Force in kg. | Resonant Frequency in cps. | Maximum amplitude in m.m. | Spring constant in kg/cm.* | *Damping Factor |
| 1 | 3.1 | 390 | .0070 | 25000 | .089 |
| 2 | 3.6 | 400 | .0115 | 26200 | .060 |
| 3 | 5.0 | 400 | .0150 | 26250 | .064 |
| 4 | 5.1 | 395 | .0110 | 26000 | .091 |
| 5 | 7.2 | 395 | .0125 | 26100 | .110 |

*Assuming the beam as rigid

d. Long Beam

| Beam dimension = 32" x 2" x 1/2" | | | | Weight of the Beam 3.93kg. | |
|----------------------------------|-----------------|----------------------------------|---------------------------------|----------------------------|-----------------|
| Sr.N. | Force in kg. | Resonant Frequency in cps. | Maximum amplitude in m.m. | Spring constant kg/cm.* | *Damping Factor |
| 1 | 3.1 | 490 | 0.0130 | 38000 | .010 |
| 2 | 4.5 | 495 | 0.0185 | 38700 | .010 |
| 3 | 6.1 | 500 | 0.0223 | 39500 | .011 |
| 4 | 7.5 | 500 | 0.0290 | 39500 | .011 |

*Assuming the beam as rigid

Table 2.7

Data for Natural Soil Deposit

a. Circular Plate

Plate dimension = 9" dia. 1/2" thickness Weight of the plate=4.048kg.

| Sr.No. | Force in kg. | Resonant Frequency in cps. | Maximum amplitude in m.m. | Spring constant in kg/cm. | Damping factor |
|--------|-----------------|----------------------------------|---------------------------------|------------------------------|----------------|
| 1 | 3.0 | 390 | 0.0066 | 25000 | .090 |
| 2 | 4.0 | 390 | 0.0079 | 25050 | .100 |
| 3 | 5.5 | 395 | 0.0096 | 25800 | .121 |
| 4 | 6.2 | 390 | 0.0103 | 25150 | .119 |

b. Square Plate

Plate dimension 8" x 8" x 1/2"

Weight of the plate=4.055kg.

| Sr.No. | Force in kg. | Resonant frequency in cps. | Maximum amplitude in m.m. | Spring constant in kg/cm. | Damping factor |
|--------|-----------------|----------------------------------|---------------------------------|------------------------------|----------------|
| 1 | 3.1 | 385 | 0.0070 | 24500 | .090 |
| 2 | 3.9 | 390 | 0.0079 | 25400 | .099 |
| 3 | 5.0 | 390 | 0.0096 | 25500 | .103 |
| 4 | 6.5 | 395 | 0.0116 | 26000 | .108 |

c. Rectangular Plate

Plate dimension = 16" x 4" x 1/2"

Weight of the plate=4.032

| Sr.No. | Force in kg. | Resonant Frequency in cps. | Maximum amplitude in m.m. | Spring constant in kg/cm.* | Damping factor* |
|--------|-----------------|----------------------------------|---------------------------------|-------------------------------|-----------------|
| 1 | 3.3 | 445 | .012 | 32250 | .043 |
| 2 | 5.5 | 425 | .014 | 29700 | .060 |
| 3 | 6.7 | 425 | .016 | 29800 | .065 |

*Assuming the beam as rigid

d. Long Beam

Beam dimension = 32" x 2" x 1/2"

Weight of the plate=3.93

| Sr.No. | Force in kg. | Resonant Frequency in cps. | Maximum amplitude in m.m. | Spring constant in kg/cm.* | Damping factor* |
|--------|-----------------|----------------------------------|---------------------------------|-------------------------------|-----------------|
| 1 | 3.2 | 485 | .015 | 37300 | .0090 |
| 2 | 4.3 | 490 | .018 | 38600 | .0105 |
| 3 | 5.1 | 490 | .022 | 38500 | .0100 |
| 4 | 6.3 | 495 | .026 | 39200 | .0099 |

*Assuming the beam as rigid

L. I. T. MARBUR
CENTRAL LIBRARY
Acc. No. A 50248

Table 2.8

Increase in Spring Constant Ratio for $L/B=16$

| $L/B = 16$ | Experimental Values | | Theoretical Values Barkan (3) | |
|----------------------------|---------------------------|---------------------------------|----------------------------------|---------------------|
| | Treating beam as rigid | Treating beam as flexible | Beam as Rigid | Beam as Flexible |
| Beam on Sandy Soil | 1.683 | 1.810 | 1.50 | 1.51 |
| Beam on Stabilized Soil | 1.595 | 1.503 | 1.50 | 1.51 |
| Beam on Natural Soil | 1.520 | 1.432 | 1.50 | 1.51 |

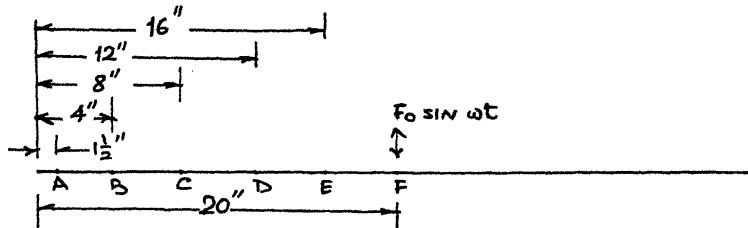
Table 2.9

Details of Beam and Spring used for Winkler Model Idealisation

| Beam Size | | | Density in kg/cm^3 | Young's modulus of Elas- ticity kg/cm^2 | EI Kg.cm^2 | Spring | |
|------------------|-----------------|---------------------|--------------------------------|--|--------------------------|--------|--------------------------------|
| length in cm. | Width in cm. | Thickness in cm. | | | | L | constant K kg/cm^2 |
| 101.5 | 5.04 | 1.26 | 7.8×10^{-3} | 2.1×10^6 | 1.76×10^6 | 3.2 | 7.0 |

Table 2.10

Displacement Values with Frequency at Force Level 9.4kg.



| Sr. No. | Frequency cps | Displacement at A in m.m. | Displacement at B in m.m. | Displacement at C in m.m. | Displacement at D in m.m. | Displacement at E in m.m. | Displacement at F. in m.m. |
|---------|------------------|---------------------------------|---------------------------------|---------------------------------|------------------------------|------------------------------|----------------------------------|
| 1 | 35 | 0.800 | 0.680 | 0.540 | 0.400 | 0.300 | 0.050 |
| 2 | 40 | 0.900 | 0.720 | 0.440 | 0.200 | 0.032 | 0.200 |
| 3 | 45 | 0.750 | 0.550 | 0.260 | 0.020 | 0.170 | 0.200 |
| 4 | 50 | 0.800 | 0.520 | 0.220 | 0.130 | 0.350 | 0.400 |
| 5 | 55 | 0.700 | 0.460 | 0.100 | 0.240 | 0.500 | 0.550 |
| 6 | 60 | 0.450 | 0.280 | 0.024 | 0.220 | 0.350 | 0.400 |
| 7 | 65 | 0.400 | 0.220 | 0.028 | 0.190 | 0.300 | 0.350 |
| 8 | 70 | 0.220 | 0.120 | 0.035 | 0.160 | 0.230 | 0.200 |
| 9 | 75 | 0.160 | 0.075 | 0.046 | 0.140 | 0.190 | 0.180 |
| 10 | 80 | 0.150 | 0.050 | 0.050 | 0.110 | 0.150 | 0.150 |
| 11 | 90 | 0.060 | 0.022 | 0.027 | 0.064 | 0.080 | 0.100 |
| 12 | 100 | 0.080 | 0.027 | 0.037 | 0.076 | 0.080 | - |
| 13 | 110 | 0.066 | 0.022 | 0.030 | 0.063 | 0.067 | - |
| 14 | 120 | 0.063 | 0.015 | 0.022 | 0.050 | 0.045 | - |

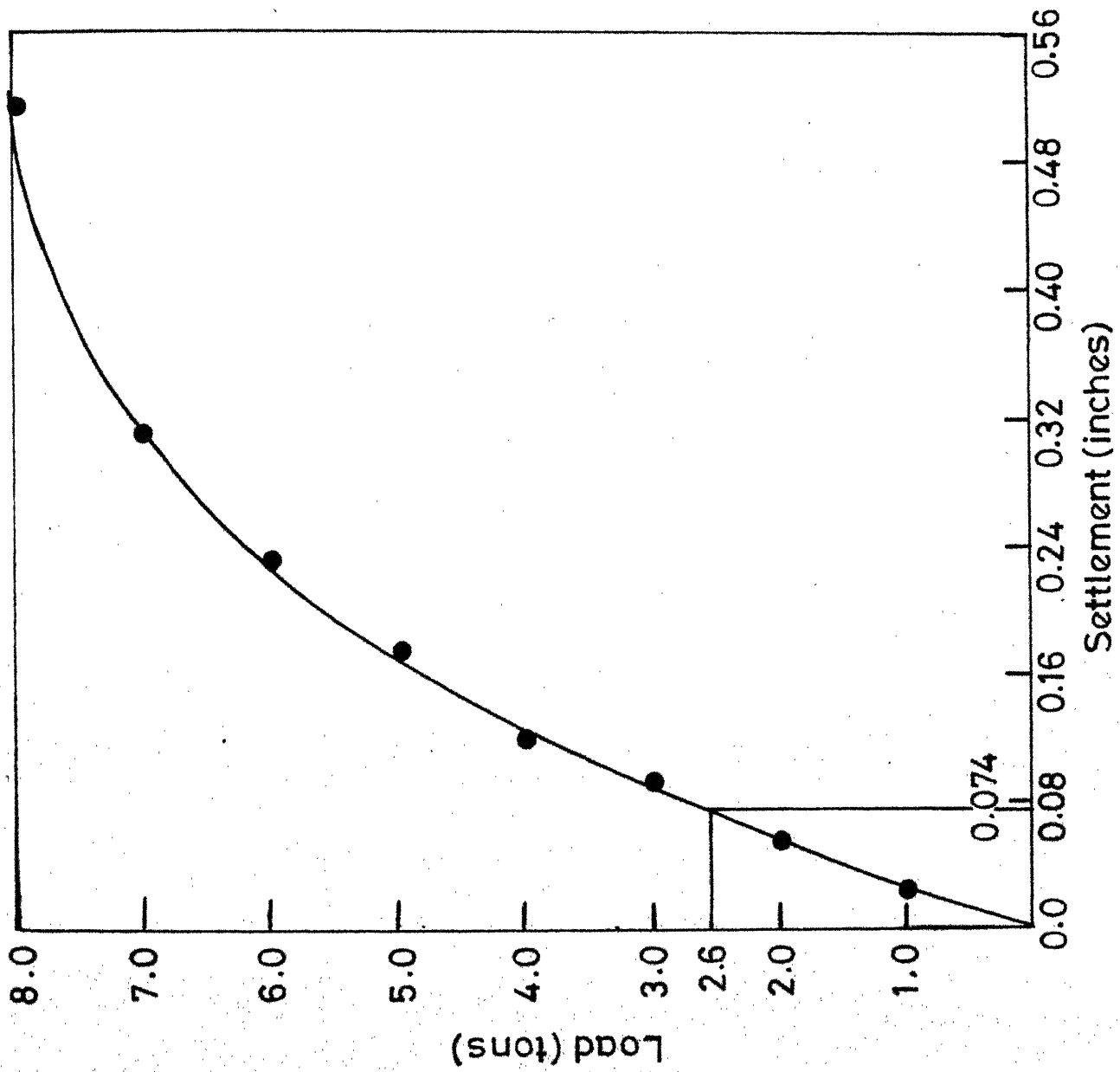


Fig.2.1 Results of plate load test of a 1640 cm² plate on stabilized soil

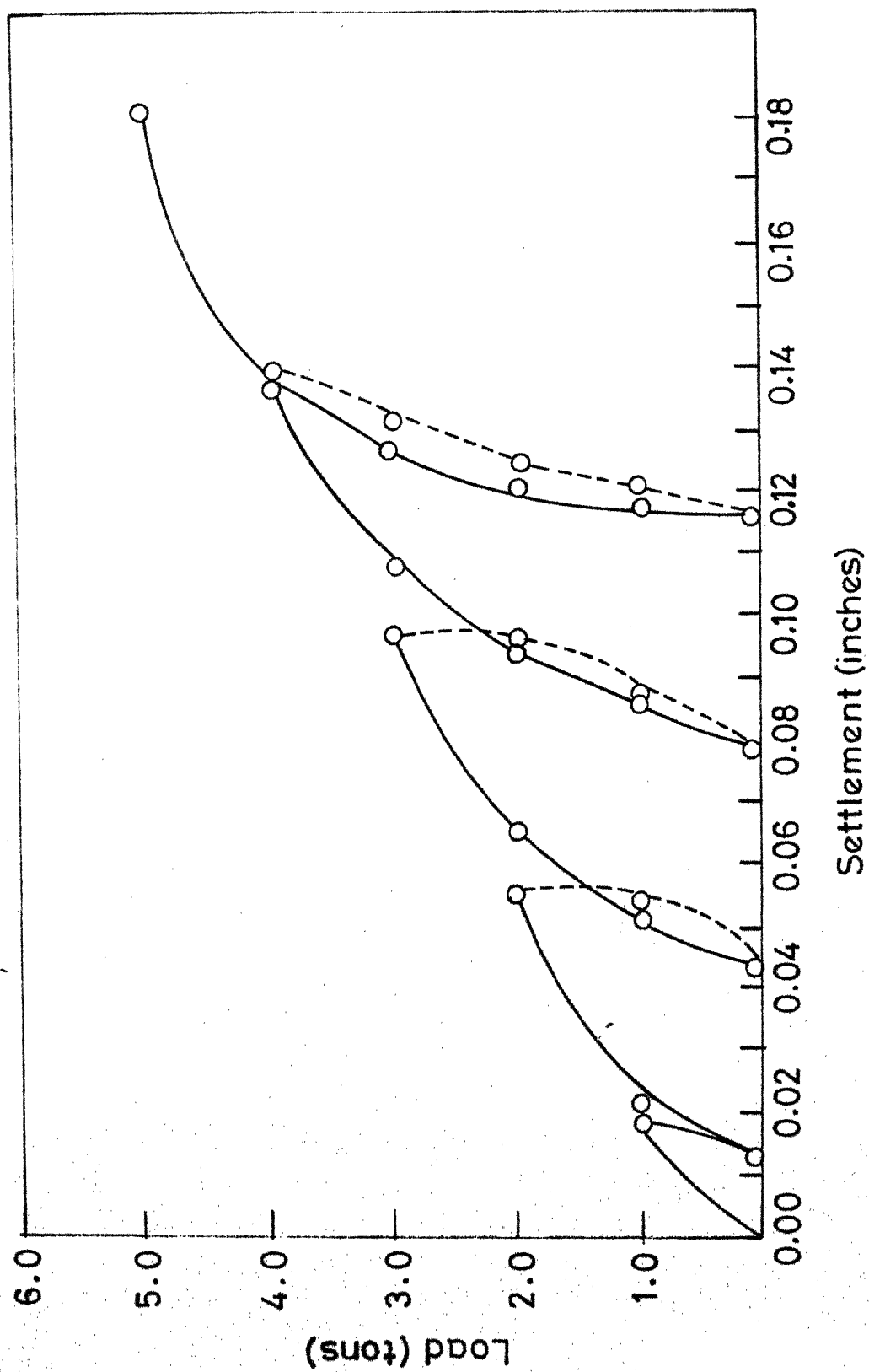


Fig.2.2 Results of a Cyclic plate load test of a 1640 cm² plate on stabilized soil

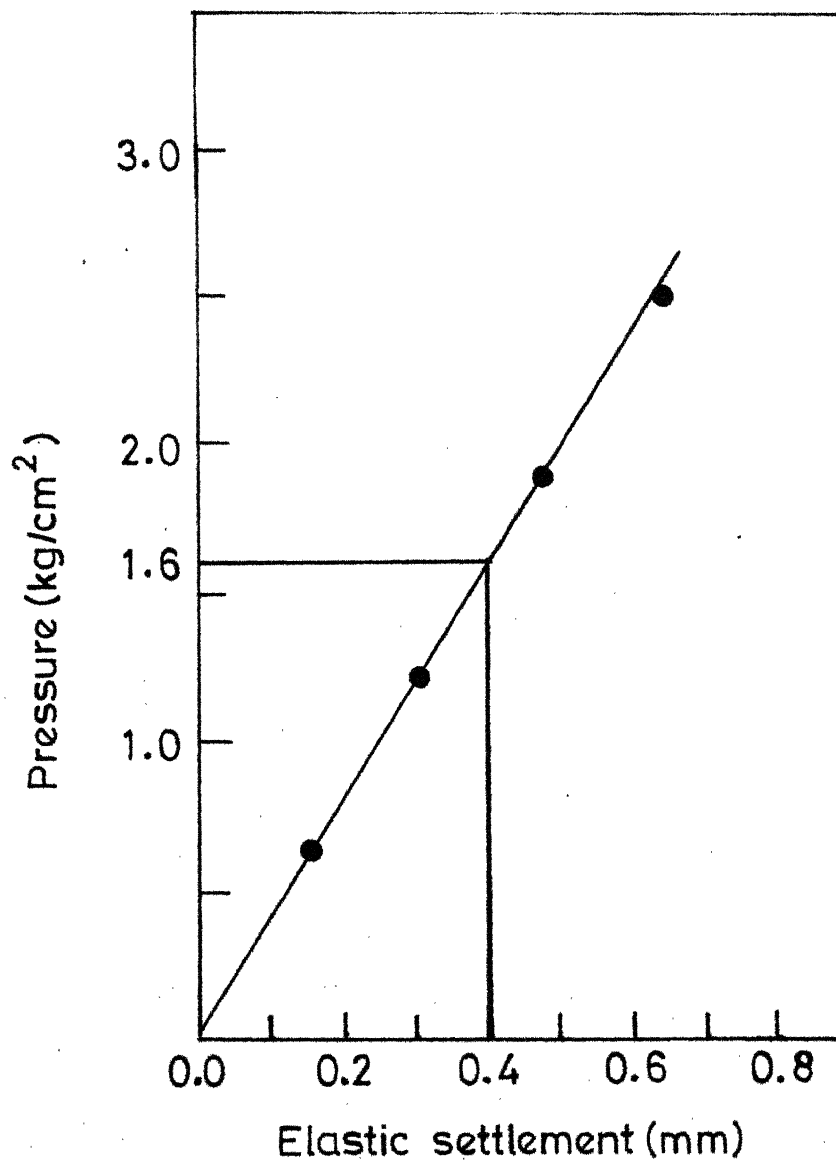


Fig.2.3 Relationship between pressure versus elastic settlement of a 1640 cm² plate on stabilized soil

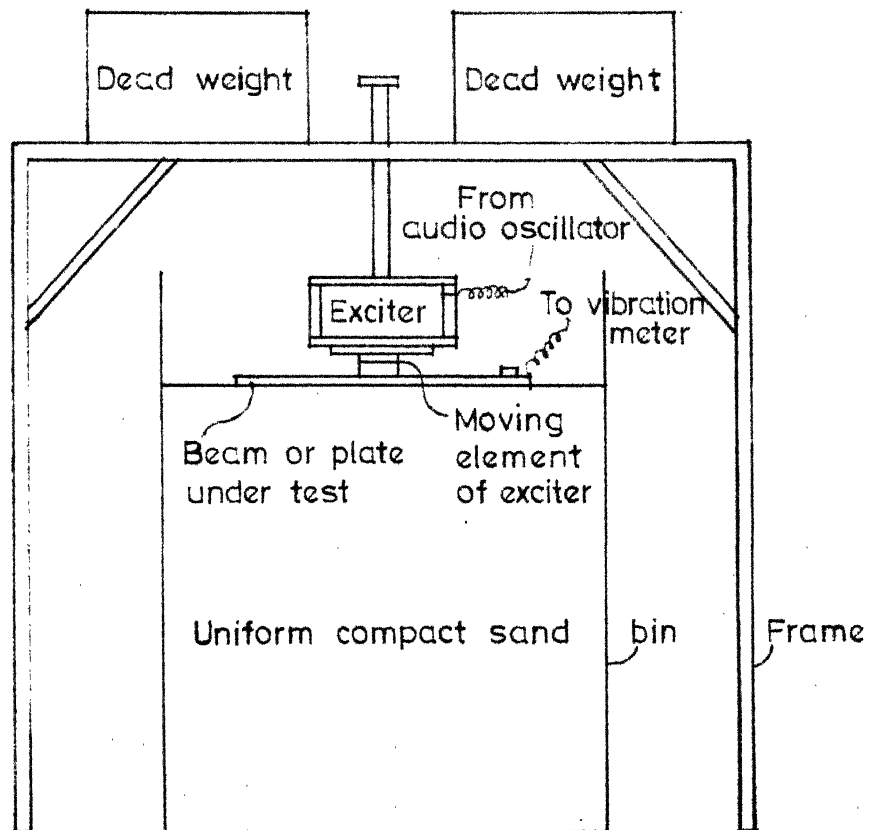


Fig.2.4 A schematic diagram of the test frame for soil contained in a bin

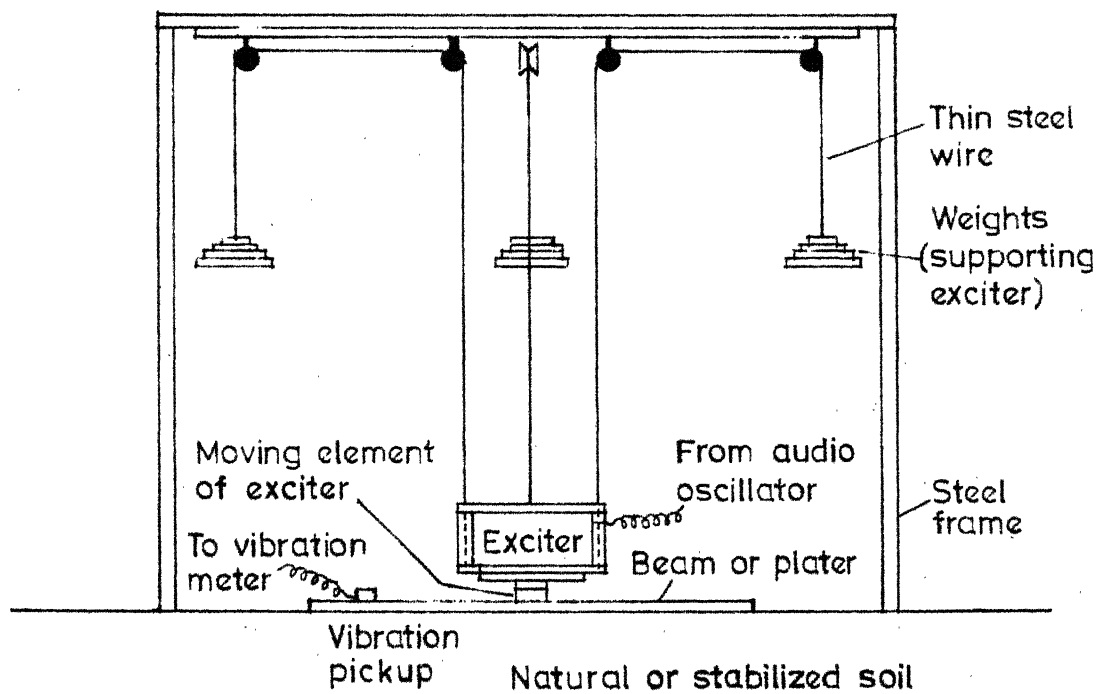


Fig.2.5 A schematic diagram of the test frame for field tests

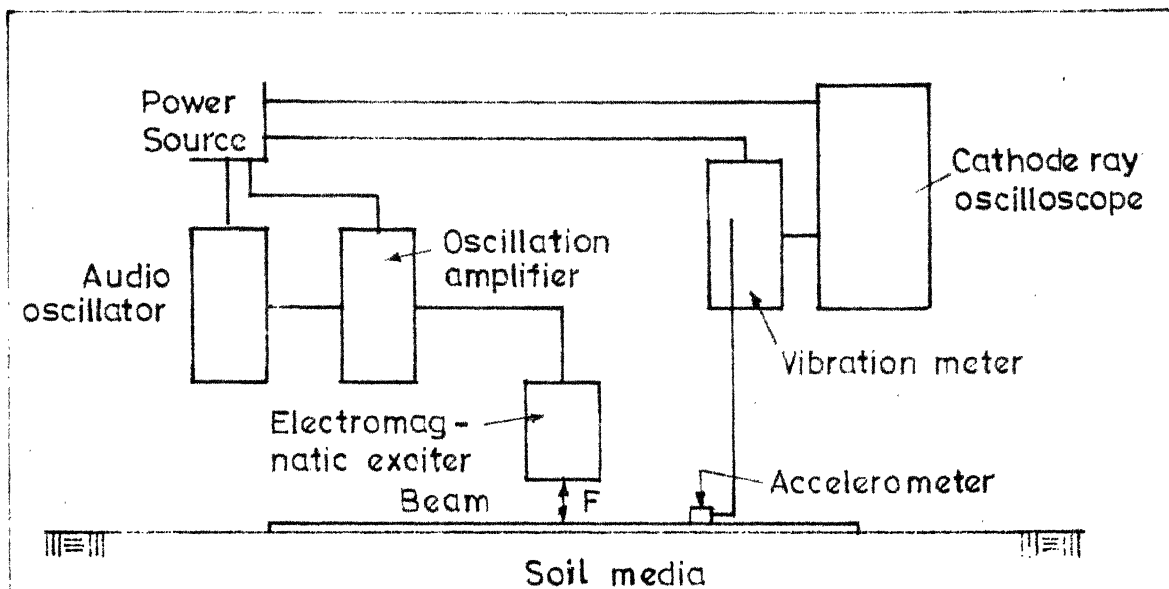


Fig.2.6 (a) A block diagram showing the arrangements of instruments for constant amplitude excitation on the footings

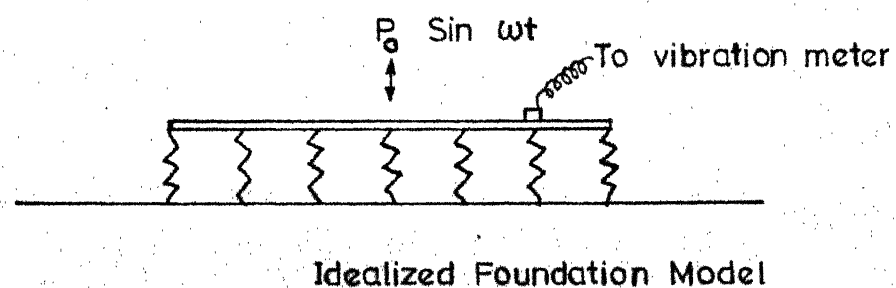


Fig.2.6 (b) Idealized Winkler Model

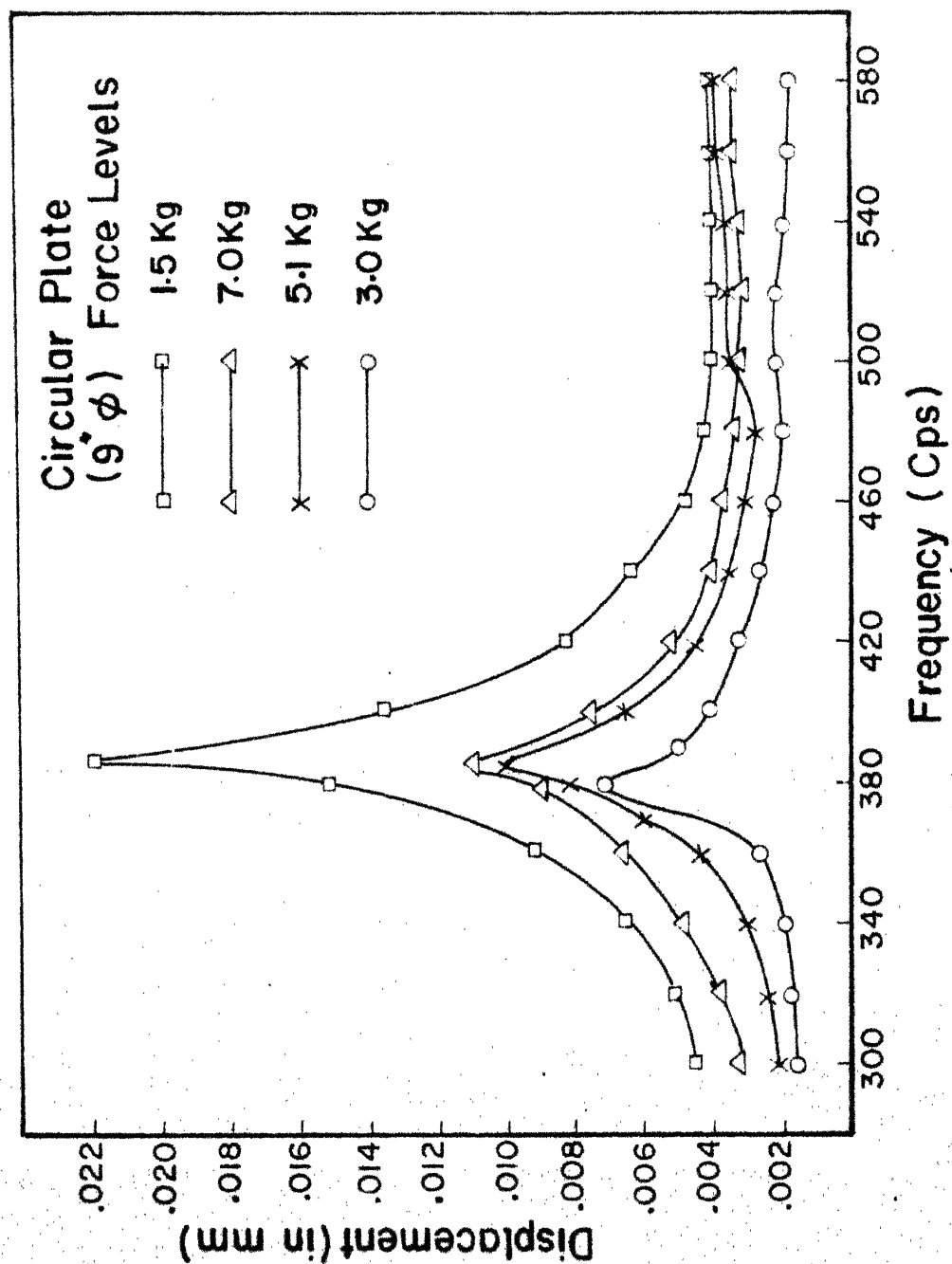


Fig.2.7 Displacement frequency curve for soil contained in the bin (for circular plate)

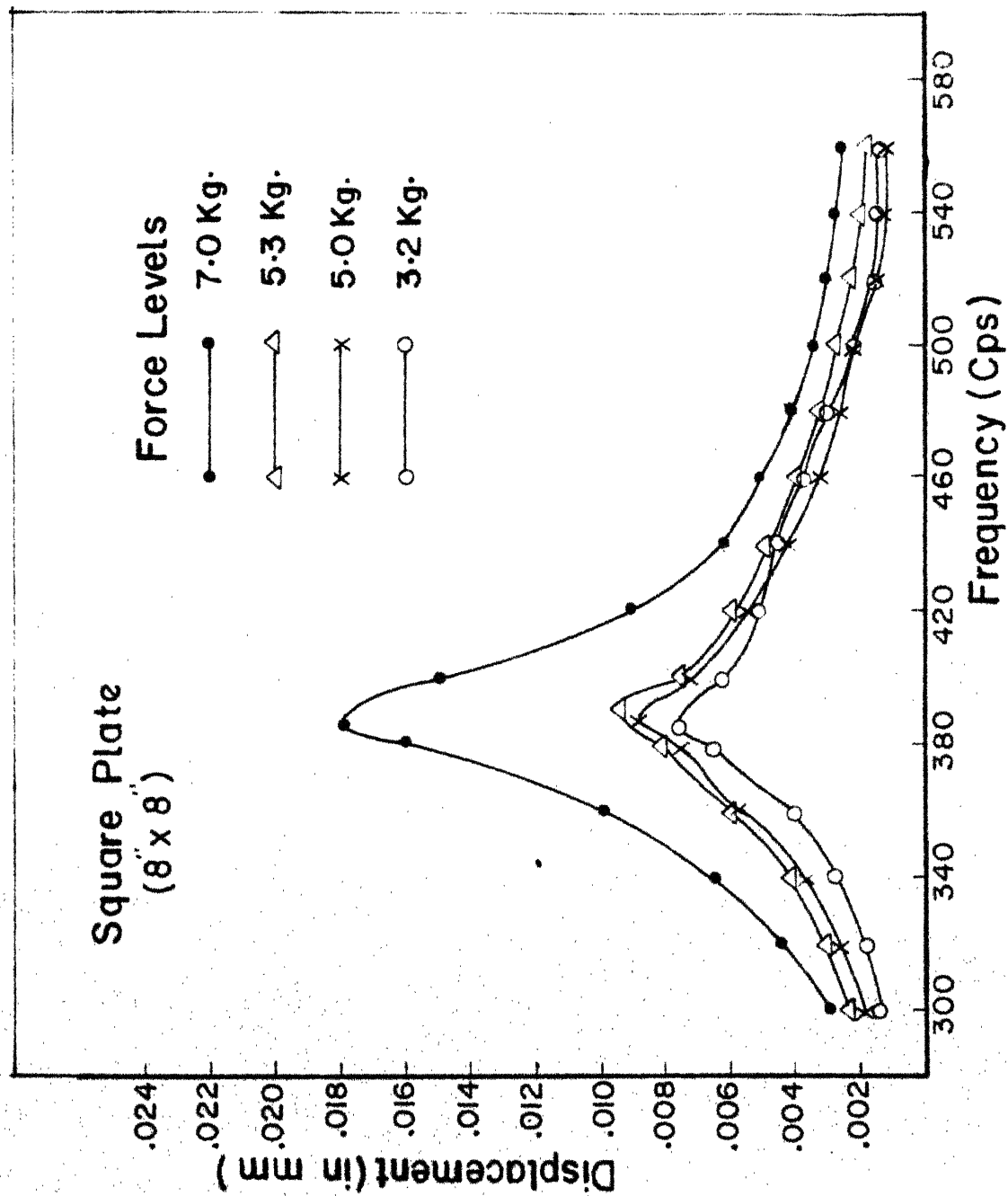


Fig.2.8 Displacement frequency response curve for soil contained in the bin (for square plate)

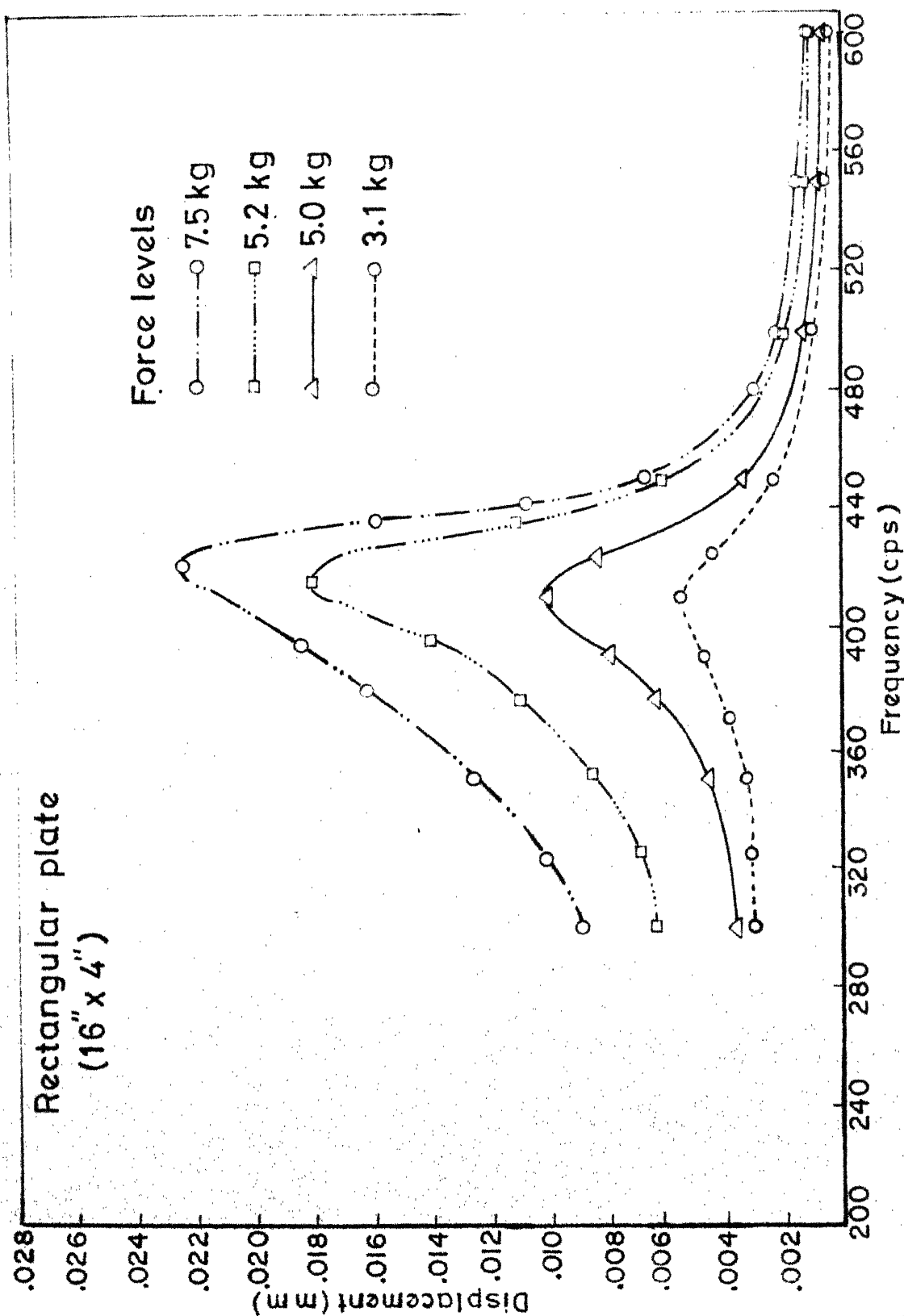


Fig.2.9 Displacement frequency response curve for soil contained in the bin (for rectangular plate)

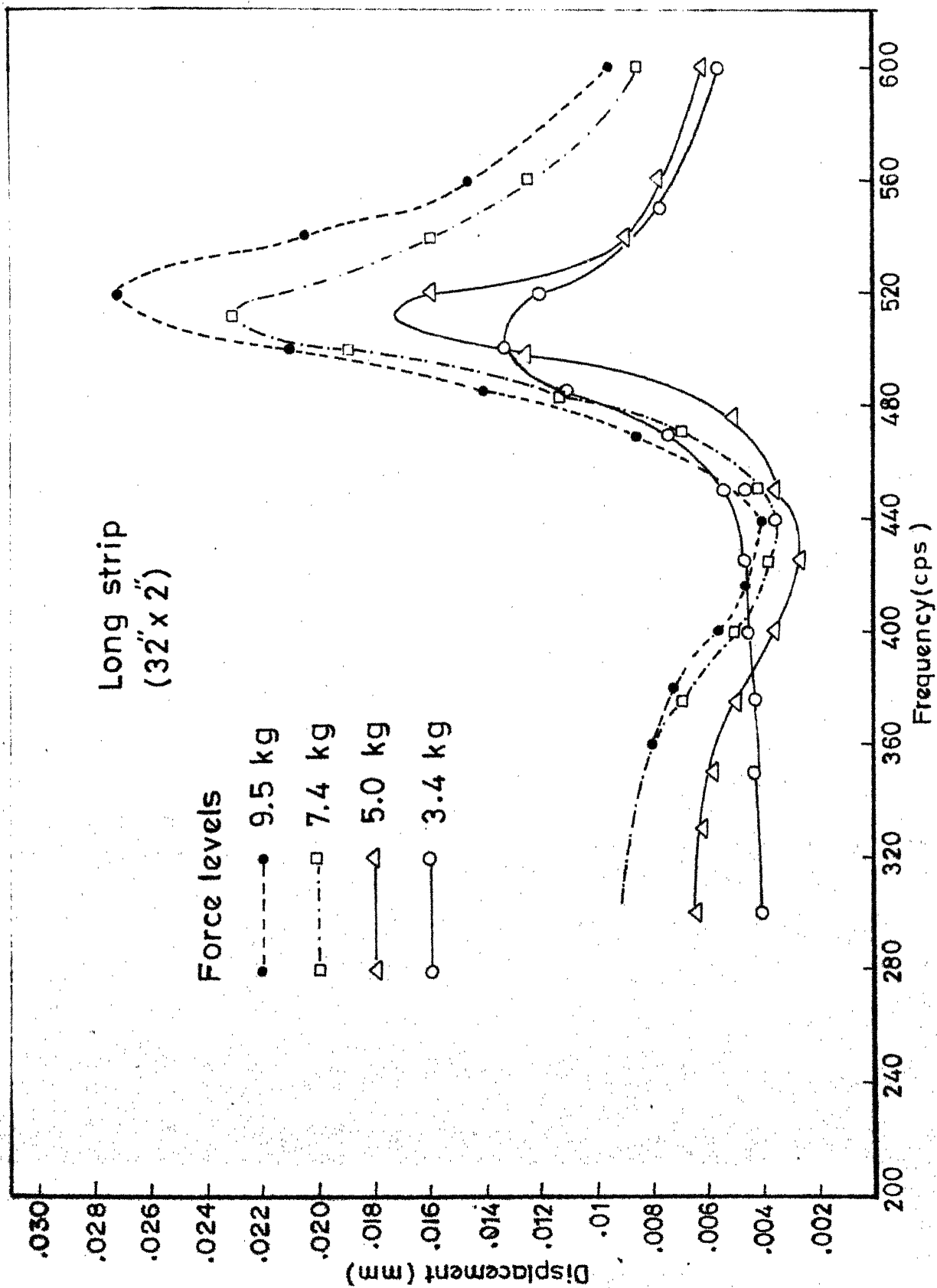


Fig.2.10 Displacement frequency response curve for soil contained in the bin (for long strip)

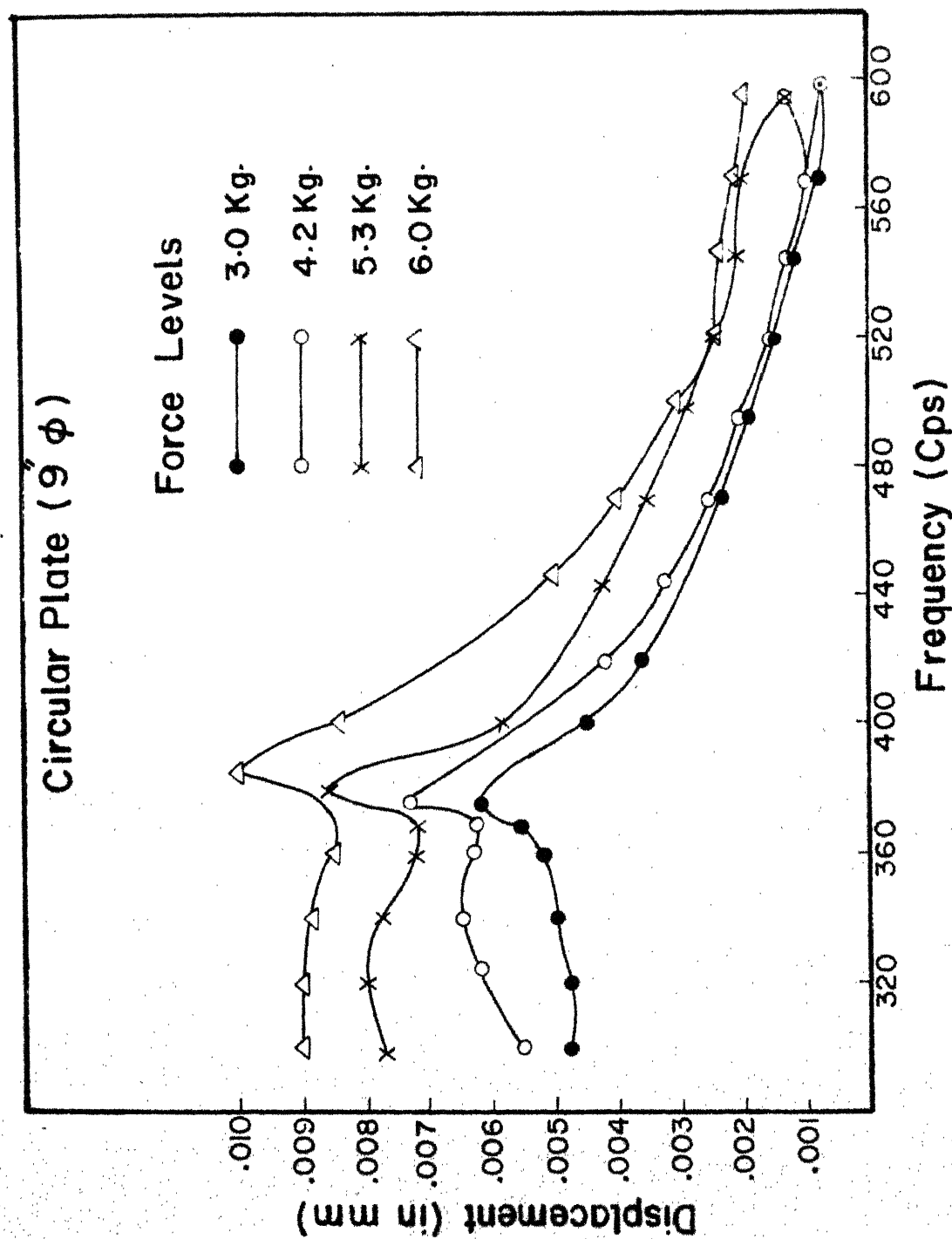


Fig.2.11 Displacement frequency response curve for stabilised soil (for circular plate)

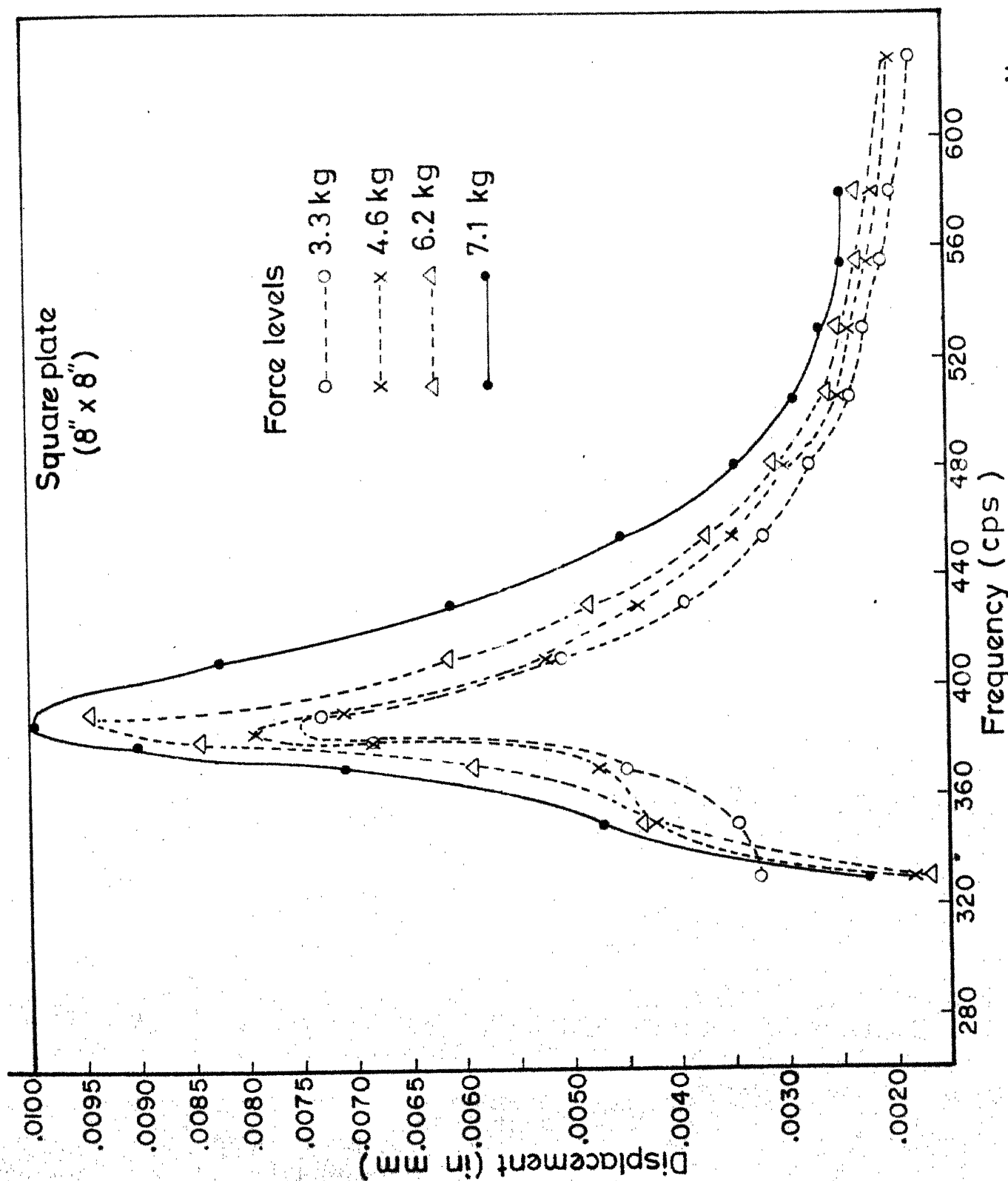


Fig. 2.12 Displacement frequency response curve for stabilised soil
(for square plate)

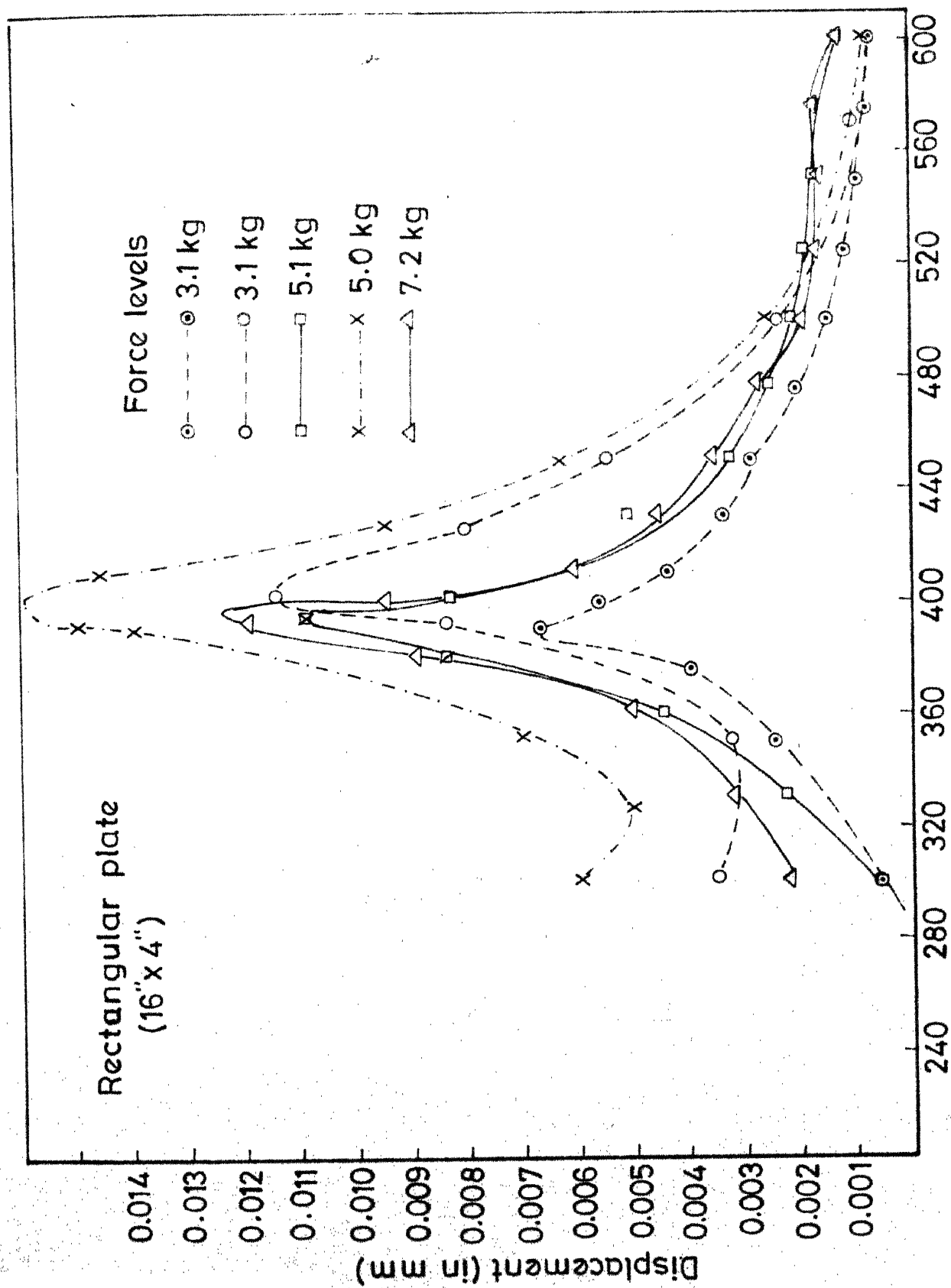


Fig.2.13 Displacement frequency response for stabilized soil
(for rectangular plate)

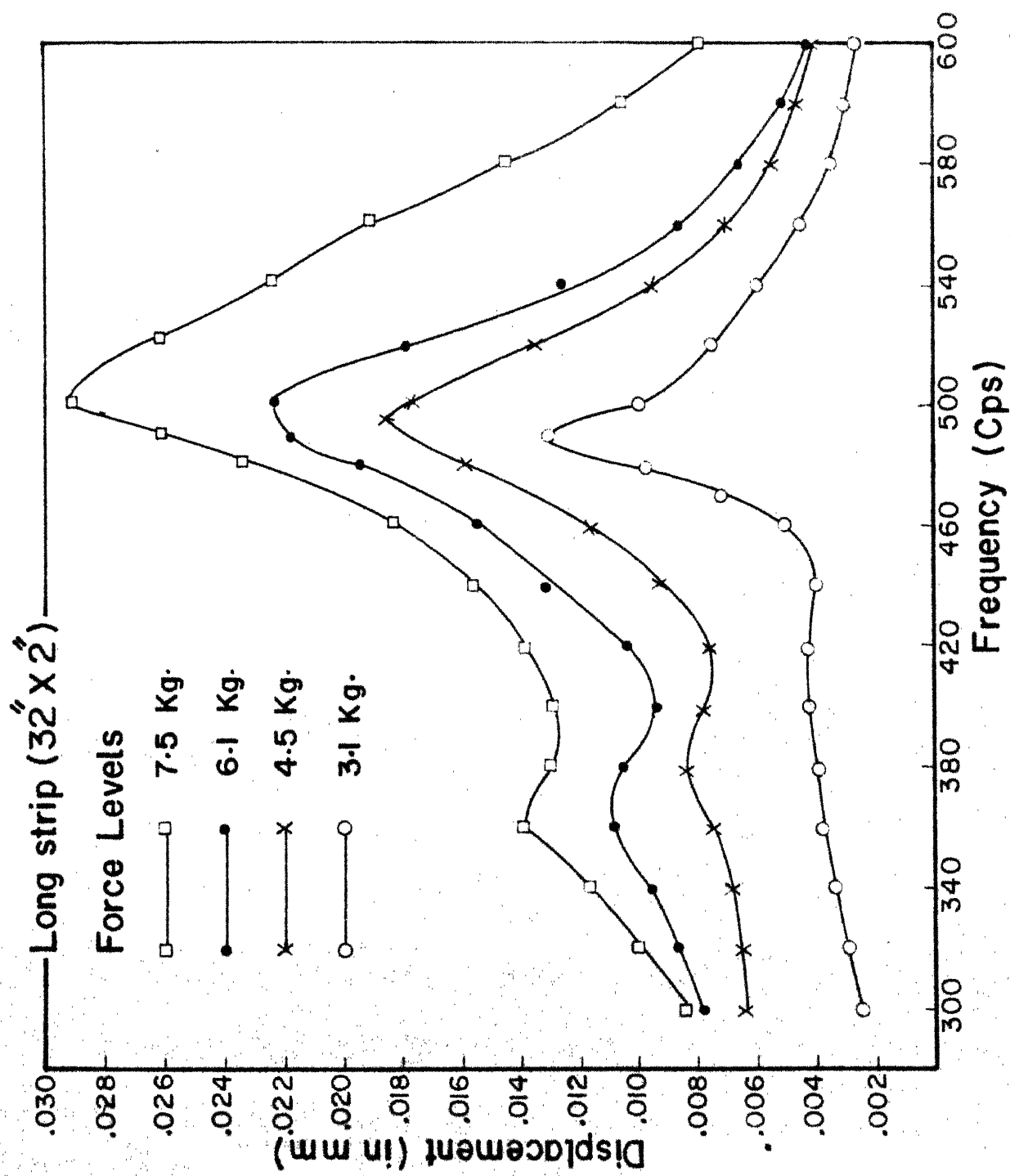


Fig.2.14 Displacement response curve for stabilised soil(for long strip)

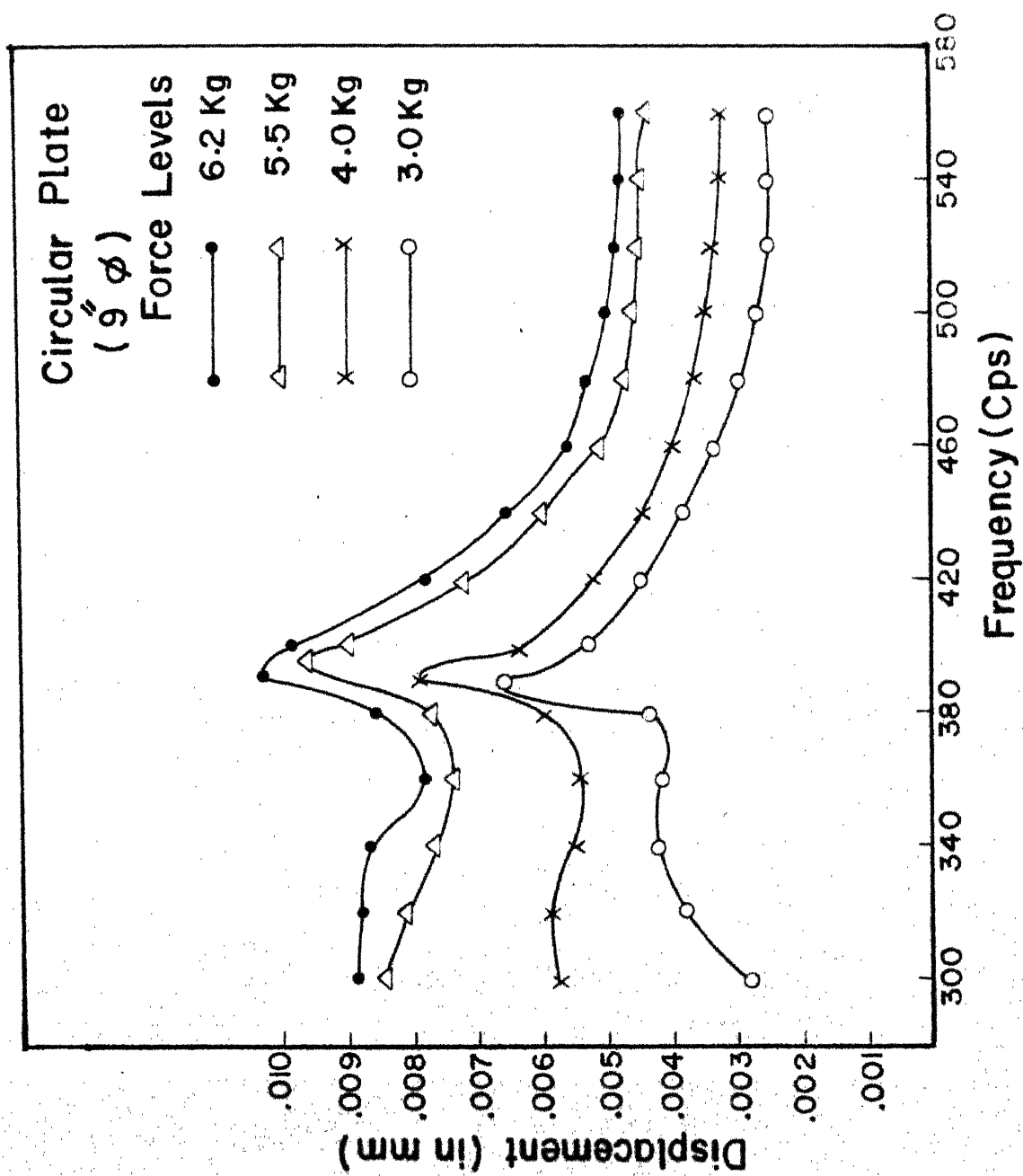


Fig.2.15 Displacement frequency response curve for natural soil (for circular plate)

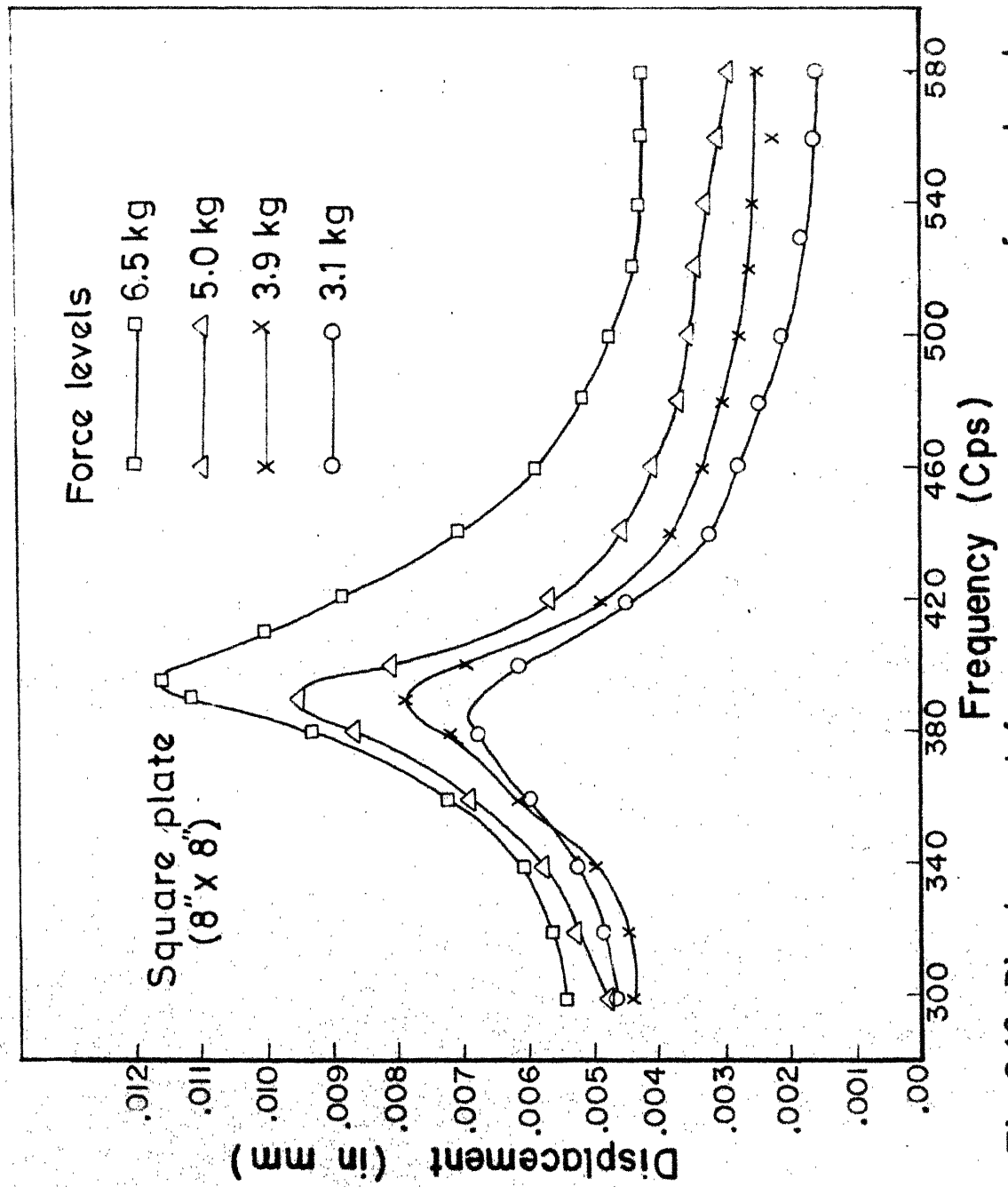


Fig.2.16 Displacement frequency response curve for natural soil (for square plate)

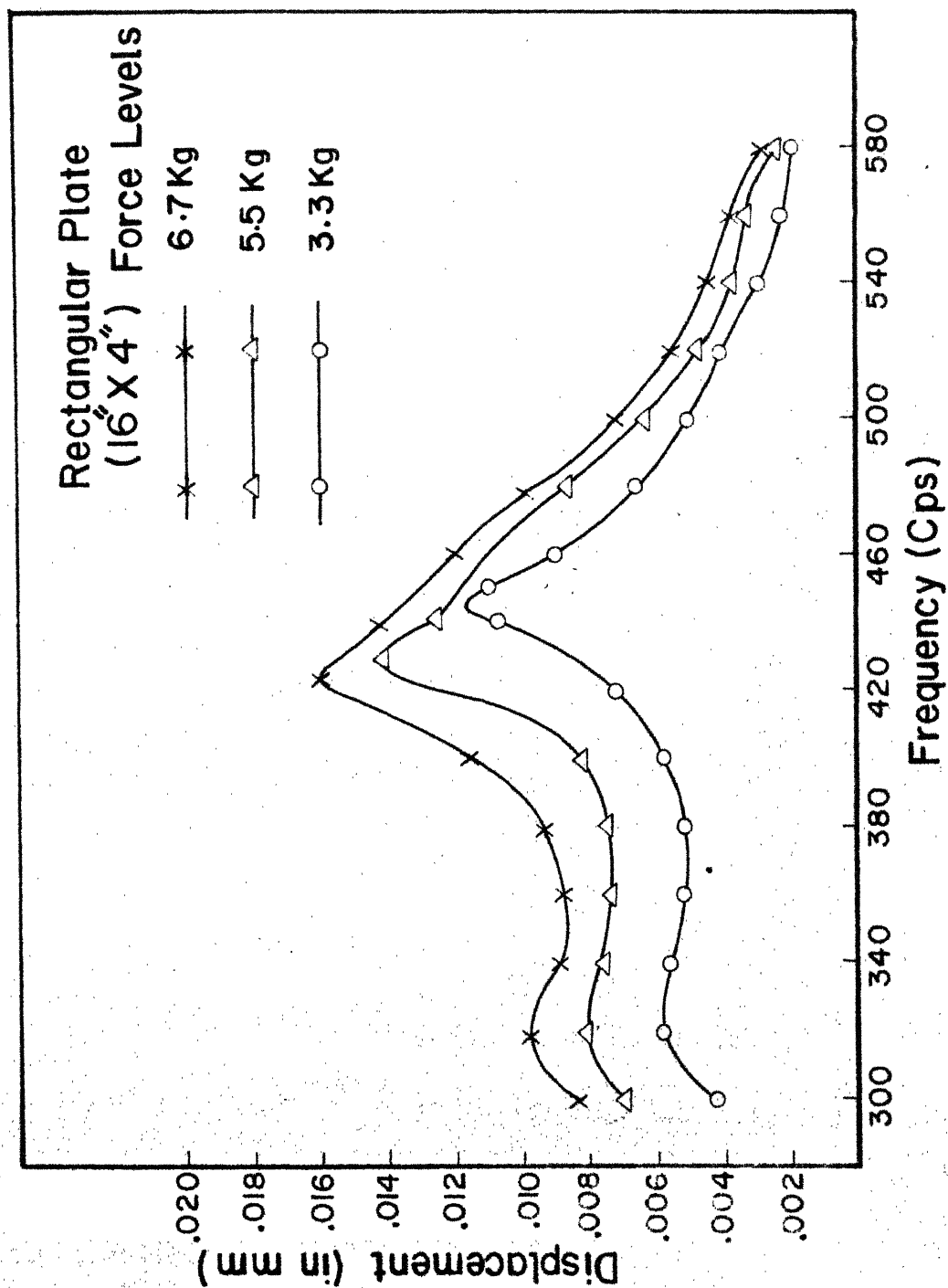


Fig.2.17 Displacement frequency response curve for natural soil (for rectangular plate)

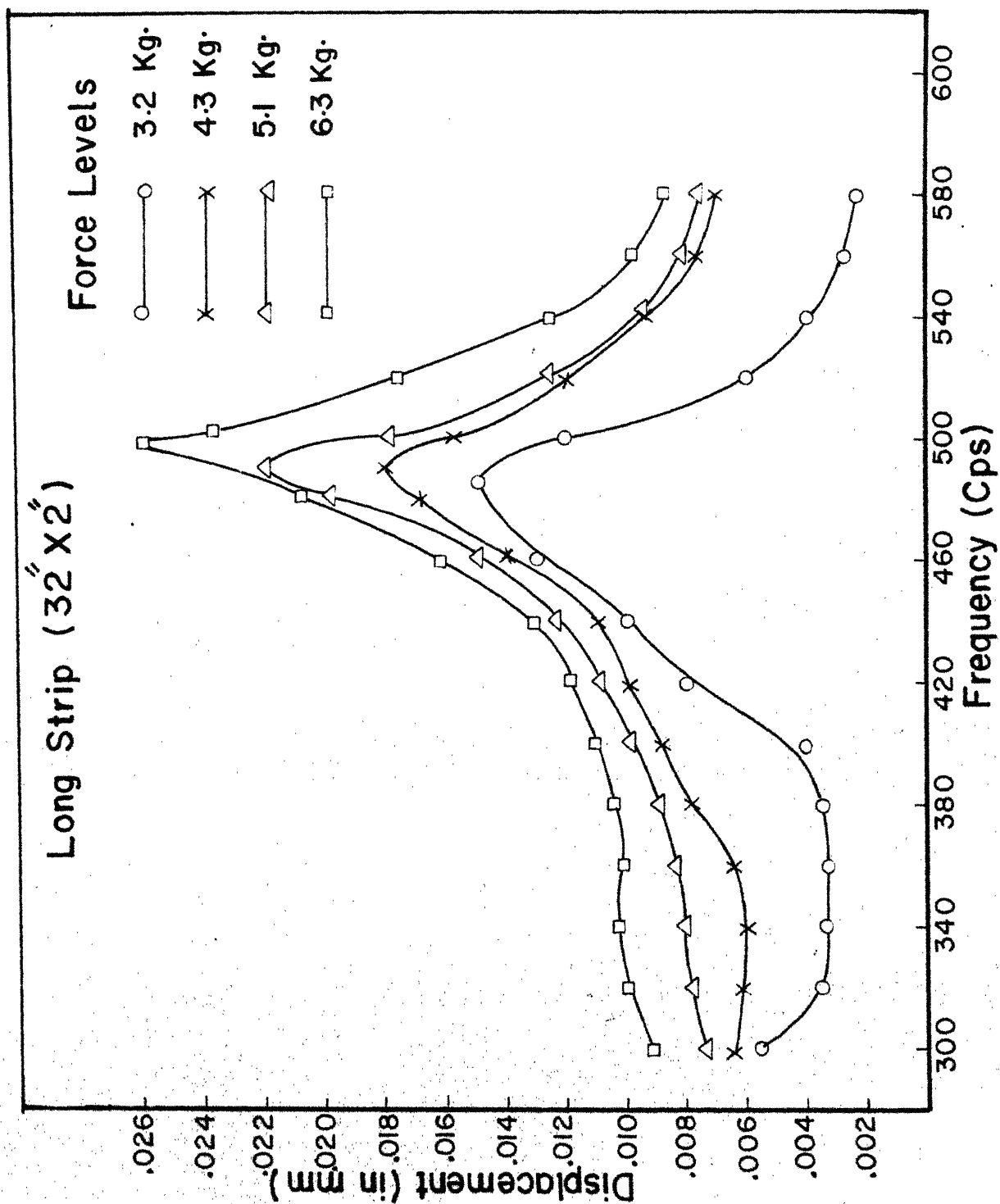


Fig.2.18 Displacement frequency response curve for natural soil (for long strip)

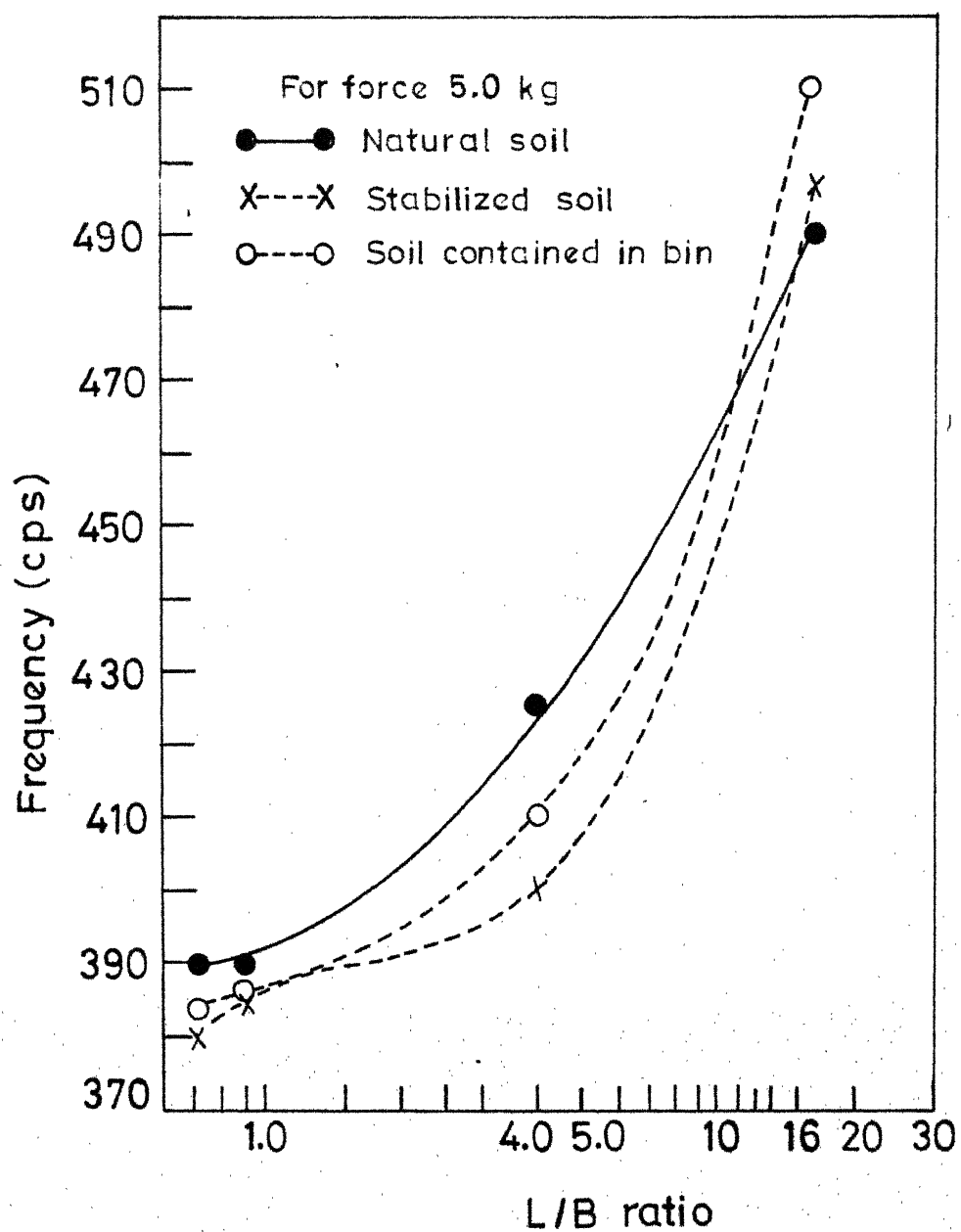


Fig.2.19 Variation of frequency with L/B ratio

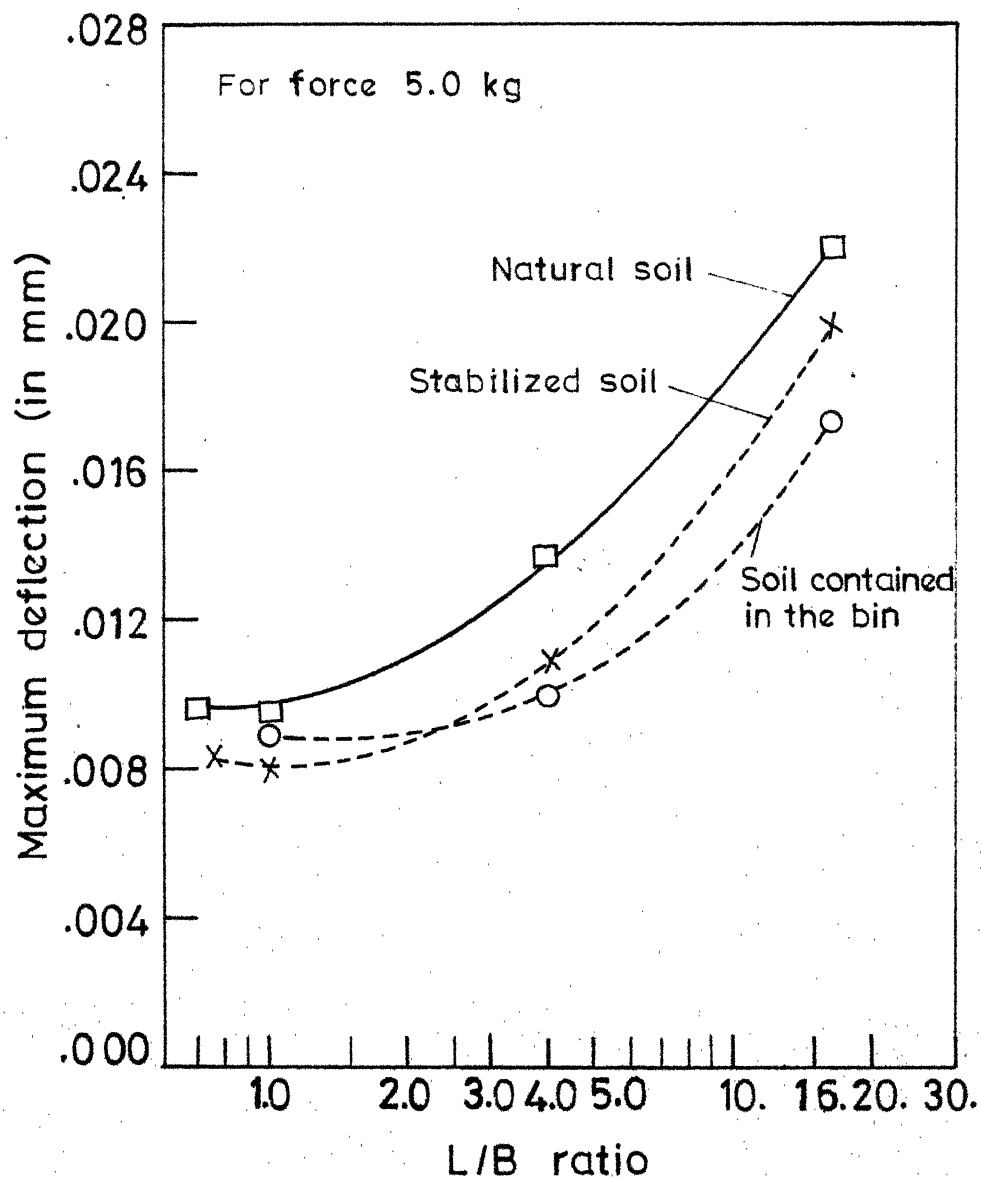


Fig.2.20 Variation of maximum deflection with L/B ratio

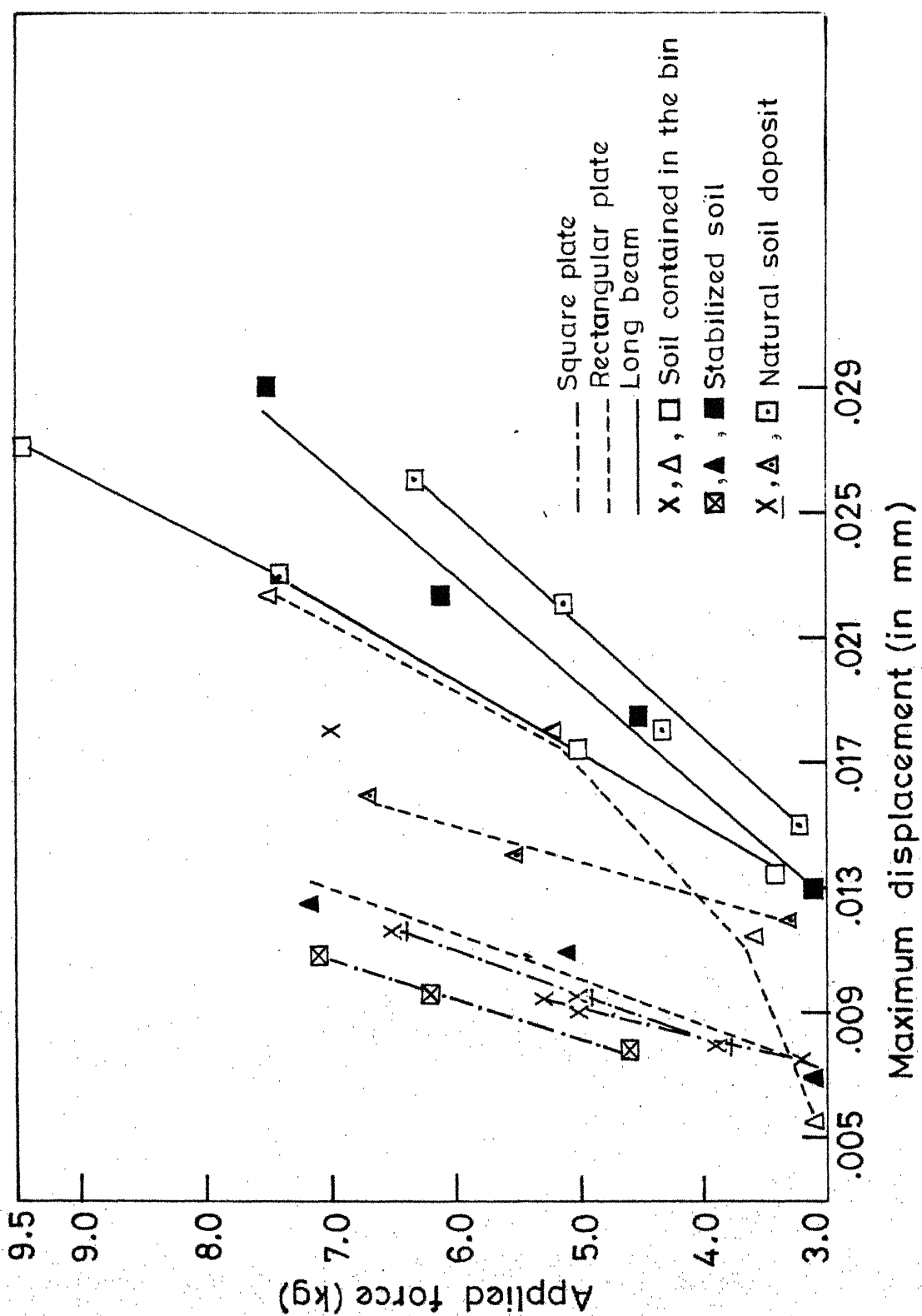


Fig.2.21 Variation of maximum displacement with force

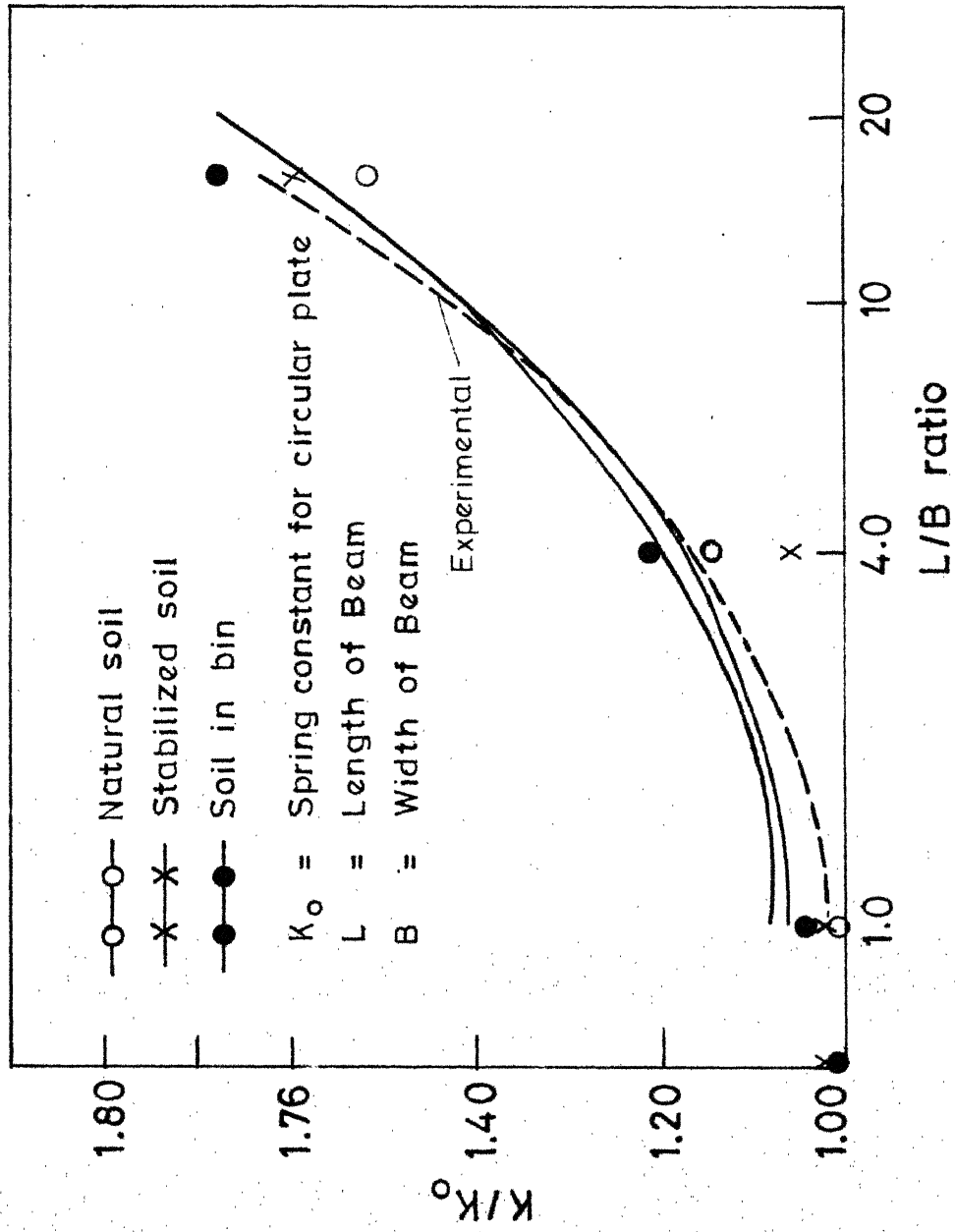


Fig.2.22 Variation of spring constant ratio with L/B ratio

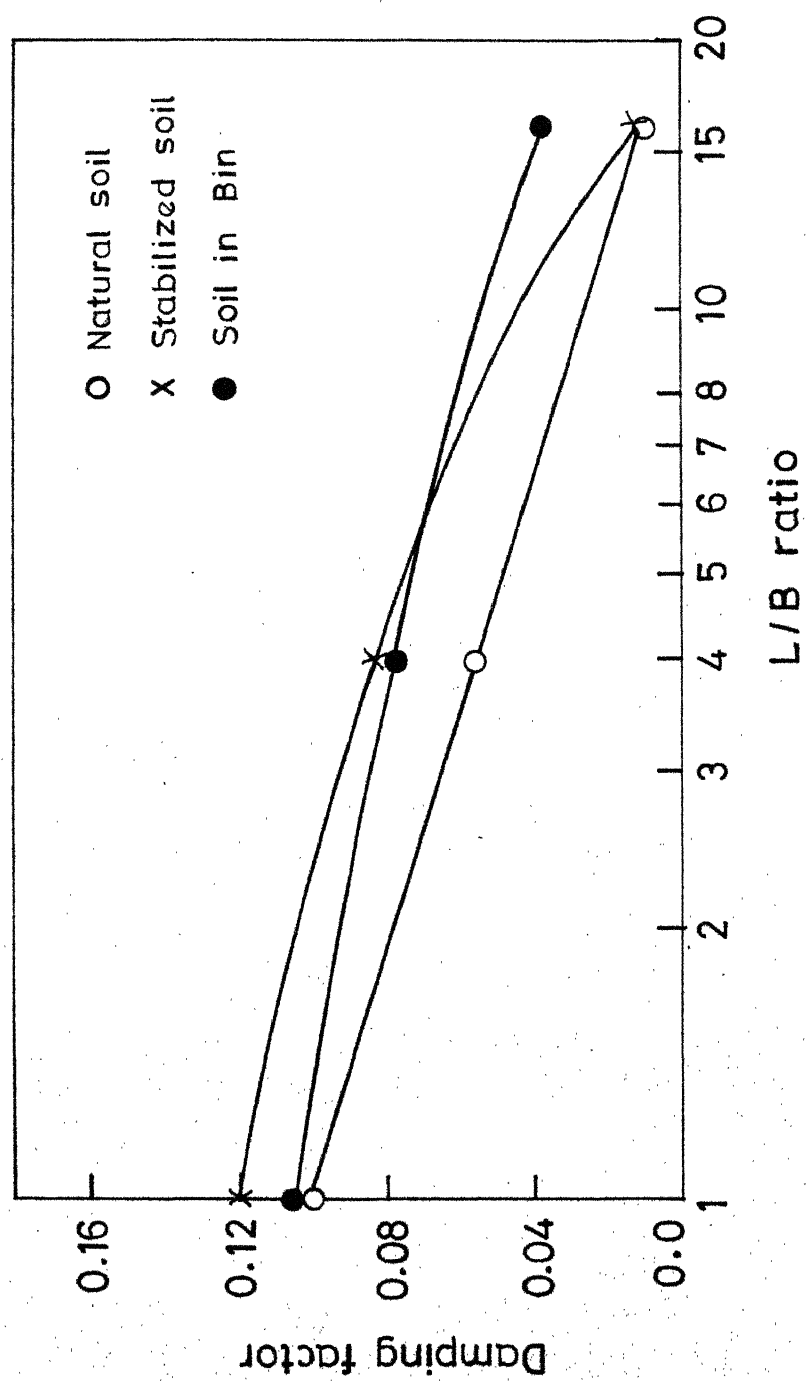


Fig.2.23 Variation in Damping factor with L/B ratio

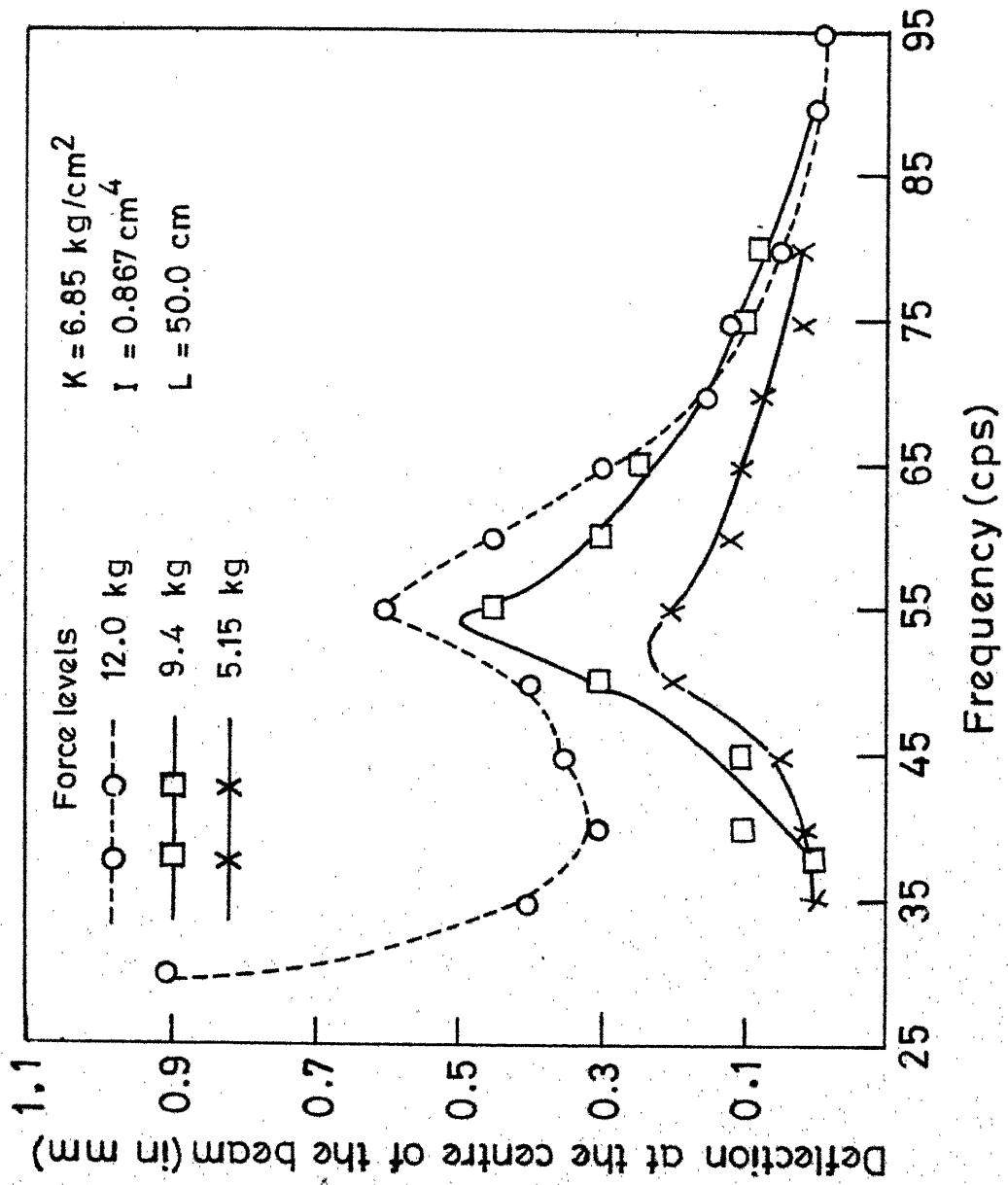


Fig. 2.24 Displacement frequency response curve for a beam resting on ideal springs

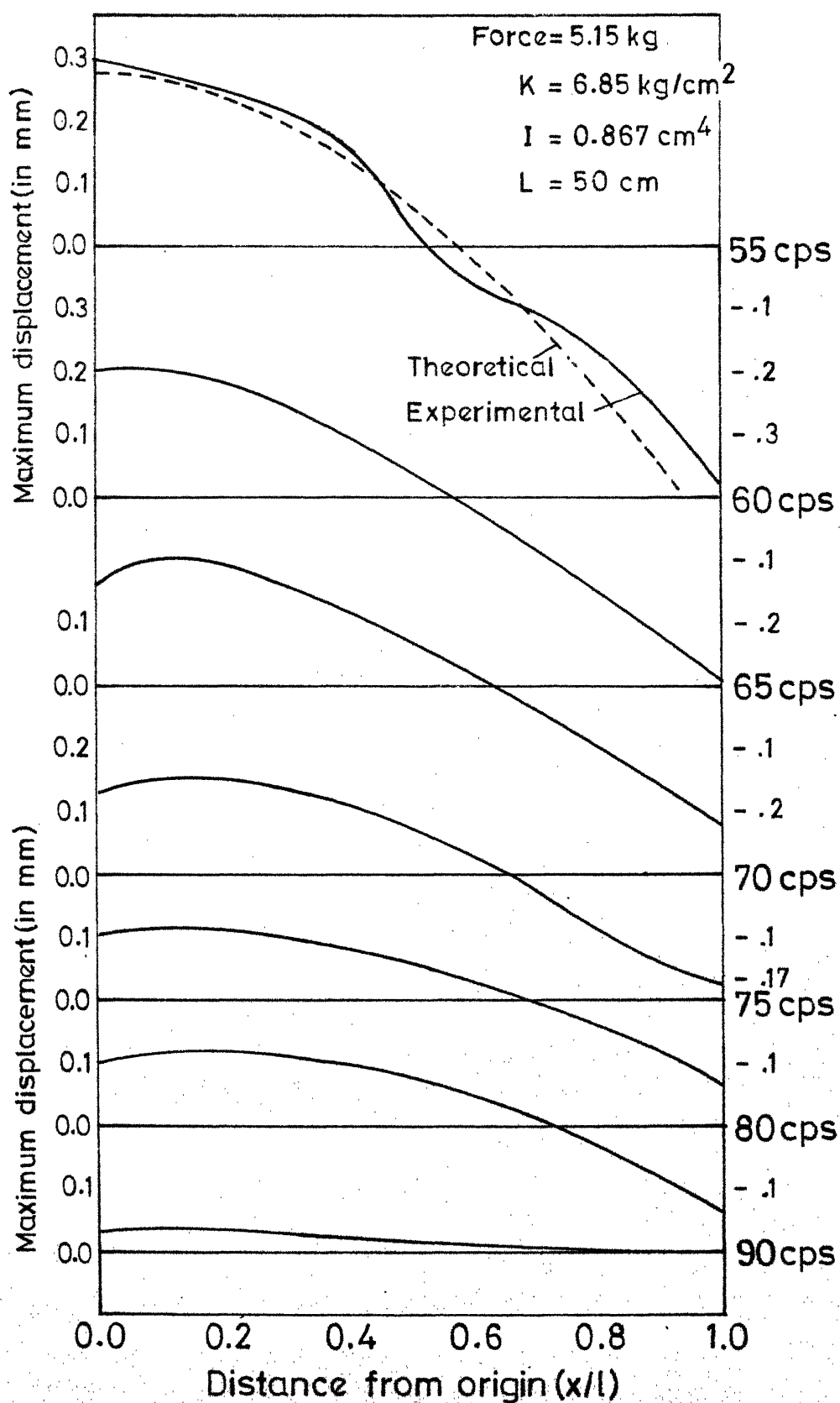


Fig.2.25 Maximum displacement variation along the length of beam at different frequencies for force 5.15 kg.

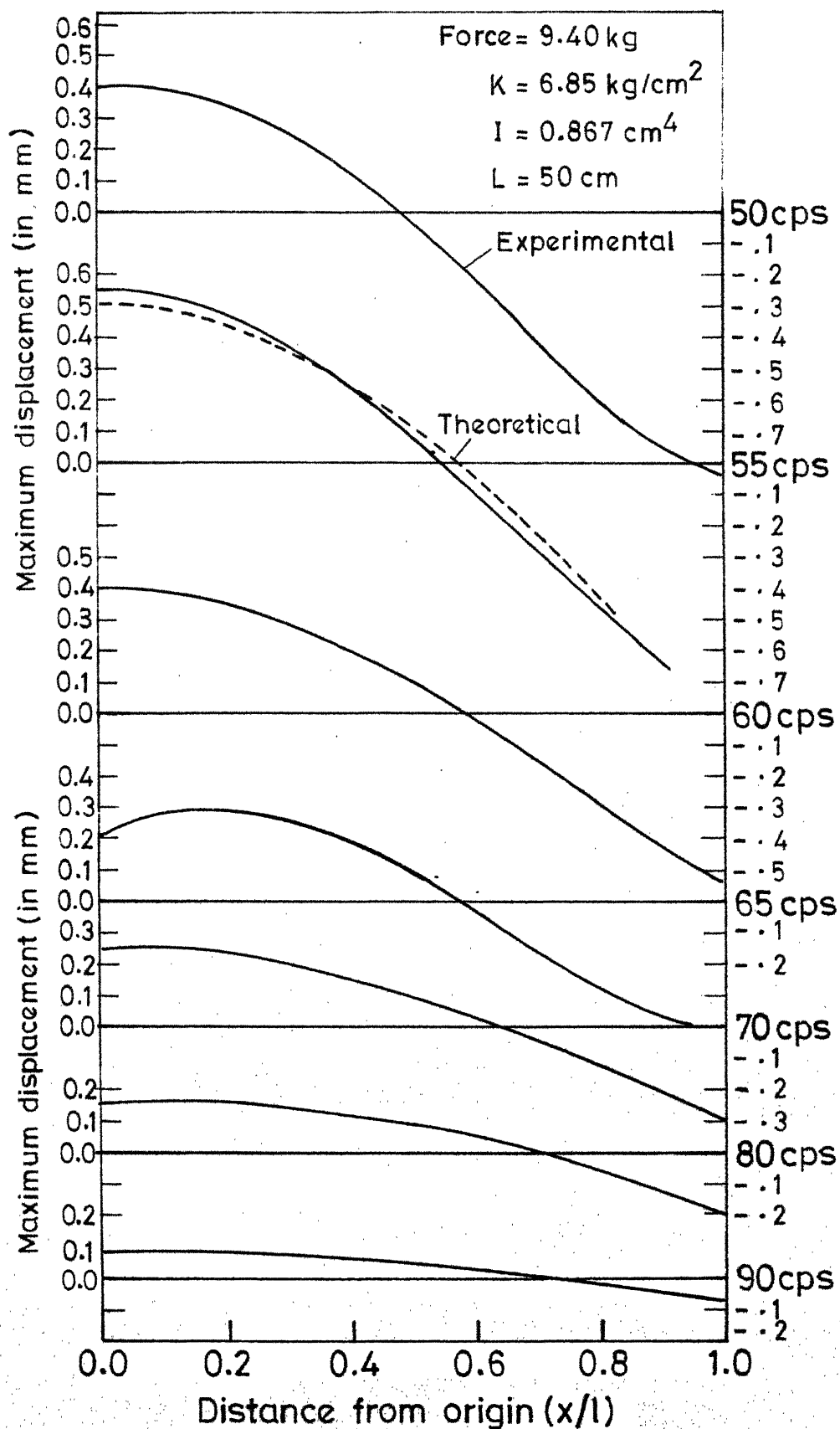


Fig.2.26 Maximum displacement variation along the the length of the beam at different frequencies for force 9.40 kg.

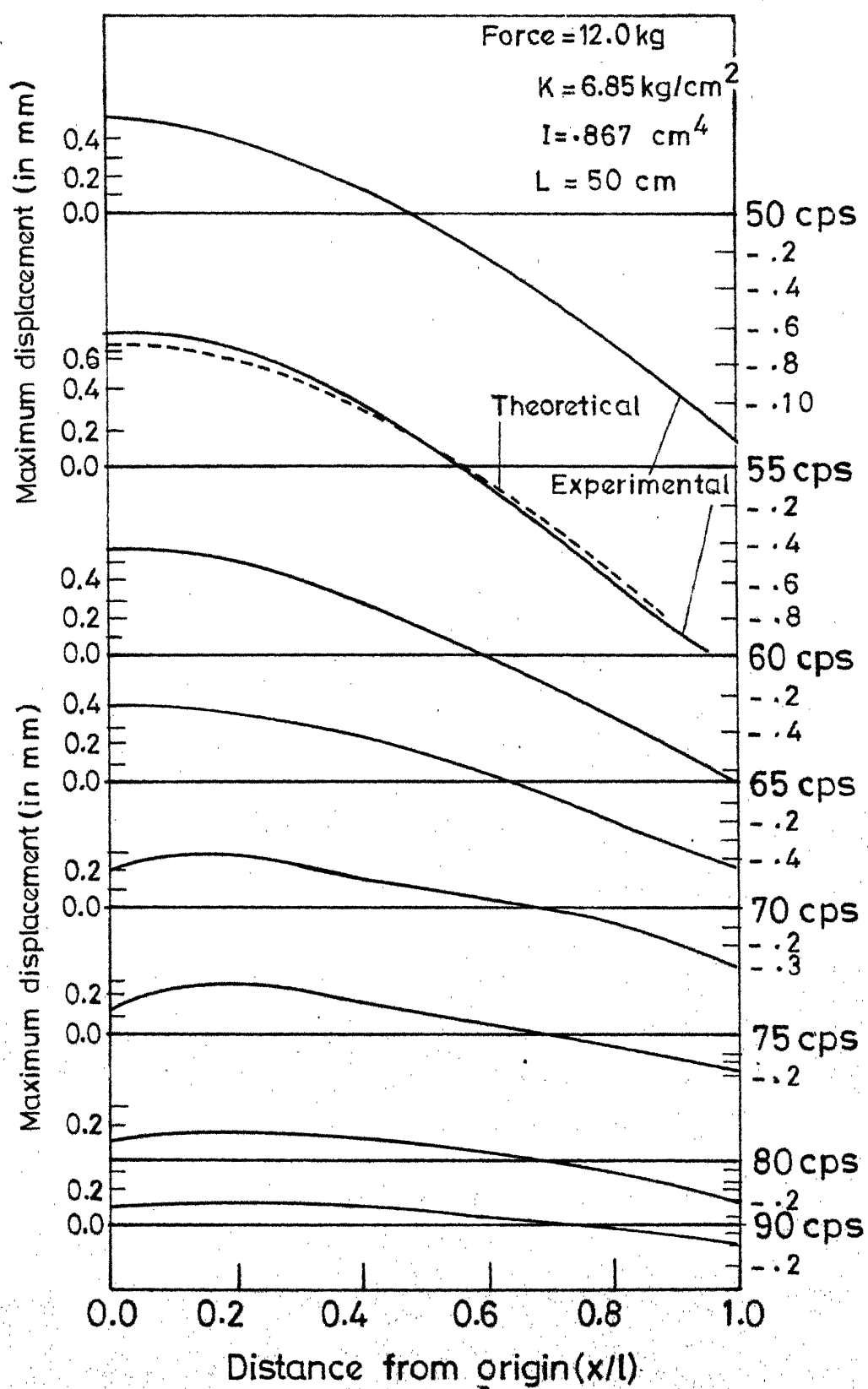


Fig.2.27 Maximum displacement variation along the length of beam at different frequencies for force 12.0 kg.

CHAPTER 3

DYNAMIC RESPONSE OF BEAMS ON ELASTIC FOUNDATION CARRYING A CONCENTRATED MASS

3.1 GENERAL

This chapter deals with the analytical solution of Euler-Bernoulli beam, carrying a concentrated mass attached to it, resting on elastic foundation and subjected to a steady state dynamic force. This problem has a lot of bearing on practical situations. A machine resting on deep beam, a column on strip footing, a mechanical oscillator (to produce a high force oscillation) on footing, for the determination of soil properties, are the few examples which simulate this problem.

In the literature, solutions for beams carrying concentrated mass and simply supported at the ends without foundation are available (12, 2, 15, 49, 22). So far no solution is reported for beams on elastic foundations with concentrated mass attached to it. In this chapter, the equations for displacement of beams with concentrated mass attached to it at the centre of the beam and resting on elastic foundation are developed using the Pasternak foundation model and the Winkler foundation model. The damping in the foundation is included for the analysis. The theory and the results are presented for beams of finite and infinite length.

The general solution for any arbitrary position of concentrated mass on the beam can easily be developed by adding suitable boundary

conditions and continuity conditions in the derivation. However, solutions for beam with concentrated mass at the centre of the beam, resting on Pasternak and Winkler foundation have been dealt here. The results are presented in non-dimensional form and the solutions are compared with existing solutions wherever possible. The theoretical results are also compared with experimental values obtained by conducting experiments on a very large channel, resting on elastic foundation of natural soil deposit and attached with a mechanical oscillator (of considerable mass) at its centre. The oscillator generates a frequency dependent harmonic force.

3.2 GENERAL THEORY

The differential equation of transverse vibration of an Euler-Bernoulli beam on elastic foundation subjected to a dynamic load can be written as -

$$EI \frac{\partial^4 w}{\partial x^4} - G_o \frac{\partial^2 w}{\partial x^2} + Kw + c \frac{\partial w}{\partial t} + \rho A_c \frac{\partial^2 w}{\partial t^2} = q(x,t) \quad (3.2.1)$$

where

E is Young's modulus of elasticity,

I is moment of Inertia of the beam,

G_o is shear modulus of the soil medium,

K is spring constant of the soil medium,

c is damping coefficient of the soil medium,

ρA_c is mass density of the ~~soil medium~~, *beam*.

w is vertical displacement of beam,

EI is modulus of rigidity of beam,

and $q(x,t)$ is dynamic forcing function.

In equation (3.2.1) the soil medium is idealized as a Pasternak foundation model characterized by the foundation constants G_o and K .

Defining the constant and the variables as

$$\lambda = 4\sqrt{\frac{4EI}{K}}, z = \frac{x}{\lambda}, y = \frac{w}{\lambda}, r = \frac{\omega}{\omega_n}, \theta = \omega_n t, c_c = 2\sqrt{K\rho A_c} \quad (3.2.2)$$

$$D = \frac{c}{c_c}, \eta = \sqrt{\frac{4EI}{G_o}}, r\theta = \omega t,$$

where

- λ is the characteristic length,
- z is non-dimensional distance variable,
- y is non-dimensional Displacement variable,
- r is dimensionless forced frequency,
- θ is non-dimensional time variable,
- c_c is critical Damping constant,
- D is damping factor,

and η is characteristic shear value of soil medium.

Equation (3.2.1) can be written in the non-dimensional form as

$$\frac{\partial^4 y}{\partial z^4} - \frac{4\lambda^2}{\eta^2} \frac{\partial^2 y}{\partial z^2} + 4y + 8Dr \frac{\partial y}{\partial \theta} + 4r^2 \frac{\partial^2 y}{\partial \theta^2} = \frac{\lambda^2}{EI} g(z, \theta) \quad (3.2.3)$$

For the unloaded surface of the foundation, outside the finite beam, $q(z, \theta)$ will be zero. Thus the equation of motion of this portion can be written as

$$G_o \frac{\partial^2 w_f}{\partial x^2} - K w_f + c \frac{\partial w_f}{\partial t} = 0 \quad (3.2.4)$$

where w_f is the foundation deflection beyond the length of the beam.

Equation (3.2.4) can be expressed in nondimensional form as

$$\frac{\partial^2 y_f}{\partial z^2} - \frac{\eta^2}{\lambda^2} (1 + 2Dr) y_f = 0 \quad (3.2.5)$$

where y_f is the nondimensional displacement of foundation beyond beam.

The general solution of equation (3.2.5) can be obtained as

$$y_f(z, \theta) = \left[e^{-\frac{\eta}{\lambda}(z)} C_1 \sin 2Dr \frac{\eta}{\lambda} z + e^{-\frac{\eta}{\lambda}(z)} C_2 \sin 2Dr \frac{\eta}{\lambda} z \right] e^{i r \theta} \quad \dots (3.2.6)$$

3.2.1 Boundary Conditions for Finite Beam

Fig. (3.1b) shows a uniform finite beam, supported by a Pasternak foundation, a mass 'M' and a sinusoidal force $F = F_0 e^{i\omega t}$ is concentrated at the middle point. This point is taken as the origin of the coordinates. Because of symmetry, only the right side of the beam is considered. At the origin, the slope of the deflection curve is zero and the total shear force applied is equal to shear force restored. The shear force applied will consist of the steady state constant exciting force $F_0 e^{i\omega t}$ at this point, and the inertia force, due to the concentrated mass M attached at the point. The restoring shear force will be provided by the beam and the shear layer of the Pasternak foundation. In mathematical form, these can be written as

$$\text{at } z = 0 \quad \frac{\partial y}{\partial z} = 0 \quad (3.2.7)$$

$$\text{and } -\frac{EI}{\lambda^2} \left[\frac{\partial^3 y}{\partial z^3} - 4 \frac{\lambda^2}{\eta^2} \frac{\partial y}{\partial z} \right] = -\frac{F_0}{2} + \frac{M}{2} \lambda^2 \omega^2 y$$

$$\text{or } \frac{\partial^3 y}{\partial z^3} - A^2 \frac{\partial y}{\partial z} = + \frac{F_o \lambda^2}{2EI} - 4\alpha R r^2 y \quad \text{at } z = 0 \quad (3.2.8)$$

At the free end of the beam, the bending moment will be zero, deflection of the beam will be equal to deflection of the foundation just away from the beam, and total shear force will be equal to the concentrated foundation pressure. In mathematical form these boundary conditions at the free end can be written as

$$\text{at } z = R \quad \frac{\partial^2 y}{\partial z^2} = 0 \quad (3.2.9)$$

$$y(R) = y_f(R) \quad (3.2.10)$$

$$\text{and } -\frac{EI}{\lambda^2} \left[\frac{\partial^3 y}{\partial z^3} - 4 \frac{\lambda^2}{n^2} \frac{\partial y}{\partial z} \right] = G_o \frac{\partial y}{\partial z}$$

$$\text{or } \frac{\partial^3 y}{\partial z^3} - A^2 \frac{\partial y}{\partial z} = A^2 \frac{\partial y_f}{\partial z} \quad \text{at } z = R \quad (3.2.11)$$

At infinity, the deflection of the free surface of the foundation must vanish. Thus

$$y(f) \rightarrow \infty = 0 \quad (3.2.12)$$

Using these conditions (3.2.7 to 3.2.12), the basic differential equation is solved by Laplace transform.

3.2.2 General Solution for Finite Beam

The general solution of Eq. (3.2.3) can be taken as

$$y(z, \theta) = y(z) e^{i(r\theta - \phi)} \quad (3.2.13)$$

Putting this solution in basic differential equation for homogeneous solution, (3.2.3) yields

$$e^{i(r\theta-\phi)} \frac{\partial^4 y}{\partial z^4} - 4 \frac{\lambda^2}{n^2} \frac{\partial^2 y}{\partial z^2} e^{i(r\theta-\phi)} + 4y e^{i(r\theta-\phi)} + 8 \text{Dir } y e^{i(r\theta-\phi)} + 4(-r^2) e^{i(r\theta-\phi)} y = 0 \quad (3.2.14)$$

After arranging the equation (3.2.14), it can be written as

$$\frac{\partial^4 y}{\partial z^4} - 4 \frac{\lambda^2}{n^2} \frac{\partial^2 y}{\partial z^2} + 4(1 - r^2 + 2\text{Dir})y = 0 \quad (3.2.15)$$

For maximum deflection in a time cycle

$$\mu^4 = \sqrt{(1 - r^2)^2 + (2\text{Dir})^2} \quad (3.2.16)$$

Thus, equation (3.2.15) can be expressed as

$$\frac{\partial^4 y}{\partial z^4} - 4 \frac{\lambda^2}{n^2} \frac{\partial^2 y}{\partial z^2} + 4\mu^4 y = 0 \quad (3.2.17)$$

For the solution, the Laplace transform of equation (3.2.17) can be written as

$$L\left(\frac{\partial^4 y}{\partial z^4}\right) = p^4 \bar{y}(p) - p^3 y(0) - p^2 y'(0) - py''(0) - y'''(0)$$

$$L\left(\frac{\partial^2 y}{\partial z^2}\right) = p^2 \bar{y}(p) - p y(0) - y'(0) \quad (3.2.18)$$

$$L(y) = \bar{y}(p)$$

where $L(F)$ denotes the Laplace transform of the function F

(p) is transform variable.

On putting these transform values in equation (3.2.17) and solving for $\bar{y}(p)$, the resulting expression is

$$\bar{y}(p) = \frac{(p^3 - A^2 p) y(0)}{(p^2 + C_a^2)(p^2 - D_a^2)} + \frac{(p^2 - A^2) y'(0)}{(p^2 + C_a^2)(p^2 - D_a^2)} + \frac{p y''(0)}{(p^2 + C_a^2)(p^2 - D_a^2)} + \frac{y'''(0)}{(p^2 + C_a^2)(p^2 - D_a^2)} \dots \quad (3.2.19)$$

where $A = 2\lambda / \eta$

$$C_a^2 = -\frac{A^2 + \sqrt{A^4 + 4\beta^4}}{2} \quad (3.2.20)$$

$$D_a^2 = A^2 + C_a^2$$

$$\beta = \sqrt{2}\mu$$

Inverting the Laplace transform, equation (3.2.19) can be written as

$$\begin{aligned} y(z) = \frac{1}{C_a^2 + D_a^2} & \left[(C_a^2 \cosh D_a z + D_a^2 \cos C_a z) y(0) + \frac{1}{C_a D_a} (C_a^3 \sinh D_a z + \right. \\ & + D_a^3 \sin C_a z) y'(0) + (\cosh D_a z - \cos C_a z) y''(0) \\ & \left. + \frac{1}{C_a D_a} (C_a \sinh D_a z - D_a \sin C_a z) y'''(0) \right] \quad (3.2.21) \end{aligned}$$

The boundary conditions can, now, be expressed as

$$\text{at } z = 0, \quad \frac{\partial y}{\partial z} = 0 \quad (3.2.7)$$

$$y'''(0) - A^2 y'(0) = -4\alpha Rr^2 y(0) - \frac{F_o \lambda^2}{2EI} \quad (3.2.8)$$

Thus equation (3.2.8) can be written as

$$y'''(0) = -4\alpha Rr^2 y(0) - \frac{F_o \lambda^2}{2EI} \quad (3.2.22)$$

$$y''(R) = 0 \quad (3.2.9)$$

$$y(R) = y_f(R) \quad (3.2.10)$$

$$y'''(R) - A^2 y'(R) = -A^2 y_f'(R) \quad (3.2.11)$$

On solving these boundary conditions, the initial parameters can be obtained as

$$y'''(0) = -4\alpha Rr^2 y(0) - \frac{F_o \lambda^2}{2EI} \quad (3.2.22)$$

$$y''(0) = \frac{F_o \lambda^2}{2EI} \frac{D_a \sinh D_a R + C_a \sin C_a R}{D_a^2 \cosh D_a R + C_a^2 \cos C_a R} + y(0) \left[4\alpha Rr^2 \frac{(D_a \sinh D_a R + C_a \sin C_a R)}{D_a^2 \cosh D_a R + C_a^2 \cos C_a R} - \frac{C_a^2 D_a^2 (\cosh D_a R - \cos C_a R)}{D_a^2 \cosh D_a R + C_a^2 \cos C_a R} \right] \quad (3.2.23)$$

$$y'(0) = 0 \quad (3.2.7)$$

and

$$y(0) = -\frac{F_o \lambda^2}{2EI} \left[\{ 2C_a^3 D_a^3 + C_a D_a (C_a^4 + D_a^4) \cosh D_a R \cos C_a R + C_a^2 D_a^2 (D_a^2 - C_a^2) \sinh D_a R \sin C_a R \} + 2(D_a^2 + C_a^2)(D_a^2 - C_a^2)^{1/2} \{ 1 + (2Dr)^2 \}^{1/2} \right. \\ \left. \frac{(D_a \cosh D_a R \sin C_a R - C_a \sinh D_a R \cos C_a R)}{[C_a^2 D_a^2 (C_a^2 + D_a^2)(D_a^3 \cosh D_a R \sin C_a R + C_a^3 \sinh D_a R \cos C_a R) - C_a D_a \cosh D_a R \cos C_a R (C_a^2 + D_a^2) 2(D_a^2 - C_a^2)^{1/2} \{ 1 + (2Dr)^2 \}^{1/2} - 4\alpha Rr^2 (C_a^2 + D_a^2) 2(D_a^2 - C_a^2)^{1/2} \{ 1 + (2Dr)^2 \}^{1/2} (D_a \cosh D_a R \sin C_a R - C_a \sinh D_a R \cos C_a R) - 4\alpha Rr^2 \{ 2C_a^3 D_a^3 + C_a D_a (C_a^4 + D_a^4) \}]} \right] \quad (3.2.24)$$

As the $y(0)$, $y'(0)$, $y''(0)$, $y'''(0)$ (the initial parameters) are known, the displacement at any point along the length of the beam can be determined using equation (3.2.21).

3.2.3 Slope, Bending Moment, Shear Force and Soil Reaction Expressions for Finite Beam

The expressions for the slope of the deflection curve, the bending moment, shear force and soil reaction for the finite beam on Pasternak foundation can be derived from the displacement equation (3.2.21). These are as follows.

Slope of the deflection curve

$$S(z) = \frac{1}{C_a^2 + D_a^2} \left[C_a D_a (C_a \sinh D_a z - D_a \sin C_a z) y(0) + (D_a \sinh D_a z + C_a \sin C_a z) y''(0) + (\cosh D_a z - \cos C_a z) y'''(0) \right] \quad (3.2.25)$$

Bending moment of beam

$$M(z) = \frac{EI}{\lambda(C_a^2 + D_a^2)} \left[C_a^2 D_a^2 (\cosh D_a z - \cos C_a z) y(0) + (D_a^2 \cosh D_a z + C_a^2 \sin C_a z) y''(0) + (D_a \sinh D_a z + C_a \sin C_a z) y'''(0) \right] \quad (3.2.26)$$

$$\begin{aligned} \text{Shear force } T(z) = \frac{EI}{\lambda^2(C_a^2 + D_a^2)} & \left[C_a^2 D_a^2 (D_a \sinh D_a z + C_a \sin C_a z) y(0) \right. \\ & + (D_a^3 \sinh D_a z - C_a^3 \sin C_a z) y''(0) + (D_a^2 \cosh D_a z \\ & \left. + C_a^2 \cos C_a z) y'''(0) \right] \quad (3.2.27) \end{aligned}$$

$$\begin{aligned}
\text{Soil Reaction } P(z) = & \frac{EI}{\lambda^3 (C_a^2 + D_a^2)} \left[C_a^2 D_a^2 (D_a^2 \cosh D_a z + C_a^2 \cos C_a z) y(0) \right. \\
& + (D_a^4 \cosh D_a z - C_a^4 \cos C_a z) y''(0) \\
& \left. + (D_a^3 \sinh D_a z - C_a^3 \sin C_a z) y'''(0) \right] \quad (3.2.28)
\end{aligned}$$

3.3 FINITE BEAM ON WINKLER FOUNDATION

The solutions for deflections, slope, bending moment, shear force and soil reaction are presented for the finite beam on Winkler foundation. Making the shear coefficient term, A , zero in equation (3.2.1), the differential equation of transverse vibration of the beam, can be written as

$$EI \frac{\partial^4 w}{\partial x^4} + Kw + c \frac{\partial w}{\partial t} + \rho A_c \frac{\partial^2 w}{\partial t^2} = q(x, t) \quad (3.3.1)$$

And in non-dimensional form it can be expressed as

$$\frac{\partial^4 y}{\partial z^4} + 4y + 8Dr \frac{\partial y}{\partial \theta} + 4r^2 \frac{\partial^2 y}{\partial \theta^2} = \frac{\lambda^2}{EI} q(z, \theta) \quad (3.3.2)$$

For free-end beam, the boundary conditions can be listed as

$$\text{at } z = 0, \frac{\partial y}{\partial z} = 0 \quad (3.3.3)$$

$$\text{at } z = 0, \frac{\partial^3 y}{\partial z^3} = -\frac{F_0 \lambda^2}{2EI} + 4\alpha Rr^2 y \quad (3.3.4)$$

$$\text{at } z = R, \frac{\partial^2 y}{\partial z^2} = 0 \quad (3.3.5)$$

$$\text{and } \frac{\partial^3 y}{\partial z^3} = 0 \quad (3.3.6)$$

Assuming the general solution as

$$y(z, \theta) = y(z) e^{i(r\theta - \phi)}$$

and solving equation (3.3.2) for boundary conditions (3.3.3 to 3.3.6), the expression for general solution can be obtained as

$$\begin{aligned} y(z) = & \frac{1}{2} (\cosh \beta z + \cos \beta z) y(0) + \frac{1}{2\beta} (\sinh \beta z + \sin \beta z) y'(0) \\ & + \frac{1}{2\beta^2} (\cosh \beta z - \cos \beta z) y''(0) + \frac{1}{2\beta^3} (\sinh \beta z - \sin \beta z) y'''(0) \\ & \dots \quad (3.3.7) \end{aligned}$$

where

$$y'''(0) = -4\alpha Rr^2 y(0) - \frac{F_o \lambda^2}{2EI} \quad (3.3.8)$$

$$y''(0) = y'''(0) \left[\frac{S(R) U(R) - T^2(R)}{S(R) T(R) - U(R) V(R)} \right] \quad (3.3.9)$$

$$y'(0) = 0 \quad (3.3.10)$$

$$\begin{aligned} y(0) = & -\frac{F_o \lambda^2}{2EI} \frac{T(R) V(R) - S^2(R)}{\left[\beta^3 \{U(R) V(R) - S(R) T(R)\} + 4\alpha Rr^2 \{S^2(R) \right.} \\ & \left. - T(R) V(R)\} \right]} \quad \dots \quad (3.3.11) \end{aligned}$$

Thus the general expressions for displacement of the beam, slope of the deflection curve, bending moment, shear force and soil reaction can be expressed as

$$\begin{aligned} y(z) = & -\frac{F_o \lambda^2}{2EI} \frac{\left[\{V(R) T(R) - S^2(R)\} S(\beta z) + \{S(R) U(R) - T^2(R)\} U(\beta z) \right.} \\ & \left. + \beta^3 \{S(R) T(R) - U^2(R)\} V(\beta z) \right]}{\left[\beta^3 \{S(R) T(R) - U(R) V(R)\} + 4\alpha Rr^2 \{T(R) V(R) - S^2(R)\} \right]} \quad (3.3.12) \end{aligned}$$

Slope of the deflection curve

$$S(z) = V(\beta z)\beta y(0) + S(\beta z) y'(0) + \frac{1}{\beta} T(\beta z) y''(0) + \frac{1}{\beta^2} U(\beta z) y'''(0) \dots (3.3.13)$$

Bending moment

$$M(z) = \frac{EI}{\lambda} \left[\beta^2 U(\beta z) y(0) + \beta V(\beta z) y'(0) + S(\beta z) y''(0) + \frac{1}{\beta} T(\beta z) y'''(0) \right] \dots (3.3.14)$$

Shear force

$$T(z) = \frac{2EI}{\lambda^2} \left[\beta^3 T(\beta z) y(0) + \beta^2 U(\beta z) y'(0) + \beta V(\beta z) y''(0) + S(\beta z) y'''(0) \right] \dots (3.3.15)$$

Soil Reaction

$$P(z) = \frac{2EI}{\lambda^3} \left[\beta^4 S(\beta z) y(0) + \beta^3 T(\beta z) y'(0) + \beta^2 U(\beta z) y''(0) + \beta V(\beta z) y'''(0) \right] \quad (3.3.16)$$

where

$$\begin{aligned} S(\beta z) &= \frac{\cosh \beta z + \cos \beta z}{2} \\ T(\beta z) &= \frac{\sinh \beta z + \sin \beta z}{2} \\ U(\beta z) &= \frac{\cosh \beta z - \cos \beta z}{2} \\ V(\beta z) &= \frac{\sinh \beta z - \sin \beta z}{2} \end{aligned} \quad (3.3.17)$$

3.4 INFINITE BEAM ON PASTERNAK FOUNDATION

The solution for infinite beam can be obtained from the differential equation (3.2.3) by changing the boundary conditions suitably. The solution can be expressed as

$$y(z) = C_1 e^{D_a z} \cos C_a z + C_2 e^{-D_a z} \cos C_a z + C_3 e^{D_a z} \sin C_a z + C_4 e^{-D_a z} \sin C_a z \quad (3.4.1)$$

C_a, D_a are defined by equation (3.2.20).

For infinite beam at $z \rightarrow \infty$, the displacement, slope, Bending moment, shear force will have some finite values, thus the terms containing $e^{D_a z}$ is to be omitted. At $z = 0$, the boundary conditions will be as follows

$$\text{at } z = 0, \quad \frac{\partial y}{\partial z} = 0 \quad (3.4.2)$$

$$\text{and } \frac{\partial^3 y}{\partial z^3} - A^2 \frac{\partial y}{\partial z} = 4 \alpha r^2 y - \frac{F_o \lambda^2}{2EI} \quad (3.4.3)$$

Using these boundary conditions in equation (3.4.1), the solution can be obtained as

$$y(z) = -\frac{F_o \lambda^2}{2EI} \frac{1}{(2C_a D_a (C_a^2 + D_a^2) + 2\alpha r^2 C_a)} \left[C_a e^{-D_a z} \cos C_a z + D_a e^{-D_a z} \sin C_a z \right] \quad \dots \quad (3.4.4)$$

and expressions for other functions can be written as

$$\text{slope } S(z) = -\frac{F_o \lambda^2}{2EI} \frac{(C_a^2 + D_a^2) e^{-D_a z} \sin C_a z}{(2C_a D_a (C_a^2 + D_a^2) + 2\alpha r^2 C_a)} \quad (3.4.5)$$

$$\text{Bending Moment } M(z) = -\frac{F_o \lambda}{2} \frac{(C_a^2 + D_a^2)}{(2C_a D_a (C_a^2 + D_a^2) + 2\alpha r^2 C_a)} \times \left[-D_a e^{-D_a z} \sin C_a z + C_a e^{-D_a z} \cos C_a z \right] \quad (3.4.6)$$

$$\text{Shear force } T(z) = -\frac{F_o}{2} \frac{(C_a^2 + D_a^2)}{\left[2C_a D_a (C_a^2 + D_a^2) + 2\alpha r^2 C_a \right]} \times \left[(D_a^2 - C_a^2) e^{-D_a z} \sin C_a z - 2C_a D_a e^{-D_a z} \cos C_a z \right] \quad \dots (3.4.7)$$

$$\text{and Soil Reaction } P(z) = \frac{\frac{F_o}{2\lambda} \times (C_a^2 + D_a^2)}{\left[2C_a D_a (C_a^2 + D_a^2) + 2\alpha r^2 C_a \right]} \left[-(D_a^3 e^{-D_a z} \sin C_a z + C_a^3 e^{-D_a z} \cos C_a z) + 3C_a D_a (C_a \sin C_a z + D_a \cos C_a z) \right] \quad \dots (3.4.8)$$

3.5 INFINITE BEAM ON WINKLER FOUNDATION

If the shear coefficient A is made zero, then equation (3.4.4) can be modified to give the deflection equation for Winkler foundation.

Thus

$$y(z) = -\frac{F_o \lambda^2}{2EI} \frac{e^{-\beta z} (\cos \beta z + \sin \beta z)}{(4\beta^3 + \alpha r^2)} \quad (3.5.1)$$

$$S(z) = -\frac{F_o \lambda^2}{2EI} \frac{2\beta e^{-\beta z} \sin \beta z}{(4\beta^3 + \alpha r^2)} \quad (3.5.2)$$

$$M(z) = -\frac{F_o \lambda}{2} \frac{2\beta^2 e^{-\beta z} (\cos \beta z - \sin \beta z)}{(4\beta^3 + \alpha r^2)} \quad (3.5.3)$$

$$\dot{T}(z) = + \frac{F_o}{2} \frac{4\beta^3 [e^{-\beta z} \cos \beta z]}{(4\beta^3 + \alpha r^2)} \quad (3.5.4)$$

$$P(z) = - \frac{F_o}{2\lambda} \frac{4\beta^4 e^{-\beta z} [\cos \beta z + \sin \beta z]}{(4\beta^3 + \alpha r^2)} \quad (3.5.5)$$

3.6 RESULTS

The response curves are plotted for displacement, frequency etc. and are presented in dimensionless form. The equations derived for displacement, slope, bending moment, shear force and soil reaction for these two foundation models can be used for the response curves. Various results of the responses are presented below.

3.6.1 Finite Beam on Winkler Foundation

The response curves are plotted in terms of displacement ratio and frequency ratio. Displacement ratio can be defined as the ratio of displacement at any frequency ratio, divided by the displacement at zero frequency ratio. Figs. 3.2 to 3.7 present the displacement-frequency response of finite beam of various lengths, for various values of damping factor and concentrated mass. Some of these figures present the responses at various points along the length of the beam.

Fig. 3.2 presents a typical response of a finite beam of dimensionless length $R = 0.5$, with no concentrated mass attached to it. The response curve is for $z = 0.3$ (dimensionless distance from origin x/l). The variation of displacement with frequency is plotted for various values of damping factor D (0.0, 0.05, 0.10, 0.15). While the maximum displacement

ratio is infinite at resonant frequency for undamped foundation, the maximum displacement becomes finite and decreases with increase in damping factor. The response at higher frequency, approaches the same magnitude of displacement for any damping factor.

The response of a beam of $R = 0.8$ with concentrated mass is quite similar to that in the Fig. 3.2. The response curves shown in Fig. 3.3 are for $z = 0$ and $R = 0.8$. The displacement ratio is infinite for undamped foundation and no concentrated mass attached to the beam. However, when the concentrated mass is attached to the beam, the maximum displacement becomes finite even without damping. The maximum displacement is decreasing with increasing α (concentrated mass ratio). As in the Fig. 3.2, the displacement values tend to approach the same value at higher frequency.

For beam of unit nondimensional length ($R = 1.0$), the displacement at the centre (the point at which the force is applied) of the beam with frequency ratio is plotted in Fig. 3.4. For various values of α (from 0.0 to 0.6), the displacement-frequency response are plotted, taking the value of damping factor equal to 0.1. Maximum displacement can be observed to be decreasing with concentrated mass ratio, just as in Fig. 3.3. The displacement values approach the same value at frequency ratio 2. After that, the displacement decreases fast with higher concentrated mass ratios.

Figs. 3.5, 3.6, 3.7, present the displacement-frequency response for beams of nondimensional lengths $R = 0.6, 0.8, 1.0$ respectively. These

curves are for the case in which the foundation has the damping factor of 0.1 and the value of concentrated mass ratio $\alpha = 0.3$. Each figure shows the displacement-frequency curves at many points along the length of the beam. Maximum displacement occurs at $z = 0$ and with the increase in z , the maximum displacement decreases. At one particular frequency ratio of 1.4, the displacement along the length of the beam can be seen to be the same, whatever be the length of the beam. Beyond this frequency, the displacement increases with z . While the displacement at the centre of the beam decreases with increase in frequency, the displacement at other points on the beam, increases slowly with the increase in frequency. With increase in z , the rate of increase of displacement increases with frequency. For beams of $R = 0.8$ and 1.0, the displacement values, for frequency ratios between 0 to 1.0 are less than the displacement values at frequency ratio 0. For z less than 0.8, the displacement values in this frequency range are always greater than the value at frequency ratio 0.0. For $R = 0.8$ and above, the value of displacement can be seen to increase beyond the resonant frequency ratio.

From these basic response curves, the maximum displacement variation with damping can be plotted for various concentrated mass ratios. Fig. 3.8 shows the variation of maximum displacement with damping, of a finite beam ($R = 0.6$) at its centre for various values of concentrated mass ratio ($\alpha = 0.0, 0.1, 0.2, 0.3$). It can be observed that, with increasing damping, the maximum displacement is decreasing. The rate of decrease is high for the beam with no

concentrated mass attached to it. This rate comes down with α increasing.

Fig. 3.9 shows the maximum displacement variation along the length of the beam resting on Winkler foundation with no damping for various values of concentrated mass ratios ($\alpha = 0.2, 0.3, 0.5, 0.6, 0.7$). As the z increases, the maximum displacement decreases. This decrease is not proportional. For lower values of z , the rate of decrease is small. For the higher values of z , the rate is high. With higher values of α , the rate decrease of maximum displacement is small.

This can be clearly observed from Fig. 3.14. This figure presents the variation of maximum displacement with concentrated mass ratio α . The beam length is $R = 0.8$, and foundation has no damping. The maximum displacement variation at points along the length of the beam has, more or less, the same rate of decrement.

For beams of finite length ($R = 0.5, 0.6, 0.8, 1.0$), resting on Winkler foundation and damping included, ($D = 0.1$), the variation of maximum displacement along the length of the beam for various values of concentrated mass ratio, are shown in Figs. 3.10, 3.11, 3.12, 3.13. It can be observed from these figures that the maximum displacement is decreasing with z increasing. However, the rate of decrease is less in this damped case compared to the undamped case. With increasing concentrated mass ratio α , the rate of decrease of maximum displacement can be seen to be the same.

Figs. 3.15, 3.16, 3.17, 3.18 present the maximum displacement variation with concentrated mass ratio for finite beam of lengths

$R = 0.5, 0.6, 0.8, 1.0$ respectively, resting on Winkler foundation with damping ($D = .1$). The decrease in maximum displacement with concentrated mass ratio is not proportional. As the value of α increases, the rate of decrease becomes small. For different values of z , the rate of decrease of maximum displacement is nearly the same.

It can, again, be observed from these figures that the maximum displacement is increasing as the length of the beam (R) is increasing. Fig. 3.19 presents the variation of maximum displacement at the centre with the dimensionless length of the beam. These curves are plotted for various values of $\alpha(0.1, 0.2, 0.3)$. From the figure, it can be observed that the increase in the maximum displacement is very marginal.

3.6.2 Infinite Beam on Winkler Foundation

For infinite beam on Winkler foundation with damping ($D = 0.1$), a typical displacement frequency response for $\alpha = 0.1$ is shown in Fig. 3.20, for various values of z . The maximum displacement (not the ratio) occurs at the centre of the beam at frequency ratio 1. This maximum displacement decreases along the length of the beam. With increase in concentrated mass ratio, this maximum displacement, again, decreases. Fig. 3.21 shows the variation of maximum displacement with concentrated mass ratio for damped and undamped foundation model. In undamped foundation model, the displacement at resonant frequency is quite high, thus the displacement corresponding to frequency ratio 0.9 is presented in this figure. The decrease in maximum displacement is almost linear. Fig. 3.22 presents the maximum displacement variation

for damped and undamped foundation model of the beam with z values. Out of the two curves, one curve is for the beam not carrying the concentrated mass and the other for beam with concentrated mass attached to it. ($\alpha = 0.1$). As usual, the maximum displacement decreases slowly at lower values of z and then faster at higher values of ' z '.

3.6.3 Infinite Beam on Pasternak Foundation

Using the equation (3.3.12) for infinite beam the response curves for deflection of beam resting on Pasternak foundation are shown in Figs. 3.23 to 3.28 for various cases. Displacement-frequency response curves are presented for varying values of concentrated mass ratio, shear coefficient A of shear layer of Pasternak foundation, damped and undamped cases and at various points along the length of the beam away from the centre.

Fig. 3.23 presents displacement-frequency response of an infinite beam with no concentrated mass on it for damped and undamped cases, at points on the beam away from the centre. The value of shear coefficient A is 1.0. Maximum displacements occur at resonant frequency and is maximum at the centre of the beam. As z increases, the displacement decreases. While in undamped case, the maximum displacement is reasonably high, in damped case, the maximum value is very low.

The displacement ratio is plotted against frequency ratio to present the response curve of an infinite beam resting on Pasternak foundation ($A = 0.5$, $D = 0.1$, $\alpha = 0.0$) in Fig. 3.24. These response curves are for various values of z from the origin. As can be observed from the

figure, the maximum displacement ratio is quite high. The maximum displacement values decrease with increasing z . But this decrement is very small. At other frequency ratios, the displacement values are very close to each other for all the values of z . Only at resonance, there is difference in displacement values.

Figs. 3.25, 3.26, 3.27 present the response curves between displacement ratio and frequency ratio for $\alpha = 0.00, 0.2, 0.4$ respectively, with $D = 0.0$. The response curves have been shown for various values of shear coefficient A . For lower values of shear coefficient, the magnitude of maximum displacement can be seen to be very high. At higher values of shear coefficient, the maximum displacement ratio is low. It can also be observed from these figures, that at frequency ratio 1.4, the displacement ratio is same for any value of shear coefficient A . At higher frequency ratios, the displacement ratio values increase with increasing shear coefficient.

Fig. 3.28 shows a typical set of response curves for foundation having damping ratio 0.1. With shear coefficient increasing, maximum displacement ratio decreases very fast. It can again be observed that the displacement ratio at the frequency ratio 1.4 is the same for any value of shear coefficient as in the undamped case. The displacement ratio values are higher for higher values of shear coefficient at higher frequencies.

Variation of maximum displacement ratios with concentrated mass ratios for various values of shear coefficients are plotted in Fig. 3.29

for $D = 0.1$. It can be observed, that the maximum displacement ratio decreases with higher values of concentrated mass. But as the shear coefficient becomes high, the effect of higher concentrated mass on maximum displacement is less. For $A = 1.0$, the maximum displacement decreases reasonably with concentrated mass ratio. For $A = 3.0$, there is hardly any decrease in maximum displacement ratio with α .

Maximum displacement along the length of the beam decreases, as can be seen from Fig. 3.30. Response curves are plotted for various values of shear coefficients. The beam is attached with a concentrated mass of value $\alpha = 0.1$. Foundation has the damping $D = 0.1$. The rate of decrease of maximum displacement for z values is nearly same, but the reduction in the maximum displacement is quite high with higher shear coefficient.

In figure 3.31, curves are drawn showing variation of maximum displacement of the centre point of the beam with shear coefficient A . These curves include the cases of undamped and damped foundation and $\alpha = 0.0$, and 0.2 . The maximum displacement decreases very fast for undamped and damped cases. The maximum displacement for undamped case is higher than for damped case. Above shear coefficient value $A = 2.0$, the maximum displacement for damped and undamped case become almost equal. The effect of concentrated mass is appreciable at lower values of shear coefficient.

3.6.4 Finite Beam on Pasternak Foundation

The response curves of a finite beam on Pasternak foundation can be drawn, using the deflection equations (3.2.24). Figs. 3.32 and 3.33

present the displacement frequency response curves for various values of concentrated mass ratio. The beam is free at the ends and the concentrated mass is attached at centre of the beam. A sinusoidal force is applied at this point. The nondimensional length of the beam is 0.7071. The results are plotted for damped and undamped cases.

Fig. 3.32, presents the displacement-frequency response curves for damped and undamped cases for beam resting on Pasternak foundation. For $A = 0$, the foundation will reduce to Winkler model. The response for $A = 0$ is compared with the response for $A = 1.4141$. While for $A = 0$, the maximum deflection occurs at frequency ratio 1.0, for $A = 1.4141$, the resonant frequency shifts from 1 to 1.3. Rades' solution gives the same response for $R = 0.7071$ and $A = 1.4141$.

In Fig. 3.33, Displacement response curves are drawn for shear coefficient $A = 1.4141$, damping factor $D = 0.1$. These displacement values are at the centre of the beam. As in Fig. 3.32, the maximum displacement occurs at frequency ratio of 1.3. With increasing concentrated mass ratio, the maximum displacement decreases. At higher frequency ratios, the values of displacement decrease and for any value of α , these are nearly equal.

The responses were calculated for shear coefficient values of 0.5 and 0.7071 also. The variation of maximum displacement is shown in Fig. 3.34 for $\alpha = 0.0, 0.1, 0.2$ for various values of shear coefficient A . The rate of decrease in maximum displacement of the beam with no concentrated mass is small at lower shear coefficient values. At higher

values of A , the rate increases. As the concentrated mass on the beam increases, the rate of decrease tends to be uniform.

Fig. 3.35 shows the variation of maximum displacement along the length of the beam for $R = 0.7071$, $\alpha = 0.1$ and $D = 0.1$. With ' z ' increasing, the maximum amplitude can be seen to be decreasing. The rate of decrease for different values of A seems to be similar.

The general trend in the variation of maximum displacement with other variables for finite beam is similar as was observed for the infinite beam on Pasternak foundation.

3.7 VERIFICATION OF SOLUTIONS AND RESULTS

In this section, the general solution for beam carrying concentrated mass at its centre and resting on elastic foundation is compared with the existing solutions for beam, resting on Pasternak foundation and beams carrying concentrated mass, simply supported at the ends. The analytical results of the solutions are compared with experimental values, obtained by conducting the experiments on a long beam with concentrated mass attached to it and resting on the soil medium.

3.7.1 Verification of General Solutions

The displacement expression for beams on Pasternak foundation and Winkler foundation are given by equations (3.2.24), (3.3.11). If the concentrated mass term α is made zero, these expression will be as follows.

The displacement equation for beam on Pasternak foundation is,

$$\begin{aligned}
 & - \frac{F_o \lambda^2}{2EI} \left[2C_a^3 D_a^3 + C_a D_a (C_a^4 + D_a^4) \cosh D_a R \cos C_a R + C_a^2 D_a^2 (D_a^2 - C_a^2) \times \right. \\
 & \left. \sinh D_a R \sin C_a R + 2 (D_a^2 + C_a^2) (D_a^2 - C_a^2)^{1/2} \right] \\
 y(0) = & \frac{(1 + (2Dr)^2)^{1/2} (D_a \cosh D_a R \sin C_a R - C_a \sinh D_a R \cos C_a R)}{\left[C_a^2 D_a^2 (C_a^2 + D_a^2) (D_a^3 \cosh D_a R \sin C_a R + C_a^3 \sinh D_a R \cos C_a R) \right.} \\
 & \left. - \cosh D_a \cos C_a R (C_a^2 + D_a^2)^2 2 (D_a^2 - C_a^2)^{1/2} (1 + (2Dr)^2)^{1/2} \right] \\
 & \dots (3.7.1)
 \end{aligned}$$

and the displacement equation for beam on Winkler foundation is

$$\begin{aligned}
 & \left[\frac{1}{4} (\sinh \beta R + \sin \beta R) (\sinh \beta R - \sin \beta R) - \frac{1}{4} (\cosh \beta R \right. \\
 & \left. + \cos \beta R)^2 \right] \\
 y(0) = & \frac{F_o \lambda^2}{2EI} \frac{\left[\beta^3 \left\{ \frac{1}{4} (\cosh \beta R - \cos \beta R) (\sinh \beta R - \sin \beta R) - \right. \right.}{\left. \left. \frac{1}{4} (\cosh \beta R + \cos \beta R) (\sinh \beta R + \sin \beta R) \right\} \right]}{\dots (3.7.2)}
 \end{aligned}$$

The same (Eq. (3.7.2)) can be simplified as

$$y(0) = \frac{F_o \lambda^2}{2EI \beta^3} \frac{[1 + \cosh \beta R \cos \beta R]}{[\cosh \beta R \sin \beta R + \sinh \beta R \cos \beta R]} \dots (3.7.3)$$

Rades (40) has presented the solution of Euler-Bernoulli beam of finite length on Pasternak foundation and subjected to steady state dynamic force. The deflection expression for beam is given by

$$y(0) = -\frac{F_0 L^2 + 2\bar{\mu}^2 \bar{\lambda}^2 - \gamma(\bar{\mu}^4 - \bar{\lambda}^4)(\bar{\lambda} \cosh \bar{\lambda} \sin \bar{\mu} - \bar{\mu} \sinh \bar{\lambda} \cos \bar{\mu})}{2EI \left[\bar{\mu}^2 \bar{\lambda}^2 (\bar{\mu}^2 + \bar{\lambda}^2)(\bar{\lambda}^3 \cosh \bar{\lambda} \sin \bar{\mu} + \bar{\mu}^3 \sinh \bar{\lambda} \cos \bar{\mu}) - \gamma \bar{\lambda} \bar{\mu} (\bar{\lambda}^2 - \bar{\mu}^2)(\bar{\mu}^2 + \bar{\lambda}^2)^2 \cosh \bar{\lambda} \cos \bar{\mu} \right]} \quad (3.7.4)$$

where

F_0 = Force applied

$$\bar{\lambda} = (2m^2 + 2(m^4 + n^4)^{1/2})^{1/2}$$

$$\bar{\mu} = (-2m^2 + 2(m^4 + n^4)^{1/2})^{1/2}$$

$$m = \left(\frac{G L^2}{4EI}\right)^{1/2}, \quad n = \left(\frac{K L^4}{4EI}\right)^{1/4} (1-r^2)^{1/4}$$

$$\gamma = \left(\frac{K L^2}{G}\right)^{1/2}$$

For Winkler foundation, the expression is given by

$$y_0 = \frac{-F_0 L^2 (\cosh \xi \cos \xi + 1)}{2EI \xi^3 (\cosh \xi \sin \xi + \sinh \xi \cos \xi)} \quad (3.7.5)$$

Term C_a, D_a in the expression (3.7.2) are corresponding to $\bar{\mu}, \bar{\lambda}$ respectively.

Damping is zero in Rades equation and γ corresponds to

$$\gamma = \frac{2}{(D_a^2 - C_a^2)^{1/2}} \quad (3.7.6)$$

Equation of beam on Winkler foundation (3.7.3) is same as equation (3.7.5). The term ξ is equivalent to βR . Thus the general solution of a finite beam carrying a concentrated mass on Pasternak foundation boils down to Rades equation (40) if the concentrated mass ratio α is made zero.

The general solution of the beam with concentrated mass can be derived for other boundary conditions. The solution of the beam deflection and frequency of simply supported beam carrying a concentrated mass at its centre is presented by Das and Deshmukh (15). In the derivation, the effect of rotary inertia and shear of the beam are also taken into account. If the rotary inertia and shear effect is neglected, the frequency equation can be written as

$$2 = \frac{M}{m} \frac{b}{2} (\bar{\beta} \tan \frac{b\bar{\beta}}{2} - \bar{\beta} \tanh \frac{b\bar{\beta}}{2}) \quad (3.7.7)$$

where M is concentrated mass attached to the beam and

$$b = \sqrt{\frac{\rho A_c}{EI}} L^2 \omega^2$$

$$\bar{\beta} = \frac{1}{\sqrt{b}} .$$

Simplification of Eq. (3.7.7) gives

$$(\tan \frac{\sqrt{b}}{2} - \tanh \frac{\sqrt{b}}{2}) \frac{M}{2 \rho A_c} \sqrt{b} = 4 \quad (3.7.8)$$

The general solution for beam on Winkler foundation is given by equation (3.3.7). For boundary conditions of simply supported case, this solution can be used to derive frequency equation.

Boundary conditions are

$$\text{at } z = 0 ; \frac{\partial y}{\partial z} = 0, \frac{\partial^3 y}{\partial z^3} = 4\alpha R r^2 y$$

and at $z = R ; y = 0,$

$$\frac{\partial^2 y}{\partial z^2} = 0$$

(3.7.9)

The frequency equation can be written as

$$y(0) (\cosh \beta R + \cos \beta R)(\sinh \beta R + \sin \beta R) + y'''(0) \frac{1}{2\beta^2} (\cosh \beta R - \cos \beta R) \\ (\sinh \beta R + \sin \beta R) + \frac{y'''(0)}{2\beta^3} (\sinh^2 \beta R - \sin^2 \beta R) = 0 \quad (3.7.10)$$

If there is no foundation below the beam, then $\beta = r$. Solving equation (3.7.10) for boundary conditions (3.7.9) it yields,

$$M\omega^2 (\tanh rR - \tan rR) + 4EI r^3 = 0 \\ \text{or } (\tan rR - \tanh rR) \frac{M\omega^2}{4EI r^3} = 4 \quad (3.7.11)$$

where $rR = \frac{\sqrt{b}}{2}$, and $\frac{M\omega^2}{4EI r^3} = \frac{M}{2\rho A_c} \sqrt{b}$

Equation (3.7.11) and (3.7.8) can be seen to be identical.

3.7.2 Verification of Results with Experimental Values

Field experiments have been conducted to verify the analytical results. A line diagram showing the experimental set up is shown in Fig. 3.36.

3.7.2.1 Experimental set up

Fig. 3.36(a) shows the line diagram of a channel section, 10.0 m long resting on the natural soil deposit. The mechanical oscillator (Saraswati SEA 350) was fixed at the centre of the beam. This mechanical oscillator, which acted as a concentrated mass attached at the centre, was producing frequency dependent sinusoidal force. A variable speed motor

was connected through a flexible shaft to drive the oscillator. Fig. 3.36(b) the block diagram of test set up. The variable speed motor runs the oscillator. The magnitude of the force level was controlled by changing the eccentricity of the rotating mass on the shaft of the oscillator and the frequency was varied by changing the speed of variable speed motor. The amplitudes of maximum dynamic displacement at the centre and the points along the length of the beam were measured through a system of vibration Pickups (MB 126,127) and vibrationmeter (MB 737). The oscilloscope was used for the visual check of the forcing function. The Pickups used in this experiments were the velocity type. In this, the voltage induced in the coil is directly proportional to the relative velocity between the coil and the magnetic field. The signal from this pickup was fed into vibrationmeter which is essentially a voltage meter calibrated to indicate the voltage in terms of the velocity of vibration system. The displacement and acceleration could be measured as the vibration meter had an integrating circuit and a differentiating circuit. A brief description of the oscilloscope is given in Chapter 2. In this test, the mechanical oscillator was tightly fixed to the beam (channel section). This oscillator utilizes the centrifugal force of unbalanced eccentric masses to generate a harmonic force. Two shafts with equal eccentric mass and rotating in opposite direction and when in phase, produce a vertical sinusoidal force. With the increase in speed of rotation the magnitude of force also increases.

The oscillator which has the total weight 75.4 kg, was attached with beam at the centre, firmly. The beam data are shown in Fig. 3.36.

The spring constant of the soil was 525 kg/cm^2 and the concentrated mass ratio $\alpha = 0.34$.

The tests were run for three different phase angles of eccentric mass ($\phi = 40^\circ, 55^\circ, 70^\circ$). The speed was varied from 600 rpm to 1400 rpm. The displacement and the velocity were measured at the centre and points along the length of beam at 1 m interval. For each eccentricity, the tests were repeated a number of times and average of readings were noted. The values of velocity were recorded for cross check.

3.7.2.2 Results and Discussion

Fig. 3.37 presents the magnitude of displacements with increase in frequency for various phase angles ($40^\circ, 55^\circ, 70^\circ$), at the centre of the beam. While the rate of increase of magnitude of displacement is slow for phase angles $40^\circ, 55^\circ$ the increase for 70° phase angle is quite rapid. The variation of maximum displacement along the length of the beam is presented in Fig. 3.38. As in the previous figure, curves are drawn for 3 phase angles of eccentric masses ($\phi = 40^\circ, 55^\circ, 70^\circ$). Beyond $x = 0.8$, the displacements have been observed to be negligible. It can be observed from the figure that maximum displacement decreases very fast with distance. For $\phi = 70^\circ$, the amplitude of deflection is very high compared to other values of phase angles ($\phi = 40^\circ, 55^\circ$).

Fig. 3.39, presents the theoretical results for the beam resting on the soil medium, as described above. The curves are drawn for $\alpha = 0$ and $\alpha = 0.34$, and force levels of 274 kg and 210 kg. While the

experimental curves are for frequency dependent force, the theoretical responses are for constant force excitation. Solid lines present the theoretical curve for $\alpha = 0.34$, the dotted lines are experimental curves. For experimental curves, the force is frequency dependent. Thus at points (A) and (B) in Fig. 3.39, the force level of theoretical and experimental results are same. From these points, it can be observed that the experimental values of displacements are quite close to theoretical values.

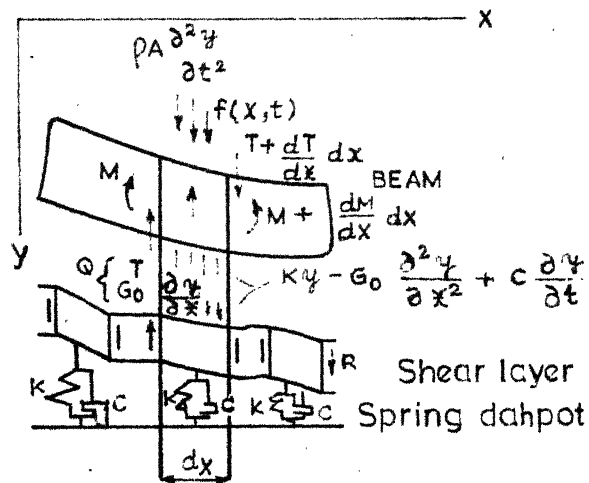


Fig.3.1(a) A beam element on Pasternak foundation

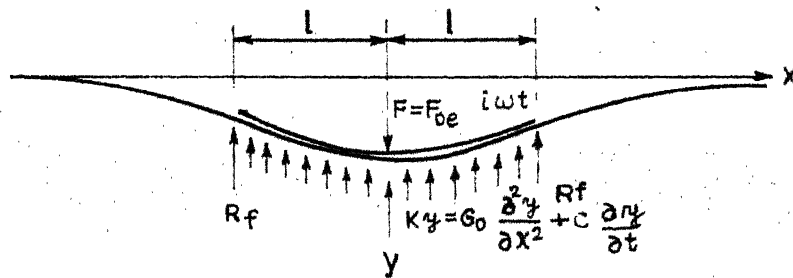


Fig.3.1(b) A uniform beam on Pasternak foundation

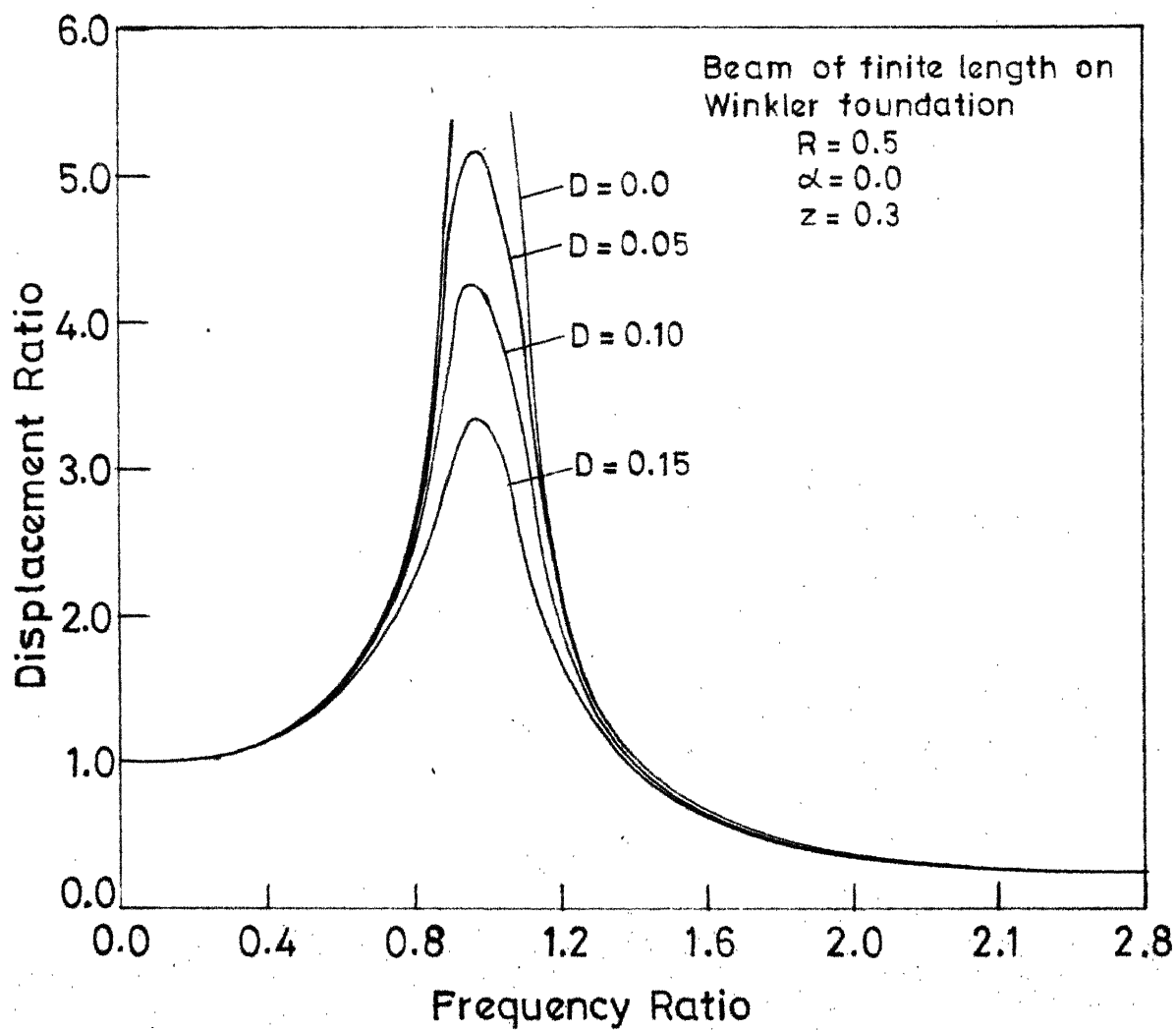


Fig. 3.2 Displacement frequency response curves for beam on Winkler foundation

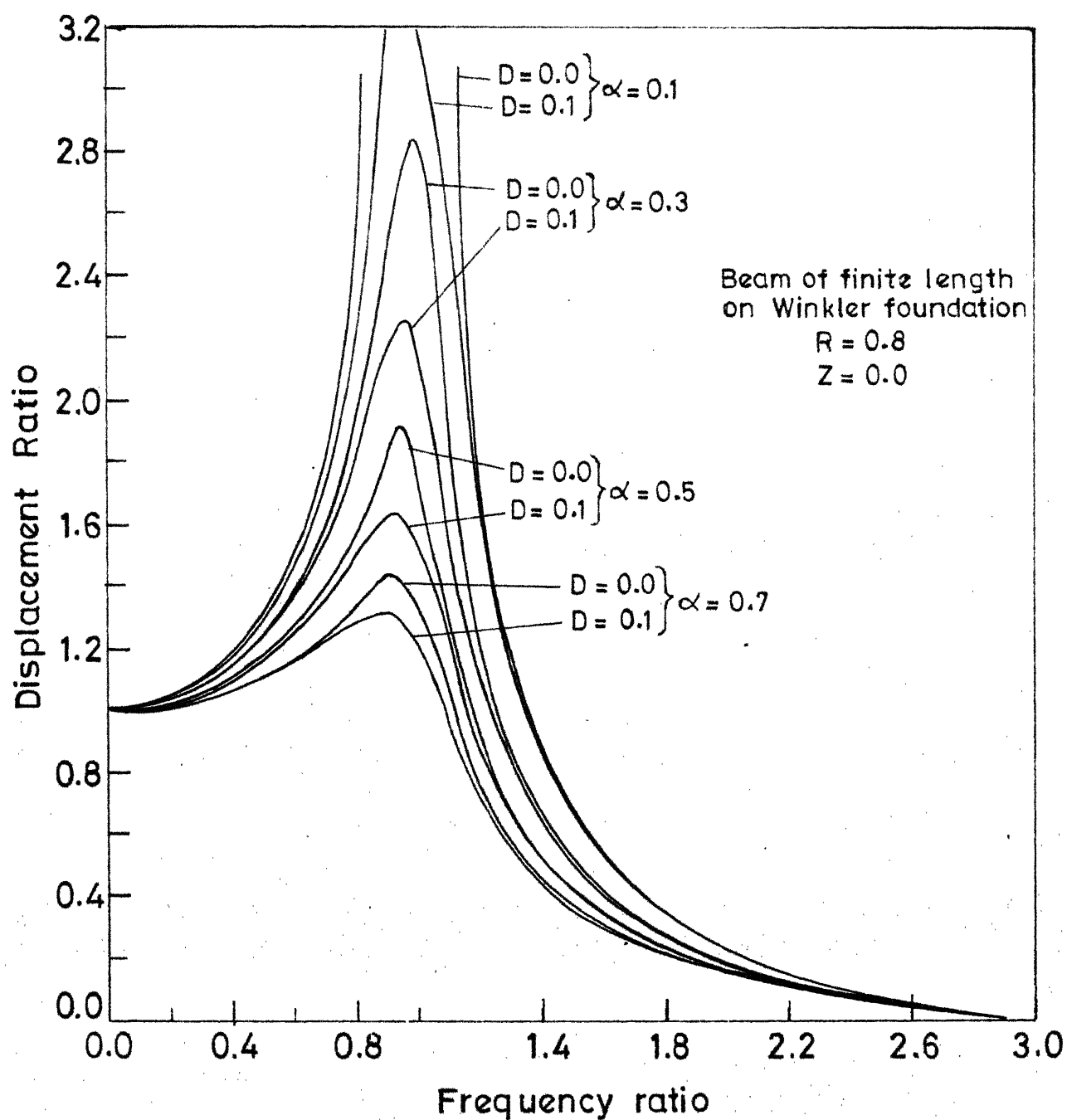


Fig.3.3 Displacement response curve for beam with concentrated mass at the centre of beam resting on Winkler foundation

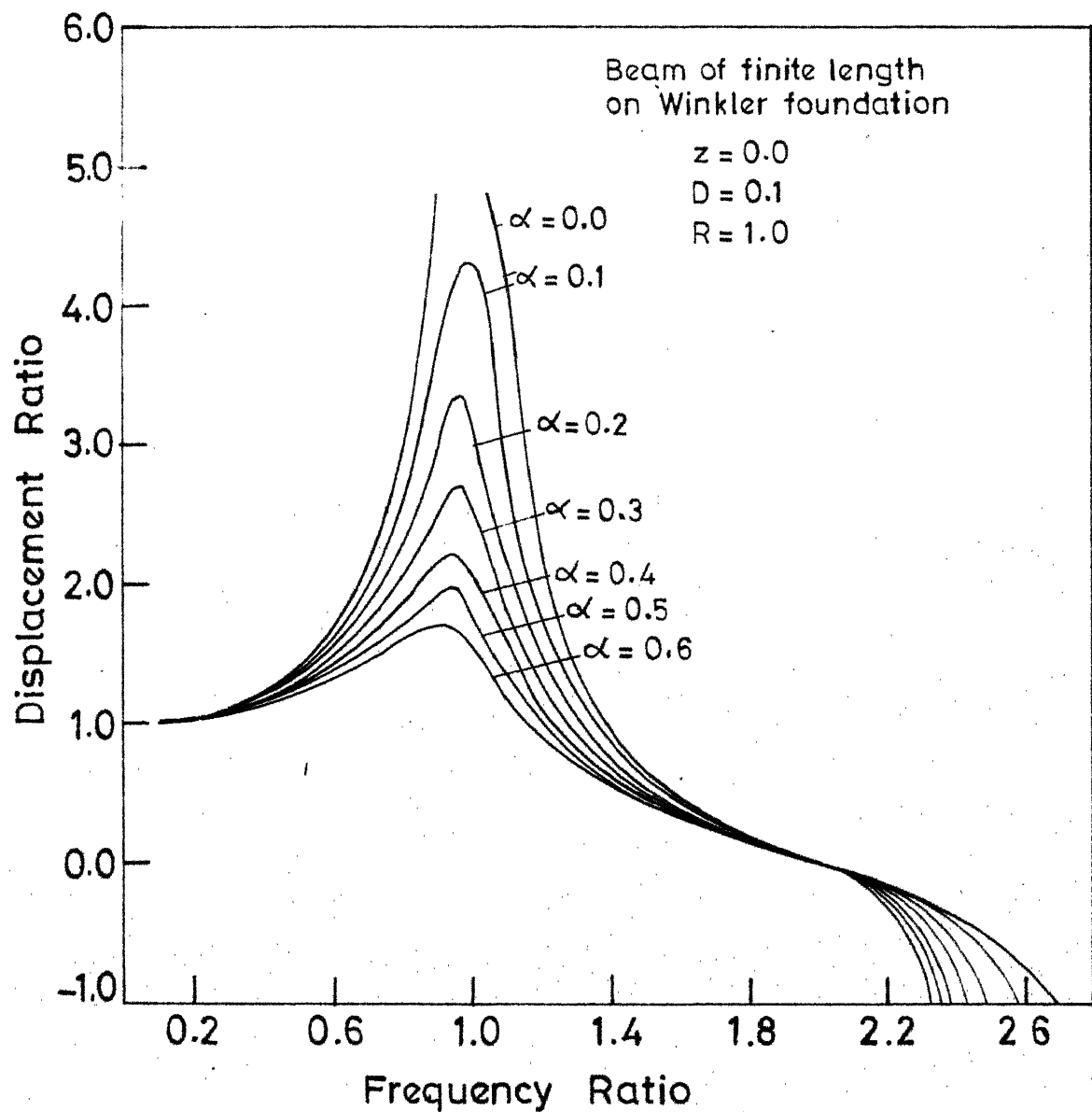


Fig.3.4 Displacement frequency response for beam with concentrated mass and resting on Winkler foundation ($R=1.0$)

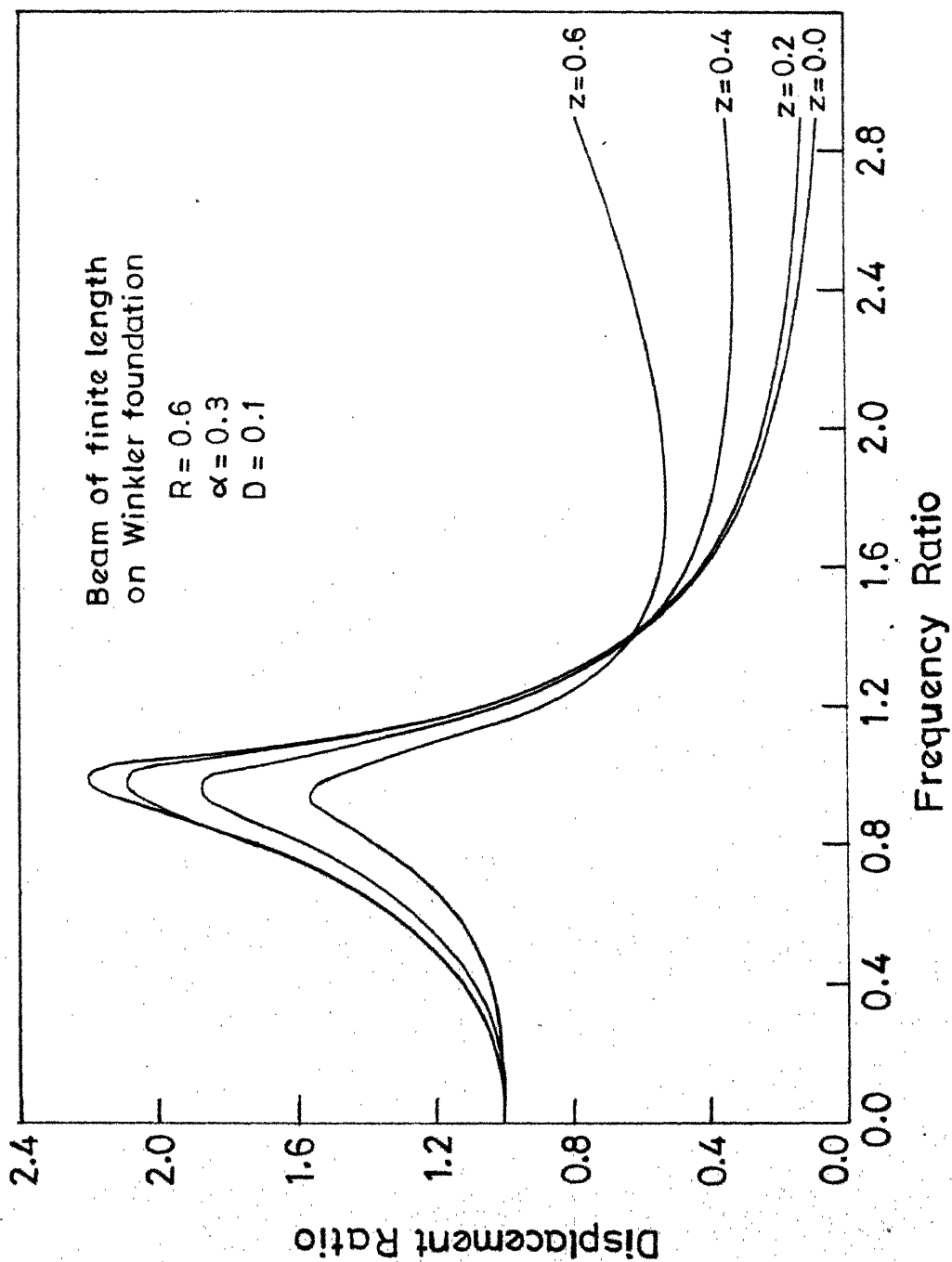


Fig.3.5 Displacement frequency responses at various points along the length of beam ($R=0.6$)

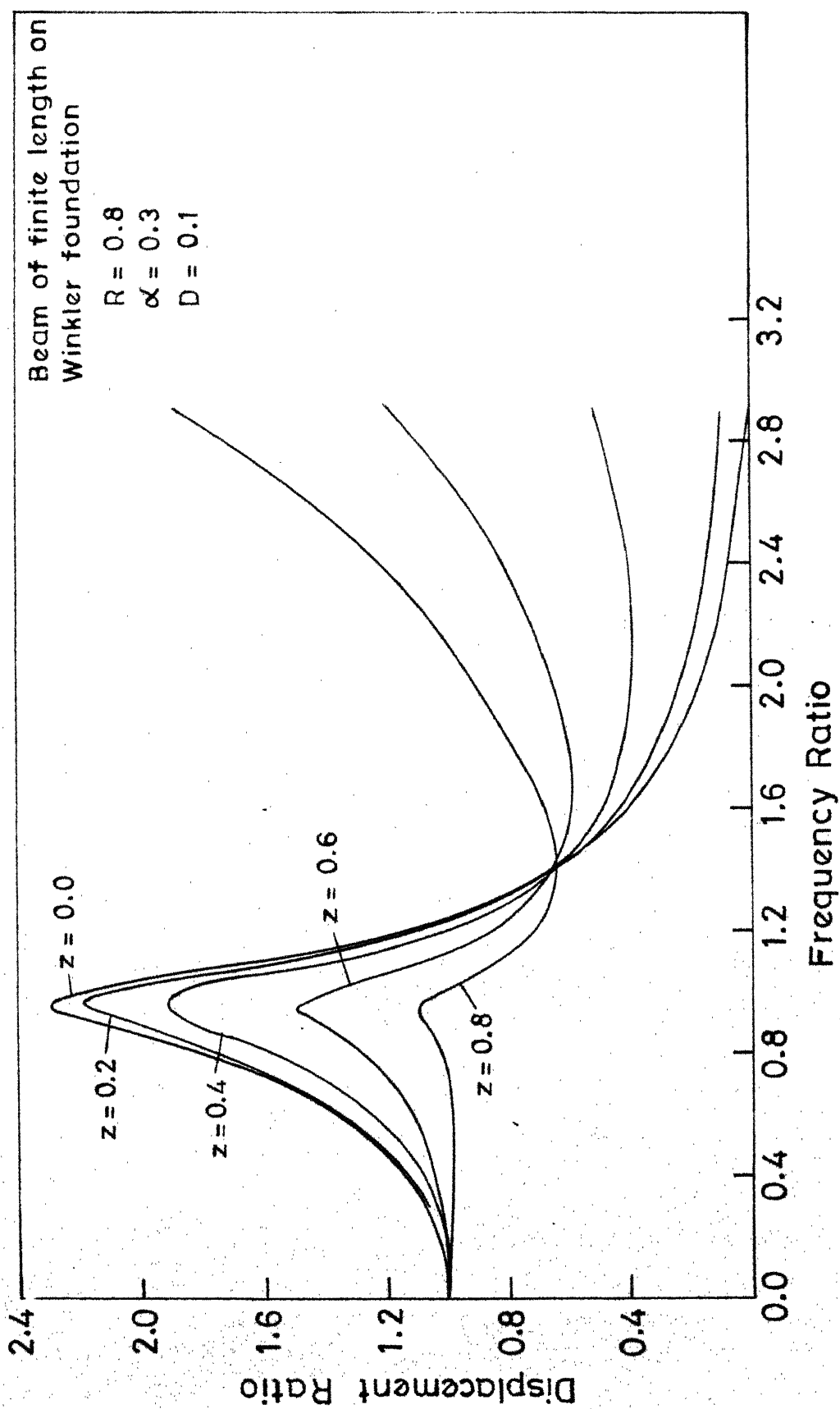


Fig.3.6 Displacement frequency response at various points along the length of beam ($R = 0.8$)

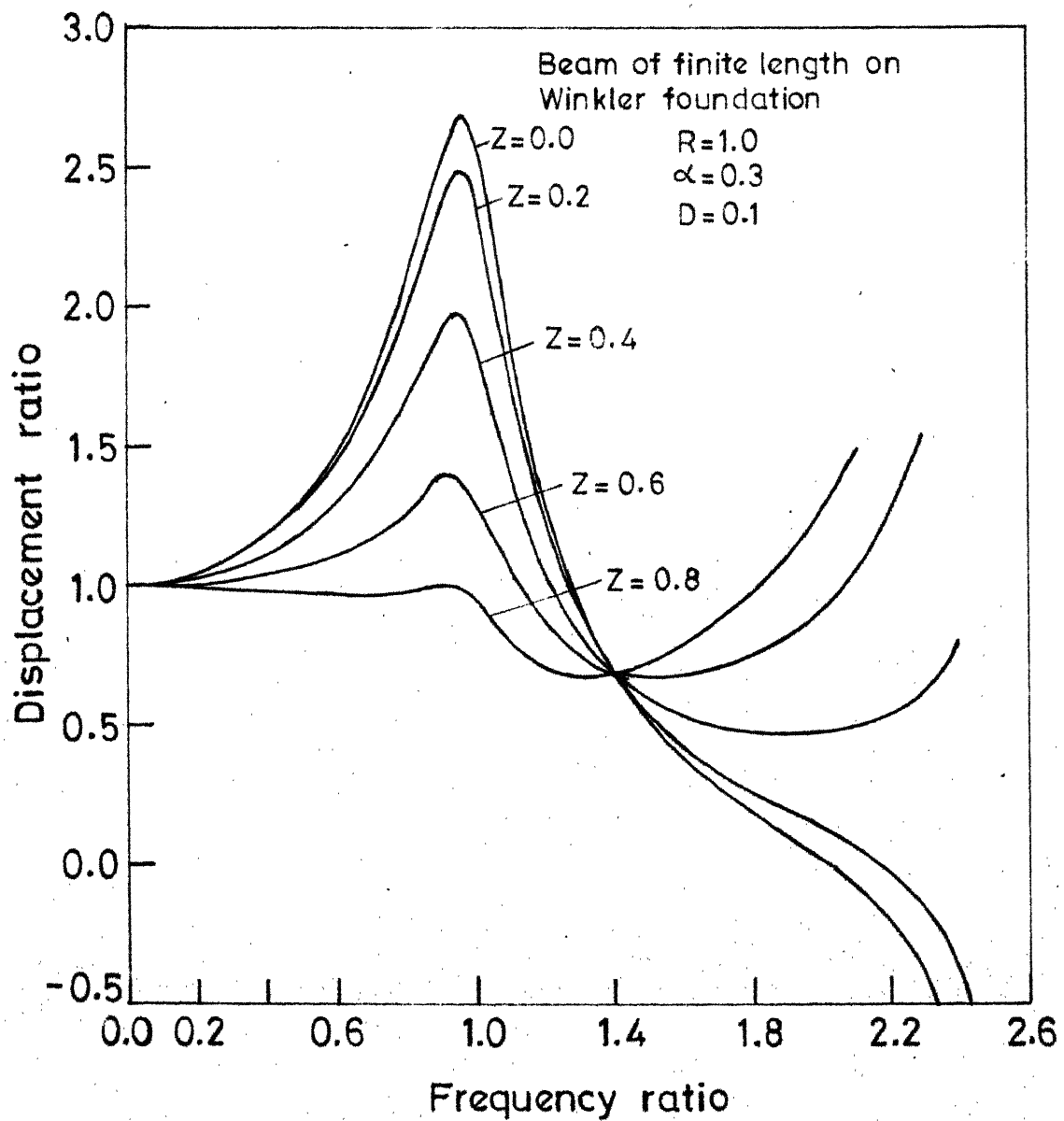
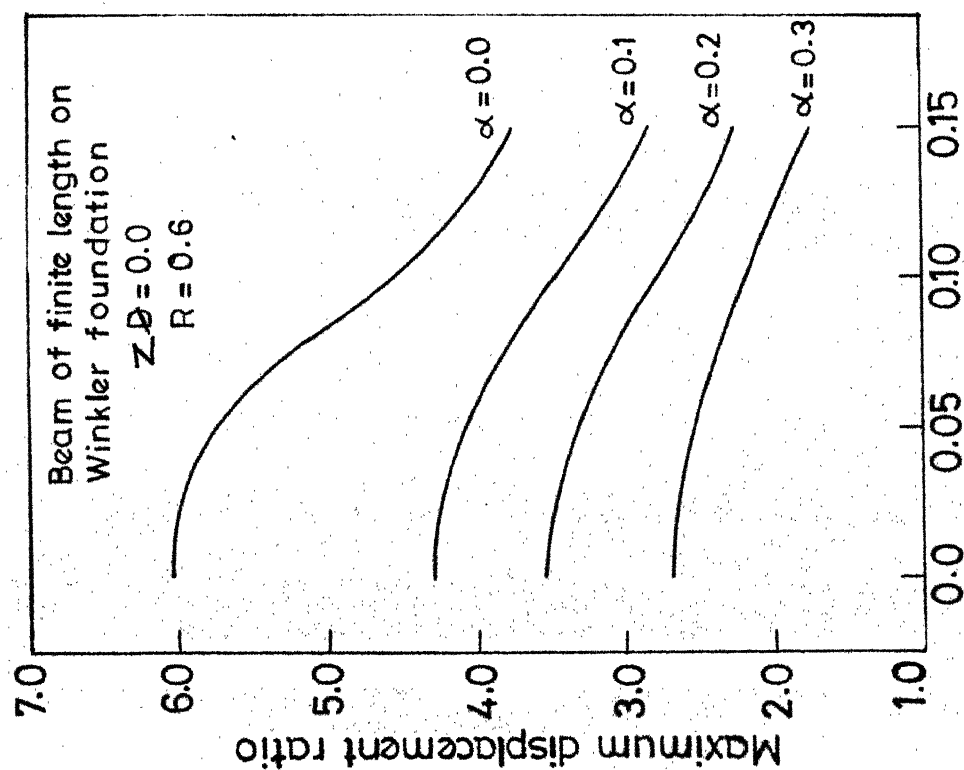
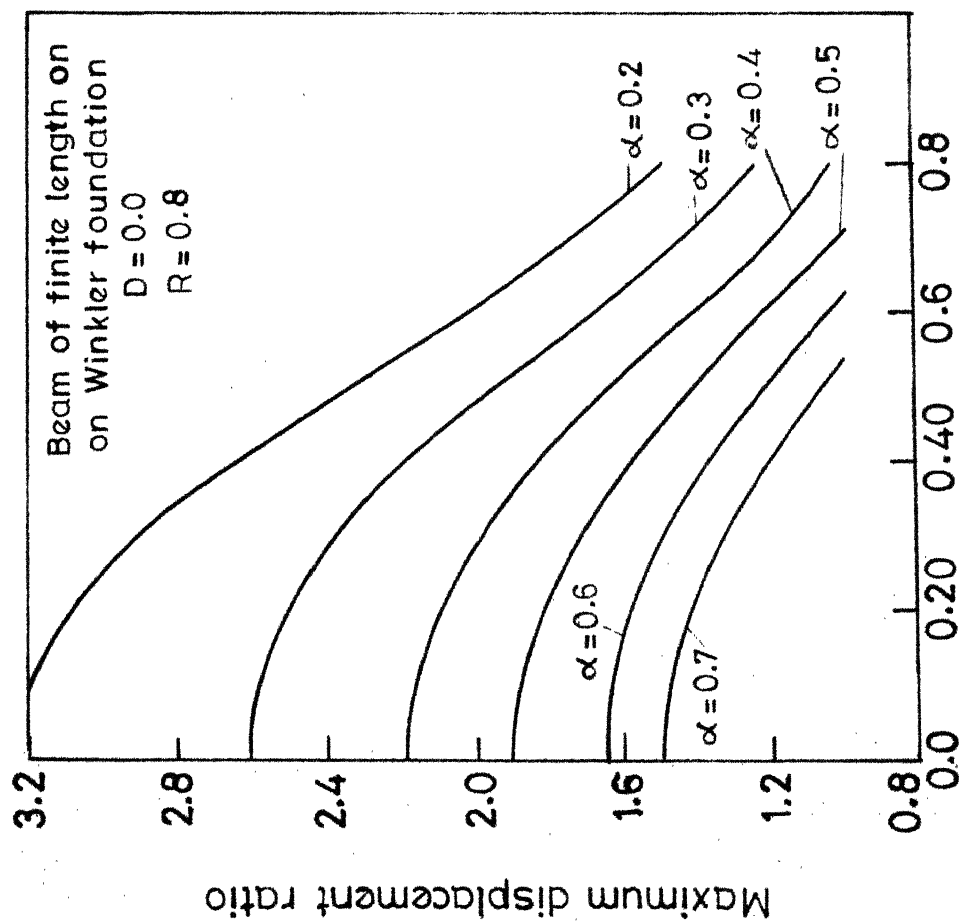


Fig.3.7 Displacement frequency response at various points along the length of beam ($R=1.0$)



Damping factor D

Fig.3.8 Variation of maximum displacement with damping factor for various concentrated mass ratio.



Distance from origin (x/l)

Fig.3.9 Displacement variation along the length of the beam for undamped case.

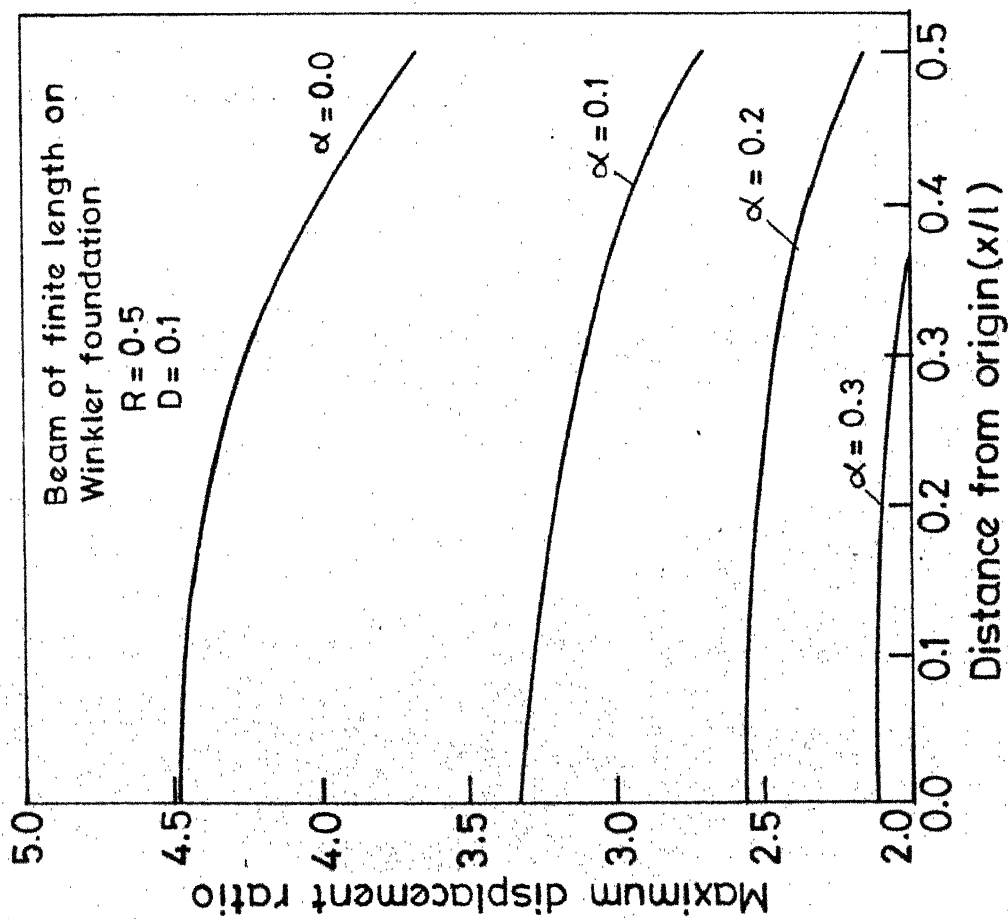


Fig.3.10 Displacement variation along the length of beam for damped case ($R = 0.5$).

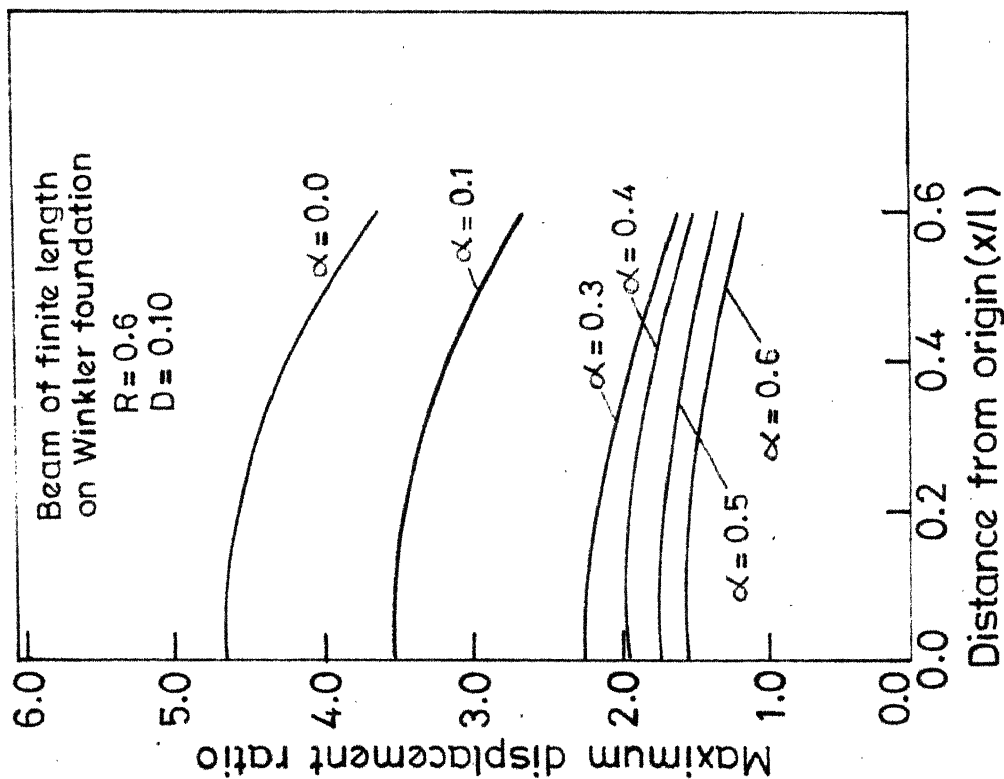


Fig.3.11 Displacement variation along the length of beam for damped case ($R = 0.6$).

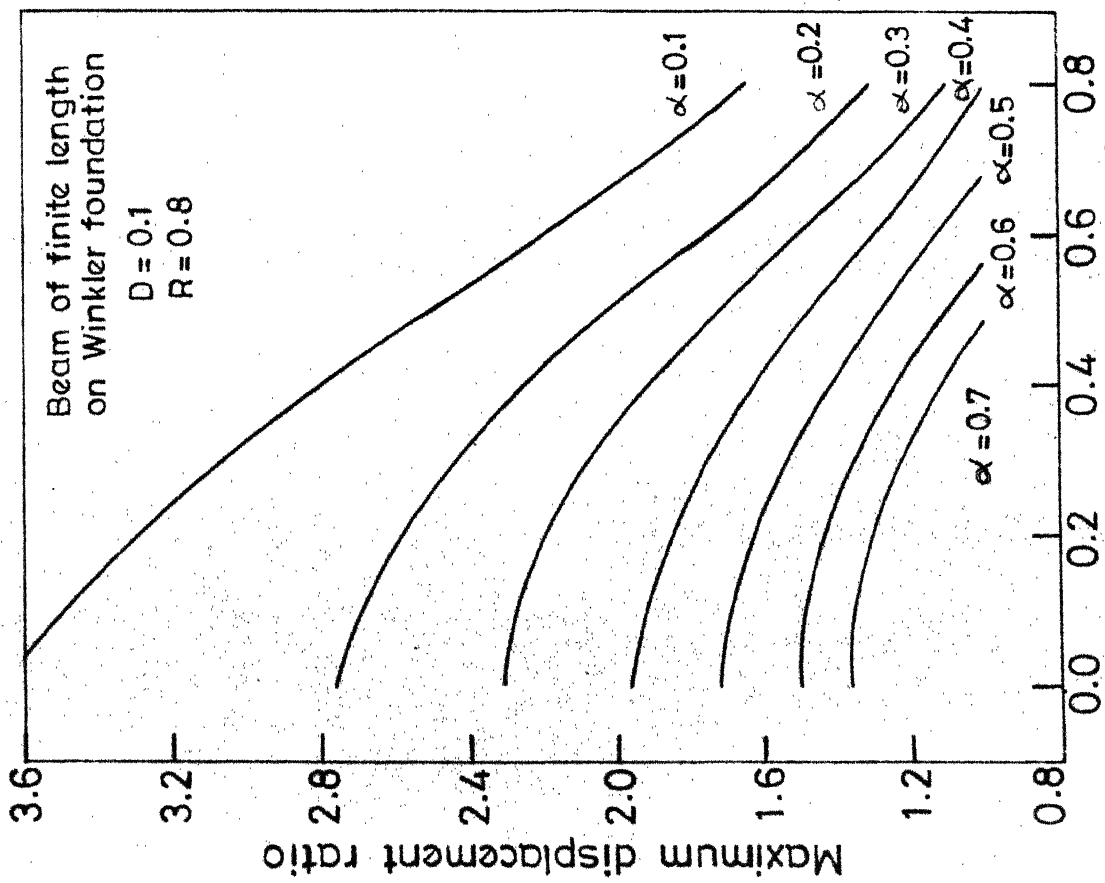


Fig.3.12 Displacement variation along the length of beam for damped case ($R=0.8$)

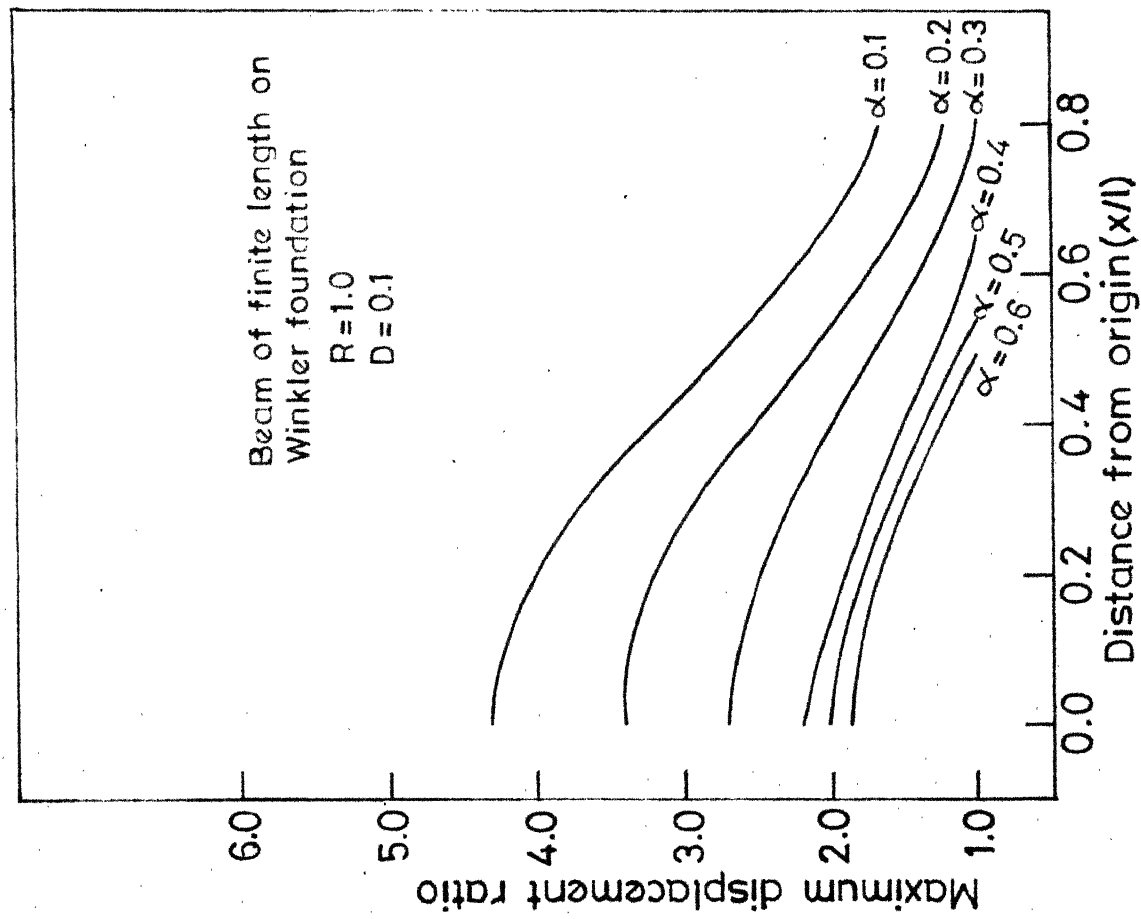


Fig.3.13 Displacement variation along the length of beam for damped case ($R=1.0$)

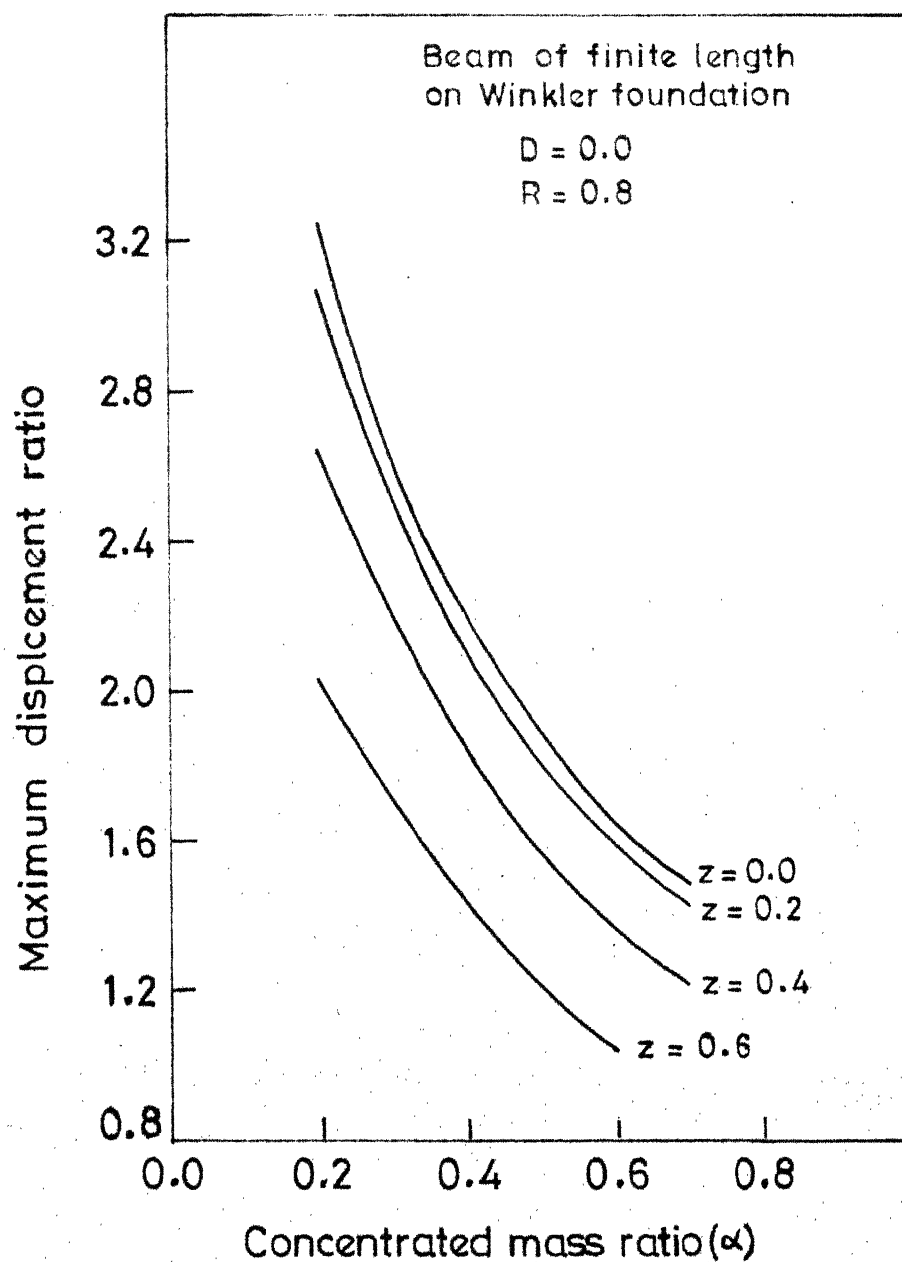


Fig.3.14 Variation of displacement with concentrated mass ratio for undamped case.

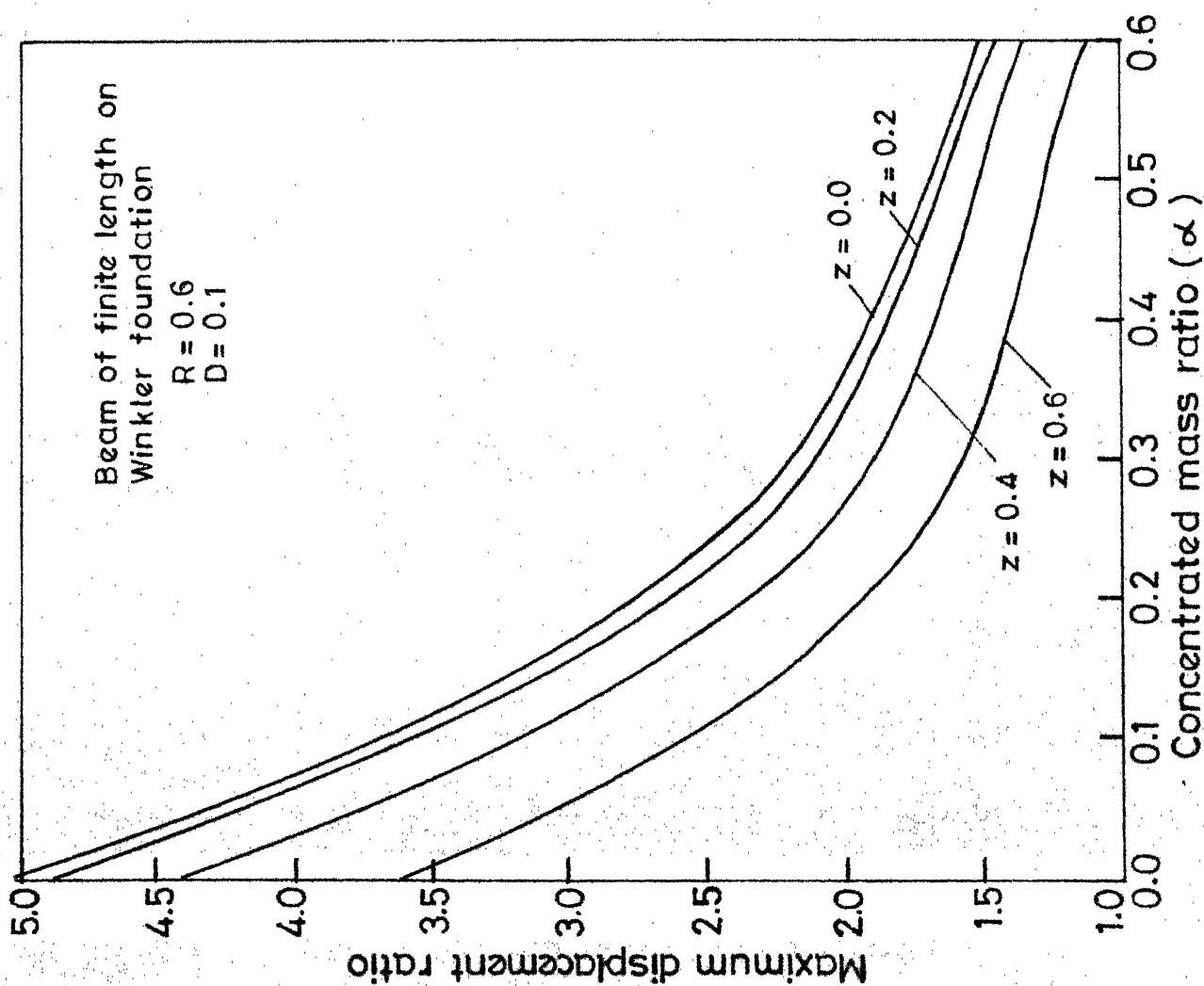


Fig.3.16 Variation of displacement with concentrated mass ratio for damped case ($R=0.6$)

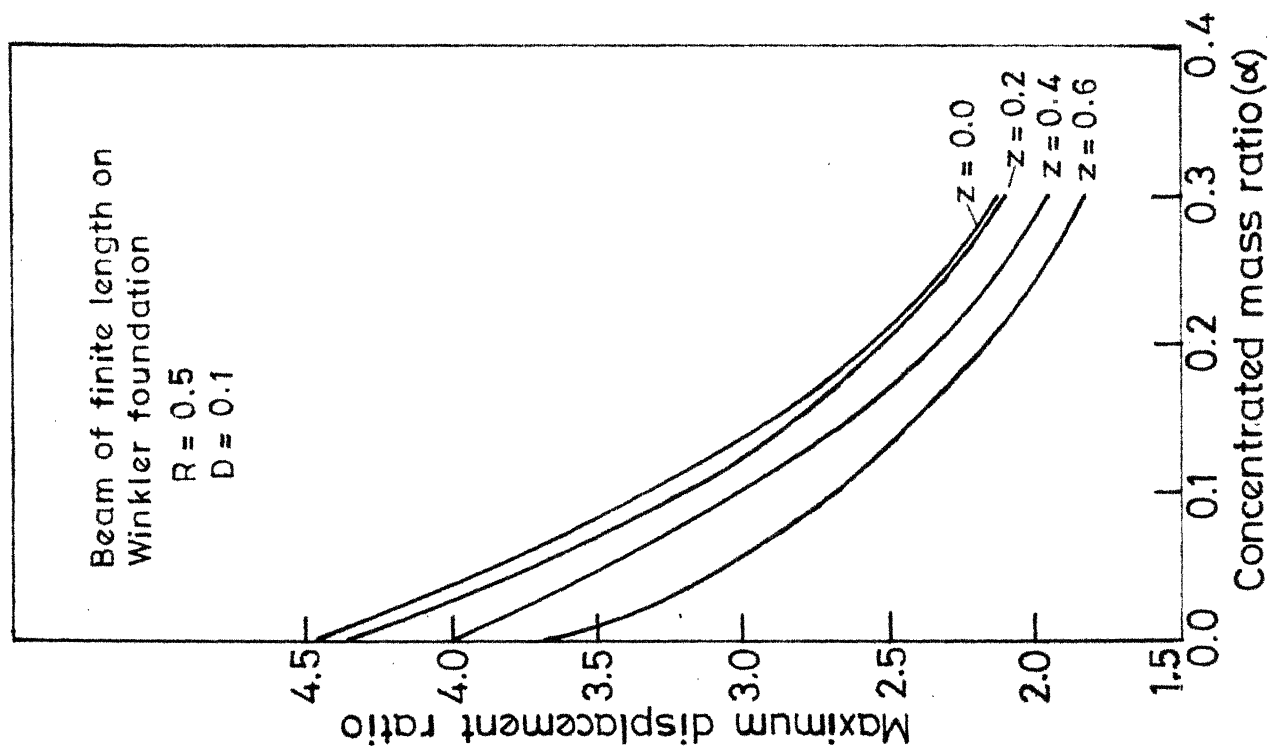


Fig.3.15 Variation of displacement with concentrated mass ratio for damped case ($R=0.5$)

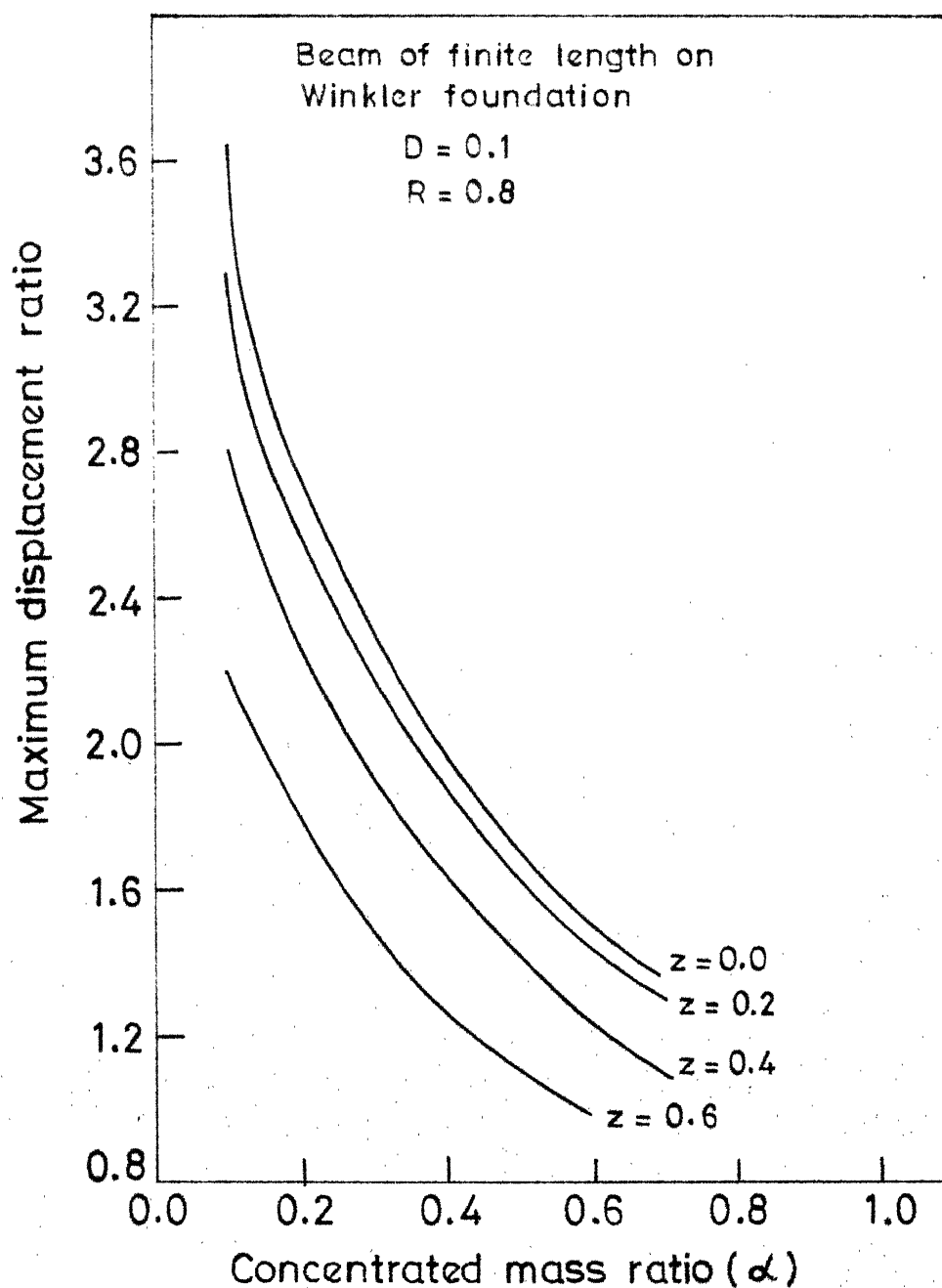


Fig. 3.17 Variation of displacement with concentrated mass ratio for damped case ($R=0.8$)

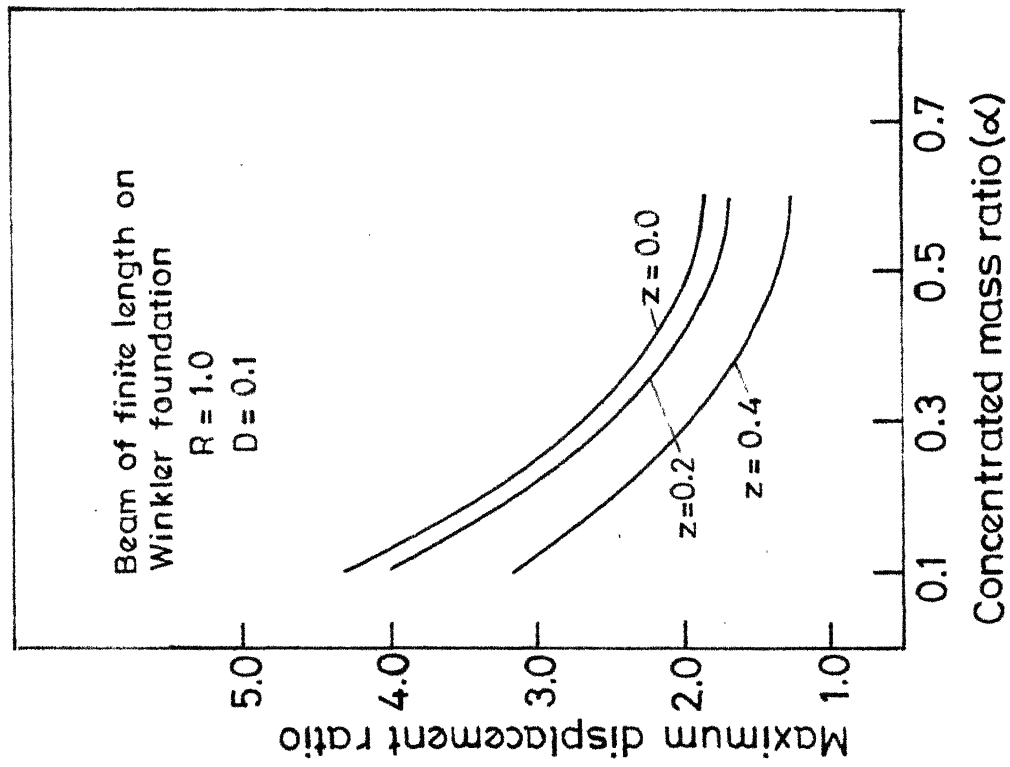


Fig.3.18 Variation of displacement with concentrated mass ratio for damped case ($R=1.0$)

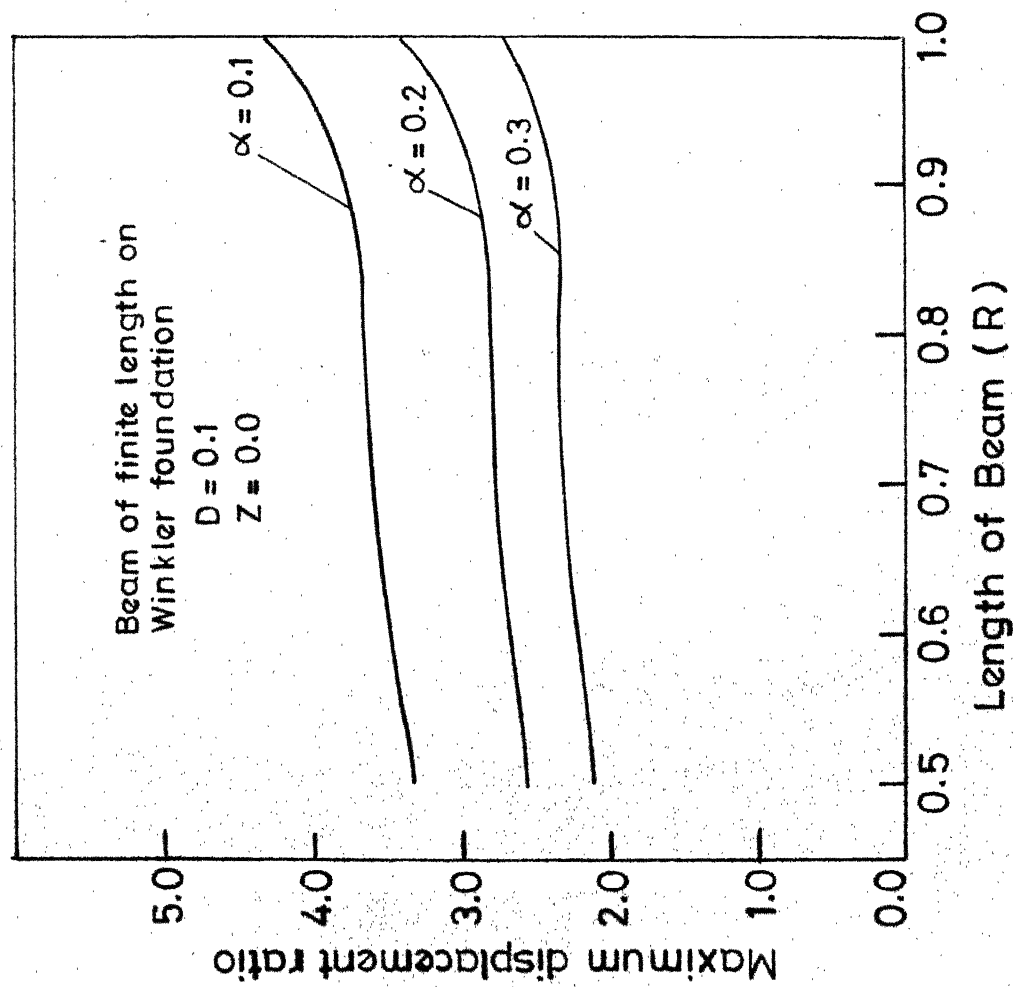


Fig.3.19 Displacement variation with non-dimensional length R .

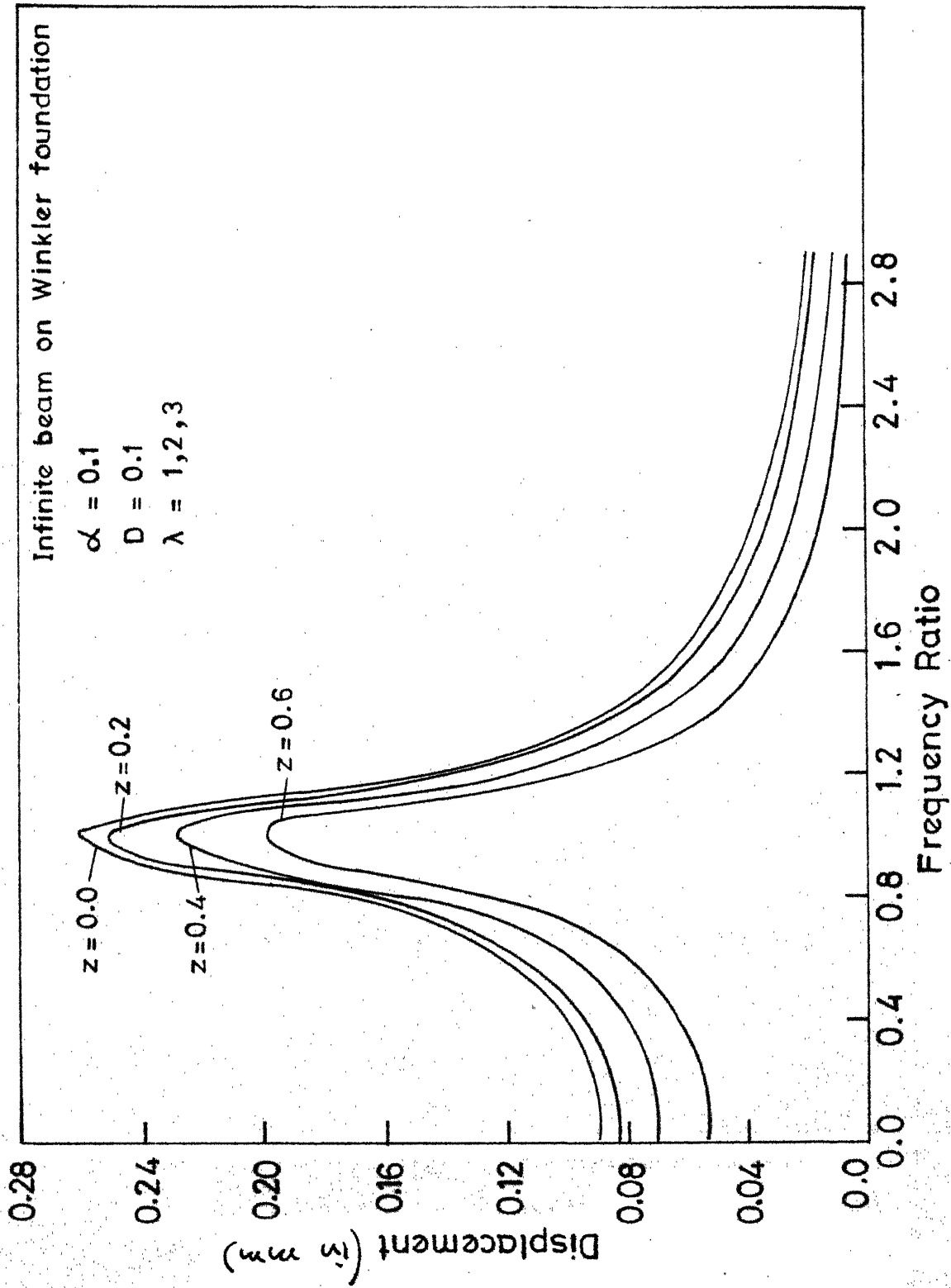


Fig.3.20 Displacement frequency response of an infinite beam along the length of the beam

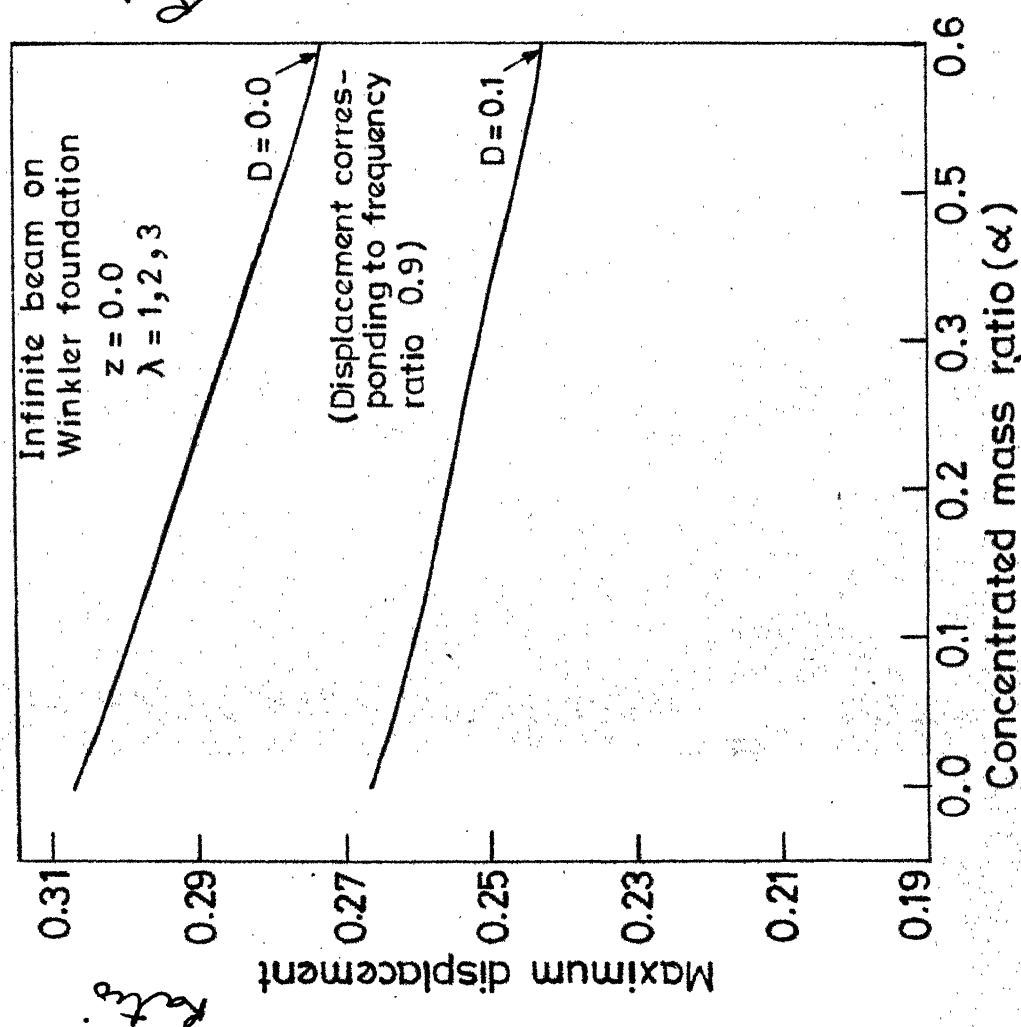


Fig.3.21 Variation of maximum displacement with concentrated mass ratio.

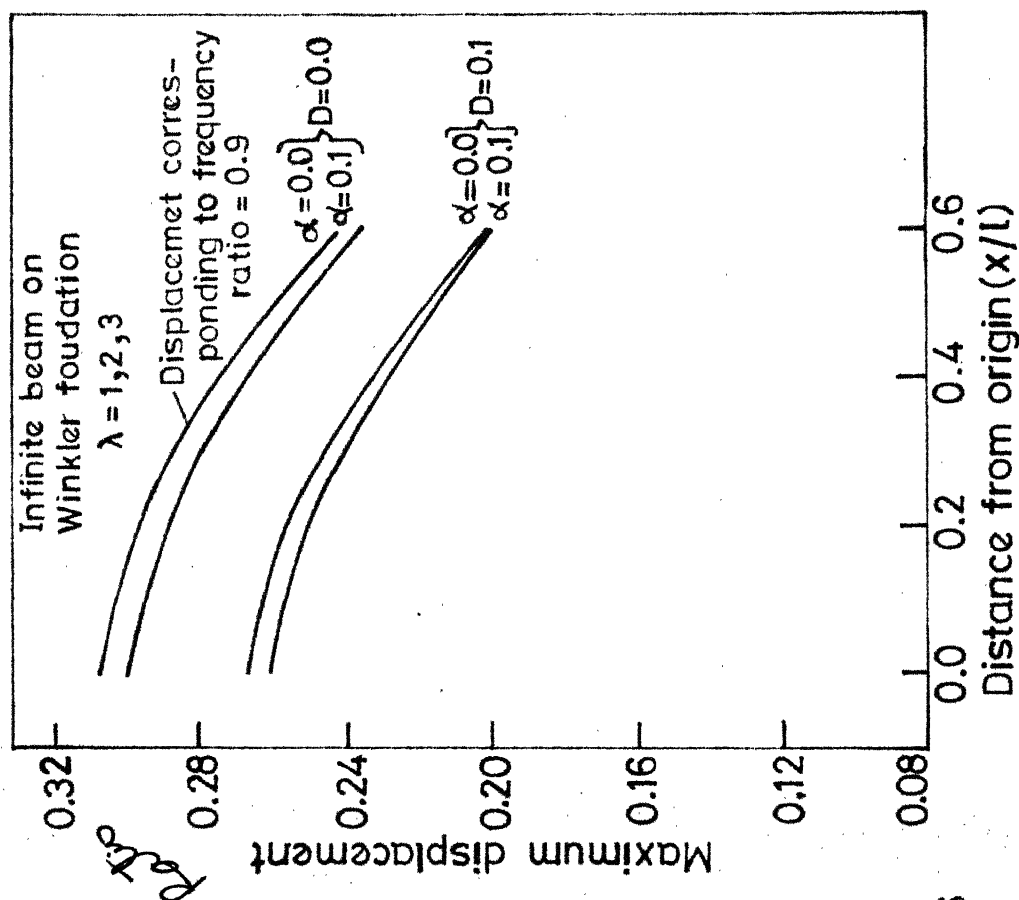


Fig.3.22 Variation of maximum displacement along the length of the beam.

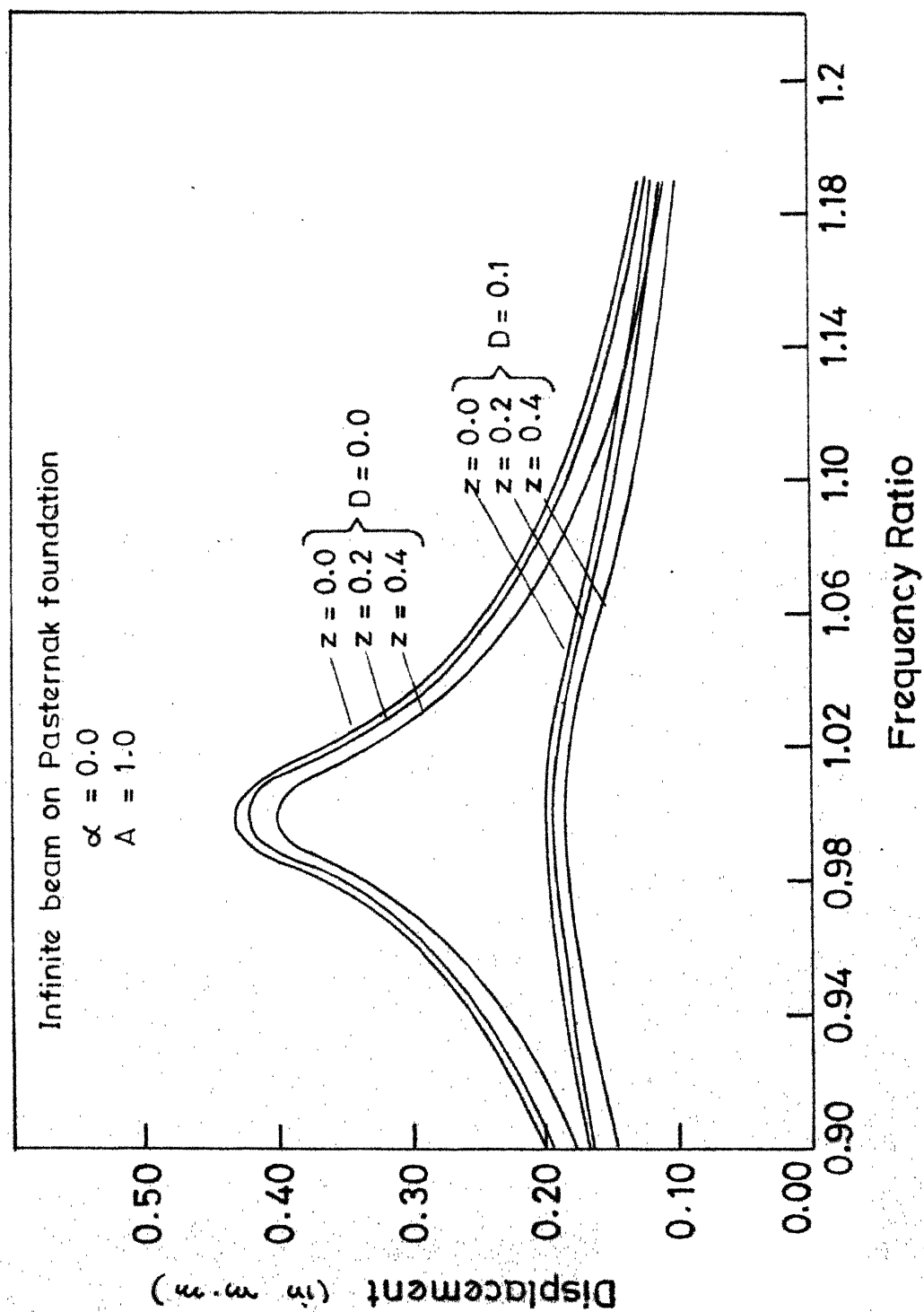


Fig. 3.23 Displacement frequency response curve for an infinite beam on Pasternak foundation (variation along the length of the beam) $A = 1.0$

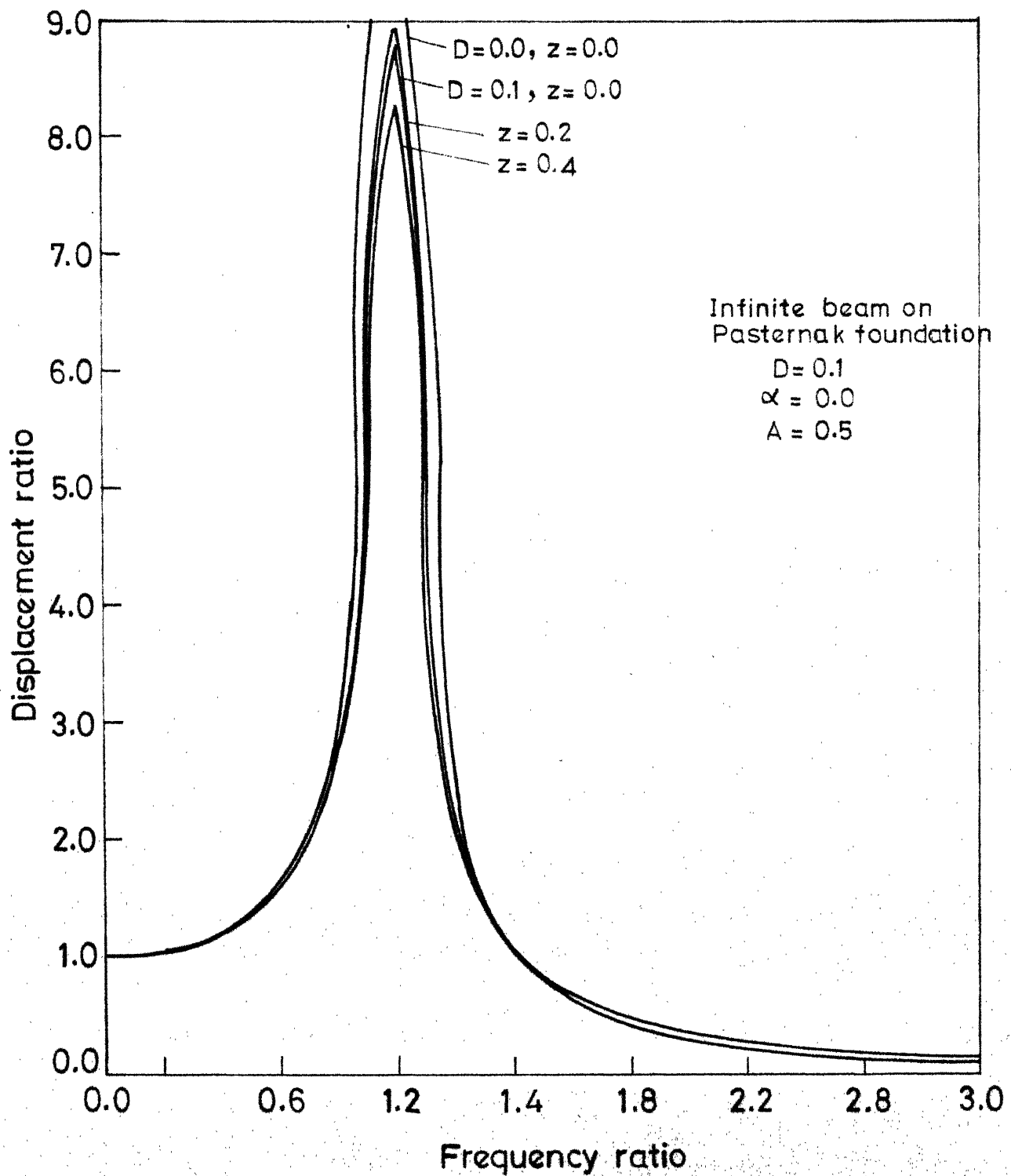


Fig. 3.24 Displacement frequency response for an infinite beam on Pasternak foundation ($A=0.5$). (variation along the length of the beam)

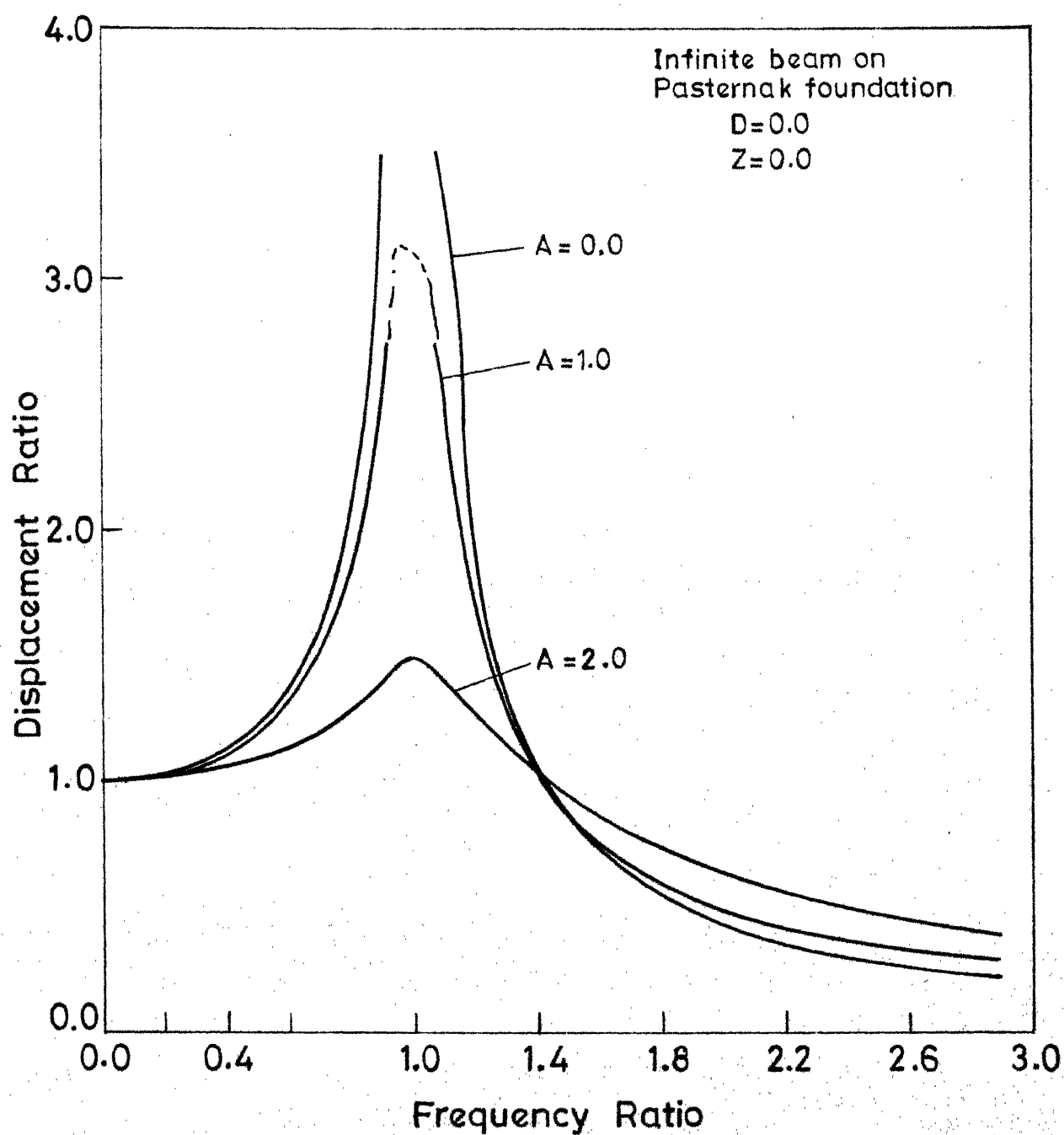


Fig.3.25 Displacement frequency response for an infinite beam with no concentrated mass (variation with shear coefficient A)

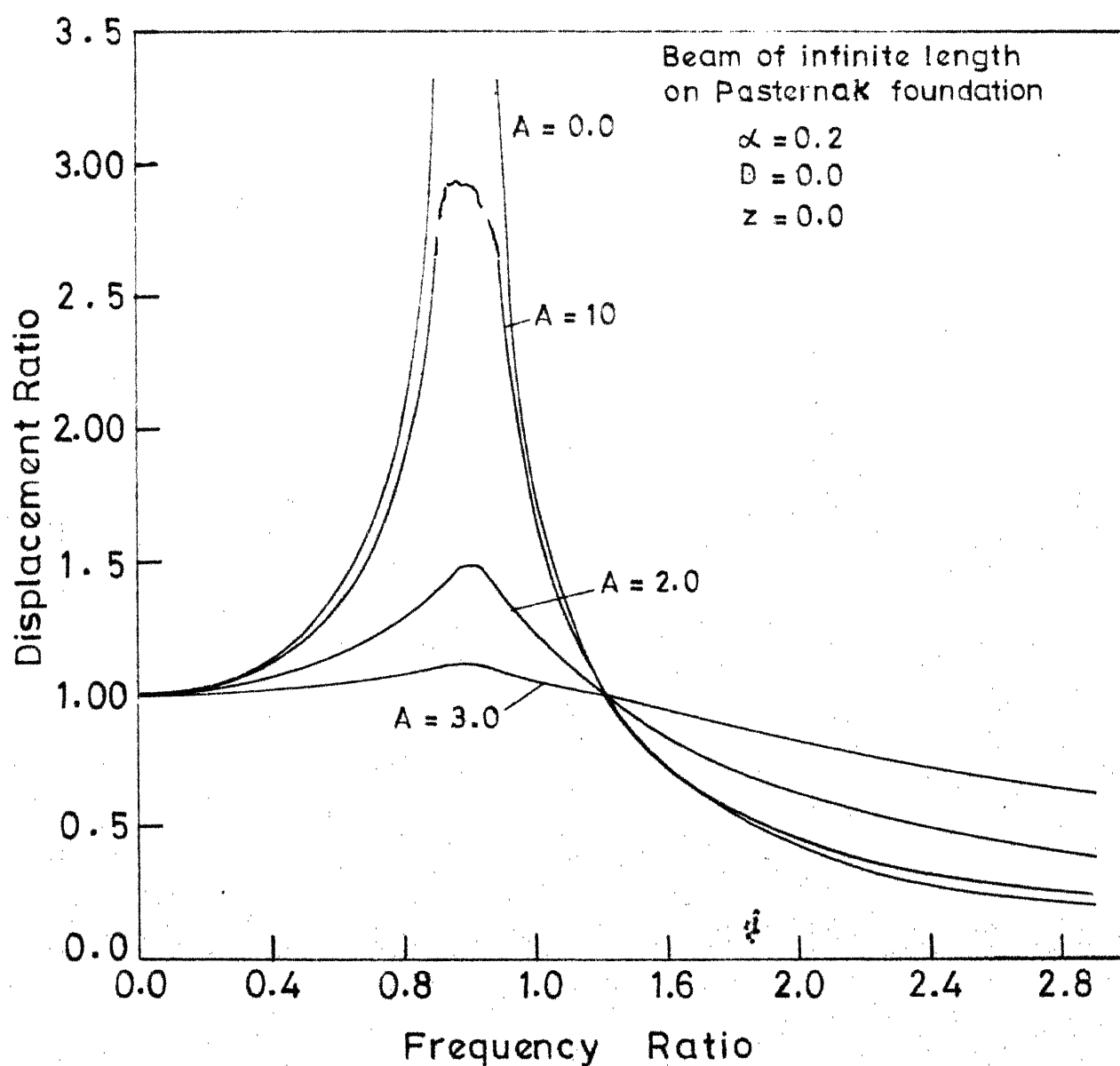


Fig.3.26 Displacement frequency response of infinite beam with concentrated mass (variation with shear coefficient A)

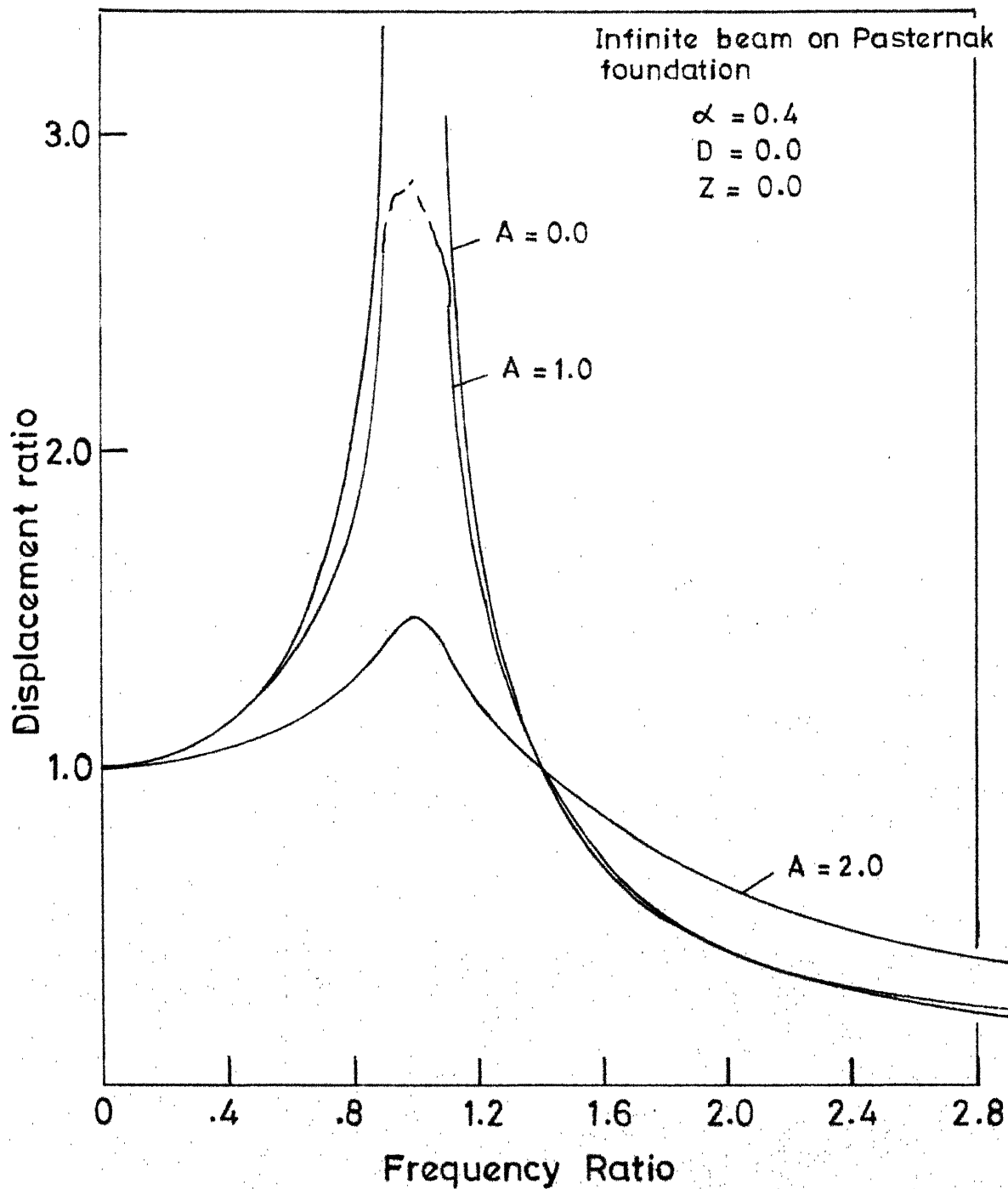


Fig.3.27 Displacement frequency response of an infinite beam with concentrated mass ($\alpha = 0.4$) (variation with the shear coefficient A)

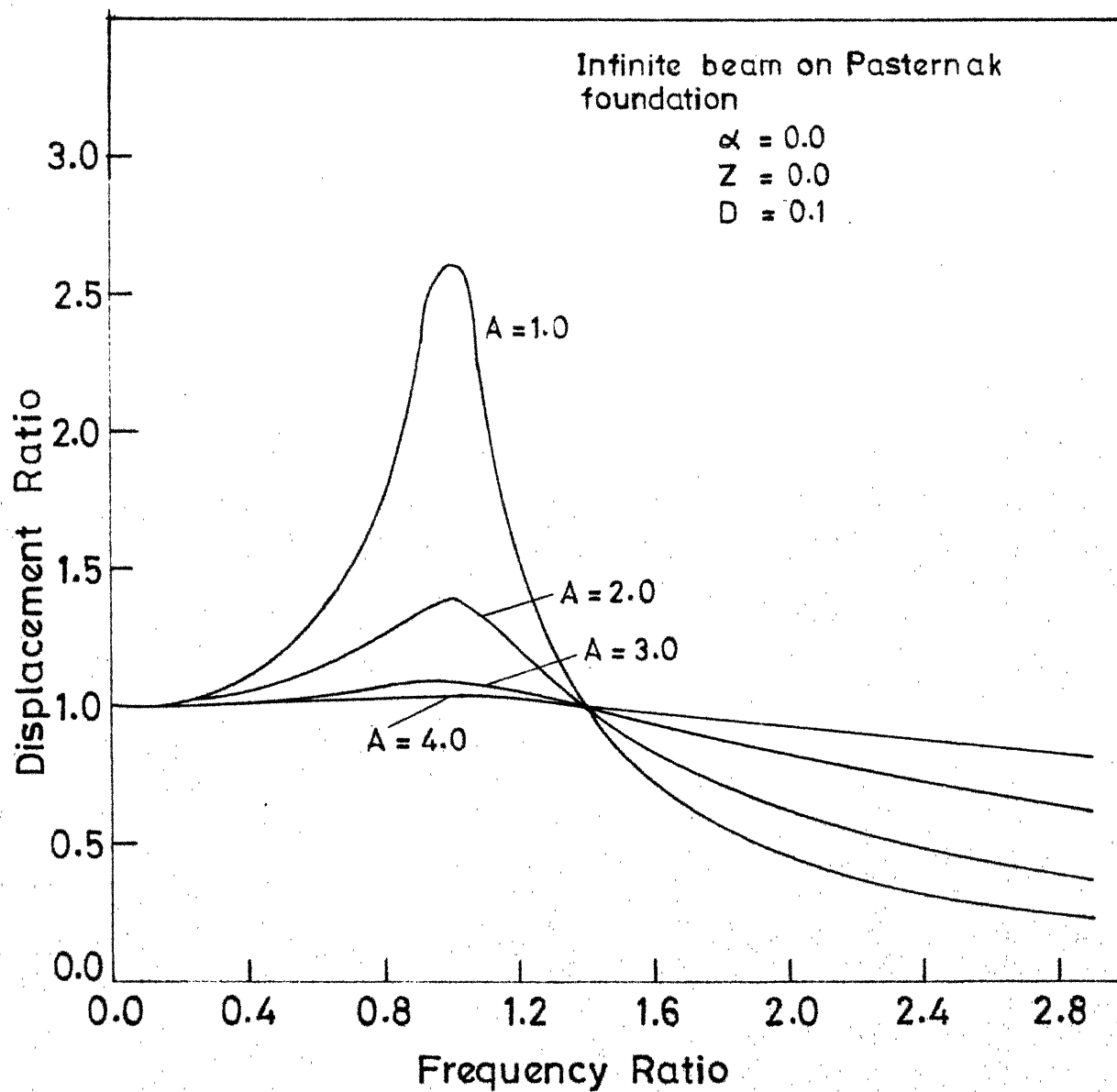


Fig. 3.28 Displacement frequency response for an infinite beam on Pasternak foundation with damping.

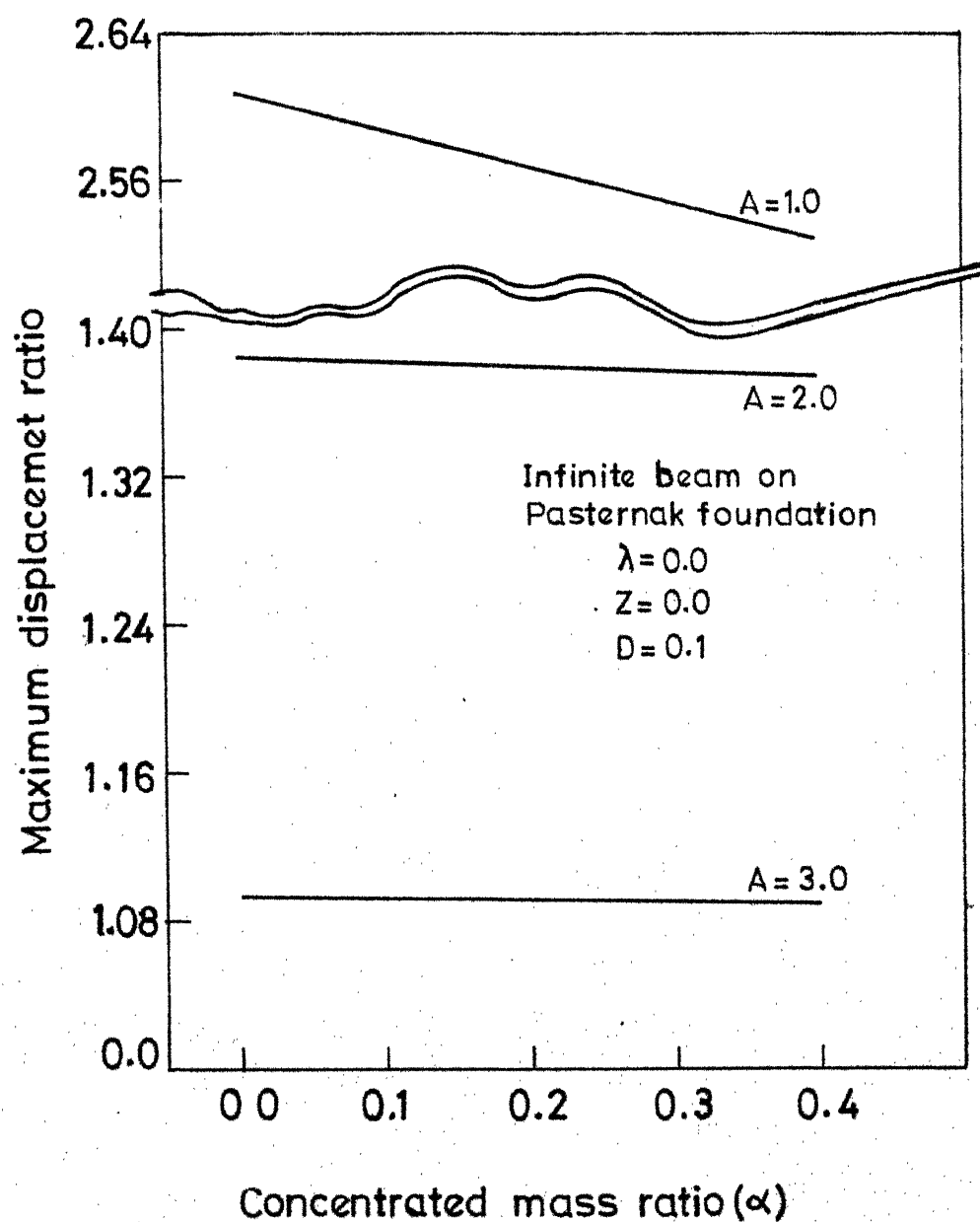


Fig.3.29 Maximum displacement variation with concentrated mass ratio.

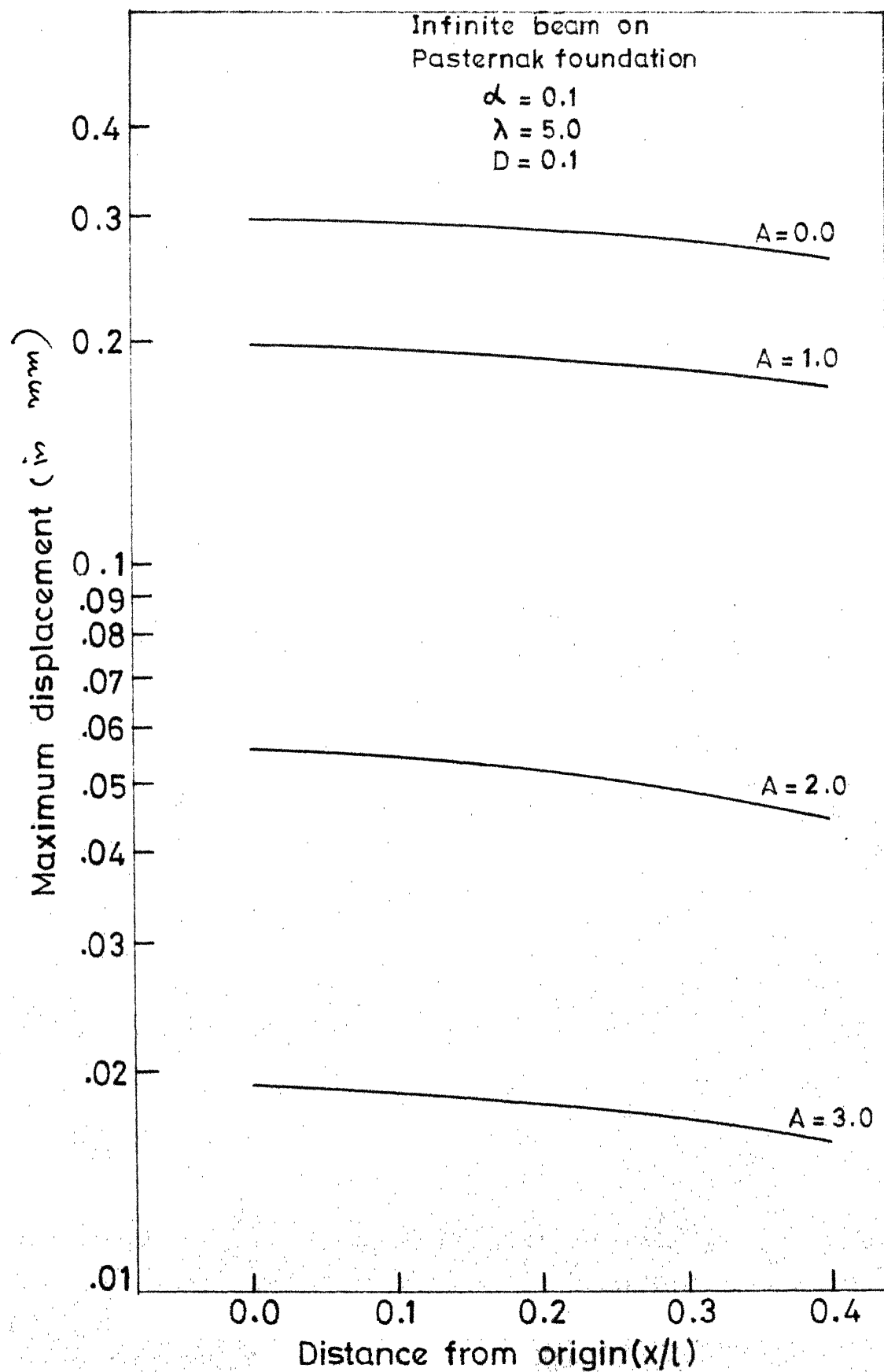


Fig.3.30 Displacement variation along the length of the beam

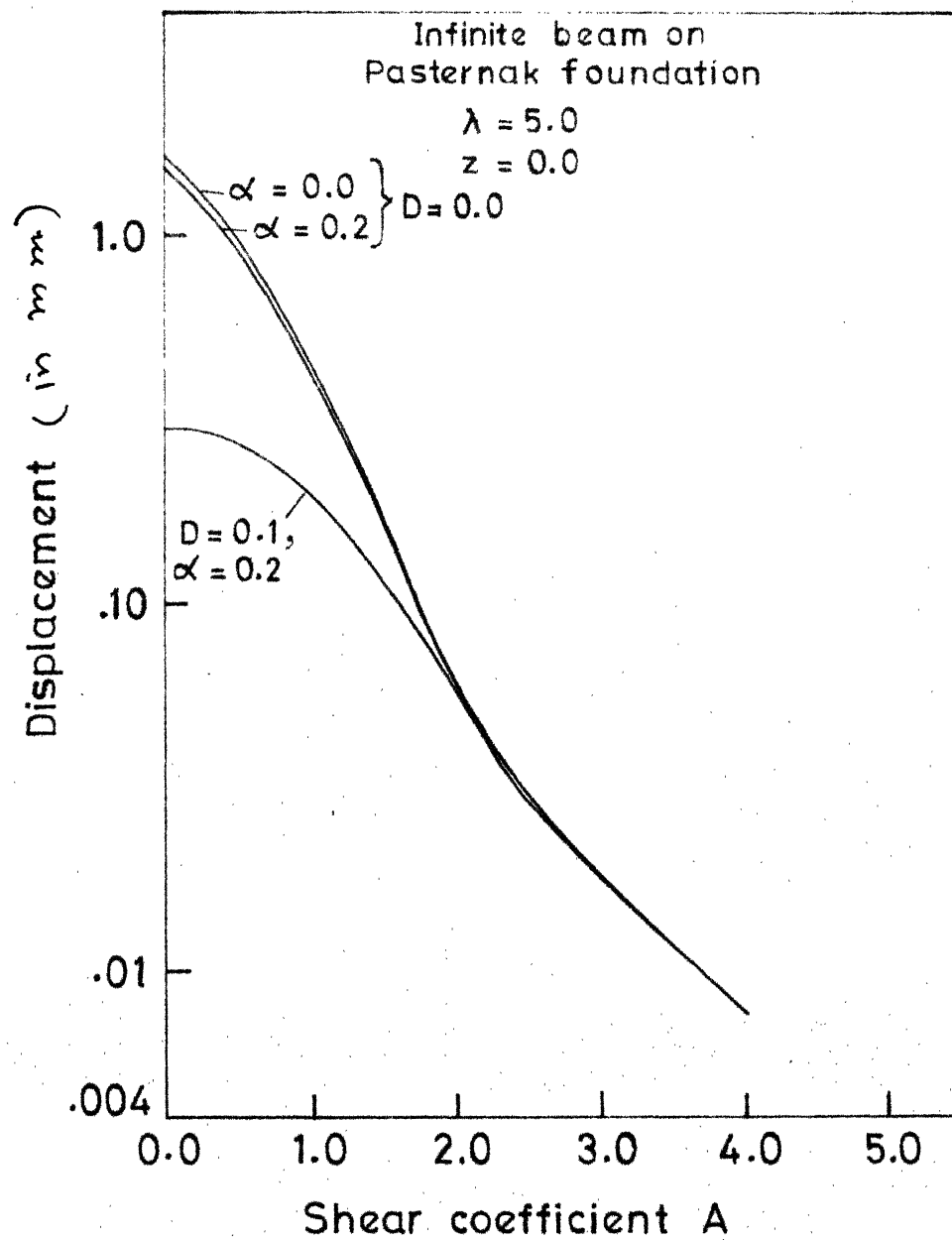


Fig.3.31 Maximum displacement variation
with shear coefficient A

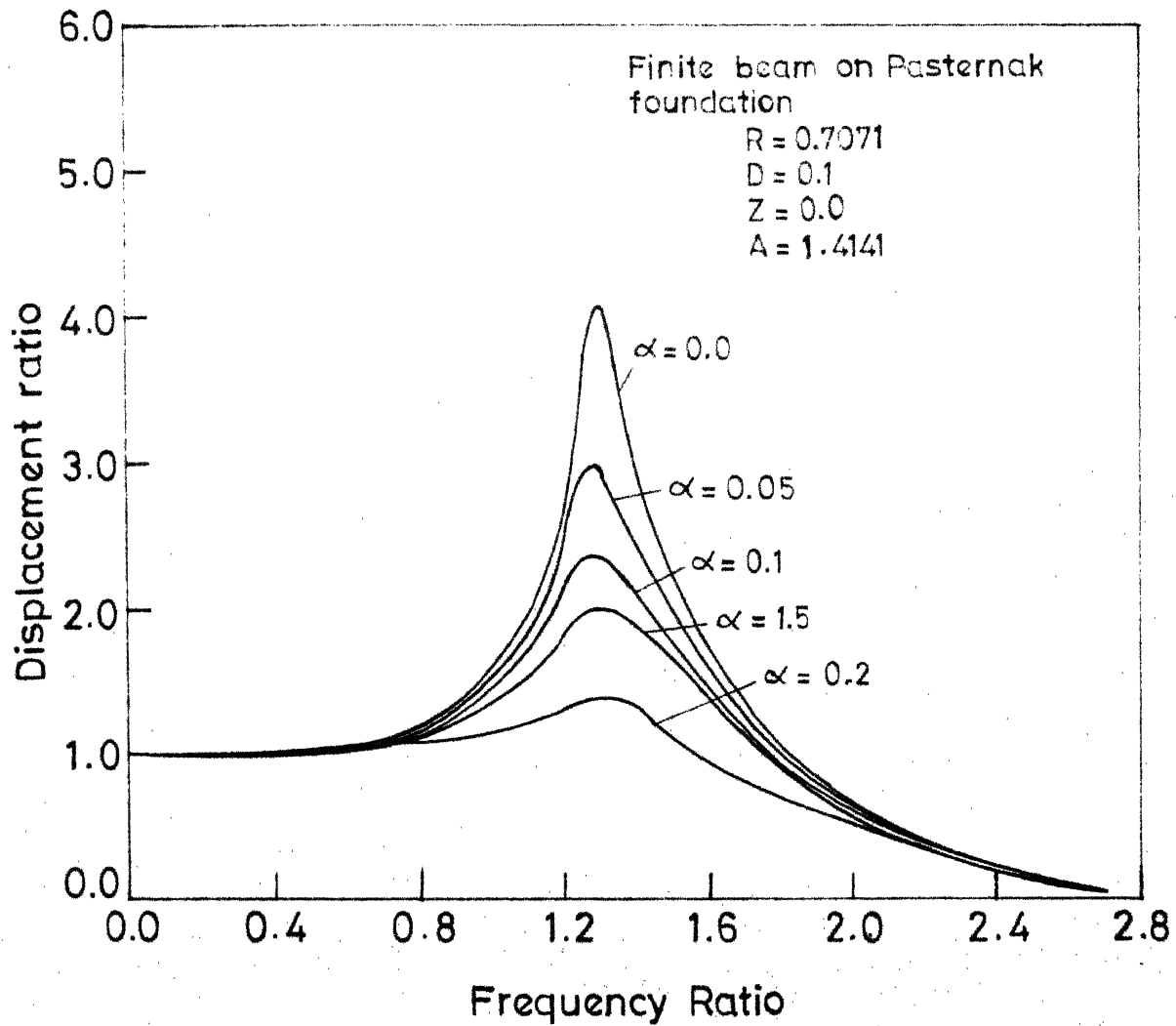


Fig. 3.33 Displacement frequency response of a finite beam on Pasternak foundation ($A=1.4141$) (variation of concentrated mass).

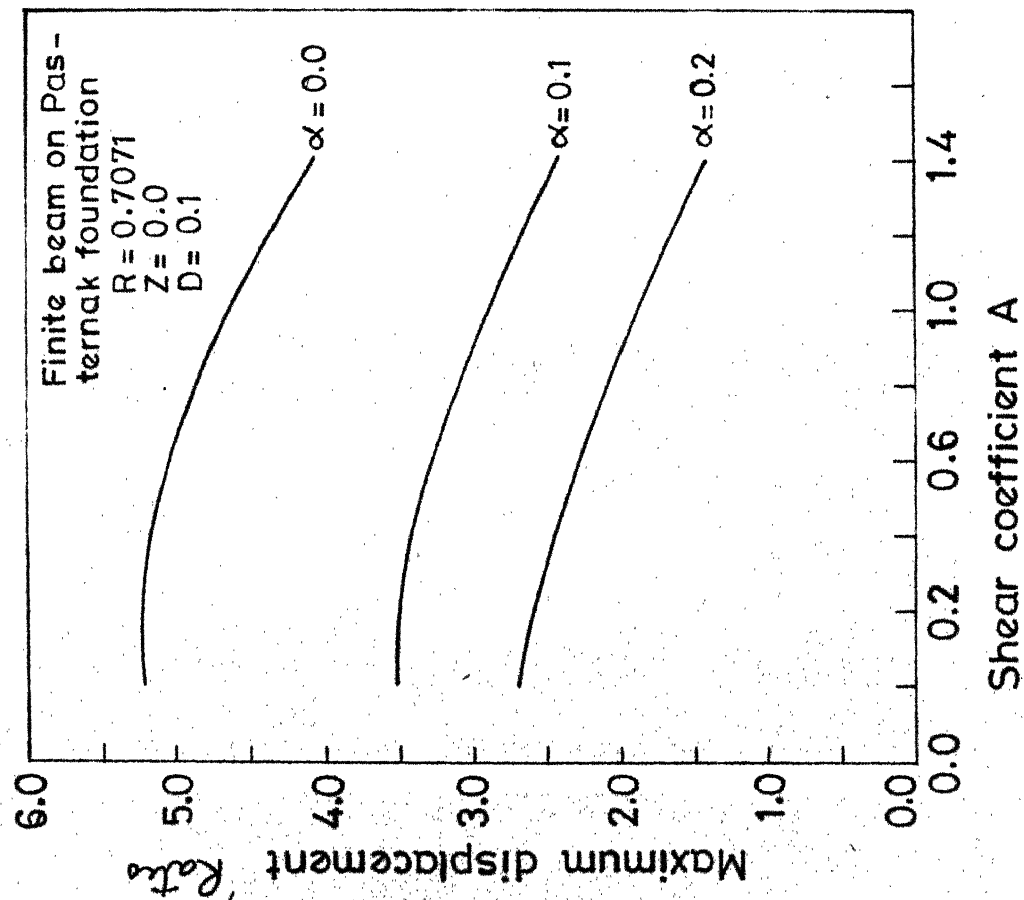


Fig.3.34 Variation of maximum displacement with shear coefficient.

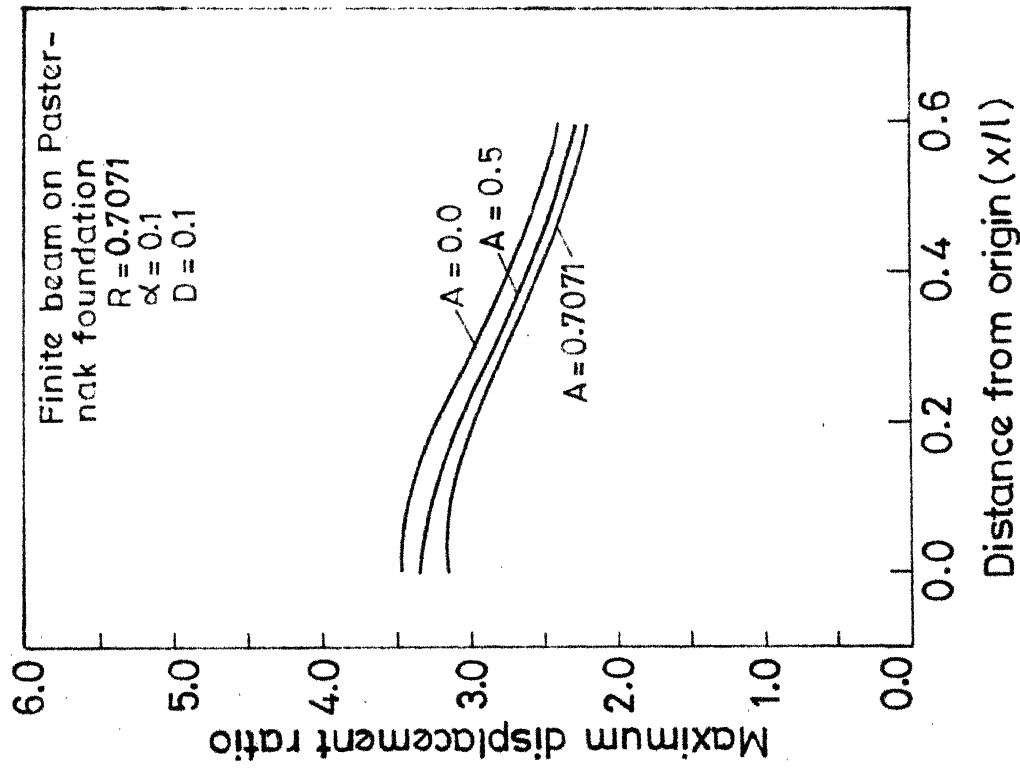


Fig.3.35 Variation of maximum displacement along the length of the beam.

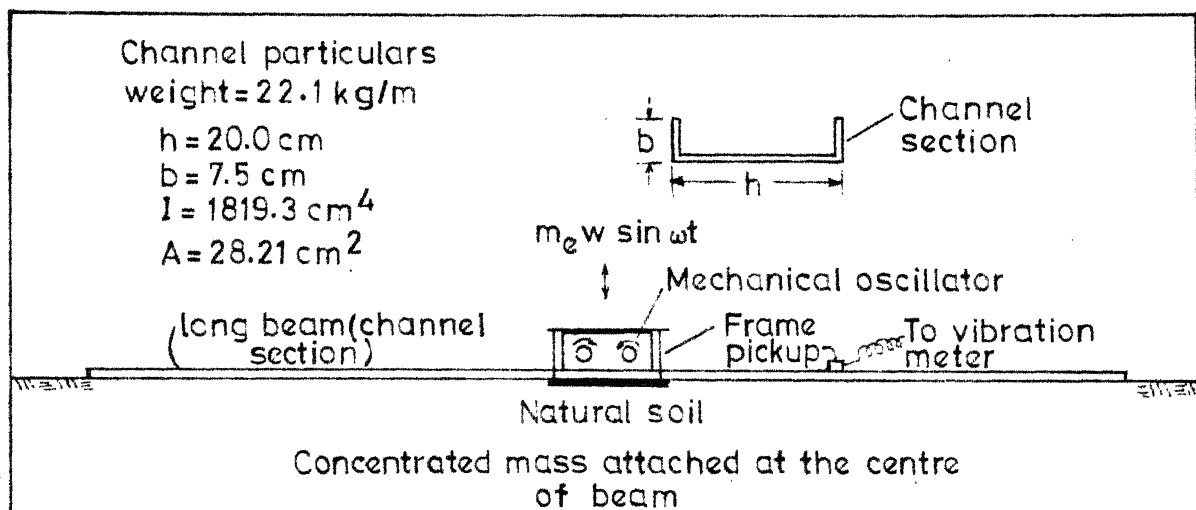


Fig.3.36(a) A line diagram of test arrangement

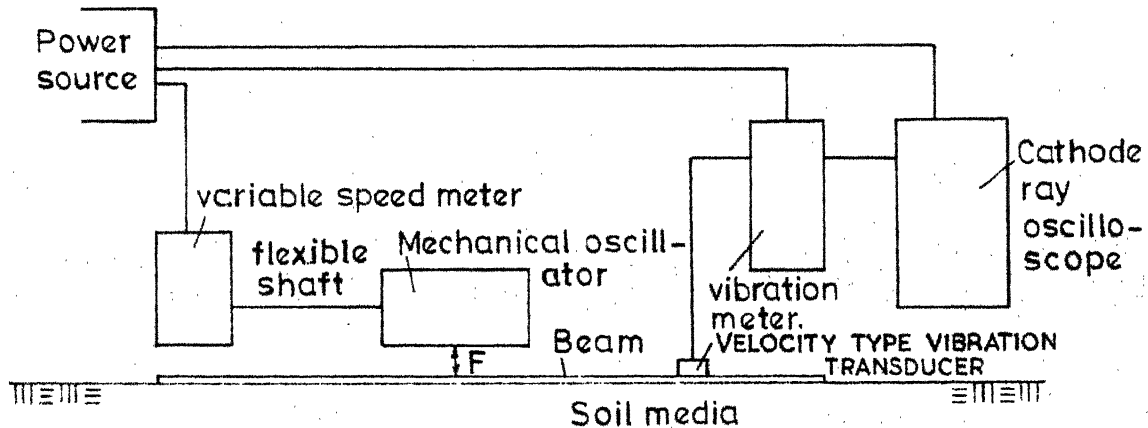


Fig.3.36(b) A block diagram for the test of a beam carrying a concentrated mass at its centre.

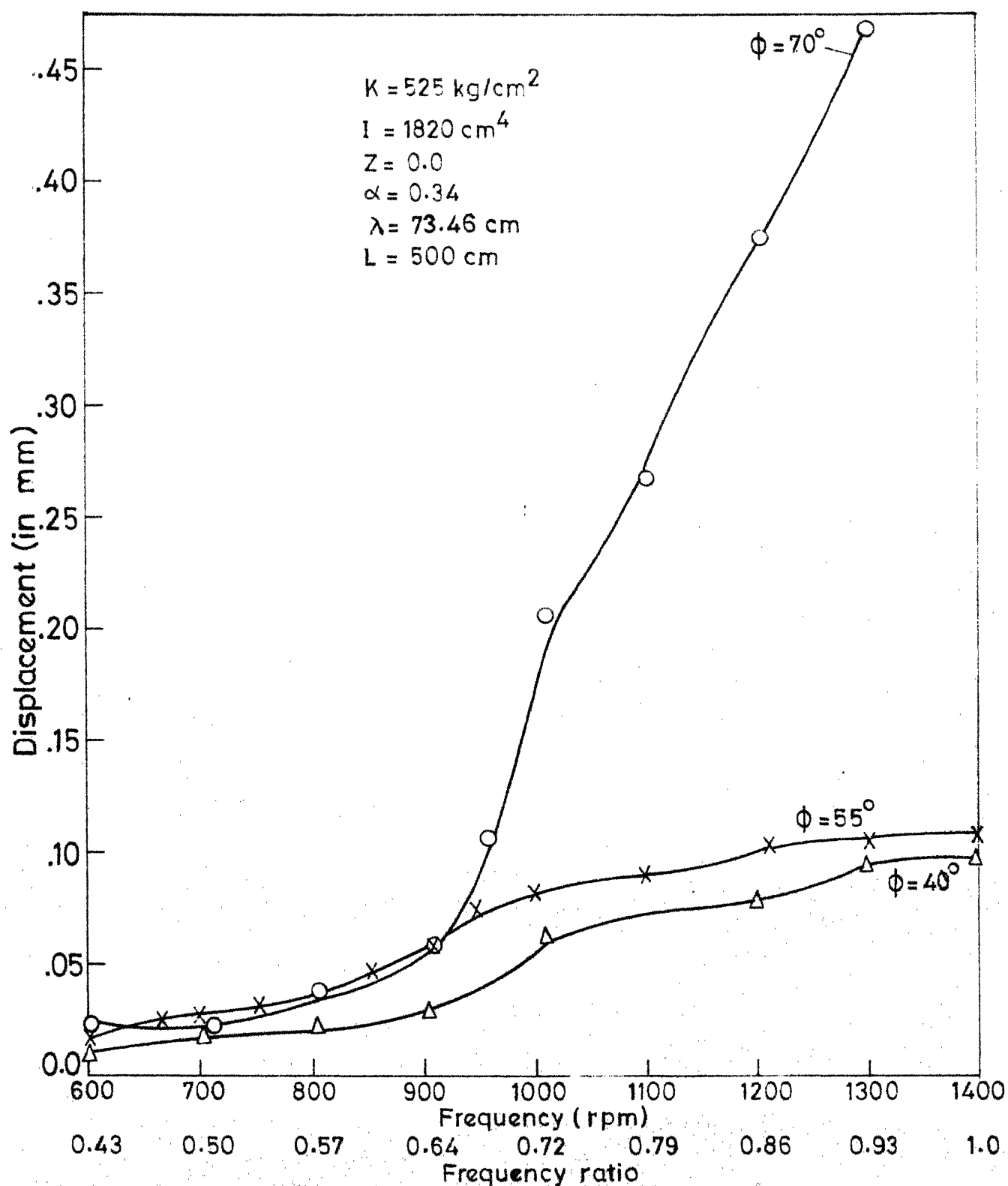


Fig.3.37 Displacement frequency response of channel section for frequency dependent force.

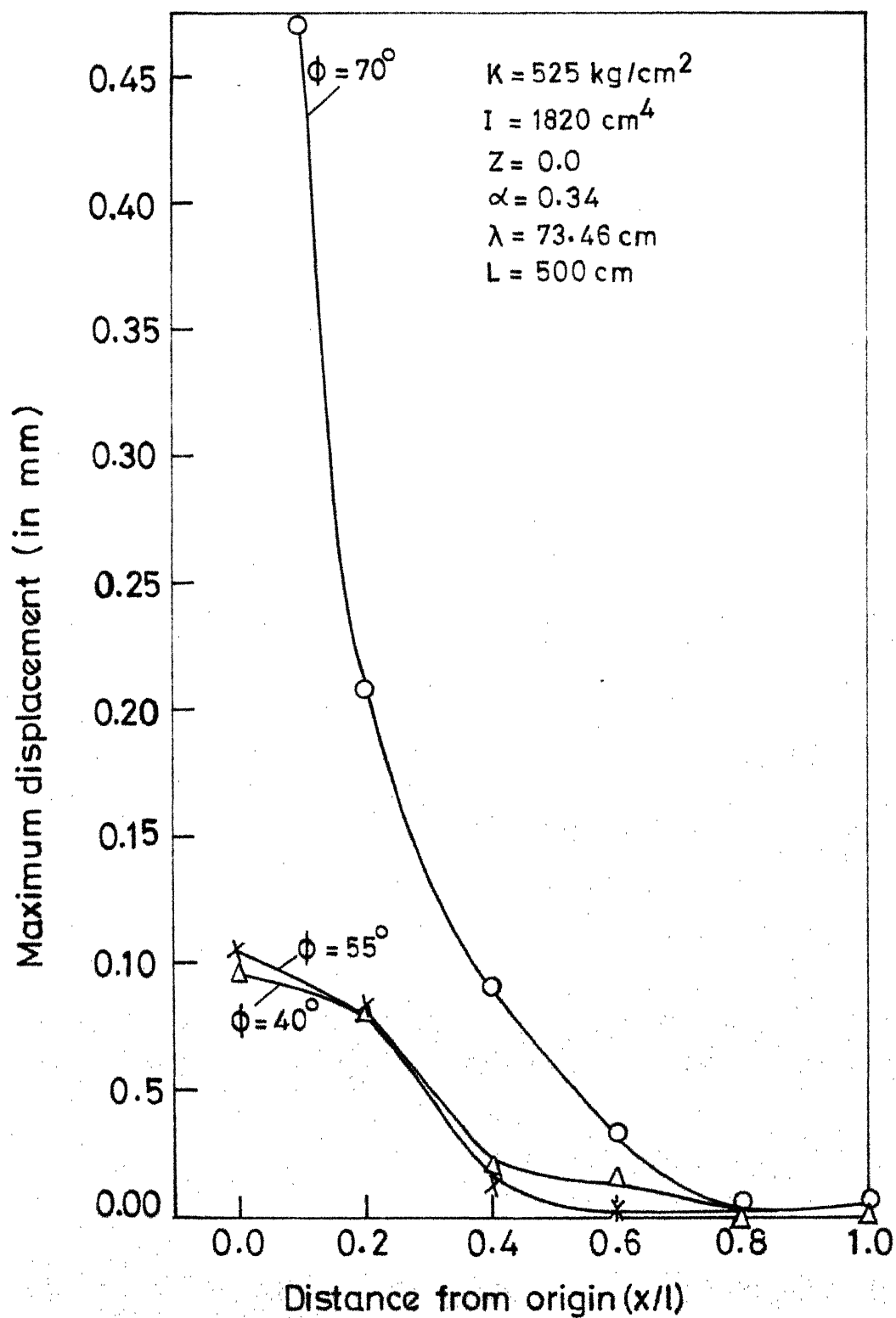


Fig. 3.38 Maximum displacement variation along the length of channel for frequency dependent force.

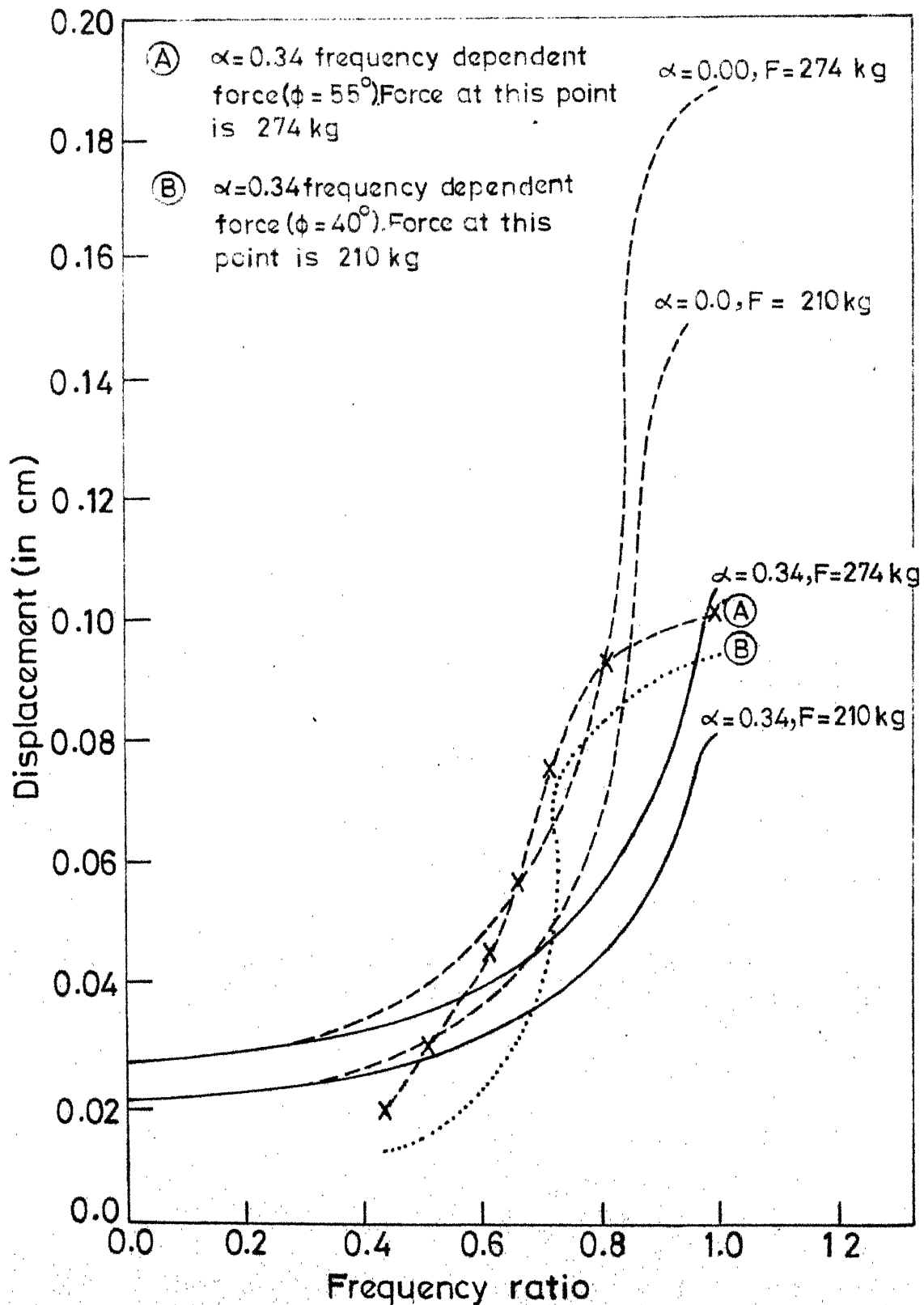


Fig.3.39 Comparison of test results with theoretical results for beam with concentrated mass on it and resting on elastic foundation.

CHAPTER 4

DYNAMIC RESPONSE OF BEAMS ON ELASTIC FOUNDATION SUBJECTED TO IMPULSE LOADS

4.1 GENERAL.

The beams on elastic foundations subjected to impulse loads have been the subject of great interest. The dynamic loading effects on stationary structures such as railway tracks, landing of aircrafts on runways, transient loads on pavements, footings subjected to impulse loads are some examples. In this chapter, the beam resting on elastic foundations subjected to impulse loads is analysed, treating the soil medium as Pasternak foundation model and Winkler foundation model with damping.

The governing differential equation for such a problem taking into the consideration the so called internal damping and external damping has been given by Hoppman (21), as

$$EI \frac{\partial^4 w}{\partial x^4} + c_e I \frac{\partial^5 w}{\partial x^4 \partial t} + c_f \frac{\partial w}{\partial t} + Kw + \rho A_c \frac{\partial^2 w}{\partial t^2} = F(x,t) \quad (4.1.1)$$

where c_e is external damping coefficient,
 c_f is internal damping coefficient,
 EI is modulus of rigidity of beam,
 I is moment of Inertia,
 K is spring constant of foundation,
 ρA_c is unit mass of beam.

The second term in the equation (4.1.1) is due to external damping. Hoppman (21) again developed an expression for impulse load in terms of coefficient of restitution e_o . For the impact of a sphere on beam, the contact force is given by

$$f(t) = m_s v_o (1+e_o) \frac{\pi}{2T_L} \sin \frac{\pi t}{T_L} \text{ for } 0 < t < T_L \quad (4.1.2)$$

where m_s is the mass of the sphere,
 v_o is velocity of sphere just before striking the beam,
 e_o is coefficient of restitution
 T_L is time of contact

Stadler and Shreeves (50) developed the differential equation with some modifications. Instead of external damping, the foundation consisted of a shear layer, besides the spring constant. The differential equation is similar to the one described by Pasternak (29) in his foundation model of soil medium and is given by

$$EI \frac{\partial^4 w}{\partial x^4} + G_o \frac{\partial^2 w}{\partial x^2} + Kw + c \frac{\partial w}{\partial t} + \rho A_c \frac{\partial^2 w}{\partial t^2} = F(x,t) \quad (3.2.1)$$

Stadler and Shreeves (50) gave the solution for impulse load at origin, as the general solution is difficult to be obtained due to complexity in deriving the solution. However, by numerical analysis, the above differential equation can be solved for responses at any arbitrary point of the beam.

In this chapter, the solution of the governing differential equation is attempted by Laplace transform. Several Laplace transform inversion

techniques were tried for the solution, and Berger's inversion technique (6) was used successfully for the general solution. The results are presented for infinite and finite beams resting on elastic foundation. An approximate solution for an infinite beam resting on Winkler foundation with damping, using Post & Widder's formula (4), is derived and results are presented. Solutions have been compared with existing results.

4.2 GENERAL FORMULATIONS.

The basic differential equation of a Euler-Bernoulli beam resting on Pasternak foundation is given by equation (3.2.3) and is given by

$$\frac{\partial^4 y}{\partial z^4} - A^2 \frac{\partial^2 y}{\partial z^2} + 4y + 8Dr \frac{\partial y}{\partial \theta} + 4r^2 \frac{\partial^2 y}{\partial \theta^2} = 0 \quad (3.2.3)$$

The impulse load is applied at the origin at time $t=0$. This impulse can be incorporated in boundary conditions with appropriate initial conditions at the origin. Hence, applying the Laplace transform with respect to θ , the equation (3.2.3) can be written as

$$\frac{\partial^4 \bar{y}}{\partial z^4} - A^2 \frac{\partial^2 \bar{y}}{\partial z^2} + 4(1 + 2Dp + p^2) \bar{y} = 0 \quad (4.2.1)$$

where

$$y(z, p) = \int_0^\infty y(z, \theta) e^{-p\theta} d\theta \quad (4.2.2)$$

p is Laplace transform variable

\bar{y} is Laplace transform of the displacement

4.2.1 Initial and Boundary Conditions

(a) Initial Conditions. Just before the application of impulse load, the beam has zero displacement and slope of the deflection curve. These initial conditions can be written as

$$y(z, \theta) = 0, \text{ at } \theta = 0, \quad \frac{\partial y}{\partial \theta} = 0 \text{ at } \theta = 0 \quad (4.2.3)$$

(b) Boundary Conditions for Finite Beam on Pasternak Foundation.

The origin is taken at the centre of the beam. As the point is at the centre of the beam, the slope of the deflection curve is zero. The shear forces acting at this point are from the impulse load, shear resistance of the beam and the foundation. At the free ends, the moment is zero while the shear resistance of the beam is balanced by the shear resistance of the foundation. In mathematical form, these boundary conditions can be expressed as

$$\left. \begin{aligned} \text{at } z = 0, \quad \frac{\partial y}{\partial z} = 0, \text{ and } \frac{\partial^3 y}{\partial z^3} - A^2 \frac{\partial y}{\partial z} &= \text{Imp.} \frac{\lambda^2 \omega_n}{2EI} \\ \text{at } z = R, \quad \frac{\partial^2 y}{\partial z^2} = 0, \text{ and } \frac{\partial^3 y}{\partial z^3} - A^2 \frac{\partial y}{\partial z} &= -A^2 \frac{\partial y_f}{\partial z} \end{aligned} \right] \quad (4.2.4)$$

For unloaded surface of the foundation, the boundary conditions are

$$\frac{\partial^2 y_f}{\partial z^2} - \frac{n^2}{\lambda^2} (1+2Dr)y_f = 0 \quad \text{and as } z \rightarrow \infty \quad y_f = 0 \quad (4.2.5)$$

(c) Infinite Beam on Pasternak Foundation. The boundary conditions at the origin are the same as for finite beam. At infinity, the response functions have finite values. These boundary conditions, in mathematical form, can be written as

$$\left. \begin{aligned}
 &\text{at } z = 0, \frac{\partial y}{\partial z} = 0, \text{ and } \frac{\partial^3 y}{\partial z^3} - A^2 \frac{\partial y}{\partial z} = \text{Imp. } \frac{\lambda^2 \omega_n}{2EI} \\
 &\text{and as } z \rightarrow \infty, y \neq \infty, \frac{\partial y}{\partial z} \neq \infty, \frac{\partial^2 y}{\partial z^2} \neq \infty, \frac{\partial^3 y}{\partial z^3} \neq \infty
 \end{aligned} \right] \quad (4.2.6)$$

(d) Finite Beam on Winkler Foundation. For Winkler model the shear coefficient A is zero. Accordingly, the boundary conditions can be written as

$$\left. \begin{aligned}
 &\text{at } z = 0, \frac{\partial y}{\partial z} = 0, \text{ and } \frac{\partial^3 y}{\partial z^3} = \text{Imp. } \frac{\lambda^2 \omega_n}{2EI} \\
 &\text{and} \\
 &\text{at } z = R, \frac{\partial^2 y}{\partial z^2} = 0, \text{ and } \frac{\partial^3 y}{\partial z^3} = 0
 \end{aligned} \right] \quad (4.2.7)$$

(e) Infinite Beam on Winkler Foundation. The boundary conditions at $z \rightarrow \infty$ are the same as for Pasternak foundation. However, at $z = 0$, the shear force equation is to be modified. The boundary conditions, in this case, can be expressed as

$$\left. \begin{aligned}
 &\text{at } z = 0, \frac{\partial y}{\partial z} = 0, \text{ and } \frac{\partial^3 y}{\partial z^3} = \text{Imp. } \frac{\lambda^2 \omega_n}{2EI} \\
 &\text{as } z \rightarrow \infty, y \neq \infty, \frac{\partial y}{\partial z} \neq \infty, \frac{\partial^2 y}{\partial z^2} \neq \infty, \frac{\partial^3 y}{\partial z^3} \neq \infty
 \end{aligned} \right] \quad (4.2.8)$$

Crandell (14) derived an expression for the response of an infinite beam subjected to impulse load at its centre, resting on Winkler foundation with damping included. He gave the expression for the boundary conditions as described by (4.2.8).

4.2.2 General Solution Using Laplace Transform.

The general solution of the homogeneous equation (4.2.1) based on equation (4.2.2) can be written as

$$\bar{y}(z) = C_1 \bar{\phi}_1(z) + C_2 \bar{\phi}_2(z) + C_3 \bar{\phi}_3(z) + C_4 \bar{\phi}_4(z) \quad (4.2.9)$$

where C_1, C_2, C_3, C_4 are initial parameters, and $\bar{\phi}_i(z)$ expression are as follows

$$\begin{aligned} \bar{\phi}_1(z) &= \frac{1}{\bar{C}_a^2 + \bar{D}_a^2} (\bar{C}_a^2 \cosh \bar{D}_a z + \bar{D}_a^2 \cos \bar{C}_a z) \\ \bar{\phi}_2(z) &= \frac{1}{\bar{C}_a^2 + \bar{D}_a^2} \left(\frac{\bar{C}_a^2}{\bar{D}_a} \sinh \bar{D}_a z + \frac{\bar{D}_a^2}{\bar{C}_a} \sin \bar{C}_a z \right) \\ \bar{\phi}_3(z) &= \frac{1}{\bar{C}_a^2 + \bar{D}_a^2} (\cosh \bar{D}_a z - \cos \bar{C}_a z) \\ \bar{\phi}_4(z) &= \frac{1}{\bar{C}_a^2 + \bar{D}_a^2} \left(\frac{1}{\bar{D}_a} \sinh \bar{D}_a z - \frac{1}{\bar{C}_a} \sin \bar{C}_a z \right) \end{aligned} \quad (4.2.10)$$

where the expression for \bar{C}_a and \bar{D}_a are given by

$$\begin{aligned} \bar{C}_a^2 &= \frac{-A^2 + \sqrt{A^2 + 4\beta_1^4}}{2} \\ \bar{D}_a^2 &= \frac{+A^2 + \sqrt{A^2 + 4\beta_1^4}}{2} \end{aligned} \quad (4.2.11)$$

$$\text{and } \beta_1^4 = 4 (1 + 2Dp + p^2) \quad (4.2.12)$$

Thus \bar{C}_a and \bar{D}_a are the functions of 'p'.

(a) General Solution for Finite Beam on Pasternak Foundation.

The general solution of equations (4.2.9) and (4.2.10) can be solved for boundary conditions as described by equations (4.2.4), (4.2.5). The solution in Laplace transform for these boundary conditions can be written as

$$\bar{y}(z) = C_1 \bar{\phi}_1 + C_3 \bar{\phi}_3(z) - \bar{\phi}_4(z) \quad (4.2.13)$$

where C_1, C_3 are initial parameters and can be expressed as

$$C_1 = \frac{\left[\bar{\phi}_3''(R) \bar{\phi}_4'''(R) - \bar{\phi}_4''(R) \bar{\phi}_3'''(R) - 4\bar{D}_a^2 \{ \bar{\phi}_3''(R) \bar{\phi}_4'(R) \bar{\phi}_4''(R) \bar{\phi}_3' \right. \\ \left. + \frac{2}{(\bar{D}_a^2 - \bar{C}_a^2)^{1/2}} \{ \bar{\phi}_3'''(R) \bar{\phi}_4(R) - \bar{\phi}_4'''(R) \bar{\phi}_3(R) \} \right]}{\left[\bar{\phi}_3''(R) \bar{\phi}_1'''(R) - \bar{\phi}_1''(R) \bar{\phi}_3'''(R) - 4\bar{D}_a^2 \{ \bar{\phi}_3''(R) \bar{\phi}_1'(R) - \bar{\phi}_1''(R) \bar{\phi}_3'(R) \right. \\ \left. + \frac{2}{(\bar{D}_a^2 - \bar{C}_a^2)^{1/2}} \{ \bar{\phi}_3''(R) \bar{\phi}_1(R) - \bar{\phi}_1''(R) \bar{\phi}_3(R) \} \right]}$$

and

$$C_3 = \frac{\left[\bar{\phi}_4''(R) \bar{\phi}_1'''(R) - \bar{\phi}_1''(R) \bar{\phi}_4'''(R) - 4\bar{D}_a^2 \{ \bar{\phi}_4''(R) \bar{\phi}_1''(R) - \bar{\phi}_1''(R) \bar{\phi}_4'(R) \right. \\ \left. + \frac{2}{(\bar{D}_a^2 - \bar{C}_a^2)^{1/2}} \{ \bar{\phi}_4''(R) \bar{\phi}_1(R) - \bar{\phi}_1''(R) \bar{\phi}_4(R) \} \right]}{\left[\bar{\phi}_3''(R) \bar{\phi}_1'''(R) - \bar{\phi}_1''(R) \bar{\phi}_3'''(R) - 4\bar{D}_a^2 \{ \bar{\phi}_3''(R) \bar{\phi}_1''(R) - \bar{\phi}_1''(R) \bar{\phi}_3'(R) \right. \\ \left. + \frac{2}{(\bar{D}_a^2 - \bar{C}_a^2)^{1/2}} \{ \bar{\phi}_3''(R) \bar{\phi}_1(R) - \bar{\phi}_1''(R) \bar{\phi}_3(R) \} \right]} \quad (4.2.14)$$

The solution at $z = 0$ can be written, after solving equations (4.2.13) and (4.2.14), as

$$\begin{aligned}
& \left[2(\bar{D}_a^2 + \bar{C}_a^2)(\bar{D}_a^2 - \bar{C}_a^2)^{1/2}(1+2Dp)(\bar{D}_a \cosh \bar{D}_a R \sin \bar{C}_a R - \bar{C}_a \sinh \bar{D}_a R \cos \bar{C}_a R) \right. \\
& \quad \left. - \bar{C}_a \bar{D}_a \{2\bar{D}_a^2 \bar{C}_a^2 + (\bar{C}_a^4 + \bar{D}_a^4) \cosh \bar{D}_a R \cos \bar{C}_a R \right. \\
& \quad \left. + \bar{C}_a \bar{D}_a (\bar{D}_a^2 - \bar{C}_a^2) \sinh \bar{D}_a R \sin \bar{C}_a R \} \right] \\
\bar{y}(0,p) = \text{Imp } \frac{\lambda^2 \omega_n}{2EI} & \frac{\left[\bar{C}_a^2 \bar{D}_a^2 (\bar{C}_a^2 + \bar{D}_a^2) \{ \bar{D}_a^3 \cosh \bar{D}_a R \sin \bar{C}_a R + \bar{C}_a^3 \sinh \bar{D}_a R \cos \bar{C}_a R \} \right.}{\left[\bar{C}_a^2 \bar{D}_a^2 (\bar{D}_a^2 - \bar{C}_a^2)^{1/2} (\bar{C}_a^2 + \bar{D}_a^2)^2 (1+2Dp) \cosh \bar{D}_a R \cos \bar{C}_a R \right]} \\
& \quad \left. - 2\bar{C}_a \bar{D}_a (\bar{D}_a^2 - \bar{C}_a^2)^{1/2} (\bar{C}_a^2 + \bar{D}_a^2)^2 (1+2Dp) \cosh \bar{D}_a R \cos \bar{C}_a R \right] \quad (4.2.15)
\end{aligned}$$

(b) Infinite Beam on Pasternak Foundation. As the response functions at infinity have to be finite, the terms $e^{\bar{D}_a z}$ will have to be omitted in the expression (4.2.15). After simplifying the expression, the general solution for deflection at the centre of the beam can be written as

$$\bar{y}(0,p) = \text{Imp } \frac{\lambda^2 \omega_n}{2EI} \left[\frac{\bar{C}_a e^{-\bar{D}_a R} \cos \bar{C}_a R + \bar{D}_a e^{-\bar{D}_a R} \sin \bar{C}_a R}{2\bar{C}_a \bar{D}_a (\bar{C}_a^2 + \bar{D}_a^2)} \right] \quad (4.2.16)$$

(c) Finite Beam on Winkler Foundation. If the shear coefficient A is made zero, the equation (4.2.15) will represent the solution of a finite beam on Winkler foundation. For boundary conditions described by (4.2.7), the general solution can be expressed as

$$\bar{y}(0,p) = \text{Imp } \frac{\lambda^2 \omega_n}{2EI} \frac{1}{\beta_1^3} \left[\frac{1 + \cos \beta_1 R \cosh \beta_1 R}{\sin \beta_1 R \cosh \beta_1 R + \cos \beta_1 R \sinh \beta_1 R} \right] \quad (4.2.17)$$

(d) Infinite Beam on Winkler Foundation. For infinite beam, solution boils down to a simple expression, for the boundary conditions described by equation (4.2.8) and can be written as

$$\bar{y}(0, p) = \text{Imp} \frac{\lambda^2 \omega_n}{2EI} \frac{1}{\beta_1^3} \quad (4.2.18)$$

and general expression can be written as

$$\bar{y}(z) = \text{Imp} \frac{\lambda^2 \omega_n}{2EI} \frac{e^{-\beta_1 z}}{\beta_1^3} [\cos \beta_1 z + \sin \beta_1 z] \quad (4.2.19)$$

4.3 INVERSION OF LAPLACE TRANSFORM

Laplace transform methods bringout a close correspondance between visco-elastic and elastic problems. In fact, any problem of wave propagation in a visco-elastic medium can be reduced to Laplace inversion problem, so long as a solution can be found for an elastic solid subject to the same boundary conditions (7). Thus the techniques for inversion of Laplace transform can be applied for the present problem. Cost (13) has reviewed a number of inversion techniques. For impulse function, Post and Widder's approximate solution (4) can be used for simple general equations. Other approximate solutions which can be used are Ter-haar's solution, Schapery's direct method, Papoulis inversion method etc. (13). In this section, solution for an infinite beam on Winkler foundation is derived using Post & Widder's approximate solution. As this method involves the nth derivatives, it becomes quite tedious to develop expressions for finite beam on Winkler foundation or Pasternak foundation. Another inversion technique which may be used for complex problems, has been tried successfully for the inversion of Laplace transform expressions. This technique, developed by Berger (6), is an inversion formula for the Laplace transform in terms of a series expansion of Jacobi polynomials.

4.3.1. Post & Widder's Approximate Solution (4).

The Post and Widder's approximate solution is used for the infinite beam on Winkler foundation. The expression is

$$f(t) = \lim_n \left[(-1)^n \frac{p^{n+1}}{n!} \frac{d^n}{dp^n} f(p) \right] \quad p = n/t \quad (4.3.1)$$

The general solution for infinite beam using (4.3.1) can be solved by breaking the trigonometric and exponential functions into series form. The general solution given by equation (4.2.19) can be written in series form as

$$\bar{y} = \text{Imp} \frac{\lambda^2 \omega}{2EI} n \left[\frac{1}{\beta_1^3} - \frac{2.1}{2!} \frac{z^2}{\beta_1} + \frac{2.2}{3!} z^3 - \frac{2.2}{4} z^4 \beta_1 + \frac{2.4}{6!} z^6 \beta_1^3 - \frac{2.8}{7!} z^7 \beta_1^4 + \frac{2.8}{8!} z^8 \beta_1^5 - \frac{2.16}{10!} z^{10} \beta_1^7 + \dots \right] \quad (4.3.2)$$

Taking the inversion term by term

$$A_1 = L^{-1} \left[\frac{1}{\beta_1^3} \right] = e^{-D\theta} \frac{\pi^{1/2}}{\sqrt{3/4}} \left(\frac{\theta}{2\sqrt{1-D^2}} \right)^{1/4} J_{1/4}(\sqrt{1-D^2} \theta) \quad (4.3.3)$$

$$A_2 = L^{-1} \left[\frac{1}{\beta_1} \right] = e^{-D\theta} \frac{\pi^{1/2}}{\sqrt{1/4}} \left(\frac{2\sqrt{1-D^2}}{\theta} \right) J_{-1/4}(\sqrt{1-D^2} \theta) \quad (4.3.4)$$

For $n=5$

The derivatives of the terms of the series are

$$\text{for} \quad \beta_1 = \left[(5/\theta + D)^2 + (1-D^2) \right]^{1/4} = \left[(5/\theta + D)^2 + s^2 \right]^{1/4} \quad (4.3.5)$$

$$\begin{aligned}
\frac{\partial^5 \beta_1}{\partial \theta^5} = & - \frac{15 \cdot 11 \cdot 7 \cdot (5)^5 \cdot 3 \cdot 2}{4 \cdot 4 \cdot 4} (N_1)^{-19/4} (N_2)^5 + \frac{11 \cdot 7 \cdot (5)^4 \cdot 5 \cdot 3 \cdot 2}{4 \cdot 4} (N_1)^{-15/4} (N_2)^3 N_4 \\
& - \frac{7 \cdot (5)^4 \cdot 3 \cdot 3 \cdot 2}{4 \cdot 4} (N_1)^{-11/4} (N_2) (N_4)^2 - \frac{7 (5)^3 \cdot 3 \cdot 3 \cdot 3 \cdot 2}{4} (N_1)^{-11/4} (N_2)^2 (N_3) \\
& + \frac{(5)^2 \cdot 5 \cdot 3 \cdot 3 \cdot 2 \cdot 2}{4} (N_1)^{-7/4} (N_3) (N_4) + \frac{(5)^2 \cdot 5 \cdot 3 \cdot 3 \cdot 2 \cdot 2}{4} (N_1)^{-7/4} (N_2) (N_5) \\
& - 5 \cdot 5 \cdot 3 \cdot 2 \cdot 2 (N_1)^{-3/4} (N_6) \quad (4.3.6)
\end{aligned}$$

where $N_1 = \left(\frac{5}{\theta} + D\right)^2 + s^2$

$$N_2 = \frac{5}{\theta^3} + \frac{D}{\theta^2}$$

$$N_3 = \frac{10}{\theta^5} + \frac{D}{\theta^4}$$

$$N_4 = \frac{15}{\theta^4} + \frac{2D}{\theta^3}$$

$$N_5 = \frac{25}{\theta^6} + \frac{2D}{\theta^5}$$

$$N_6 = \frac{15}{\theta^7} + \frac{D}{\theta^6}$$

and $s = 1 - D^2$

For $\beta_1^3 = N_1^{3/4}$

$$\begin{aligned}
\frac{\partial^5 \beta_1^3}{\partial \theta^5} = & - \frac{13 \cdot 9 \cdot (5)^6 \cdot 3 \cdot 2}{(4)^3} (N_1)^{-17/4} (N_2)^5 + \frac{9 \cdot (5)^7 \cdot 3 \cdot 2}{(4)^2} (N_1)^{-13/4} (N_2)^3 (N_4) \\
& - \frac{(5)^5 \cdot (3)^2 \cdot 2}{(4)^2} (N_1)^{-9/4} (N_2) (N_4)^2 - \frac{(5)^5 (3)^2 \cdot 2}{4} (N_1)^{-9/4} (N_2)^2 (N_3) \\
& + (5)^3 (3)^2 (N_1)^{-5/4} (N_4) (N_5) \\
& + (5)^3 (3)^2 (N_1)^{-5/4} (N_5) (N_2) - (5)^2 \cdot 4 \cdot (3)^2 (N_1)^{-1/4} (N_6) \quad (4.3.7)
\end{aligned}$$

For $\beta_1^5 = (N_1)^{5/4}$

$$\begin{aligned} \frac{\partial^5 \beta_1^5}{\partial \theta^5} = & \frac{11 \cdot 7 \cdot (5)^6 \cdot 3 \cdot 2}{(4)^3} (N_1)^{-15/4} (N_2)^5 - \frac{7 \cdot (5)^6 \cdot 3 \cdot 2}{(4)^2} (N_1)^{-11/4} (N_2)^3 (N_4) \\ & + \frac{(5)^5 (3)^2 \cdot 2}{(4)^2} (N_1)^{-7/4} (N_2) (N_4)^2 \\ & + \frac{(5)^4 \cdot (3)^2 \cdot 2}{4} (N_1)^{-7/4} (N_2)^2 (N_3) - (5)^4 \cdot 3 (N_1)^{-3/4} (N_4) (N_3) \\ & - (5)^4 \cdot 3 (N_1)^{-3/4} (N_2) (N_5) \\ & - (5)^3 \cdot 3 \cdot (2)^2 (N_1)^{1/4} (N_6) \end{aligned} \quad (4.3.8)$$

$$\text{For } \beta_1^4 = (N_1) \quad , \quad \frac{\partial^5 \beta_1^4}{\partial \theta^4} = -10 \cdot 60 \cdot 2 (N_6) \quad (4.3.9)$$

Denoting the derivatives as

$$\begin{aligned} A_3 = -1/5(5/\theta)^6 \frac{\partial^5 \beta_1}{\partial \theta^5} \quad , \quad A_4 = -1/5(5/\theta)^6 \frac{\partial^5 \beta_1^3}{\partial \theta^5} \quad , \quad A_5 = -1/5(5/\theta)^6 \frac{\partial^5 \beta_1^4}{\partial \theta^5} \quad \text{and} \\ A_6 = -1/5(5/\theta)^6 \frac{\partial^5 \beta_1^5}{\partial \theta^5} \end{aligned}$$

The general solution can now be written as

$$y(z, \theta) = \frac{\lambda^2 \omega_n}{4EI} \text{Imp} \left[A_1 - A_2 z^2 - \frac{A_3}{3} z^4 + \frac{A_4}{90} z^6 - \frac{1}{315} A_5 z^7 + \frac{A_6}{2520} z^8 \right] \quad (4.3.10)$$

4.3.2 Laplace Inversion by Series Solution.

Papoulis (37) constructed an inversion formula of the one dimensional laplace transform in terms of series expansions of trigonometric functions and Legendre Polynomials. Berger (6) constructed this

inversion formula in terms of series expansion of Jacobi polynomials. Berger's (6) technique seems to be better than the methods adopting Legendre polynomials or trigonometric functions. Berger's technique is presented below in brief.

The one dimensional Laplace transform of $f(\theta)$ can be defined as

$$F(p) = \int_0^{\infty} e^{-p\theta} f(\theta) d\theta \quad (4.3.11)$$

$$\text{Let } f(x) = f \left[\left(-\frac{1}{\sigma} \right) \log \left(\frac{1-x}{2} \right) \right] \quad (4.3.12)$$

$$p = (m+1)\sigma + g-1 \quad (4.3.13)$$

where $\sigma > 0$, m is a positive integer and g is a parameter and assuming

$$\psi(x) = \sum_{n=0}^{\infty} g_n P_n^{(p_1, p_2)}(x) \quad (4.3.14)$$

the solution can be expressed as

$$f(x) = \psi(x) (1-x)^{p_1} (1+x)^{p_2} \left(\frac{1-x}{2} \right)^{(1-g/\sigma)} \quad (4.3.15)$$

where $P_n^{(p_1, p_2)}$ is the Jacobi polynomial.

Considering the time variable given by

$$\theta = \left[-1/\sigma \right] \log \left(\frac{1-x}{2} \right) \quad (4.3.16)$$

and substituting (4.3.12), (4.3.13), (4.3.14), (4.3.15), (4.3.16) into (4.3.11) and changing the order of summation, integration of equation (4.3.11) gives

$$F \left[\begin{matrix} (m+1)\sigma + g - 1 \\ (p_1, p_2) \end{matrix} \right] = (1 + \sigma 2^{m+1}) \sum_{n=0}^{\infty} g_n \int_{-1}^{+1} (1-x)^{m+p_1} (1+x)^{p_2} P_n^{(p_1, p_2)}(x) dx \quad (4.3.17)$$

Equation (4.3.17) may be expressed as

$$F \left[\begin{matrix} (m+1)\sigma + g - 1 \\ (p_1, p_2) \end{matrix} \right] = \frac{2^{(p_1 + p_2)}}{\sigma} \sum_{n=0}^m g_n B(m, n, p_1, p_2) \quad (4.3.18)$$

$$\text{where } B(m, n, p_1, p_2) = \frac{\Gamma(p_1 + m + 1) \Gamma(p_2 + n + 1) \Gamma(n - m)}{n! \Gamma(-m) \Gamma(p_1 + p_2 + m + n + 2)} \quad (4.3.19)$$

Γ denotes gamma function

The coefficient g_n may be computed from the equation (4.3.18) recursively and may be obtained as

$$g_n = \left[\frac{2\sigma}{h_n} \right]_{(p_1, p_2)} \sum_{k=0}^n (-1)^k C(k, n, p_1, p_2) F \left[\begin{matrix} (k+1)\sigma + g - 1 \\ (p_1, p_2) \end{matrix} \right] \quad (4.3.20)$$

$$\text{where } h_n = \frac{2^{p_1 + p_2 + 1}}{2n + p_1 + p_2 + 1} \frac{\Gamma(p_1 + n + 1)}{\Gamma(n + 1)} \frac{\Gamma(p_2 + n + 1)}{\Gamma(p_1 + p_2 + n + 1)} \quad (4.3.21)$$

$$\text{and } C(k, n, p_1, p_2) = \frac{1}{n!} \binom{n}{k} (n + p_1 + p_2 + 1) \dots (n + p_1 + p_2 + k) (p_1 + k + 1) \quad (4.3.22)$$

The Jacobi Polynomial is given by

$$P_n^{(p_1, p_2)}(x) = \sum_{k=0}^n C(k, n, p_1, p_2) \left(\frac{x-1}{2} \right)^k \quad (4.3.23)$$

Knowing the values of Jacobi Polynomials for any n , $P_n(p_1, p_2)$, and coefficient g_n , the function $\psi(x)$ can be determined. Then the response function $f(x)$ can be evaluated through equation (4.3.15).

4.4 RESULTS

Before determining the response values, the Laplace inversion technique was verified for displacement-time response at the centre of an infinite beam, resting on Winkler foundation. The exact solution in terms of fractional Bessel's function, at the centre of an infinite beam, resting on Winkler foundation, is available. The solution in Laplace transform is given by (14)

$$\begin{aligned}\bar{y}(0,p) &= \text{Imp} \frac{\lambda^2 \omega_n}{8EI} \frac{1}{(1+2Dp+p^2)^{3/4}} \\ &= \text{Imp} \frac{\lambda^2 \omega_n}{8EI} \frac{1}{(p^2+s^2)^{3/4}}\end{aligned}\quad (4.4.1)$$

where $s^2 = 1-D^2$ $p^2 = (p+D)^2$

Thus after inversion

$$y(0,\theta) = \text{Imp} \frac{\lambda^2 \omega_n}{8EI} \frac{\sqrt{\pi}}{\left[\frac{3}{4}\right]} \left(\frac{\theta}{2\sqrt{1-D^2}}\right)^{1/4} J_{1/4}(\sqrt{1-D^2}\theta) e^{-D\theta} \quad (4.4.2)$$

where $\text{Imp} = \frac{W}{g}$ $v_0 = W \sqrt{\frac{2h}{g}}$ - (14) (4.4.3)

v_0 = velocity of freely falling mass $\left(\frac{W}{g}\right)$, just before striking the beam.

For the verification of the numerical inversion of Laplace transform, an impulse load ($W = 40\text{kg}$, $v_0 = 441 \text{ cm/sec.}$) was applied on an infinite beam of mass per unit length, $0.001 \text{ kg.sec.}^2/\text{cm}^2$ and moment of inertia 113.0 cm^4 , resting on Winkler foundation ($K = 6000 \text{ kg/cm}^2$). (Table 4.1). For Laplace transform inversion the values

of constants for computation are taken as $p_1 = 3.0$, $p_2 = 3.0$, $\sigma = 50.0$, $g = 0.0$. In figure 4.1 displacement time response is plotted by the dotted line for an infinite beam, resting on Winkler foundation, using numerical inversion technique. Solid curve shows the displacement time curve for beam, using the exact solution.

From this figure (Fig. 4.1) it can be observed that the response by numerical inversion is quite close to the response, by the exact solution. As the time is increasing, the time period of response, by numerical inversion, is increasing slightly. Also, the amplitudes are little higher compared to exact solution. For most of the practical problems, the response is important for initial two or three time cycles. In this range, the numerical results can be seen to be matching closely with the exact solution (36).

Fig. 4.2, shows the displacement time response of an infinite beam on Winkler foundation for another set of soil and beam parameters (Table 4.1). In this case the spring constant of the soil medium is 800 kg/cm^2 . The infinite beam of mass per unit length, equal to $.00016 \frac{\text{kg. sec}^2}{\text{cm}^2}$, has the moment of inertia 6.66 cm^4 . The impulse load was applied through a body of 10 kg, falling freely from the height of 100 cm. ($W = 10\text{kg}$, $v_0 = 441 \text{ cm/sec.}$). In this case also, the response can be seen to be close to the response, by exact solution. With increasing time, the response period is slightly increasing as was observed for the previous set of parameters. The amplitude is also increasing but very marginally. For the initial two or three time cycles, the response is matching as in Fig. 4.1.

Fig. 4.3 presents the peaks of the response curve with time for exact and numerical solution of displacement response at the centre of an infinite beam resting on Winkler foundation. While the peaks are occurring at constant interval for the response by exact solution, the time period is increasing with subsequent peaks, in response curve obtained by numerical inversion. Still, for initial two or three time cycles, it can be observed from the Figure (Fig. 4.3) that the time period is more or less constant.

4.4.1 Infinite Beam

In Fig. 4.4 the maximum displacement with time cycle is plotted for various values of damping factor D . The solid lines show the curves obtained by exact solution and dotted lines, by numerical inversion. It can be observed that with increase in time cycles, the maximum displacement is decreasing. Also, as the damping factor is increasing, the maximum displacement is decreasing. The rate of decrease in maximum displacement is higher for the damped case, compared to undamped case. The maximum displacement values obtained by numerical inversion follows the same trend but the magnitude of displacement is little higher with increasing time.

Fig. 4.5 presents the variation of maximum displacement with time for the another set of soil and beam parameters. The response curve is plotted from the results obtained by numerical inversion. As was observed in Fig. 4.4, the maximum displacement decreases with time. At lower time values, the rate of decrease is higher. With time

increasing, the rate of decrease becomes less as in Fig. 4.4. The maximum displacement values are lower for damped case and is decreasing with increase in damping factor. The rate of decrease in maximum displacement for damped case, is higher than, for the undamped case.

The variation of maximum displacement of the first peak, with damping factor is shown in Fig. 4.6, for both the sets of soil and beam parameters. Maximum displacement is decreasing with increasing damping factor.

Fig. 4.7 presents the variation of maximum displacement, along the length of the beam for the set 1 of soil and beam parameters given in table 4.1. Responses are plotted for three values of damping factor (0.0, 0.05, 0.10). The maximum displacement (first peak) decreases along the length of the beam. While at lower values of z , the rate of decrease is slow, the displacement decreases fast at higher values of z . For all the values of damping factors, the decrease in maximum displacement follows the same trend.

The variation of maximum displacement along the length of the infinite beam is shown in Fig. 4.8 for set 2 of soil and beam parameters (Table 4.1). The maximum displacement is decreasing as ' z ' is increasing. For lower values of z , the rate of decrease is less. After that, the maximum displacement decreases fast. For different values of damping factor, the rate of decrease is nearly the same, as observed for set 1.

Using Post & Widder's (4) approximate solution, the response curves for an infinite beam resting on Winkler foundation and subjected

to impulse load are drawn in Fig. 4.9 and 4.10. The curves are drawn for both damped and undamped cases.

Fig. 4.9 shows the maximum displacement (displacement at the peak of first cycle) variation along the length of the beam for undamped and damped ($D = 0.05$) Winkler foundation. The soil and beam parameters are as follows

| | |
|-------------------|--|
| Spring constant | $= 5.0 \text{ kg/cm}^2$ |
| Moment of inertia | $= 65 \text{ cm}^4$ |
| Mass of the beam | $= .0016 \frac{\text{kg. sec}^2}{\text{cm}}$ |
| Impulse load | $= 40 \text{ kg sec.}$ |

The maximum displacement is decreasing with the increase in z value. The maximum displacement is higher for $D=0.0$ in comparison to the value of maximum displacement for $D = 0.05$. The rate of decrease for undamped and damped cases follow the same trend, i.e. at lower values of z the rate of decrease is slow, and at higher values of z , the decrease in maximum displacement is fast.

Fig. 4.10 presents the variation of maximum displacement at the centre of the beam with damping factor (with the same data as given above). The maximum displacement is decreasing with the increase in damping factor. It can be observed that the decrease is not quite linear. This curve is compared with the exact solution (14).

4.4.2 Finite Beam.

For finite beam, resting on Winkler foundation, the response curves are drawn using Berger's (6) numerical inversion technique

Fig. 4.11 presents the variation of maximum displacement at the centre of the beam, with the time. Fig. 4.12 shows the variation of maximum displacement along the length of the beam for damped and undamped cases.

It can be observed from Fig. 4.11 that maximum displacement decreases fast as the time passes. As for infinite beam, the decrease in maximum displacement for damped foundation is rapid, that for undamped foundation. Again, the magnitude of maximum displacement of the finite beam at any time t , is less than the amplitude for infinite beam at that time. In Fig. 4.11, the variation of maximum displacement of finite beam is compared with the displacement of infinite beam.

Fig. 4.12, shows the variation of maximum displacement along the length of beam for damped and undamped cases. The maximum displacement along the length of beam for undamped foundation is higher than for $D=0.05$. However, the rate of variation of maximum displacement along the length is more or less same for undamped and damped cases.

From these results it can be observed that Beger's technique can be used successfully for the general solution of beams on elastic foundations subjected to impulse load.

Table 4.1

Soil and Beam Parameters used for Numerical Results by Inversion
Technique

| Set | Spring constant kg/cm^2 | Modulus of Ela- sticity kg/cm | Moment of Inertia cm^4 | Mass of the Beam kg. sec^2 cm^2 | Weight of falling body kg. | Height of Fall cm. |
|----------|--|---|--|--|----------------------------------|-----------------------|
| Set No.1 | 6000.00 | 2100000.0 | 113.0 | 0.001 | 40.00 | 100.00 |
| Set No.2 | 800 .00 | 2100000.0 | 6.66 | 0.00016 | 10.00 | 100.00 |

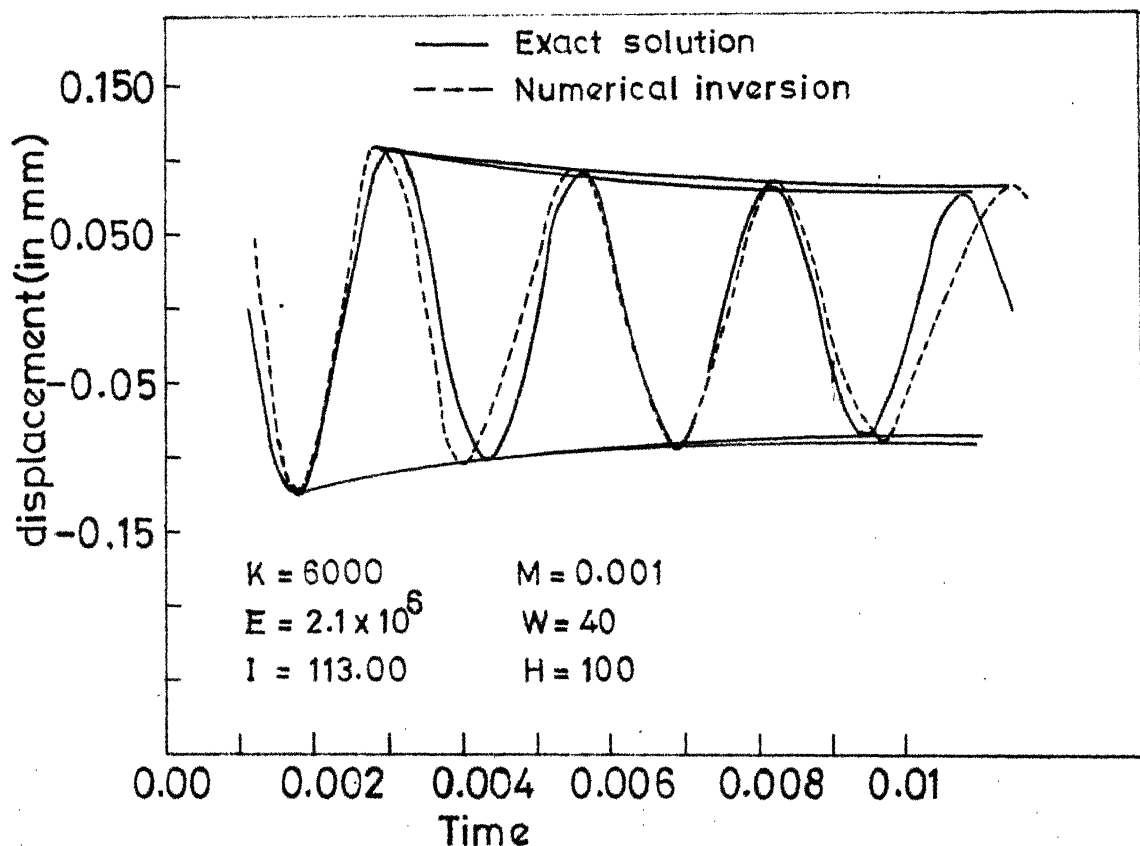


Fig.4.1 Variation of displacement with time of an infinite beam on Winkler foundation subjected to impulse load (set 1)

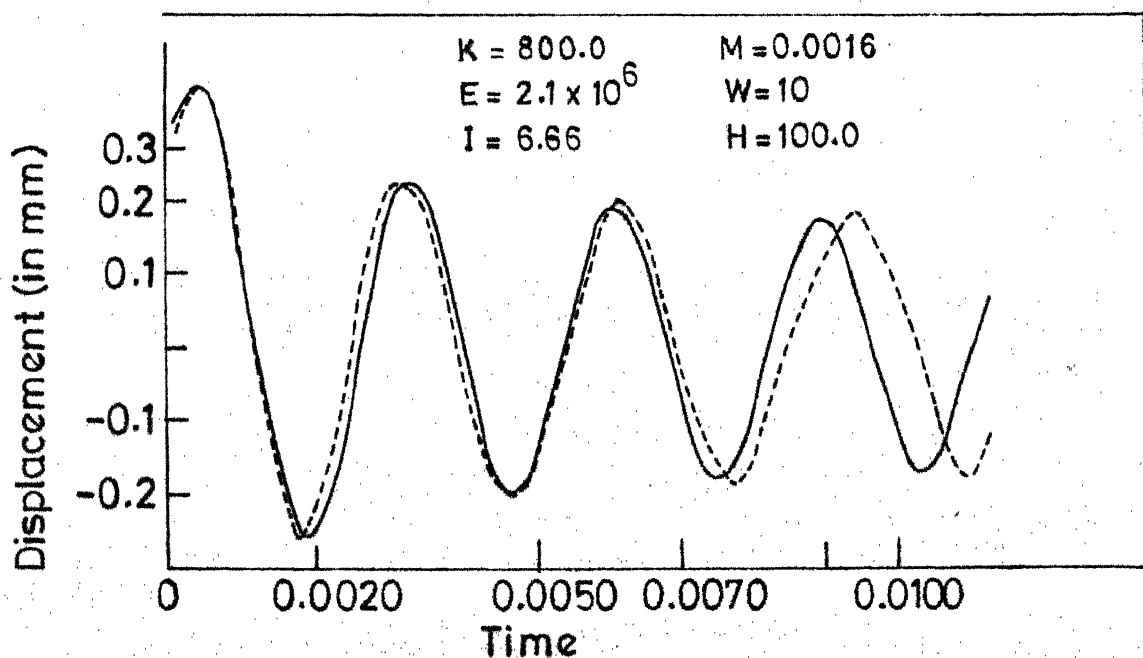


Fig.4.2 Variation of displacement with time of an infinite beam on Winkler foundation subjected to impulse load (set 2)

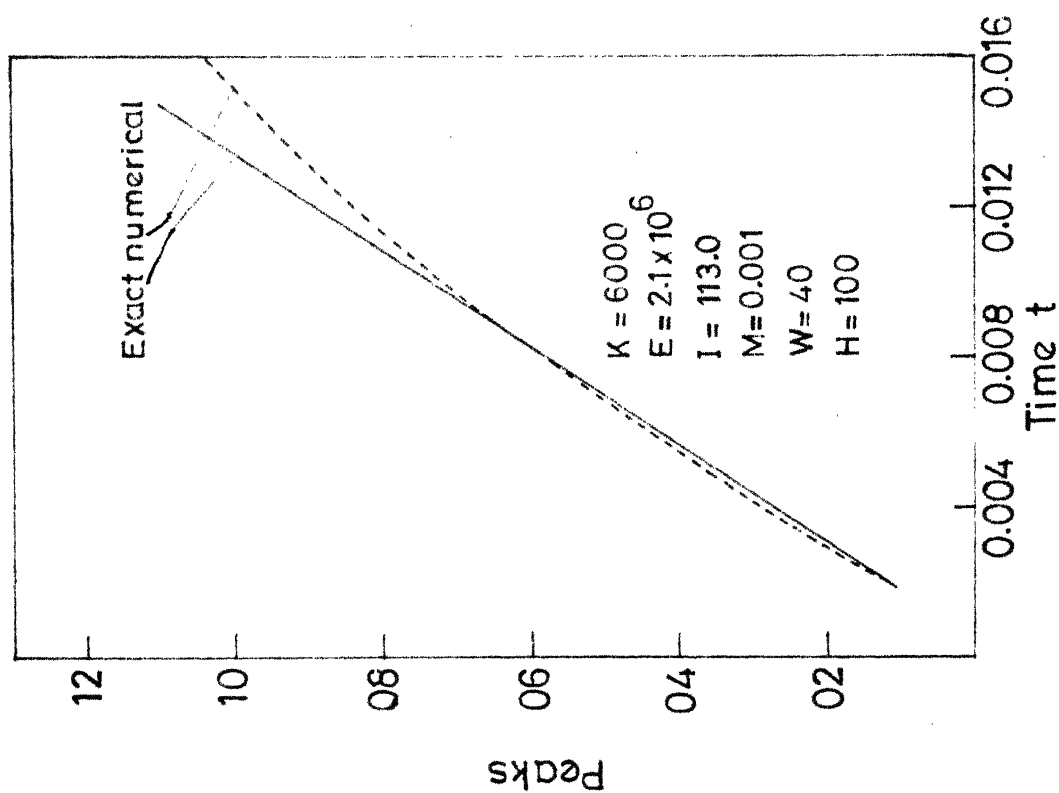


Fig.4.3 Comparison of time period of the response by numerical inversion with that of exact solution.

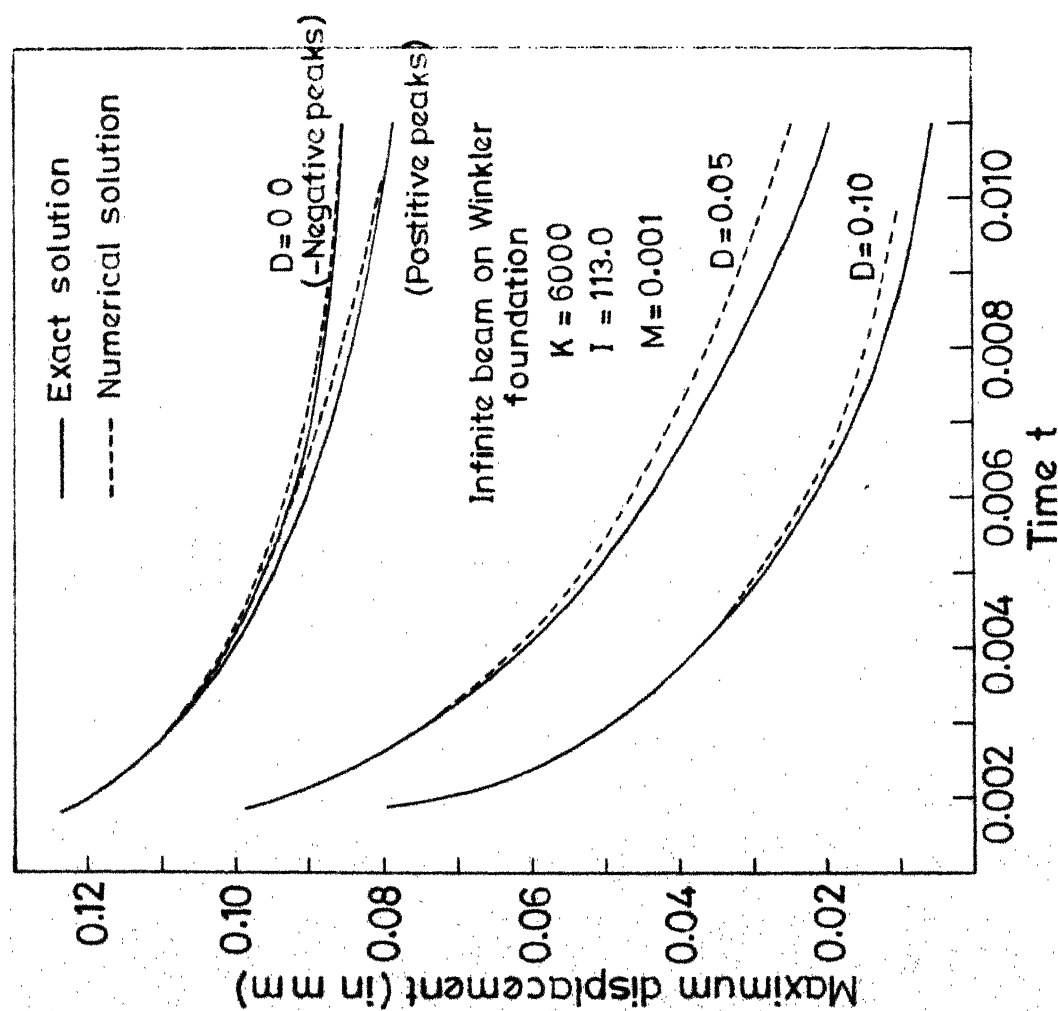


Fig.4.4 Variation of maximum displacement at the centre of the beam with time (set 1).

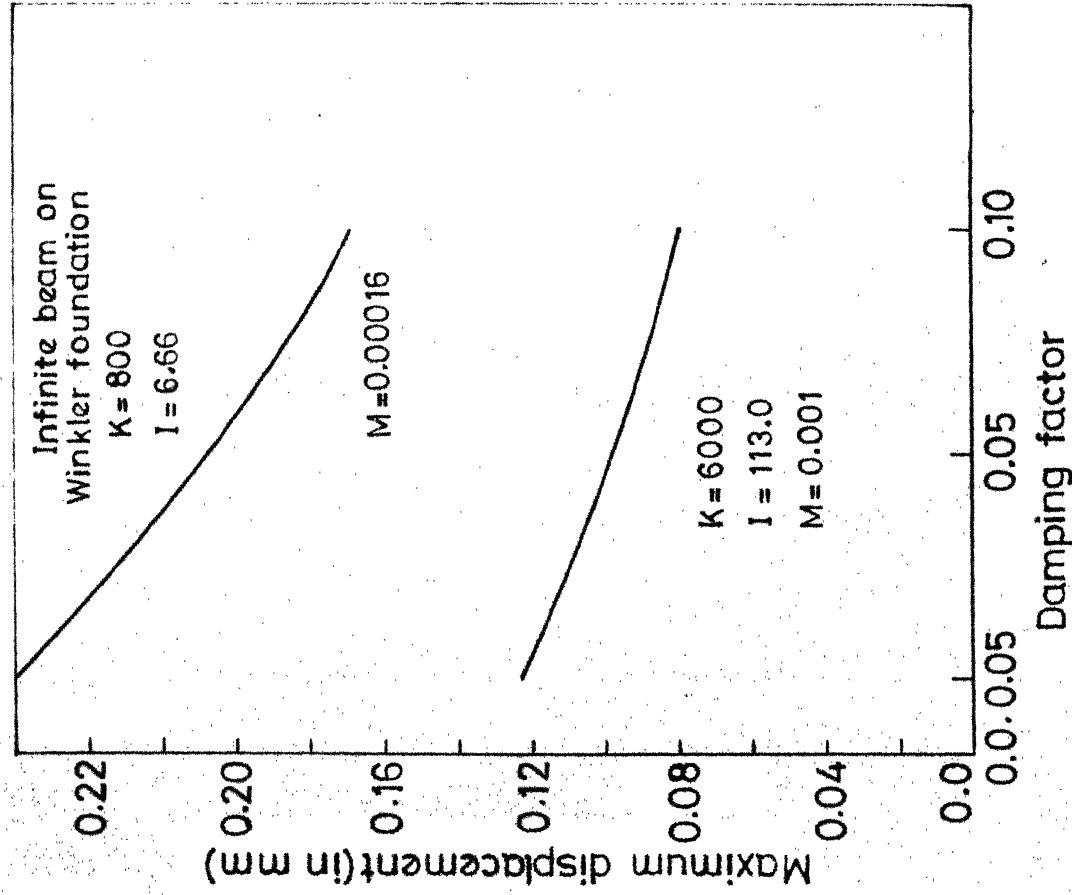


Fig.4.6 Variation of maximum displacement with damping factor (Berger's technique)

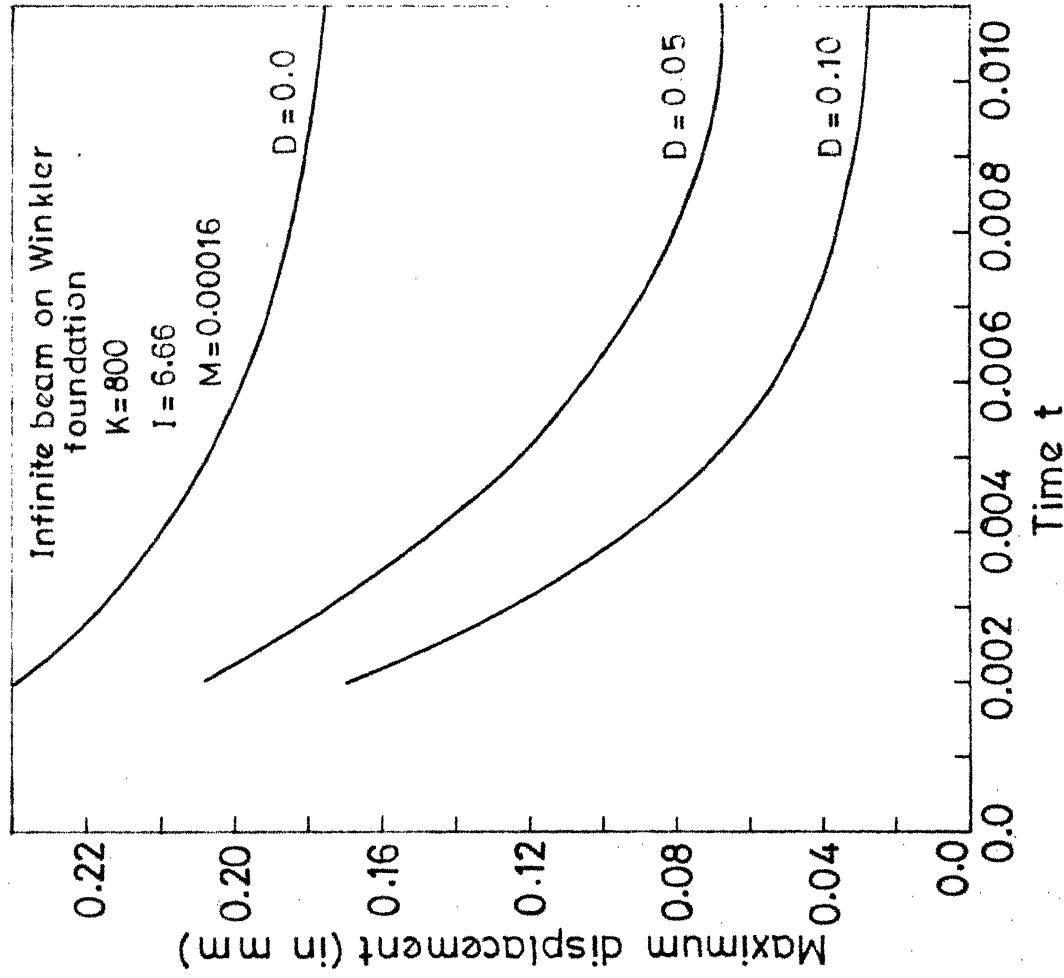


Fig.4.5 Variation of maximum displacement at the centre of the beam with time (Berger's technique) (set 2)

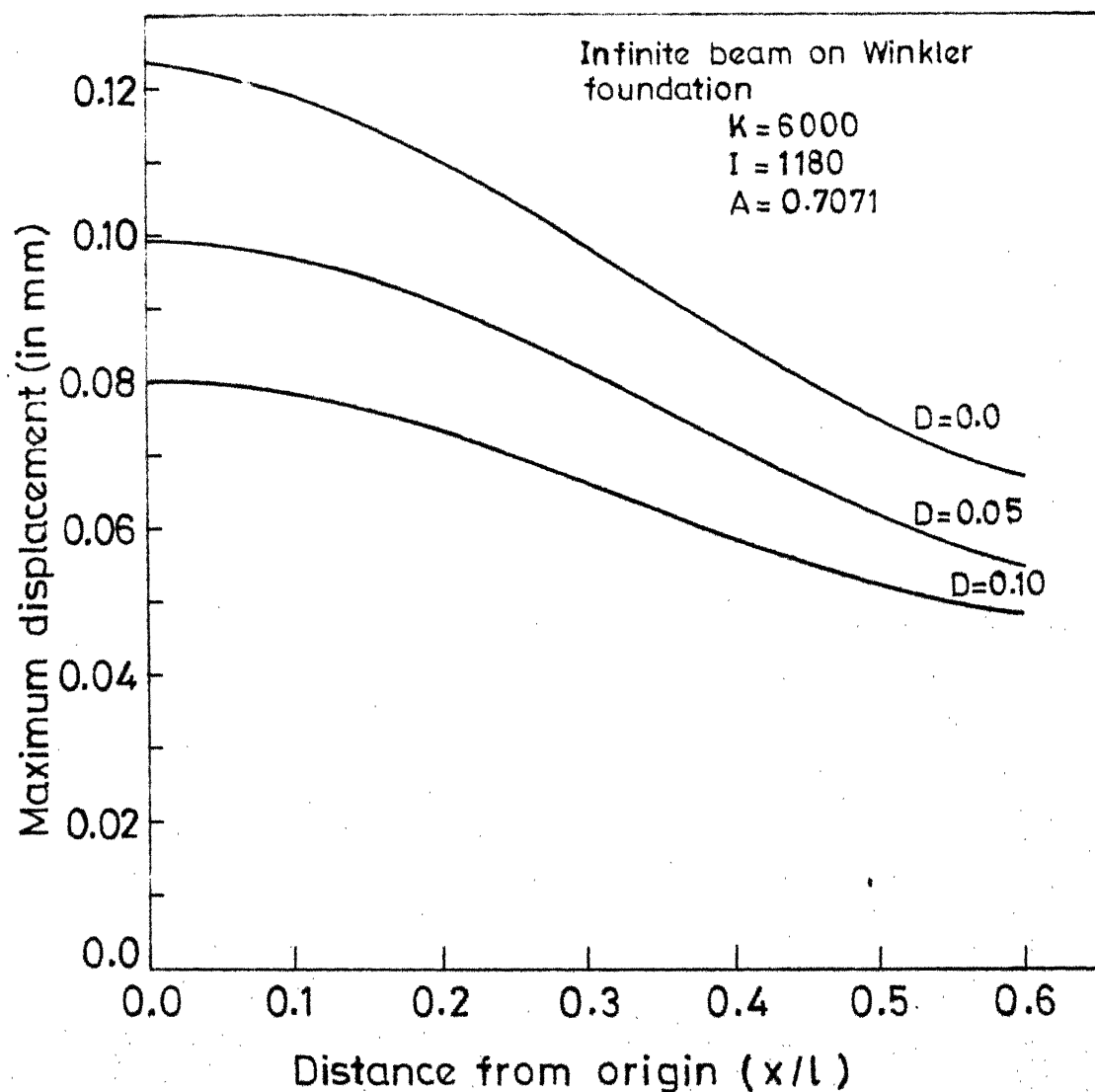


Fig.4.7 Variation of maximum displacement along the length of beam (Berger's technique) (set 1)

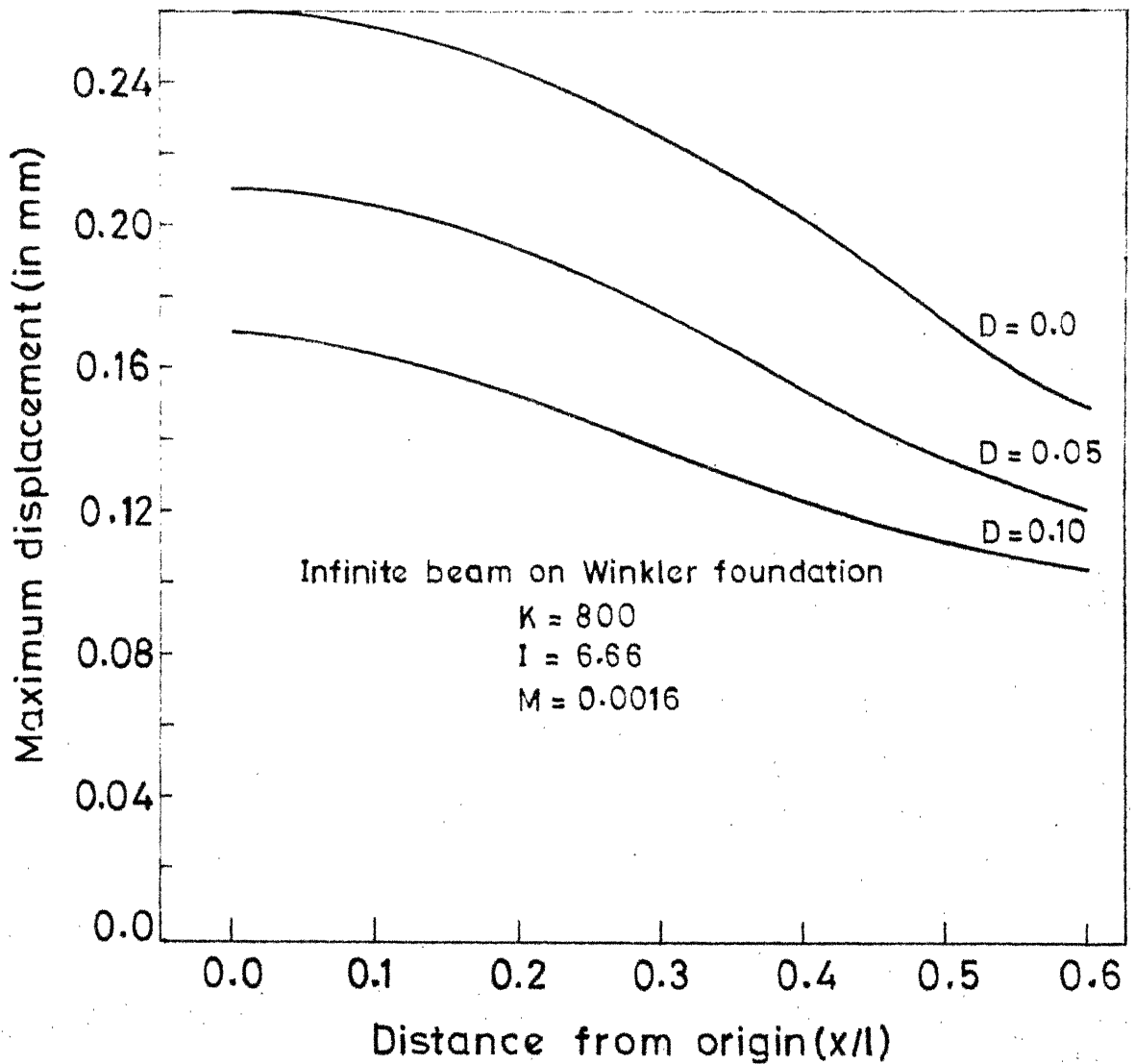


Fig.4.8 Variation of maximum displacement along the length of beam (Berger's technique) (set 2)

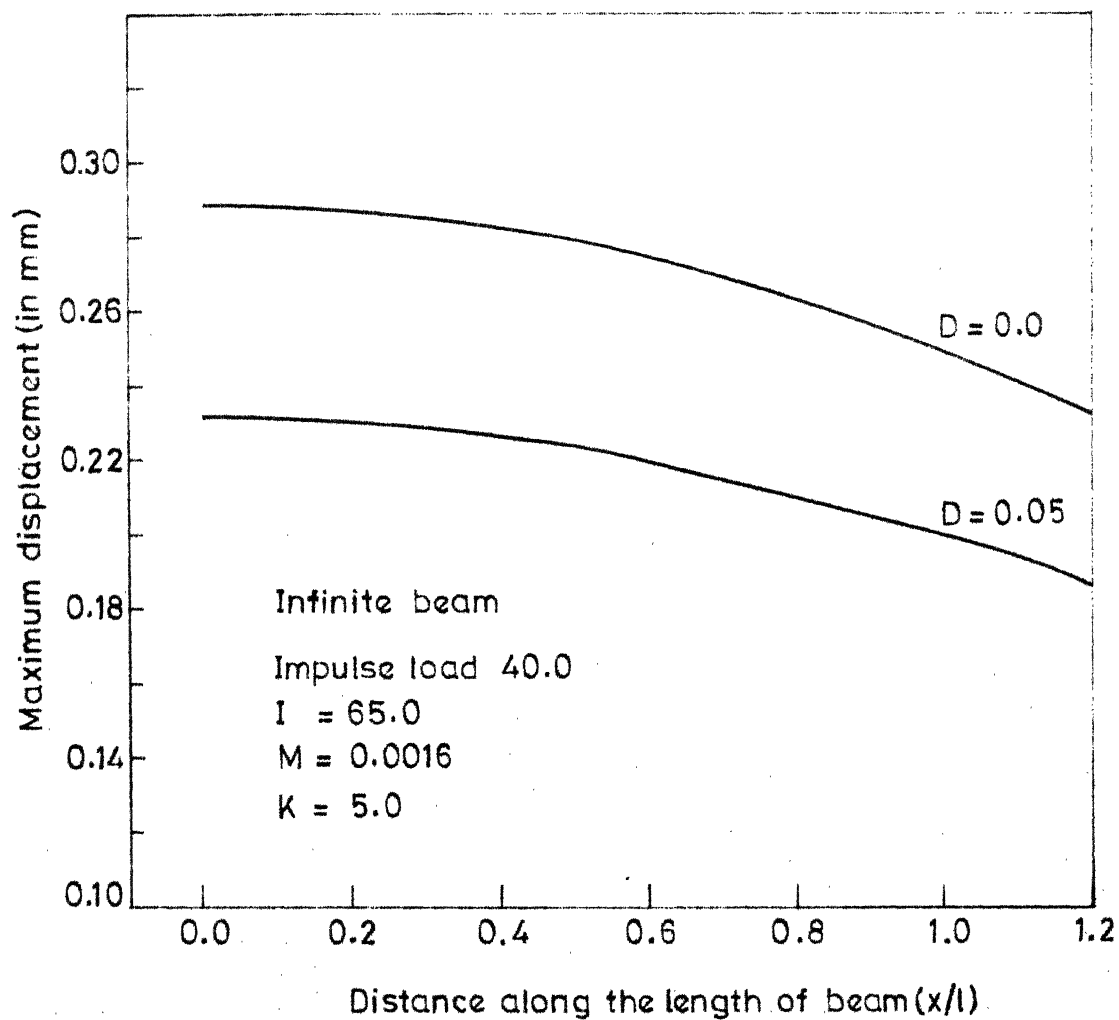


Fig. 4.9 Variation of maximum displacement along the length of beam.
(Post & Widder's technique)

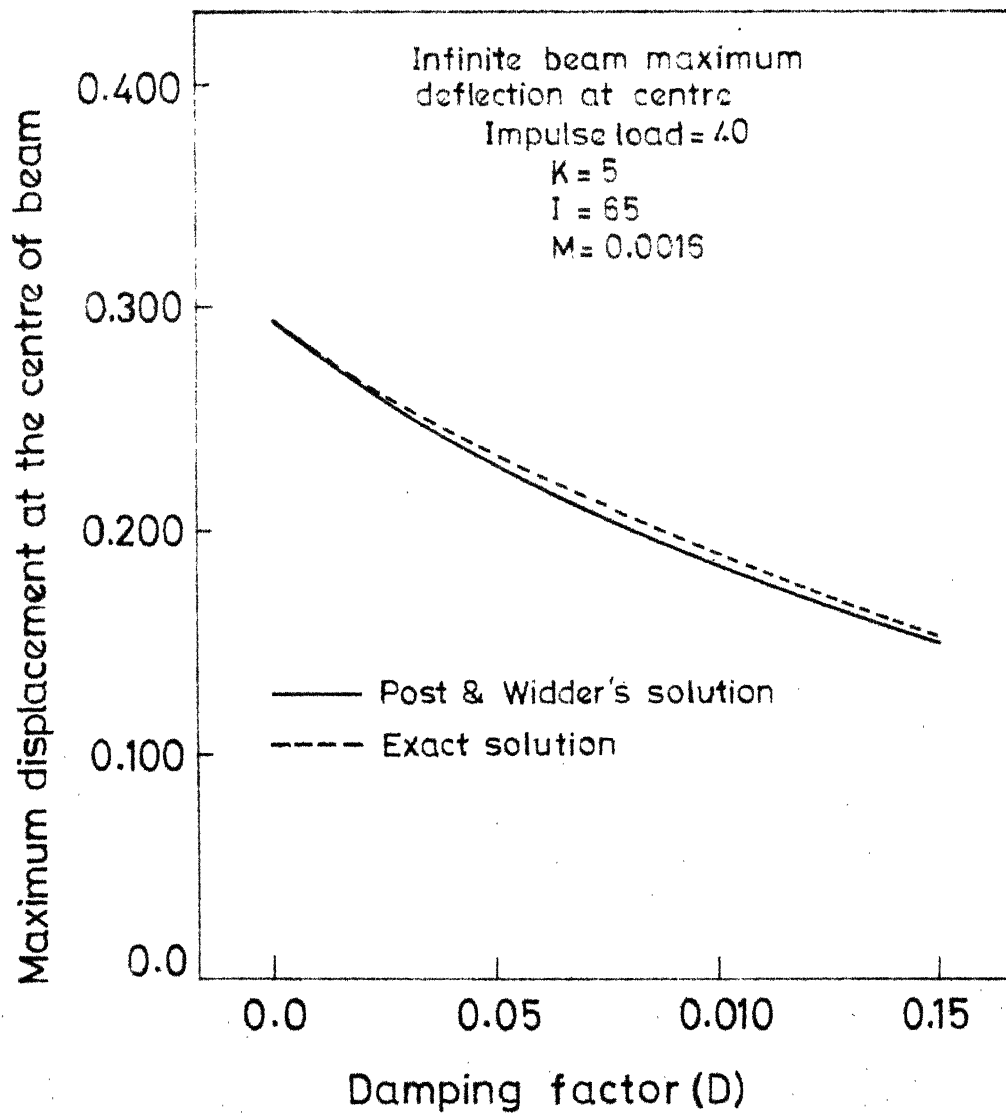


Fig.4.10 Variation of maximum displacement at the centre of beam with damping factor (Post & Widder's technique)

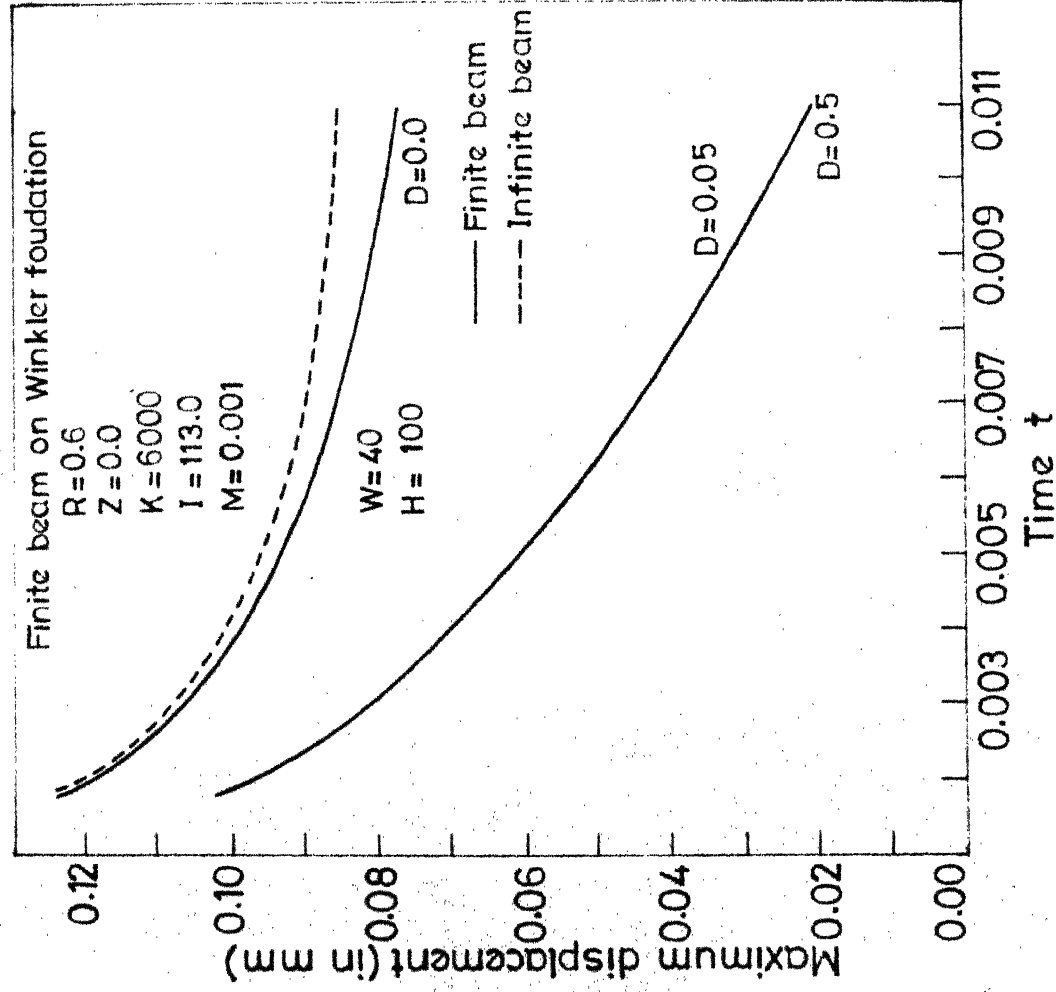


Fig. 4.11 Variation of maximum displacement at the centre of the finite beam ($R=0.6$) (Berger's technique)

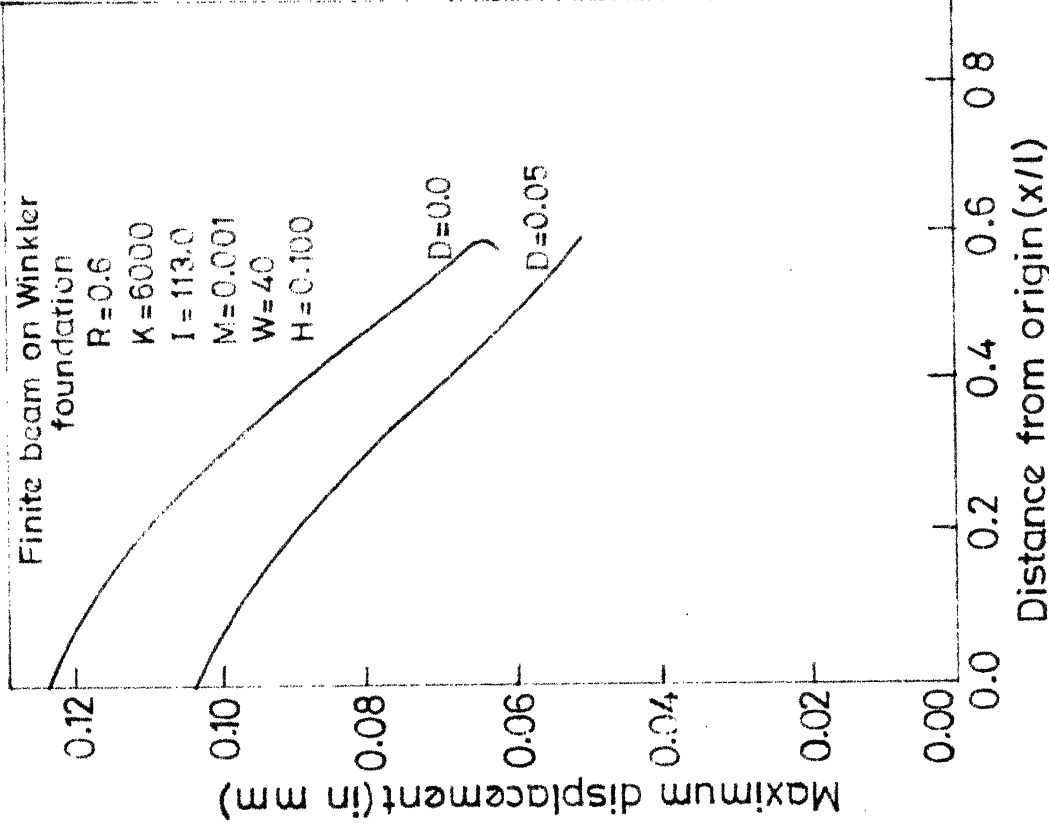


Fig. 4.12 Variation of maximum displacement of finite beam ($R=0.6$) along the length of the beam (Berger's technique)

CHAPTER 5

CONCLUSIONS AND RECOMMENDATIONS

5.1 CONCLUSIONS

Experimental and analytical investigations have been carried out on some problems in the area of dynamic soil-structure-interaction, in the present work. Results have been discussed and conclusions have been presented in each chapter separately. However, general conclusions are presented below from the present investigations.

To facilitate the correct evaluation of soil parameters which characterize the behaviour of soil medium, studies have been made on the effect of magnitude of force levels and flexibility of the footing on the foundation response. From the experimental results it can be observed that with the increase in force level, the magnitude of displacement increases more or less proportionately. The theoretical analysis of the footings on soil medium, shows that the displacement of the footing is directly proportional to the force applied. The flexibility of the footing has very little effect on spring constant. Analytical solutions based on elastic theory show that there is no difference in spring constant values due to variation in flexibility. The studies on the effect of size and shape of the foundation on soil parameters reveal that with length and width variation, the soil parameters such as spring constant, damping factor etc. vary considerably. While the spring constant is increasing with increasing L/B ratio, the

damping factor is decreasing. Thus, in the analysis of rectangular plates of higher L/B ratios and long beams, these soil parameters may have to be modified.

From the analytical results of the beam on elastic foundations (Winkler model and Pasternak model) carrying a concentrated mass on it and subjected to steady state dynamic force, it can be seen that the effect of concentrated mass on the displacement response is quite pronounced. The maximum displacement decreases very fast as the concentrated mass increases on the beam. However, for the beams resting on Pasternak foundation, the shear coefficient of the shear layer of the foundation model, plays a more important role in decreasing the displacement, not only at the centre, but also, along the length of the beam. For certain values of shear coefficient, the effect of concentrated mass is not noticeable. To compare the theoretical results, experiments have been conducted on a long beam carrying a concentrated mass and resting on the natural soil deposit. These experimental values are in close agreement with the theoretical results.

The beam resting on elastic foundation has again, been analysed for the transient load (impulse load). The beam subjected to impulse load has been analysed using Laplace transform. The solutions have been obtained using numerical inversion of Laplace transform. While the Post and Widder's formula for numerical inversion was used for infinite beam on elastic foundation, the Berger's Laplace inversion technique was used for finite and infinite beams on elastic foundations. However, Berger's technique has been shown to be more useful for complex problems,

while Post and Widder's formula can be used for simple cases. These numerical results show that the displacement along the length of the beam decreases as the distance from origin increases. With damping of the foundation, also, the displacement decreases.

5.2 RECOMMENDATIONS

The following topics are recommended for further studies

- (1) Experimental investigations on the effect of geometry on prototype foundations.
- (2) Experimental investigations for contact pressure distributions for dynamic loads.
- (3) Effect of shear deformation and rotary inertia of the beam on the beam-foundation response.
- (4) Beams subjected to periodic and aperiodic loads such as triangular pulse, rectangular pulse etc.

REFERENCES

1. Anderson, R.A. "Flexural Vibrations in Uniform Beams According to the Timoshenko Theory" Journal of App. Mech. Vol. 20, No. 4, 1953, pp (504-510).
2. Baker, W.E. "Vibration Frequencies for Uniform Beams with Central Masses" Journal of App. Mech. Vol. 31, No. 2, 1964, pp. (335-337).
3. Barkan, D.D. "Dynamics of Bases and Foundations" Mc-Graw Hill Book Co. New York 1962.
4. Bellman, R.E., Kalaba, R.E. and Lockett, J.A. "Numerical Inversion of the Laplace Transform Application to Biology, Economics, Engineering and Physics" American Elsevier Publication 1966.
5. Berger, B.S. "Dynamic Response Functions" Journal of Engg. Mech. ASCE Vol. 90, No. EM4, 1964, pp. (131-148).
6. Berger, B.S. "The Inversion of the Laplace Transform with Applications to the Vibration of Continious Elastic Bodies" Journal of App. Mech. Vol. 35, No. 4, Dec. 1968, pp. (837-839).
7. Berry, D.S. "Stress Propagation in Visco-elastic Bodies" Journal of Mechanics and Physics of Solids, Vol. 6, 1958, pp. (177-185).
8. Biot, M.A. "Bending of an Infinite Beam on an Elastic Foundation" Journal of App. Mech., Vol. 4, No. 1, ASME, 1937, pp. (A1-A7).
9. Boley, B.A. & Chao C.C. "Some Solutions of the Timoshenko Beam Equations" Journal of App. Mech., Vol. 22, No. 4, Dec. 1955, pp. (579-586).
10. Boley, B.A. and Chao, C.C. "An Approximate Analysis of Timoshenko Beams under Dynamic Loads", Journal of App. Mech., Vol. 25, No. 1, March 1958, pp. (31-36).
11. Bowles, J.E. "Foundation Analysis and Design" McGraw Hill-Kogakusha Ltd., 1968.
12. Chen, Y. "On the Vibration of Beams or Rods Carrying a Concentrated Mass" Journal of App. Mech. Vol. 30, Trans. ASME Vol. 85, 1963, pp. (310-311).

13. Cost, T.L. "Approximate Laplace Transform Inversion in Visco-elastic Stress Analysis", AIAA Journal, Vol. 2, No. 12, 1962, pp. (2157-2166).
14. Crandell, S.H. "Dynamic Analysis of a High Speed Track" Studies on Dynamics and Instrumentation of the Holloman Tract, Holloman Air force Base, New Mexico-1959.
15. Das, Y.C., Deshmukh, R.S. "Beam Vibrations with Centrally Attached Mass" Bulletin of Indian Society of Earthquake Technology, Vol. VII , No. 2, June 1970, pp. (89-95).
16. Eringen, A.C. "Transverse Impact on Beams and Plates" Journal of App. Mech. Vol. 20, No. 4, Dec. 1953, pp. (461-468).
17. Fletcher, D.Q. and Herrman, L.R. "Elastic Foundation Representation of Continuum" Journal of Engg. Mech. Div. ASCE Vol. 97, No. EM1, Feb. 1971 , pp. (95-107).
18. Funston, N.E. and Hall, W.J. "Footing Vibrations with Nonlinear Subgrade Support" Journal of Soil Mech. & Found. Division ASCE, Vol. 93, SM5, 1967, pp. (191-211).
19. Han, L.S. "On the Free Vibration of a Beam on a Nonlinear Elastic Foundation" Journal of App. Mech. Vol. 32, No. 2, 1965, pp. (445-447).
20. Hetenyi, M. "Beams on Elastic Foundation" The University of Michigan Press, Ann Arbor, Michigan, 1946.
21. Hopmann, W.H. "Impact of a Mass on a Damped Elastically Supported Beam" Journal of App. Mech. Vol. 15, No. 2, 1948 pp (125-136).
22. Hopmann II, W.H. "Forced Lateral Vibration of Beam Carrying a Concentrated Mass" Journal of App. Mech. Vol. 19, Trans ASME, Series E, 1952, pp. (301-307).
23. I.S. Code 5249-1969" Method of Test for Determination of Insitu Dynamic Properties of Soils" I.S.I. New Delhi-1969.
24. Jennings, P.C. and Bielak, J. "Dynamics of Building Soil Interaction" Bulletin of Seismology Society, Vol. 63, 1973, pp. (9-48).
25. Kameswara Rao, N.S.V. , Das, Y.C., and Anandakrishnan, M. "Dynamic Response of Beams on Generalised Elastic Foundations" International Journal of Solids & Structures Vol. 11, March, 1975, pp. (255-273).

26. Kameswara Rao, N.S.V. "Dynamics of Soil Structure Systems-a Brief Review" Journal of Structure Engg. Vol. 4, No. 4, Jan. 1977 , pp. (149-153).
27. Kausel, E. and Rosset, J.M. "Dynamic Stiffness of Circular Foundations" Journal of Engg. Mech. ASCE, Vol. 101, No. EM6, Dec. 1975, pp. (771-785)
28. Kenny, J.T. "Steady State Vibrations of Beam on Elastic Foundation for Moving Loads" Journal of App. Mech. ASME, Vol. 21, 1954, pp. (359-364).
- 29 . Kerr, A.D. "Elastic and Viscoelastic Foundation Models" Journal of App. Mech. Vol. 31, No. 3, 1964, pp. (491-498).
30. Krishna Murty, A.V. "Vibrations of Short Beams" AIAA Journal Vol. 8, No. 1, 1970, pp. (34-38).
31. Luco, J.E. and Westmann, R.A. "Dynamic Response of Circular Footings" Journal of Engg. Mech. Vol. 97, EM5, Oct. 1971 pp. (1381-1395).
32. Ludwig, K. "Deformation of a rail Elastically Supported and of Infinite Length by Loads Moving at a Constant Horizontal Velocity", Proc. 5th International Congress of Mechanics, March, 1938, (p. 650).
33. Mathews, P.M. "Vibration of a Beam on Elastic Foundation" Zeitschrift fur angewandte Mathematik and Mechanic Band-38, 1958, Seite (105-115).
34. Miklowitz, J. "Flexural Wave Solutions of Coupled Equations Representing the More Exact Theory of Bending" Journal of App. Mech. Vol. 20, No. 4, Dec. 1953, pp. (511-514).
35. Novak, M. "Effect of Soil on Structural Response to Wind & Earthquake" Journal of Earthquake Engg. and Structural Dynamics Vol. 3, 1974, pp. (79-96).
36. Nowacki, W. "Dynamics of Elastic Systems" Chapman & Hall Ltd. London 1963.
37. Papoulis, A. "A New Method of Inversion of the Laplace Transform" Quarterly of App. Mathematics, Vol. 14, 1957, pp. (405-414).
38. Parmelee, R.A. "Building Foundation Interaction Effects" Journal of Engg. Mech. Div. ASCE, Vol. 93, EM2, 1967, pp (131-152).
39. Prasad, B.B. "Impact Loads on Beams on Elastic Foundation" M. Tech. Thesis to I.I.T. Kanpur Sep. 1974.

40. Rades, M. "Steady State Response of a Finite Beam on a Pasternak type Foundation" International Journal of Solids & Structures, Vol. 6, 1970, (739-756).
41. Rainer, J.H. "Structure Ground Interaction in Earthquakes" Journal of Engg. Mech. Div. ASCE, Vol. 97, EM5, 1971, pp. (1431-1450).
42. Rainer, J.H. "Damping in Dynamic Structure Foundation Interaction" Canadian Geotechnical Journal Vol. 12, No. 1, Feb. 1975, pp. (13-22).
43. Reissner, E. "Stationary and Axially Symmetrical Vibrations of a Homogeneous Elastic Half-space Caused by Vibrating Mass" Ing. Archiv. Band VII (In German) 1936, pp.(281-396)
44. Richart, F.E., Woods, R.D. and Hall, J.R. "Vibrations of Soils and Foundations" Prentice Hall, New Jersey 1970.
45. Rosset, J., Whitman, R.V. and Dobry R. "Model Analysis for Structures with Foundation Interaction" Journal of Structural Div. ASCE, Vol. 99, 1973, pp. (399-416).
46. Saito Hideo and Tomizo Murakami, "Vibrations of an Infinite Beams on an Elastic Foundation with Consideration of Mass of a Foundation" Bulletin of JSME, Vol. 12, No.50, 1969, pp(200-205).
47. Sarrajin, M.A., Rosset, J.M. and Whitman, R.V. "Dynamic Soil Structure Interaction" Journal of Structural Div. ASCE, Vol. 98, 1972, pp. (1525-1544).
48. Schwieger Horst "Central Deflection of a Transversely Struck Beam" Experimental Mechanics, April 1970 (p. 166).
49. Srinath, L.S. and Das, Y.C. "Vibrations of Beams Carrying Mass" Journal of App. Mech. Vol. 34, No. 3, 1967, pp(384-385).
50. Stadler, W. and Shreeves, R.W. "The Transient and Steady State Response of the Infinite Bernoulli Euler Beam with Damping and on Elastic Foundation" Quarterly Journal of Mech. and App. Mathematics, Vol. 23, No. 2, 1970, pp. (197-208).
51. Stokoe II K.H. and Woods, R.D. "Insitu Shear Wave Velocity by Crosshole Method" Journal of Soil Mech. and Found Div. ASCE, Vol. 98, SM5, May 1972.

52. Szuladzinski, G. "Discrete Model of Beams on Elastic Foundation" Journal of Engg. Mech. Div. ASCE, Vol. 101, No. EM6, Dec. 1975, pp. (839-853).
53. Vlasov, V.Z. and Leontev, U.N. "Beams, Plates and Shells on Elastic Foundations" (Translated from Russian) NASA-TTE-357, 1966.
54. Veletsos, A.S. and Verbic, B. "Vibration of Viscoelastic Foundations" International Journal of Earthquake Engineering and Structural Dynamics Vol. 2, No. 1, July-Sep. 1973, pp. (87-102).
55. Veletsos, A.S. and Verbic, B. "Basic Response Functions for Elastic Foundations" Journal of Engg. Mech. Division, ASCE, Vol. 100, EM2, April 1974, pp. (189-202).
56. Vesic, A.B. "Bending of Beam Resting on Isotropic Solid" Journal of Engg. Mech., Division, ASCE, EM2, Vol. 87, 1961, pp. (35-53).
57. Vesic, A.B. "Beams of Elastic Subgrade and Winkler's Hypothesis" Proc. of 5th International Conference on Soil Mech. & Found. Engg. Vol.1, 1961 (p. 845).
58. Vesic, A.B. and Johnson, W.H. "Model Studies of Beams Resting on a Silt Subgrade" Journal of Soil Mech. & Found. Div. ASCE, Vol. 89, SM-1, Feb. 1963, pp. (1-31).
59. Whitman, R.V. "Analysis of Foundation Vibrations" Professional Paper P65-02 Soils Publication 169, Deptt. of Civil Engg., M.I.T. April 1964.